

The hydrodynamics of high-speed transom-stern vessels

Author:

Robards, Simon William

Publication Date:

2008

DOI:

<https://doi.org/10.26190/unsworks/18103>

License:

<https://creativecommons.org/licenses/by-nc-nd/3.0/au/>

Link to license to see what you are allowed to do with this resource.

Downloaded from <http://hdl.handle.net/1959.4/42782> in <https://unsworks.unsw.edu.au> on 2024-05-05

Chapter 1

Introduction

1.1 Research Outline

The prediction of the resistance is a significant aspect in vessel design, as it enables the designer to predict the final speed that will be achieved (Helmores, 1995). Accurate prediction of resistance is therefore of paramount importance in the design of a high-speed vessel due to the fact that building contracts for high-speed vessels often include heavy penalties for non-achievement of the contract speed. Much research has been conducted in the area of resistance prediction; however, further investigation of the hydrodynamics of high-speed vessels, specifically the complexities of the flow around the transom, is required.

The first aim of this research was to develop a greater understanding of the influence of a vessel's geometric particulars on its resistance characteristics. The second aim was to develop a greater understanding of the hydrodynamics of transom-stern flow separation and a method for predicting the behaviour of this flow. The third aim was to utilise the results of the transom experimentation to enhance the prediction of resistance for high-speed transom-stern displacement vessels.

1.2 Thesis Outline

The remainder of this Chapter is devoted to providing an introduction to naval architecture and, specifically, the industry importance of high-speed vessels and their design. The following two chapters provide an introduction to resistance prediction, the hydrodynamics of the transom stern, and previous research in these two areas.

An investigation of the wave-resistance prediction method originally conceived by Michell (1898) was undertaken. Specifically, the method of applying form factors to the wave-resistance, as developed by Doctors (1998c), was further developed by applying the method to a large database of collected model test data. To analyze this data the HYDROS suite of programs developed by Doctors (1999b) was utilised, but the original FORTRAN code had to be reformatted to enable it to be used on a PC running Microsoft[®] Windows[®] as its operating system. The reformatting, and validation process involved is reported in Chapter 6 and the results of the form-factor analysis are reported in Chapter 7.

An extensive experimental investigation of the influence of vessel speed, and vessel beam and draft, on the hydrodynamics of the transom stern was performed. The methods used in the conduct of these experiments and the results obtained are discussed in Chapter 4. The results of these experiments were used in developing an algorithm for the prediction of the transom hollow shape. This analysis is presented in Chapter 5

Concluding remarks on the research undertaken and recommendations for further work are presented in Chapter 8, and the majority of experimental results are listed in the Appendices.

1.3 High-Speed Vessels

In today's technologically-advanced society, time is more than ever before a precious commodity. The demand for reduced lead time in freight delivery, as well as faster



Figure 1.1: *Simply Magistic* designed by North West Bay Ships (NWBS) (*Photograph Courtesy of NWBS*)

passenger transport (Figure 1.1), efficient patrolling of national waterways (Figure 1.2) and faster deployment of troops and equipment in time of war (Figure 1.3) is ever increasing.

The largest demand for high-speed vessels has been in the passenger ferry market, and there has been a steady increase in the number of high-speed ferries (especially catamarans) in service over the past decade. Catamarans enable the designer to provide large deck areas for maximum passenger numbers, and the ability to reduce resistance with slender demihulls whilst retaining and (usually) increasing the transverse stability of the vessel. In recent years there has been an increasing interest in re-examining the question of optimal hullforms for displacement vessels. In particular, the number of hulls, or subhulls, providing optimal transport efficiency has been considered afresh (Doctors, 1999a). This has led to the development of trimaran vessels such as the 127 m trimaran ferry built by Austal Ships in Western Australia (Figure 1.4). The very long slender centre-hull offers favourable resistance



Figure 1.2: Patrol Vessels for Kuwait built by Austal Ships (*Photograph Courtesy of Austal Ships*)



Figure 1.3: The Incat-designed US Navy vessel HSV-X1 (*Photograph Courtesy of Incat*)

characteristics and supplies most of the displacement of the vessel; however, the slenderness is inherently deficient in transverse stability. The two small outrigger hulls provide significant additional transverse stability without adding considerably to the total resistance of the vessel.

Regardless of the number of hulls, a large proportion of the high-speed vessels being constructed today are designed with a flat, or transom, stern. Often a transom stern is incorporated into the design of high-speed vessels for ease of waterjet installation (a means of propulsion popular in high-speed applications). Another possible advantage of utilising the design feature of a transom stern in high-speed applications is the reduction in wetted surface area over that of a streamlined stern. Therefore, by incorporating a transom stern, the wetted surface and hence frictional resistance can be reduced while simultaneously retaining a wave pattern equivalent to that of a streamlined stern (Doctors and Day, 1997).

Comment is not offered regarding the advantages and disadvantages of transom sterns from a hydrodynamic viewpoint; rather, the work presented in this thesis is an acknowledgement of the common use of transom sterns in high-speed vessels and the resulting need to more greatly understand their complex hydrodynamic nature.

1.4 The Ship-Design Process

The design of high-speed vessels, as with the design of all marine craft, is an iterative process. The steps from contractual obligations to detailed design must be refined throughout the design process. Figure 1.5 is a diagrammatic representation of the design process, starting from the contract requirements through to the final detail design. For high-speed vessels, whether they be passenger or freight carrying, the main contractual obligation laid upon the ship builder is for the vessel to reach a certain speed at a given loaded displacement. There are usually heavy financial penalties if the contract speed cannot be achieved. Therefore, correctly determining the powering requirements is of great importance. Simply grossly overpowering the



Figure 1.4: 127 m Trimaran *Benchijigua Express* built by Austal Ships (*Photograph Courtesy of Austal Ships*)

vessel to ensure the contract speed is not the answer, as the additional fuel costs over the life of the vessel would be considerable. The propulsion engines, particularly in high-speed vessels, make up a considerable proportion of the displacement of a vessel, further influencing the final speed and fuel consumption. The required speed, therefore, affects the vessel's form, which in turn affects the required structure and powering. This changes the final weight of the vessel, which in turn influences the final speed. Hence, there is a need for continual refinement as depicted in Figure 1.5.

Paramount, therefore, in the successful design of high-speed vessels is an accurate prediction of the vessel's resistance characteristics early in the design process. This enables the designer to be confident in the powering selected to achieve the contract speed early in the design process and reduces the number of "refinement loops" required before reaching a final detailed design. Accurate prediction of the vessel's resistance characteristics can also reduce the additional capital and lifetime running costs which may occur if the resistance is overestimated and, hence, the vessel is unnecessarily overpowered.

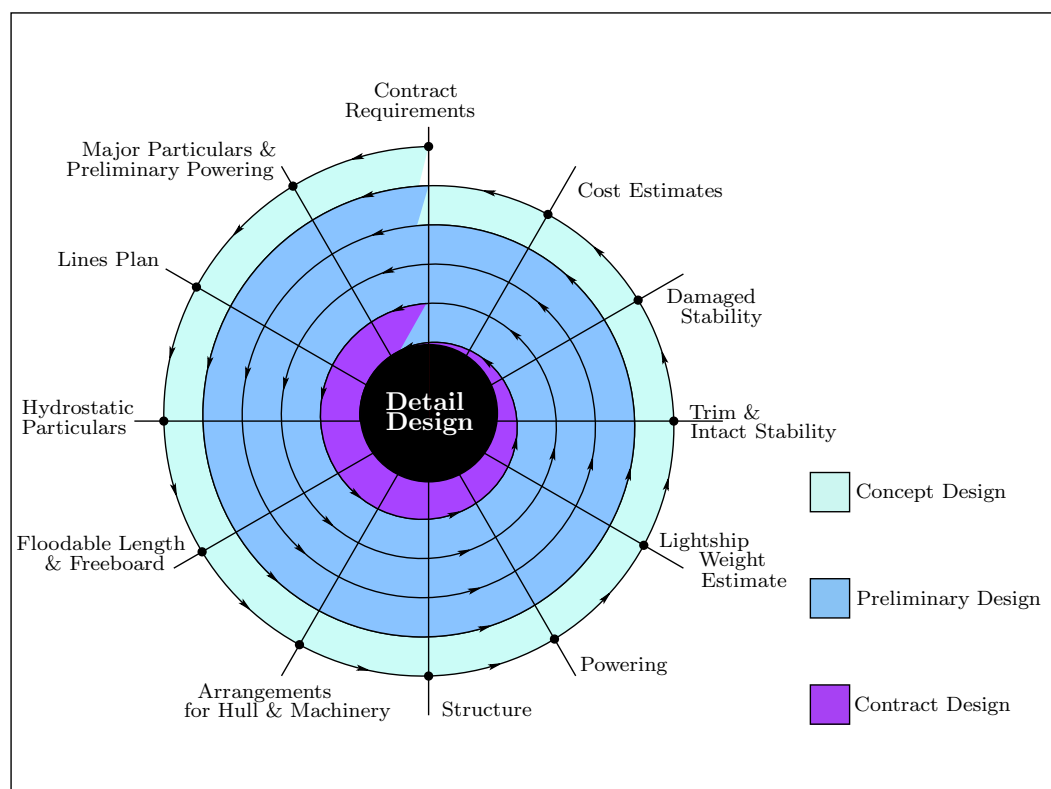


Figure 1.5: Typical Design Spiral (*Taggart, 1980*)

Chapter 2

Resistance Prediction

2.1 Ship Resistance

2.1.1 Introduction

The resistance of a vessel at a given speed is the force required to tow the vessel at that speed in calm water assuming no interference from the towing vessel (Lewis, 1988). The power necessary to overcome this resistance and achieve the required speed is referred to as the effective power and is given by

$$P_E = R_T V \quad (2.1)$$

The engine power required (often quoted as the engine brake power) is then given by

$$P_B = P_E / \eta \quad (2.2)$$

where η is the coefficient of total propulsive efficiency when all losses due to propulsion, shaft-line and gearbox efficiencies have been accounted for. The direct relationship between the vessel's resistance, and the resulting engine power required to achieve a given vessel speed, emphasizes the importance of predicting the vessel's resistance accurately.

A vessel's total resistance is made up of several components which interact in a very complex manner. The two main forms of resistance are frictional resistance and wave-making resistance. Other forms of resistance which can influence the total resistance of a vessel, but generally to a far lesser extent, are aerodynamic resistance, wave-breaking resistance and eddy-making resistance.

2.1.2 Frictional Resistance

Frictional resistance (R_F) results from the vessel's motion through a viscous fluid. The viscosity of the fluid has two main influences on restricting the vessel's forward motion. Firstly, the vessel experiences frictional forces between the hull surface and the fluid through which it passes. These frictional forces effectively carry along the fluid immediately in contact with the hull. The layer of water set in motion by the frictional forces imparted by the vessel grows in thickness along the length of the vessel and is commonly referred to as the boundary layer. The momentum supplied to the water in the boundary layer is a measure of the frictional resistance.

Secondly, the boundary layer has the effect of changing the pressure distribution over the vessel's hull. For a deeply-submerged body moving through an ideal fluid (one with no viscosity), there is no friction and, hence, no boundary layer is formed. Since the fluid has no viscosity, the pressure forces acting on the vessel act normal to the hull, so the pressure forces at the bow act to retard the vessel whereas the forces at the stern act to assist the vessel. It can be shown that the net fore-and-aft pressure distribution sums to zero; that is, there is no resistance. This outcome is referred to as d'Alembert's Paradox. The boundary layer in a real fluid, however, changes this pressure distribution such that there is a net force acting on the vessel which provides resistance to its motion. This is known as viscous pressure resistance, and can affect the wave-making resistance of the vessel.

Typically the frictional resistance of a vessel is predicted using one of the ship-model correlation lines given in Figure 2.1. All of the ship-model correlation lines in

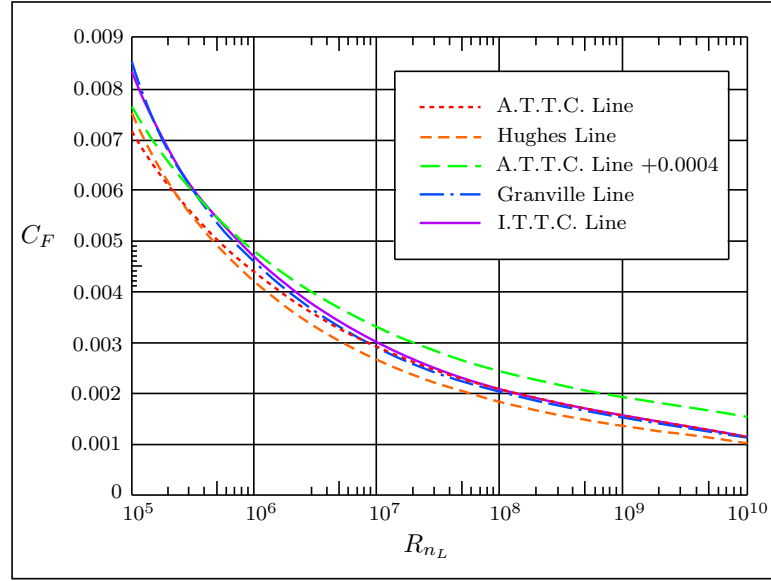


Figure 2.1: Ship-Model Correlation Lines (*Lewis, 1988*)

use today have been based on the principle of the investigations into the frictional resistance of smooth planks by Froude (1872, 1874). Froude's experiments were conducted on a series of planks of various lengths and surface finishes. From these experiments he developed a formula, with associated coefficients, for the prediction of the surface friction of ships. The results of the tests conducted by Froude are still in use today, though other superior friction formulations have been developed (Phillips-Birt, 1970).

2.1.3 Wave-making Resistance

A vessel on the surface of the water experiences a pressure distribution similar to that of the deeply-submerged body considered in Section 2.1.2. The surface vessel, however, is subject to increased pressure forces due to the free surface of the water. The bow wave associated with the forward motion of a vessel is evidence of the pressure forces acting on the forepart of the hull. The additional resistance, corresponding to the increase in net fore-and-aft pressure forces, results in the production of a wave

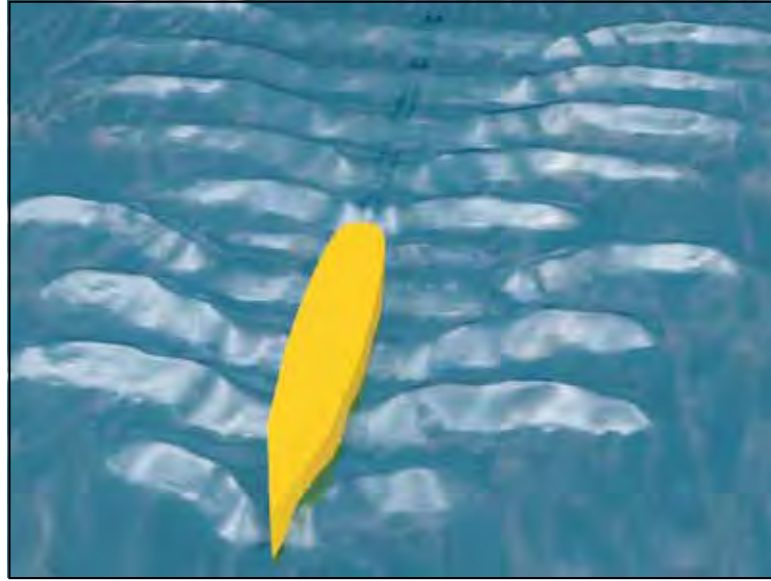


Figure 2.2: Rendered Illustration of Bow and Stern Wave Systems

system. This wave system represents a continual drain on a vessel's forward motion and is commonly referred to as wave-making or wave-pattern resistance.

The wave pattern produced by a vessel was first investigated by Lord Kelvin (1887), who considered a single pressure point travelling over the water surface, producing waves in a systematic pattern. The pattern he described reflects the observed wave systems created by full-scale vessels as depicted in Figure 2.2. The wave pattern consists of waves diverging from the bow and stern, extending out diagonally from the vessel. In addition to the diverging waves, a series of transverse waves is created perpendicular to the vessel's motion.

As the wave-making resistance is a result of the pressure forces acting normal to the hull surface, the magnitude of the wave-making resistance is largely dependent on the shape of the hull designed. Together with accurate prediction of a vessel's resistance, the refinement of the vessel's hull shape to produce the least resistance is the main objective of the naval architect in the study of ship resistance.

2.1.4 Other Forms of Resistance

Eddy-making Resistance Vessel forms which possess rapid changes in shape, or discontinuities such as steps in the hull bottom or transom sterns, are subject to separation and eddy formation. At the point of discontinuity, the flow cannot follow the dramatic change in direction and separation occurs. The eddies created represent a loss in energy for the vessel which is sometimes referred to as a separation resistance. Other causes of eddy formation, and hence further resistance, are appendages such as shaft struts and rudders.

Wave-breaking Resistance A form of resistance which is an important consideration for vessels with a fairly bluff form is wave-breaking resistance. At lower Froude numbers, vessels possessing a very full entrance create a wave in front of the bow. From Bernoulli's equation (Bernoulli, 1738),¹ it can be shown that the maximum elevation, (ζ) , of this wave is given by

$$\zeta = \frac{V^2}{2g} \quad (2.3)$$

where V is the speed of the vessel and g is the acceleration due to gravity. As the vessel's speed increases this bow wave breaks, and the energy lost due to this wave breaking is known as the wave-breaking resistance. For high-speed vessels with fine entrances, wave-breaking resistance is not a major consideration.

Spray Resistance Of much greater consideration for high-speed vessels is spray resistance. Analogous to wake-making resistance, where the production of waves by the vessel's forward motion is a loss of energy by the vessel in the form of wave-making resistance, the creation of spray by the motion of a high-speed vessel is also a loss of energy by the vessel and, hence, a form of resistance to its forward motion.

¹The modern form of the Bernoulli equation was first given by Lagrange (1788); however, the conservation principles on which the equation is based were first presented by Bernoulli

Because of the spray's complexity, experimental methods such as those by Hirano *et al.* (1990) are the only means by which the contribution of spray resistance to the total resistance can be approximated.

Aerodynamic Resistance There is more to a vessel's resistance than that below the surface of the water. Just as an aircraft experiences resistance from the air through which it travels, a vessel's superstructure experiences aerodynamic or wind resistance. For a vessel moving in still air, the aerodynamic resistance can be written as

$$R_{AA} = C_D \times \frac{1}{2} \rho_{\text{air}} A_T V^2 \quad (2.4)$$

Of interest to the designer can be the prediction of a vessel's total aerodynamic resistance, under the influence of both the vessel's speed and of the prevailing wind (V_T). Therefore, the apparent wind speed, or the wind velocity relative to the vessel (V_R) (Figure 2.3), should be used in the calculation of aerodynamic resistance

$$R_{AA} = C_D \times \frac{1}{2} \rho_{\text{air}} A_T V_R^2 \quad (2.5)$$

Research into the aerodynamic resistance of a vessel's superstructure was performed by Hughes (1930). Experiments were conducted on three different superstructures, characteristic of a tanker, a cargo ship and an Atlantic liner. The three different superstructures were towed upside-down through water at varying angles of attack and, from these experiments, Hughes developed the following equation for the determination of aerodynamic resistance

$$R_{AA} = 1.223 A_T V_R^2 K \cos \alpha \quad (2.6)$$

where α is the angle of the wind relative to the vessel and K is taken from Figure 2.4

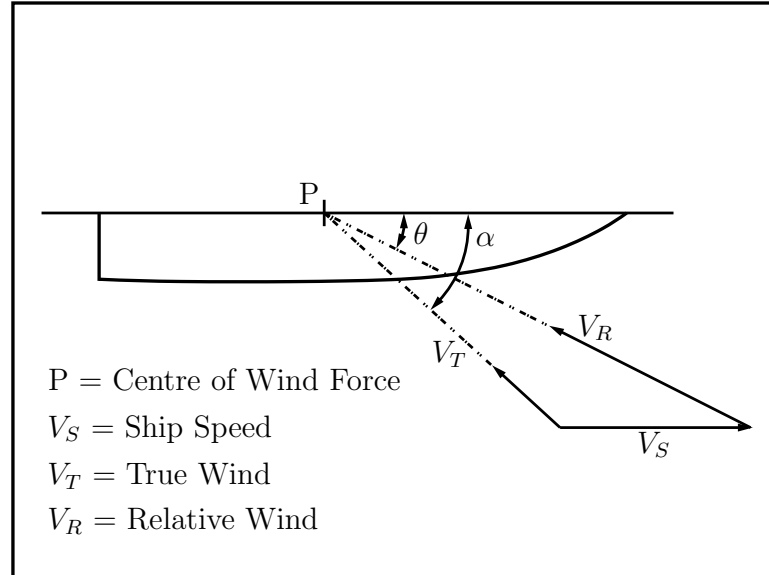


Figure 2.3: Wind Speed Relative to Vessel (*Lewis, 1988*)

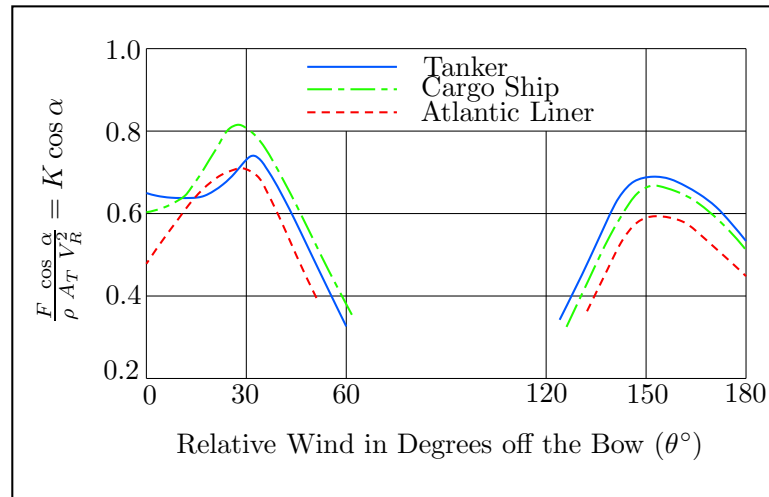


Figure 2.4: Resistance Coefficients for Relative Wind Ahead or Astern (*Lewis, 1988*)

The only means by which accurate predictions of the aerodynamic resistance can be estimated are by wind tunnel testing on scale models of a vessel's superstructure. As the aerodynamic resistance represents only a small portion of the overall resistance of a vessel; however, analytical or statistical approximations of the aerodynamic resistance are usually made.

2.1.5 Total Resistance

As discussed, the total resistance of a vessel is the result of several components which are interdependent and interact in a very complex manner. The total resistance and the relationships of the individual components are illustrated in Figure 2.5. In the current work the total resistance of a vessel is formulated as being

$$R_T = f_W R_W + f_F R_F + R_H + R_{AA} \quad (2.7)$$

where R_H is the hydrostatic resistance term resulting from the fact that for high-speed vessels, total separation occurs at the transom which “runs dry” (Chapter 3). The variables f_W and f_F are form factors for the wave-making and frictional resistance respectively, and are discussed in Section 2.3.

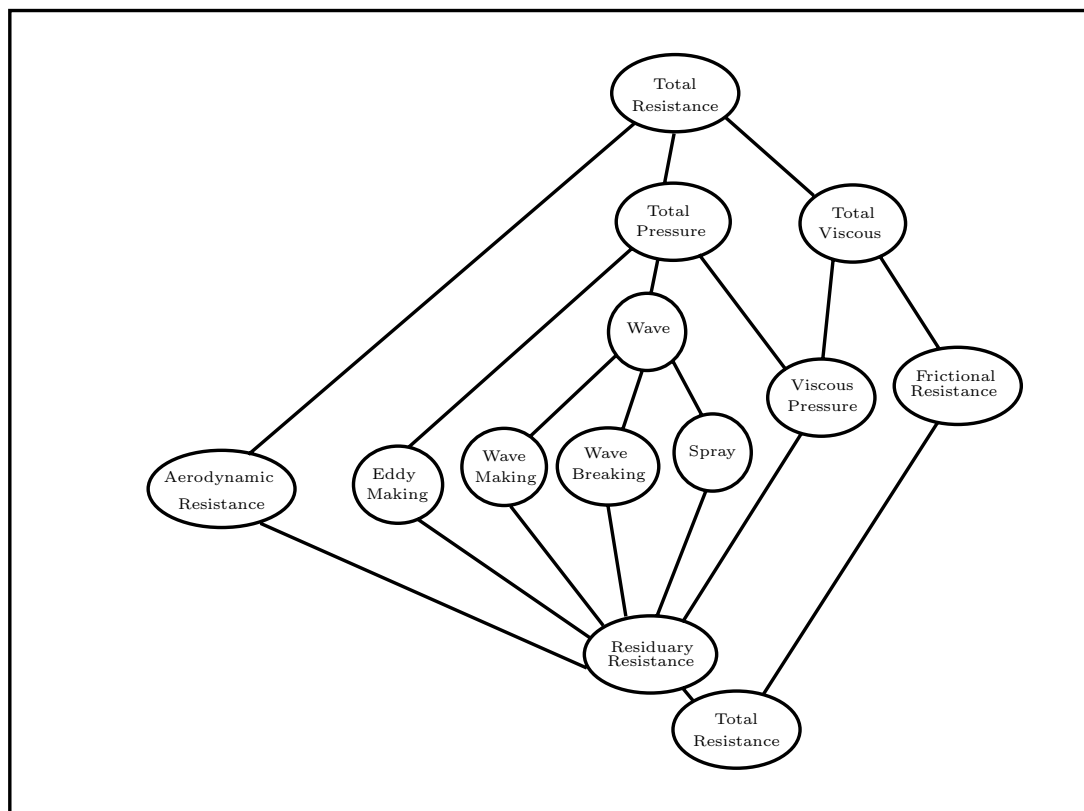


Figure 2.5: The breakdown of total resistance into its individual components and their relationships (*Modified from Couser, 1996*)

2.2 Resistance Prediction Methods

2.2.1 Introduction

The prediction of a vessel's resistance is a problem that has been grappled with for hundreds of years. Records show that Leonardo da Vinci (1452–1519) performed tests on three ship models having different fore-and-aft distributions of displacement (Tursini, 1953). Many and varied techniques have been employed in the research of ship hydrodynamics but, even with today's modern computing power, all the questions regarding ship resistance have not been answered. Much research has been done, however, and many methods are available to the ship designer and those involved in research and development.

2.2.2 Experimental

Introduction

The oldest and still the most accurate method for predicting a vessel's total resistance is experimental testing of scale models. Modern model-testing facilities provide a means by which the naval architect can test scale models at set speeds in both calm water and a variety of simulated sea states.

Facilities

Most towing-tank facilities consist of a carriage which is mechanically propelled on rails which run above the towing tank channel. The model is attached to the carriage by one or more tow posts that are free to heave with the vessel's movements underway.

Generally for the ship designer, the determination of the total resistance of the model is the main objective. This can be determined using a strain gauge on the towing post, measuring the force required to tow the vessel through the water (and air if the superstructure also has been modelled). The measurements recorded by the

strain gauge are then converted from a voltage to the equivalent force in accordance with the calibration of the gauge. Likewise, the heave of the tow post under the influence of the hydrodynamic forces experienced by the vessel is recorded using linear position transducers.

For the naval architect involved in research and/or development, the individual components of the vessel's resistance can be of most interest. The wave-making resistance of a vessel can be determined experimentally by measurement of the wave elevation in the far-field wave system. This is normally achieved using a series of capacitance wave probes arranged to record longitudinal cuts of the wave system. This technique was successfully employed by Insel (1990) and Couser (1996) in the determination of wave-making resistance. A more-expensive but non-obtrusive method of measurement would be to use laser measurement devices to record to wave elevations.

The viscous resistance can be measured by several means. One method is to measure the total loss in pressure head across the wake of the model in a transverse plane using a large matrix of pitot tubes. Alternatively, laser doppler velocimetry (LDV) can be used to measure the velocities in the wake system. Cordier and Dumez (1993) employed LDV to verify pitot tube measurements and showed that the two methods correlate well.

Scaling

The correlation of model test results with full-scale predictions of the vessel's resistance is the final stage in model testing, and presents the greatest challenge in the production of accurate predictions of a ship's resistance from the test results. The difficulty in conducting model tests to predict the full-scale resistance effects is that the different components of resistance scale according to different laws. It has been found that the forces due to pressure changes around the hull, such as wave-making

resistance, are dependant on the Froude number²

$$F_{n_L} = \frac{V}{\sqrt{gL}} \quad (2.8)$$

whereas the viscous resistance components scale according to the Reynolds number

$$R_{n_L} = \frac{VL}{\nu} \quad (2.9)$$

where ν is the kinematic viscosity of the operating fluid for the model or ship being considered.

Scaling such that the Reynolds number is the same at model and full scale requires the ratio of speeds to be equal to the scale factor. Scaling such that the Froude number is the same at model and full scale however, requires the ratio of speeds to be equal to the reciprocal of the square root of the scale factor. Experiments cannot be conducted that satisfy both Froude number and Reynolds number scaling simultaneously. However, in 1868 William Froude proposed separating the total resistance measured from model tests into the frictional resistance component and the remainder or residuary resistance (R_R) (Todd, 1966). From observations of the wave patterns of geosim models, Froude then proposed his *Law of Comparison*, which states that the coefficient of residuary resistance at corresponding speeds (that is, the same Froude number) would have the same value for ship and model. Therefore, from Froude's *Law of Comparison*, ($C_{R_{\text{model}}} = C_{R_{\text{ship}}}$), the coefficient of total resistance at full scale can be determined as

$$C_{T_{\text{ship}}} = C_{T_{\text{model}}} - (C_{F_{\text{model}}} - C_{F_{\text{ship}}}) \quad (2.10)$$

²Traditionally, the Froude number is calculated based on the waterline length of the vessel. However, due to the nature of the current work, the Froude number based on the static draft of the vessel at the stern (F_{n_T}) is primarily used.

Froude's *Law of Comparison* is still used today in ship-model correlation, the only variation being the method for determination of the frictional resistance term.

2.2.3 Statistical

For the designer, often the first estimate of a vessel's resistance is made by statistical means. Prediction methods, based on regression analysis of methodical series test data, provide an excellent means by which a designer can predict the resistance of a vessel. The accuracy of the resulting prediction is likely to be good, provided that the vessel to be designed is of a similar form to that of the series of models tested. If, however, the principal parameters of the vessel to be designed fall outside the limits of applicability of the prediction method, then the resulting prediction can be grossly inaccurate. There are several regression models available to the designer in both the displacement, semi-planing and planing regime. Some of the frequently-used prediction methods are those of Mercier and Savitsky (1973), Holtrop (1984), Fung (1991), and Lahtiharju *et al.* (1991).

2.2.4 Theoretical

Frictional Resistance

Typically, frictional resistance is estimated using one of the established ship-model correlation lines as discussed in Section 2.1.2. Prediction of frictional resistance by this method is both straightforward, reliable and, most importantly, efficient.

An alternative method, and one that potentially yields more useful information to the designer, is numerical solution of Reynolds-averaged Navier-Stokes (RANS) equations. The solving of these equations can reveal details regarding the flow around the vessel's hull which can assist in optimising the placement of appendages and propellers. However, the solution of Reynolds-averaged Navier-Stokes equations is numerically intensive and, even with today's computing power, requires vast

computing resources beyond the availability to the average designer.

Wave-making Resistance

Michell Theory A ground-breaking theory on the determination of the wave-resistance of a ship was developed by Michell (1898). Michell proposed that the wave resistance of a slender hull could be calculated by determining the resultant velocity potential in a uniform stream and, hence, the normal pressure distribution. By integrating the fore-and-aft components of this pressure distribution an expression for the wave-resistance can be derived. Further improvements to the Michell theory were made by Sretensky (1936) and Lunde (1951) through the inclusion of the influence of finite depth and finite width of the canal. Doctors and Renilson (1992) introduced the two finite-depth wave functions:-

$$\mathcal{U} = \frac{P^+ + \exp(-2kd)P^-}{1 + \exp(-2kd)} \quad (2.11)$$

$$\mathcal{V} = \frac{Q^+ + \exp(-2kd)Q^-}{1 + \exp(-2kd)} \quad (2.12)$$

where P^\pm and Q^\pm are the Michell deep-water wave functions defined by

$$P^\pm + iQ^\pm = \int_{S_0} b(x, z) \exp[i(k_x x + k_y y) \pm kz] dx dz \quad (2.13)$$

The resulting wave-resistance formulation³ is

$$R_W = \frac{2\rho g}{H} \sum_{i=0}^{\infty} \epsilon_i \frac{k_x^2 k (\mathcal{U}^2 + \mathcal{V}^2)}{2k - k_0 \tanh(kd) - k k_0 d \operatorname{sech}^2(kd)} \quad (2.14)$$

where

³For simplification the index i of the summation in Equation (2.14) has been dropped from all symbols except ϵ .

$$\epsilon_i = \begin{cases} \frac{1}{2} & \text{for } i = 0 \\ 1 & \text{for } i \geq 1 \end{cases} \quad (2.15)$$

The longitudinal and transverse wave numbers in Equation (2.14) are

$$\begin{aligned} k_x &= \sqrt{k^2 - k_y^2}, \\ k_y &= \frac{2\pi i}{H} \end{aligned} \quad (2.16)$$

while the circular wavenumber k is given by the solution of the implicit dispersion relationship

$$f = k^2 - k k_0 \tanh(kd) - k_y^2 = 0 \quad (2.17)$$

$$\frac{df}{dk} = 2k - k_0 \tanh(kd) - k k_0 d \operatorname{sech}^2(kd) \quad (2.18)$$

Finally, the fundamental wavenumber is

$$k_0 = \frac{g}{V^2} \quad (2.19)$$

Michell's theory has been shown to predict the general trends in the resistance curve with a good degree of accuracy (Doctors, 1998d), and correlates well with the experimental techniques employed by Eggert (1939).

Far-field Wave Measurement Another method for the prediction of wave-resistance proposed by Havelock (1934) is to examine the energy in the flow far astern of the vessel. The wave resistance of the vessel is a measure of the energy required to maintain the wave system. The prediction of a vessel's wave resistance by measurement of the far-field wave system has been attained experimentally by the likes of Gadd and Hogben (1962), Ward (1962), Insel (1990), and Couser (1996).

Fully Non-Linear Computation In recent times increased computing resources have meant the advent of fully non-linear codes which iterate to solve the non-linear, kinematic and dynamic free-surface conditions. The utilisation of fully non-linear codes for the determination of a vessel's resistance shows much promise as a research tool (Raven, 1992; Larson, 1993). However, the computational resources required for a single analysis are extensive. For the designer, hull optimisation, requiring repeated refinement or utilisation of a generic algorithm method such as that developed by Day and Doctors (1997b), is unattainable using non-linear techniques.

2.3 Ship Resistance Form Factors

The work of Froude on frictional resistance, as discussed in Section 2.1.2, was the result of experiments on flat planks of varying surface finishes. Likewise, Hughes (1952)⁴ conducted many experiments on planks and pontoons from which he extrapolated his skin friction formulation for plane, smooth surfaces in two-dimensional flow (Lewis, 1988). In association with his two-dimensional skin friction line, Hughes proposed that the total three-dimensional viscous resistance could be obtained through the use of a form factor k which accounts for the three-dimensional form of the vessel.

Similarly, the wave-resistance theory of Michell is based on the assumption of a thin hullform. Therefore, in much the same way as Hughes proposed a form factor for his two-dimensional skin friction line to extrapolate to the three-dimensional ship form, Doctors and Day (1997) proposed a form factor for the computed linearised wave resistance. The method was applied to a catamaran in several conditions, and the application of a single constant wave-resistance form factor resulted in more favourable agreement with experimental results.

Doctors (1998c) extended the research on form factors by proposing that both the

⁴Also refer to (Hughes, 1954).

frictional and wave-resistance form factors could be approximated in the following manner

$$f_W = \sum_{i=1}^N a_{W,i} f_i \quad (2.20)$$

$$f_F = \sum_{i=1}^N a_{F,i} f_i \quad (2.21)$$

where $a_{W,i}$ and $a_{F,i}$ are constants to be found through regression, and f_i are functions of the hull geometry. This method is further detailed in Chapter 7.

Doctors applied the method separately to three different model series, and the results were shown to be most favourable in increasing the accuracy of correlation between theory and experiment. The limitation on the form factors calculated in this research is that they only apply (with any deal of confidence), to the model series from which they were derived. One of the aims of the research reported here was to apply the method discussed to a very wide range of collected model data (refer Chapter 7). The rationale behind applying the regression to a diverse range of model test data is that the resulting form factors will have a far broader applicability in the accurate determination of a vessel's resistance when using the traditional Michell theory.

Chapter 3

The Transom Stern

3.1 Introduction

High-speed vessels often share the characteristic of possessing a truncated or transom stern. As discussed in Section 1.3, possible reasons for the incorporation of a transom stern include the desire to install waterjet propulsion which has been shown to be an efficient means of propulsion at high speeds. There is particular interest in waterjet propulsion for vessels of catamaran configuration, where waterjets offer a high degree of maneuverability. Another possible advantage of utilising the design feature of a transom stern in high-speed applications is the reduction in wetted surface area compared with that of a streamlined stern, leading to a reduction in frictional resistance while simultaneously retaining a wave pattern equivalent to that of a streamlined stern.

3.2 Transom-stern Flow

Regardless of the rationale behind its use, the transom stern presents a complex area of hydrodynamic analysis. In particular, the closure of the hollow, which is

accompanied by considerable amounts of spray¹ and unsteadiness, appears to be a formidable problem in hydrodynamics.

Observed phenomena relating to the fluid flow behind transom sterns indicate that at low speeds the transom stern is trailed by an area of circulating water. As the speed increases, a hollow is formed in the water behind the transom and the behaviour of the flow in the hollow cavity becomes more erratic. At higher speeds, the hollow deepens to the point where the flow fully separates from the transom and the length of the hollow increases with speed to the point that a “rooster tail” is formed well aft of the transom. One of the aims of the current work was to determine what influence the vessel’s beam, draft, and speed has on the depth and length of the hollow cavity (Chapters 4 and 5).

3.3 Relevance of Prediction

The total resistance for a vessel is taken to be the sum of the individual resistance components as shown in Equation 2.7. As mentioned in Section 3.2, at high speeds the flow fully separates, ventilating the transom. The hydrostatic resistance term (R_H) in Equation 2.7 was introduced to account for the additional resistance resulting from this change in pressure distribution and is calculated as

$$R_H = -\rho g \int_{-T_{\text{tran}}}^0 b(x_{\text{tran}}, z) z dz \quad (3.1)$$

The problem which arises with this formulation is that the hollow tends to fill in at lower speeds, hence the need for an accurate method for predicting the hollow depth throughout the speed range (Robards and Doctors, 2003).

In addition to improving the total resistance prediction by accounting for the influence of the hollow depth on the hydrostatic resistance term, the prediction of the

¹The point of closure of the flow in the hollow behind a transom stern is often referred to as a “rooster tail” because of the spray pattern that is thrown into the air.

hollow's length can aid in improving the wave resistance prediction. In the numerical prediction of wave-resistance, it is a common approach in the discretisation of the hull to mesh the hollow as a geometrically-smooth addition to the vessel. Therefore, of great importance in the accurate prediction of wave resistance is a method for accurately determining the length of the hollow to be discretised.

Design advantages aside, scientific endeavour throughout history has, for the most part, been undertaken in an effort to gain a greater understanding of those forces that govern our surroundings. The desire to gain a greater appreciation of the driving forces governing the behaviour of transom-stern flow is no different.

It is for these reasons that the experiments and analysis presented in Chapters 4 and 5 were performed. That is, that the prediction of total resistance using the traditional Michell theory may be improved, and that a greater understanding may be gained of the hydrodynamics of the transom stern and the driving factors determining the shape of the hollow accompanying it.

3.4 Previous Research

Very little experimental work has been performed in determining the behaviour of transom-stern flow. A small number of researchers has addressed the question of hydrodynamic flow past the transom using analytical means. An early paper on the subject was written by Milgram (1969) who modelled the wake behind the transom as a region filled with “deadwater”. Milgram assumed that the flow separated in various ways from the transom but, in the more refined version of his approach, the flow was assumed to separate tangentially to the hull surface. The traditional Michell theory was then applied to the whole body, incorporating the vessel itself and the proposed wake region.

Tulin and Hsu (1986) addressed the stern flow and the appropriate method of applying constant atmospheric pressure to the surface of the hollow. The method was limited to very high Froude numbers, which avoided the problem of analyzing

the area of the “rooster tail” as, at high Froude numbers, it would be located far from the transom. Good agreement with experimental data was achieved.

Another approach was that of Molland *et al.* (1994b), in which the water flow behind the vessel was modelled with different types of sink models. In particular, they wished to be able to model cases with lower Froude numbers, but only small improvements were made with this transom-correction method. Couser (1996) extended the ideas of Molland by modelling the transom hollow as a virtual appendage to the hull, with the length of the hollow based on the research and experiments of both Batchelor (1959) and Sinha (1981), into flows over backward-facing steps. It was noted by both Batchelor and Sinha that, for high Reynolds number turbulent flow, the streamline re-attachment length behind the step tended to be six times the step height. In this manner, Couser proposed to close the mesh of the hollow at a length of six times the half breadth of the transom. However, from experimental observations and comparisons of predicted and experimental results, it was found that the re-attachment length showed some dependance on the Froude number and the beam-to-length ratio (Couser *et al.*, 1998). Accordingly, Couser *et al.* proposed that the re-attachment length be altered in accordance with Figure 3.1 which was developed through systematic optimisation of results by means of re-attachment length variation. This approach yielded good agreement with experimental data over most of the speed range.

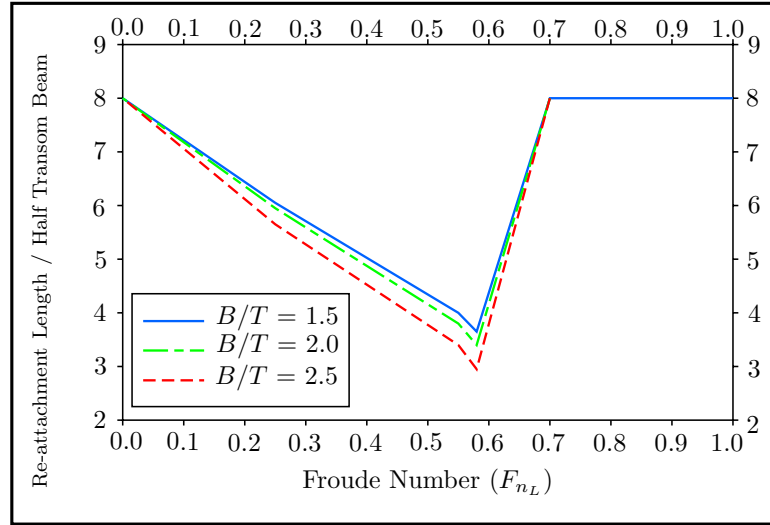


Figure 3.1: Variation in Re-attachment Length with F_{n_L} and B/T (Couser et al., 1998)

3.5 Current Research

Doctors and Day (1997) used an approach similar to that of Milgram in that the flow was assumed to separate tangentially to the vessel. Doctors and Day modelled the transom hollow based on the detailed geometry of the transom and the vessel's speed. In this study the form of the transom hollow was assumed to be parabolic in nature. The vessel was defined by means of an enclosing surface mesh, as described by Doctors (1995b), in which the vessel was represented by a network of longitudinal and girth lines (Figure 3.2). The longitudinal lines of the body were extended beyond the transom in a parabolic manner until they met at the free surface at a focal point behind the vessel (the “rooster tail”). The length of the hollow was defined as the longitudinal distance between this point and the mean longitudinal coordinate of the immersed transom girth line.

The longitudinal lines of the vessel's mesh were extended utilizing their longitu-

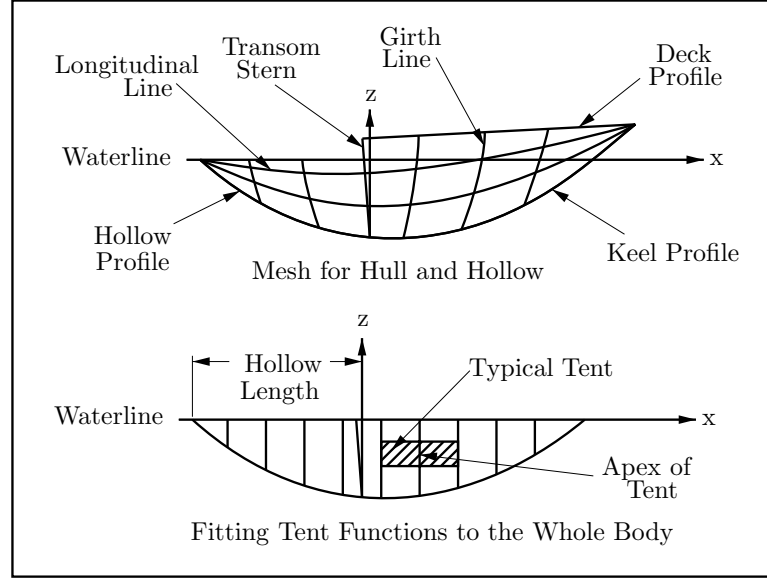


Figure 3.2: Meshing the Transom-Hollow (*Doctors, 1998e*)

dinal x and radial r coordinates, in which

$$r = \sqrt{y^2 + z^2} \quad (3.2)$$

The pair of parametric equations used for the extension to the longitudinal line was

$$x = x_i - Ut \quad (3.3)$$

$$r = r_i - U \left[\frac{dr}{dx} \right]_{x=x_i} t - \frac{1}{2} g^* t^2 \quad (3.4)$$

in which x_i and r_i were the coordinates of the relevant springing point of the hollow on the transom girth, U was the speed of the vessel (and, hence, the water past the stern, to the first order of approximation), and g^* was the effective acceleration due to gravity, which is defined as

$$g^* = f_g g \quad (3.5)$$

in which f_g was a modifying constant. Finally, t was simply a parameter which was thought of as the physical time associated with the motion of a particle of water

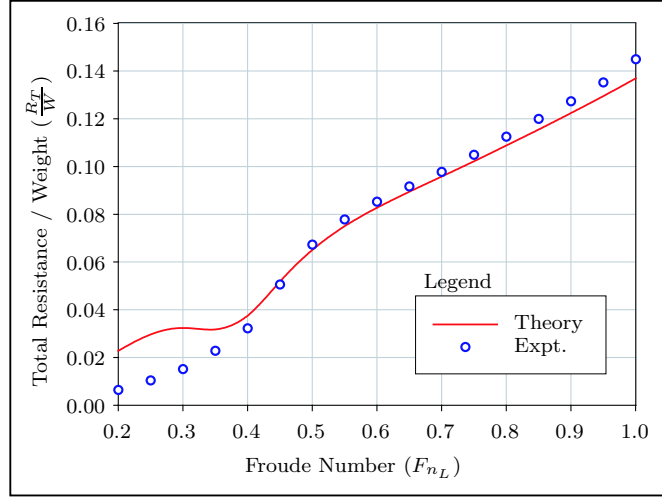


Figure 3.3: Plot of Theoretical Prediction of Total Resistance versus Experimental Measurement. (*Doctors, 1998c*)

in this kinematic and dynamic model of the hollow. The x coordinate of the end of the hollow in this radial plane was then calculated by substituting $r = 0$ into Equation 3.4.

The difficulty of the separate longitudinal lines not meeting at a single focus behind the vessel was overcome by computing a weighted focus, in which the weight was the element of transom girth associated with each longitudinal line. Furthermore, the possibility of an additional correction was permitted in this method by allowing the cavity to be stretched by a length factor, f_L .

For the purposes of numerical evaluation of the wave resistance, Doctors (1998c) discretised the hull using rectangular panels. The panels do not fit the centreplane exactly. However, the resulting error due to this non-fit at the edges was shown to be of a small order of magnitude.

The method was applied by Doctors (1998c) to the University of Southampton's series of transom-stern models. The agreement in all cases was qualitatively reasonable, although generally under-predicting the total resistance. It was noted by Doctors that there was an over-prediction of total resistance at the very low speeds

(Figure 3.3) due to the theory calculating the hydrostatic resistance based on the stern running dry at *all* speeds.

To combat the poor prediction at low speeds, where the hollow is not fully aerated,² an additional element of sophistication was added by Doctors (1998e) by estimating the depth of the hollow using potential-flow theory. The suction created at the bottom of the transom was estimated using the formulas

$$\begin{aligned}
 u &= \int_{x_1}^{x_2} \frac{\sigma(x')[x - x']}{4\pi r^3} dx' \\
 \sigma &= -2U \frac{dA}{dx} \\
 r &= \sqrt{(x - x')^2 + (y - y')^2 + (z + z')^2} \\
 q &= -Ui + u \\
 \zeta_{\text{holl.}} &= \frac{(U^2 - q^2)}{2g}
 \end{aligned} \tag{3.6}$$

where u is the perturbation velocity induced by the slender-body source distribution $\sigma(x)$ along the axis of the ship plus the hollow on the free surface, x is the coordinate at the bottom of the transom, A is the local cross section of the vessel or hollow, r is the radial distance, q is the velocity at the bottom of the transom, $\zeta_{\text{holl.}}$ is the elevation of the free-surface behind the transom, and g is the acceleration due to gravity.

Doctors applied this more-sophisticated transom-flow prediction method to the Lego series of models (Chapter 7) and further reductions in the difference between theory and experiment were achieved in terms of the root-mean-square error in values of R/W . This research by Doctors demonstrated the considerable improvements that can be achieved by estimating the drop in the water level in the transom hollow, as opposed to assuming that the transom runs dry at all speeds.

²Assuming that the buttock lines have a long easy slope ahead of the transom for 20%–30% of the waterline length and that the immersed draft is reasonably constant transversely, Saunders (1957a) surmised that full aeration of the transom would occur at $F_{nT} > 4$ or 5, where Saunders referred to F_{nT} as the submergence Froude number based on the immersed transom draft.

Considering the improvements in resistance prediction made in the research by Doctors and Day (1997) and Doctors (1998e) whereby the transom-stern effects are accounted for through estimation of the length and depth of the hollow, a large experimental programme was undertaken to determine the length and depth of the transom hollow as affected by speed and transom dimensions, the results of which are presented in Chapters 4 and 5.

Chapter 4

Transom-wake Experimentation

4.1 Introduction

Following the ideas of Doctors and Day (1997), where the hollow cavity behind the transom-stern was meshed as a geometrically-smooth addition to the vessel (Section 3.4), experiments were conducted to determine the variation in the shape of the hollow with change in the speed and geometric parameters of a vessel. The following chapter details the methods, results and analysis of the experiments conducted.

4.1.1 Hollow Model Series

There are potentially many influences affecting the shape of the transom hollow, such as bilge radius, deadrise angle, rocker, narrowing of beam from midships to transom and the rise of keel immediately forward of the transom. However, in order to minimise the size of the test matrix, the assumption was made that the major influences on the shape of the transom hollow are the vessel's transom beam, transom draft, and speed. Based on this assumption, and to avoid influences other than these three parameters, the models to be tested were designed with a flat bottom and wall sides. Figure 4.2 depicts the “Hollow Model” series with the waterline length (L) of

Table 4.1: Hollow Model Series

Hollow Model	1	2	3	4	5
Length (L) in mm	800.0	951.4	1131.4	1345.4	1600.0

the five models given in Table 4.1. The models were given a parabolic entrance for the forward one-third of their length, described by the following equation,

$$y = \frac{B}{2} \left[1 - \left(\frac{x}{L/3} \right)^2 \right] \quad (4.1)$$

All five models had a length-to-beam (L/B) ratio of 8, which was chosen so that the vessels were streamlined enough to ensure steady, uniform flow past the transom. The assumption was made that further increasing the L/B ratio would not have a substantial effect on the transom hollow.

The model size was varied by a factor of $\sqrt[4]{2}$, such that the fifth model in the series was exactly double the length and breadth of the first model in the series. All five models were tested at the same five drafts which varied from 50.0 mm to 100.0 mm by the same ratio of $\sqrt[4]{2}$, giving drafts of 50.0 mm, 59.5 mm, 70.7 mm, 84.1 mm, and 100.0 mm.

By varying the models and drafts in this way, some of the test conditions become exact geosims, as shown in Table 4.2. For example, Hollow Model 5 tested at Draft 5 (100 mm) is an exact geosim of Hollow Model 4 tested at Draft 4 (84.1 mm). Theoretically, assuming that there are no Reynolds number effects, the resistance results for geosim models at the same draft Froude number will correlate upon non-dimensionalising. Therefore, the existence of geosims in the Hollow Model series allows for a dimensional check on the experimental results obtained.

Table 4.2: Hollow Model Geosims

	Draft 1	Draft 2	Draft 3	Draft 4	Draft 5
Hollow Model 1	Geosim 4	Geosim 5	Geosim 6	Geosim 7	Unique 8
Hollow Model 2	Geosim 3	Geosim 4	Geosim 5	Geosim 6	Geosim 7
Hollow Model 3	Geosim 2	Geosim 3	Geosim 4	Geosim 5	Geosim 6
Hollow Model 4	Geosim 1	Geosim 2	Geosim 3	Geosim 4	Geosim 5
Hollow Model 5	Unique 0	Geosim 1	Geosim 2	Geosim 3	Geosim 4

4.1.2 Calculation of Required Displacement

Due to the simple nature of the models' hullforms, the displacement required to float each model at the five nominated drafts could be calculated analytically. For simplicity, the waterplane area of the model is separated into the parallel area aft (A_a) and the parabolic area forward (A_b) as shown in Figure 4.1. Due to the wall-sided nature of the models, the volume calculation is simply the waterplane area multiplied by the draft required. Therefore, using Equation 4.1 describing the parabolic entry, A_b is calculated as follows:

$$\begin{aligned}
 A_b &= 2 \times \frac{B}{2} \int_0^{L/3} \left[1 - \left(\frac{x}{L/3} \right)^2 \right] dx \\
 &= \frac{2LB}{9}
 \end{aligned} \tag{4.2}$$

Therefore, including the parallel section aft (A_a), the displacement (Δ) required for the vessel to float at draft (T) in a liquid of density (ρ) is given by:

$$\Delta = \frac{8LBT\rho}{9} \tag{4.3}$$

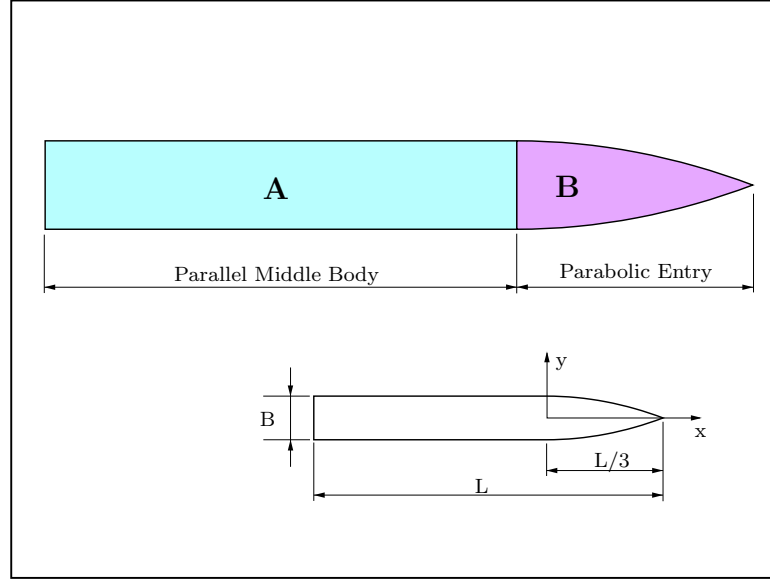


Figure 4.1: Waterplane Area Schematic

Using Equation 4.3, and taking the density of the freshwater used in the experiments as $\rho = 998.843 \text{ kg/m}^3$ (at 16.6° C), the displacement for each model at the five drafts is given in Table 4.3.

4.1.3 Measurement of the Hollow Shape

The HYDROS suite of programs developed by Professor L. J. Doctors generates the transom hollow by extending the longitudinal lines of the discretised hullform in a parabolic manner behind the transom (Section 3.5). Therefore to improve the resistance prediction made by the HYDROS suite of programs, experimental determination of only the transom depth and transom length is required negating the need for any measurements offset from the vessel's centerline.

For the purpose of the work reported here, the length of the hollow was defined as the longitudinal distance from the mean longitudinal coordinate of the immersed transom girth line, to the point of intersection of the measured hollow profile with the original static waterline (Figure 4.3).

Table 4.3: Required Model Displacement

Model	Displacement (in kg) Required to Float at Draft (T)				
	Draft 1	Draft 2	Draft 3	Draft 4	Draft 5
	$T=50.0$ mm	$T=59.5$ mm	$T=70.7$ mm	$T=84.1$ mm	$T=100.0$ mm
Hollow Model 1	3.550	4.221	5.020	5.970	7.099
Hollow Model 2	5.020	5.970	7.099	8.443	10.040
Hollow Model 3	7.099	8.443	10.040	11.940	14.199
Hollow Model 4	10.040	11.940	14.199	16.885	20.080
Hollow Model 5	14.199	16.885	20.080	23.879	28.397

For the majority of the experiments, the models were free to trim, varying the vertical location of the lowest point on the vessel's transom. As the trim of the vessel affects the depth of the transom hollow, the hydrodynamic draft instead of the hollow depth was recorded for each run. The hydrodynamic draft (T_H) is defined as the wetted depth of the transom as shown in Figure 4.3. The other advantage in recording (T_H) instead of the hollow depth is that the term varies between 0 (fully aerated) and 1 (fully wetted) when non-dimensionalised by dividing by the static draft.

To experimentally determine the length and depth of the hollow cavity, a capacitance wave probe¹ was used to measure the water elevation aft of the transom along the centreline of the vessel. One consideration was to use several wave probes aft of the transom, spaced evenly along the vessel's centreline. This would result in time-averaged results for the water elevation at known longitudinal locations. A

¹The capacitance wave-probe had wires separated by approximately 10 mm resulting in the actual measurements of the water level being 5 mm offset from the vessel's centerline. However, due to the parabolic nature of the shape of the transom hollow, the resulting error in measured length of the transom hollow would be less than one percent.

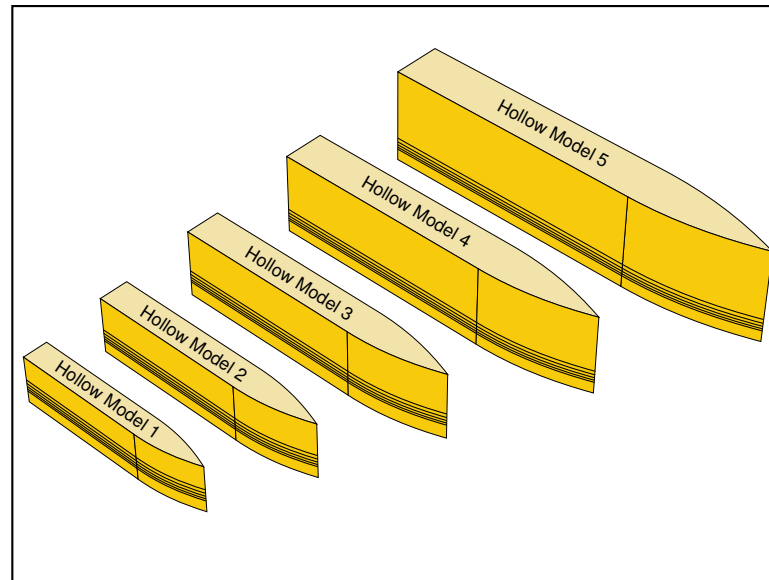


Figure 4.2: Render and Plan Schematic of Hollow Model Series

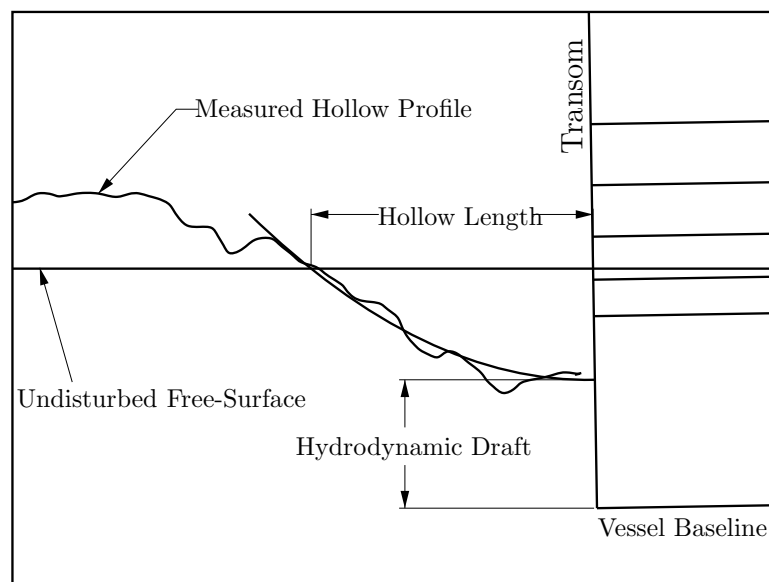


Figure 4.3: Definition of Transom-Hollow Dimensions

curve could then be fitted through the coordinates of the measured water elevation at each wave probe, and in this way produce the profile of the hollow cavity. The problem with measuring a series of points along the hollow profile with wave probes of fixed spacing is that the length of the hollow cavity changes quite dramatically with speed. This results in the fixed spacing chosen for the wave probes being ideal for only a limited number of speeds.

Instead, a movable wave-probe was employed, providing measurements of the water elevation over the entire length of the hollow profile along the centreline of the vessel. The disadvantage of using the movable wave-probe method is that the measurements at each longitudinal location cannot be time averaged. However, with the wave probe capturing 1024 data points over a distance of approximately 500 mm, the measured hollow profiles had approximately two points for every millimetre. With this many data points describing the hollow profile, a line of best fit approach provided an accurate means for determining the intersection of the hollow profile with the original static waterline.

4.2 Methods

4.2.1 Testing Facilities

The hollow model series was tested in the Ship Hydrodynamics Centre (SHC) at the Australian Maritime College (AMC) in Launceston, Tasmania. Experimental facilities at the AMC include a circulating water or “flume tank”, a cavitation tunnel, and a ship model basin; however, it was the SHC’s towing tank that was utilised for the experiments reported here.

The towing tank was approximately 60 m long², 3.6 m wide and with a maximum water depth of 1.5 m. Models were towed by a powered carriage running along rails on the topsides of the tank (Figure 4.4). The speed of the carriage can be set, and

²The towing tank facility at AMC was extended to over 100 m in length in 2005.



Figure 4.4: The Towing Tank and Carriage at The Australian Maritime College, Launceston, Tasmania (*Photograph by S. Robards*)

maintained to within 0.01 m/s, up to a maximum of approximately 4.6 m/s.

Although the current work only called for calm-water testing, waves can be produced for seakeeping analysis. A hydraulically-driven wavemaker positioned at the end of the tank can produce a wide variety of wave forms, including regular or irregular waves, and user-defined wave spectra. A “beach” for the dissipation of wave energy is located at the start of the tank, along with mechanically removable “beaches” down one side of the tank.

A ballasting dock, located at the start of the tank, is used to achieve level trim and heel of the model. Glass sides in this part of the tank enable verification of the trim of the model’s waterlines in relation to the free surface of the water.

4.2.2 Model Preparation

In preparing the models for testing, the following procedure was followed:

Step 1: Turbulence-stimulation studs were adhered to the outside of the hull in a

girth-wise direction, 150 mm aft of the bow.

Step 2: Waterlines corresponding to the five drafts were drawn on each model.

Step 3: The lower part of forward tow-post³ along with a strain gauge for resistance measurements was attached to the model 25 mm above the model's baseline. The forward-tow post was pin jointed and free to experience heave but was restricted in roll. Both tow posts were fixed transversely such that the model could not experience yaw.

Step 4: The lower part of the aft tow-post consisted of a ball-bearing slider which was attached to the model. The slider accounted for the change in the relative distance between attachment points with the change in trim of the model. The longitudinal location of the aft post was recorded with the vessel bolted in position and at level trim. Figure 4.5 shows the post attachments, and Table 4.4 gives the setup positions recorded for each model.

Step 5: Each model was ballasted to the displacement corresponding to the draft at which the model was to be examined (see Table 4.3 for drafts and displacements). The total displacement of the model included the bolts used to connect lower and upper tow-posts, as these bolts were not included in the counterbalancing of the upper posts.

Step 6: The model was attached to the towing carriage by bolting the upper and lower parts of the towing posts.

Step 7: With the model in the ballasting dock, level trim and even heel were obtained by altering the longitudinal and transverse location of the ballast.

³The upper part of both forward and aft tow posts, to which the lower parts were bolted, were permanently attached to the towing tank carriage. and counterbalanced to provide no influence on the displacement or heave of the vessel.

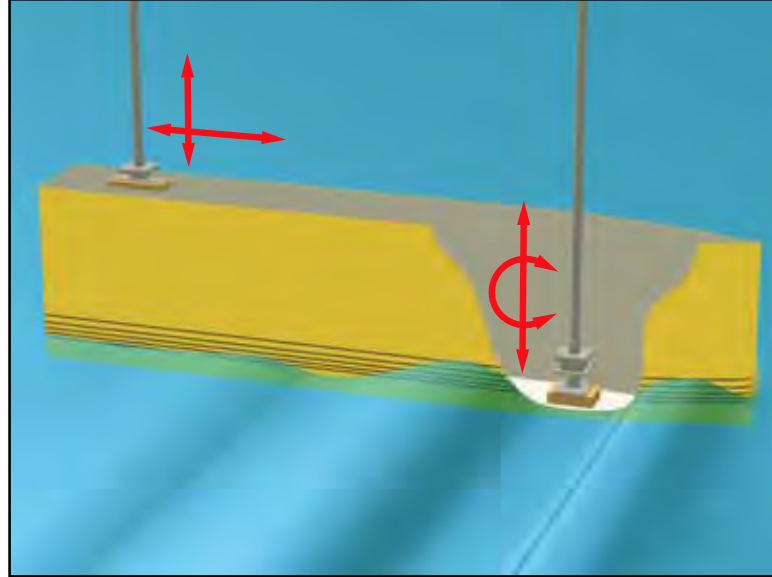


Figure 4.5: Arrangement of the Forward and Aft Tow-Posts on the Model.

Table 4.4: Measured Model Arrangements

Model	Measurements relative to midships & baseline in mm				
	Forward Post		Aft Post		Wave Probe Origin
	z_{post_F}	x_{post_F}	z_{post_A}	x_{post_A}	x_{WP_0}
Hollow Model 1	25.0	200.0	200.0	-280.0	-924.0
Hollow Model 2	25.0	237.8	250.0	-333.2	-1040.2
Hollow Model 3	25.0	282.8	300.0	-396.2	-1078.7
Hollow Model 4	25.0	336.6	350.0	-470.7	-1203.7
Hollow Model 5	25.0	408.5	400.0	-551.5	-1330.0

4.2.3 Experimental Rig

Standard Rig

The conventional two post dynamometer, designed and commissioned by AMC, was used to tow the model. The posts were both counterbalanced to provide no influence on the equilibrium of the model. Both tow posts were fitted with linear-variable-displacement transducers (LVDTs) to measure the heave motions experienced by the model underway. LVDTs are electromagnetic devices which have coils of wire wound on a hollow tube and a metal rod moving inside the tube. The LVDT's output is an alternating-current (AC) voltage proportional to the relative displacement of the rod from the tubing (in this case, the rise of the vessel).

Movable Wave Probe Rig

The rig to support the capacitance wave-probe was designed by the resident model technicians at the SHC. A solid aluminium strut was used to support the wave probe. The strut was initially of rectangular cross-section; however, early testing revealed that this inhibited the smooth forward motion of the probe through the water. To provide less resistance to the probe's forward motion the strut was ground back to a more streamlined foil shape.

The probe and associated supporting strut were attached to a sliding bracket on a ball-bearing runner of approximately 500 mm in length. A rotary potentiometer, fixed at the aft end of the slide, was used to record the longitudinal location of the bracket, and hence the wave probe, during the experiment. The wave probe's forward motion was provided manually via a pulley system attached to the probe's sliding bracket.

The entire wave-probe rig, along with a means for calibration (Section 4.2.4), was bolted to the towing carriage. The complete wave-probe setup is shown in Figure 4.6, along with a photograph of the wave probe in position behind one of the hollow models in Figure 4.7.

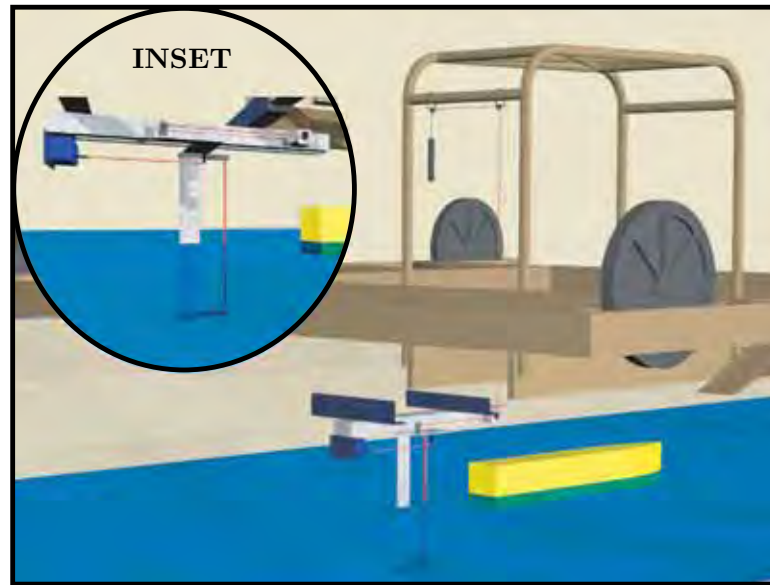


Figure 4.6: Rendered Model of Wave-probe Rig with Detailed View Inset

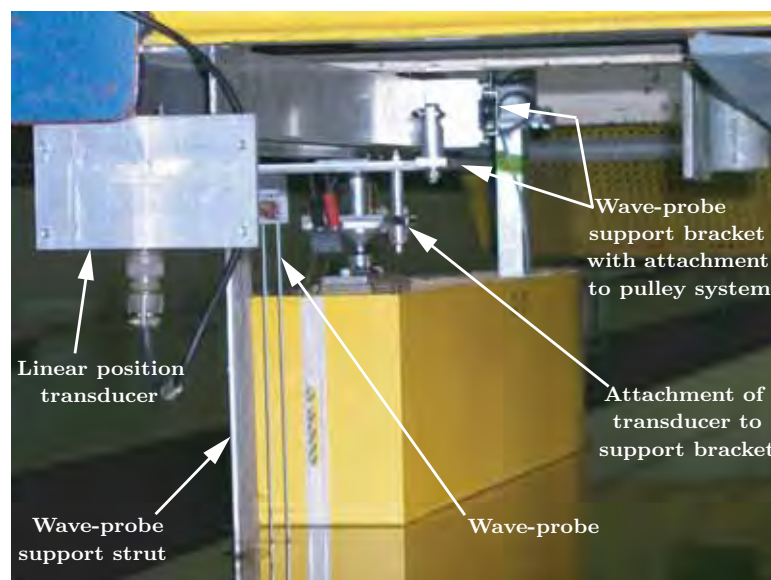


Figure 4.7: Wave Probe *in situ* Behind one of the Hollow Models (*Photograph by S. Robards*)

4.2.4 Rig Preparation

Before the prepared model could be tested, the instrumentation used to record the experimental results required calibration. The instruments were calibrated each day before experimentation commenced. The strain gauge was also calibrated between conditions due to the expected increase in resistance experienced by a larger model, or a model at a greater draft. Not all data channels were used for all testing conditions (e.g. the heave of the posts was not required for the fixed trim tests⁴); however, the calibration factors relevant to each condition can be found in Appendix B. The methods of calibration for each data channel are detailed below:

Channel 0: The speed of the carriage, was calibrated once per month by the technicians at the SHC.

Channel 1: The tow posts, used to attach the model to the towing carriage, are depicted in Figure 4.8. Both the tow posts had a slide, with slots at exactly 10 mm increments. This could be moved to align one of the slots with the zero heave position of the vessel. For fixed-trim tests the model could then be pinned in the level-trim position. The slots were also used to calibrate the linear-variable-displacement transducers used to measure the rise of the vessel. The LVDT measuring the heave of the vessel at the forward post was calibrated by systematically raising the forward post in 10 mm increments up to 50 mm of heave, then returning to the zero position. The post was then lowered to -50 mm heave in 10 mm decrements and then returned to the zero position. The calibration factor was the result of a line of best fit to the recorded values from the known movements.

⁴The majority of the hollow experiments were performed with the model free-to-trim. Hence, the vast majority of the results presented here (unless indicated otherwise) are for the model free-to-trim.

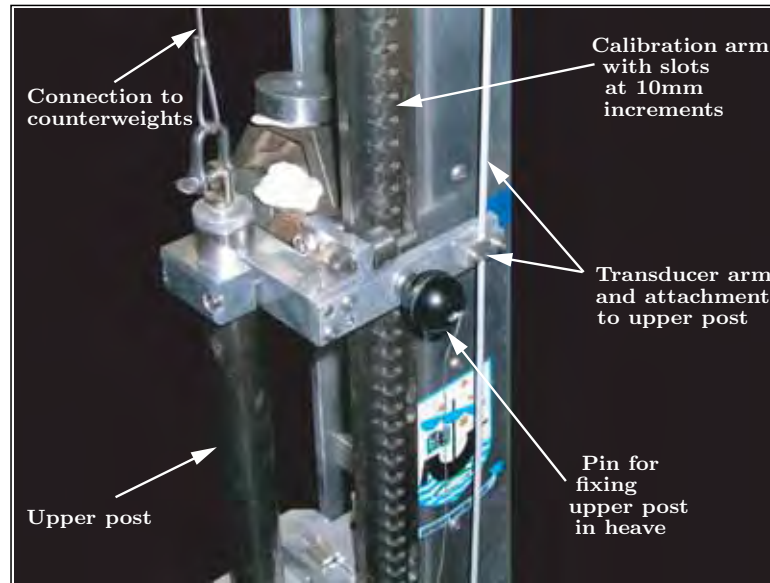


Figure 4.8: Towing Posts and Associated Calibration Slide (*Photograph by S. Robards*)

Channel 2: The LVDT measuring the heave of the vessel at the aft post was calibrated in the same manner as that of the forward post recorded on Channel 1.

Channel 3: The strain gauge used for measuring the vessel's total resistance, was calibrated by applying known forces horizontally to the vessel. Weights were applied to a set of scales designed to apply the force parallel to the waterline, via a wire attached to a hook on the model's transom. Weights were added in even increments up to a value exceeding the maximum expected resistance for the model's condition. The weights were then systematically reduced, in double the initial increments, back to the zero position. The calibration factor was determined from the line of best fit to the recorded voltages for the known forces.

Channel 4: To calibrate the rotary potentiometer measuring the longitudinal location of the movable wave-probe, use was made of the probe's pulley system.

A rule was set up parallel to the pulley wire and the probe was systematically displaced in 10 mm increments up to a maximum displacement of 100 mm. The probe was then returned to the zero mark in 10 mm increments. The calibration factor was then determined from the line of best fit to the recorded voltages for the known probe displacements.

Channel 5: The movable wave-probe was calibrated by attaching a solid aluminium shaft to the top of the wave-probe strut. The solid shaft was designed with holes drilled at precisely 10 mm increments which were used to fix the wave probe at different depths of water. The wave probe was systematically raised in 10 mm increments to a height (or simulated hollow depth) of 130 mm, and then returned to the zero point in 10 mm increments. The calibration factor was determined from the line of best fit to the recorded voltages for the successive movements.

Channel 6: For the fixed-trim experiments conducted on Hollow Model 3, an additional wave probe was placed on the transom to record a time-averaged result of the water elevation at the transom. As the wave probe was attached to the transom, calibration was achieved by systematically lowering the model in 10 mm increments to a depth of 50 mm using the increments on the tow posts. The model was then raised back to zero and then raised in 10 mm increments to a height of 50 mm. The calibration factor was determined from the line of best fit to the recorded voltages for the successive movements.

4.2.5 Experimental Procedure

Methodology

Initially, the model series was only tested free-to-trim; however, fixed-trim tests were conducted on Hollow Model 3. The models were tested at 23 draft Froude numbers⁵ (F_{n_T}) ranging from 0.7 to 4.0. For each of the 25 conditions (5 models at 5 drafts), two additional repeat runs were conducted as an experimental check. The models were tested in calm water, with approximately ten minutes of waiting time between runs. This provided enough time for the energy in the disturbed free surface from the previous run to dissipate.

Test Procedure

The following test procedure was used for each of the experimental runs:

Step 1: Digital video cameras were used to film each run. Relevant data on the run being filmed, such as model number, run number, and the carriage speed, was typed into a video-labelling system preceding each run.

Step 2: The models were tested at draft Froude numbers ranging between 0.7 and 4.0. Before each run the carriage speed was set to within 0.01 m/s of the required draft Froude number.

Step 3: Before each run, checks were made to ensure that the model was still free-to-trim and that the movable wave-probe was in the starting position.

Step 4: Once the water surface of the tank had settled from the previous run, the carriage was powered up, ready for the next run. The initial or “zero” readings for each data channel were then recorded with the vessel at rest and

⁵The draft-Froude number is based on the static draft of the vessel at the stern such that $F_{n_T} = \frac{V}{\sqrt{gT}}$

the movable wave-probe at its starting position. The towing tank's data-acquisition system calculated the "zeroes" by averaging 100 readings.

Step 5: Recording of the digital video was commenced.

Step 6: The carriage was set in motion.

Step 7: Once the carriage had reached the set speed and the the model had reached a steady state, data on all channels were recorded. The data-acquisition system was set to record 1024 data points at a sampling rate of 100 Hz.

Step 8: During data acquisition, the pulley system was used to advance the wave probe through the water towards the transom stern of the model.

Step 9: Once the data-acquisition system had finished recording, the carriage was stopped and slowly reversed back up the tank. The recording of the digital video also ceased.

Step 10: The mechanically-operated "beaches" on the side of the towing tank were lowered to absorb the energy of the created wave system.

Step 11: The data-acquisition system provided a graphical interface for plotting the data recorded on each channel. Channels 0, 1, 2, and 3 were all recording constant data such as speed, heave, and resistance. Therefore, the average of all data points was taken in each case. In the calculation of the averages, the in-house data system enabled the user to crop the recorded data to include only the steady-state period. This was important for runs where the model had not reached a steady-state before recording had begun, or where the carriage had to be stopped before recording had finished. The complete data set (all channels, uncropped) was then saved on a floppy disk.

4.2.6 Methods of Analysis

Although a strain gauge was used to determine the resistance experienced by the models, it was the shape of the transom hollow that was of primary interest. Therefore, the methods and results presented are solely for the measurement of the transom hollow.

Plotting of Hollow Profile

Microsoft® Excel® spreadsheets were primarily used for importing the experimental data and performing any initial calculations. Using the calibration factors determined, and the recorded zeroes, the voltages were converted to the relevant units. For example, the heave at the forward post (δz_F) was determined in the following manner

$$\delta z_F = (z_V - z_0) \times C \quad (4.4)$$

where z_V is the heave measurement in volts, z_0 is the zero reading recorded for the forward post, and C is the calibration factor for the forward post (determined by the methods described in Section 4.2.4).

As with the cropping of the static-data channels to include only the steady-state data, the data for the movable wave-probe also required cropping. This was necessary to remove the build up of points at the start of a run where data was being recorded too long before the probe started to move. Likewise, if the probe had reached the vessel's transom before the period of data acquisition had ceased, there was an unnecessary build up of points at the transom. To crop the extraneous data, a search was made for the last occurrence of the minimum longitudinal location of the wave-probe. All data preceding this data point were ignored. Similarly, the first occurrence of the maximum longitudinal location of the wave probe was found, and all data following this data point were disregarded.

Due to the large number of data files to be modified, small codes (or macros) were developed to automate many processes. Microsoft[®] Excel[®] provides excellent means for writing, debugging, and running macros in the Visual Basic language.

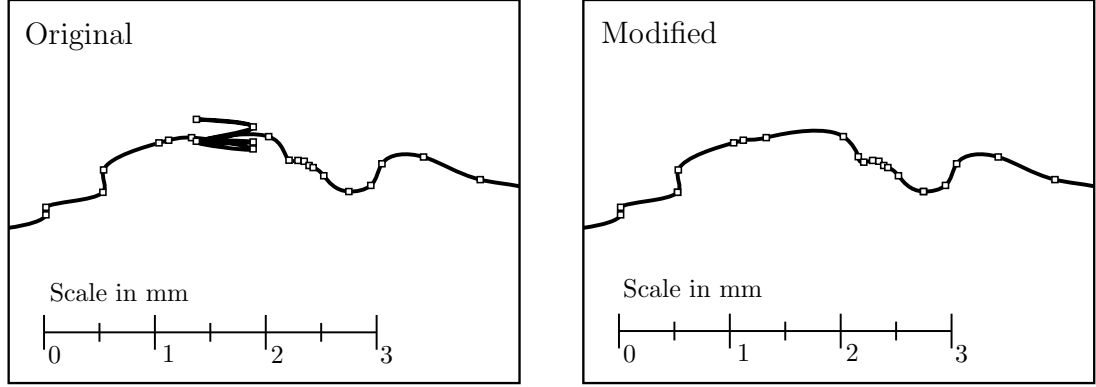
The computer-aided-drafting (CAD) package Rhinoceros[®] was used for plotting the hollow profile in association with the relevant vessel profile. Rhinoceros[®] is a powerful three-dimensional (3-D) modelling package which combines the accuracy of traditional CAD systems with the flexibility of NURBS⁶-based modelling technology. Although primarily used as a 3-D modelling tool, due to its flexibility and accuracy, Rhinoceros[®] was an ideal application for the analysis reported here.

Each of the 625 runs was imported into Rhinoceros[®] and fitted with an interpolated curve (or spline) of degree 3. Due to the fact that the wave probe was manually pulled through the water, occasionally when the probe's forward motion was irregular, there was a build up of points at the one longitudinal location. In these instances, the curve was modified as shown in Figure 4.9 to remove the extraneous points. As the scale in Figure 4.9 indicates, this did not have an effect on the measured length and depth of the transom-hollow.

Trimming of Vessel Profile

With the hollow profile produced, the next step in the analysis was to incorporate a profile of the appropriate vessel. The vessel profile was placed at the correct draft and longitudinal location with respect to the plotted hollow profile. The longitudinal location of the transom in relation to the zero position of the wave probe differed for each model. For example, calculating from Table 4.4, the distance between the wave probe origin and the transom for Hollow Model 1 was

⁶Non-Uniform Rational B-Splines (NURBS) are mathematical representations which can accurately define any shape from a simple 2-D line, circle, arc, or box to the most complex 3-D free-form organic surface or solid.

**Figure 4.9:** Modification of the Interpolated curve

$$\begin{aligned}
 x_{\text{TRAN}} &= -\left(x_{WP_0} + \frac{LWL}{2}\right) \\
 &= -(-924.0 + 400.0) \\
 &= 524.0 \text{ mm}
 \end{aligned} \tag{4.5}$$

whereas for Hollow Model 2 it was

$$\begin{aligned}
 x_{\text{TRAN}} &= -\left(x_{WP_0} + \frac{LWL}{2}\right) \\
 &= -(-1040.2 + 475.7) \\
 &= 564.5 \text{ mm}
 \end{aligned} \tag{4.6}$$

With the profile of the model positioned at the appropriate draft and in the correct longitudinal location, the recorded heave measurements at the forward and aft tow posts were used to obtain the correct trim for the model profile. In order to trim the profile of the model, the following procedure was followed:

Step 1: As shown in Figure 4.10(A), a circle of radius equal to the heave of the aft post (δz_{AFT}) was placed with its centre at the recorded starting location of the aft post (A_{POST}).

Step 2: The profile of the model was then moved vertically a distance equal to the heave experienced by the forward post (F_{POST}) as indicated in Figure 4.10(B).

Step 3: An arc was then constructed, having its centre at the modified position of the forward post (F'_{POST}). Figure 4.10(C) shows that the arc passes through point α , being the intersection of the line of the aft tow post, and the circle constructed in Step 1. The arc also intersects the top of the profile of the model at point β .

Step 4: The profile of the model was then rotated about F'_{POST} , until point β coincides with point α (β'). As can be seen in Figure 4.10(D), the original position of the aft post (A'_{POST}) moves in a vertically-constrained manner to point (A_{POST}) however, point β has moved longitudinally. Hence, there is a need for the aft post to be attached to the model using a slide as mentioned in Section 4.2.2.

Macros were developed to automate the above process for the 625 free-trim runs, and this greatly reduced the overall processing time.

Hollow Measurements

With the measured hollow profile plotted against the corresponding trimmed model profile, it was possible to determine values for the hollow length (L_H), and hydrodynamic draft (T_H) for each run. Using the functions of Rhinoceros[®], and following on from the ideas of Doctors and Day (1997) where the form of the transom hollow was assumed to be parabolic in nature, each of the plotted hollow profiles was fitted with a parabola for determination of L_H and T_H . The distance along the static waterline between the transom and the point of intersection with the parabola was then recorded as the hollow length using the distance function in Rhinoceros[®] (Figure 4.3). Likewise, the distance between the intersection of the parabola with the transom and the base of the transom was recorded as the hydrodynamic draft.

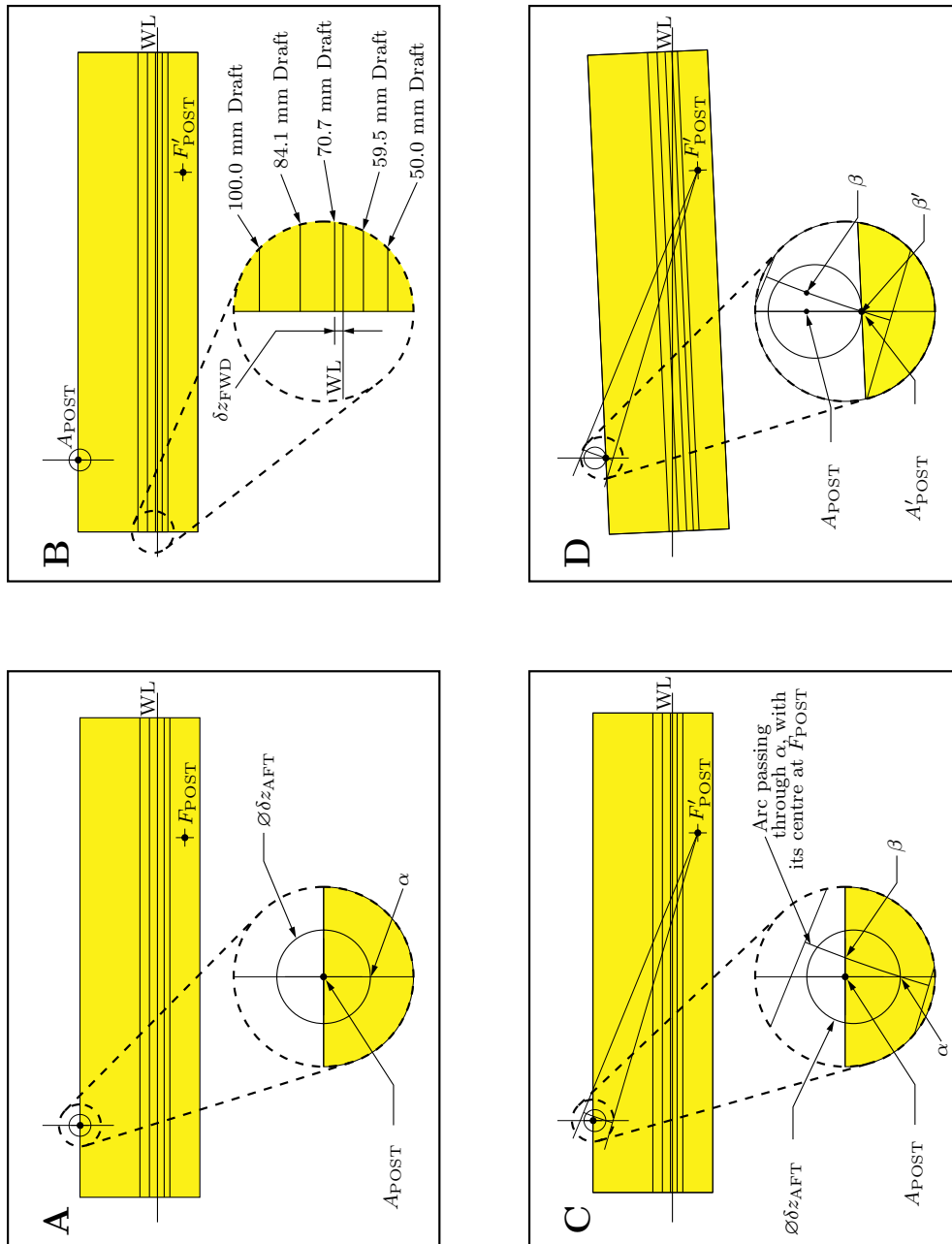


Figure 4.10: Method of Trimming Model Profile

4.3 Results

4.3.1 Measured Hollow Shape

Hollow Profiles

The main purpose for recording the hollow profile was to determine the hydrodynamic draft and hollow length and to use this data to improve the theoretical prediction of resistance. However, the measured profiles also provide a visual representation and comprehensive study of the influences of beam, draft and speed on the shape of the transom hollow.

The influence of the beam of the models on the shape of the transom hollow is evident in Figure 4.14, where comparison is made of the measured hollow profiles for each of the models at the deepest draft of 100.0 mm, and tested at a draft Froude number of 2.0. The beam of the model only has a small affect on the depth and length of the hollow, but has a dramatic influence on the amount of wake behind the hollow. With a reduced beam the inward components of velocity in the two streams which flow aft of the transom port and starboard are smaller, producing a smaller ridge of disturbed turbulent water or “rooster tail”. This supports the theoretical work of Doctors (1998f) where it was shown that the selection of long slender hulls in a catamaran configuration was superior to broader monohulls in terms of wave-wake generation.

The effect on the shape of the transom hollow of the draft at which the model is floating is less pronounced than the beam of the model. Figure 4.15 compares the measured hollow profiles for Hollow Model 5, indicating a dramatic change in the depth of the hollow with change in draft. However, Figure 4.15 presents the hollow profiles at the 5 drafts at the same draft Froude number of $F_{n_T} = 2.0$, so with increasing draft the speed is increasing. Figure 4.16 on the other hand, presents the hollow profiles for model 5 at the same beam Froude number (hence same velocity) of $F_{n_B} = 1.2$. Here the affect of draft is clearly less pronounced than the beam of

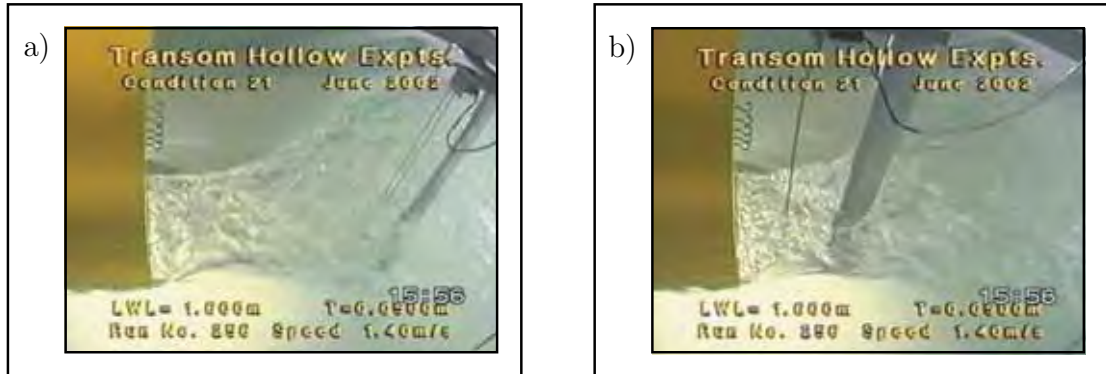


Figure 4.11: Video Screen Capture of Hollow Model 5 at Draft 1 and $F_{nT} = 2.0$

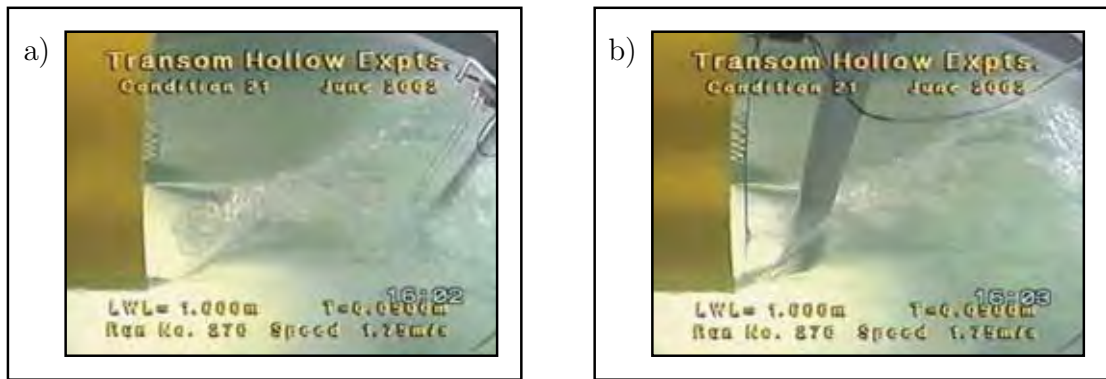


Figure 4.12: Video Screen Capture of Hollow Model 5 at Draft 1 and $F_{nT} = 2.5$

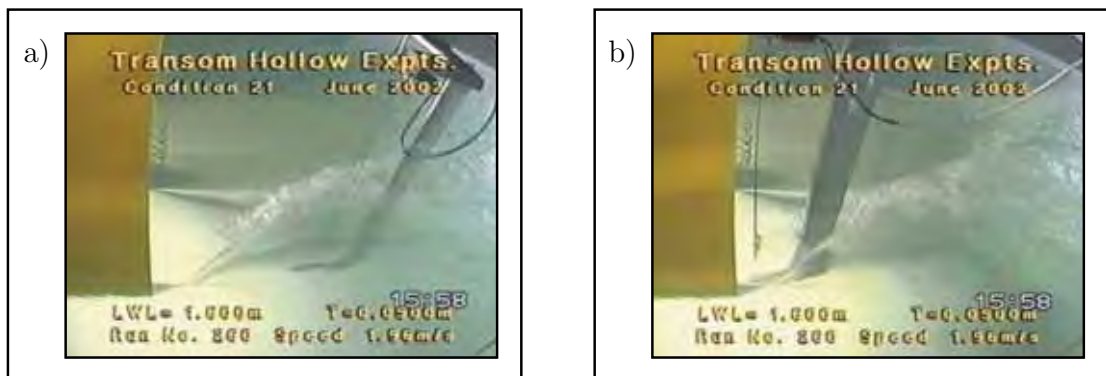


Figure 4.13: Video Screen Capture of Hollow Model 5 at Draft 1 and $F_{nT} = 2.8$

the vessel.

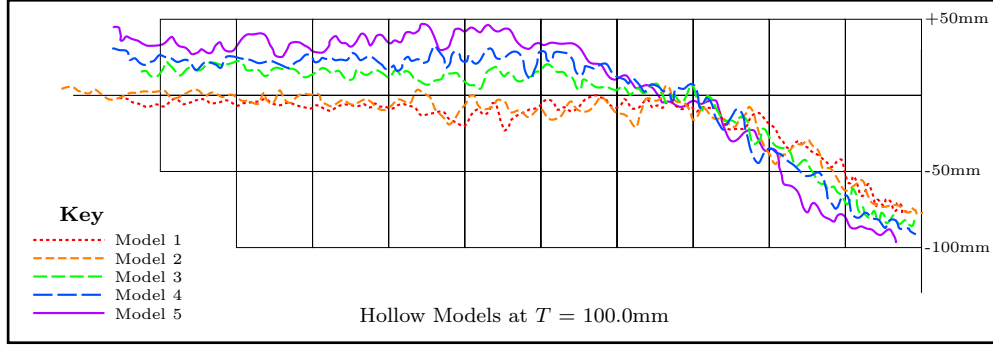


Figure 4.14: Influence of model beam on the transom hollow at $F_{nT} = 2.0$

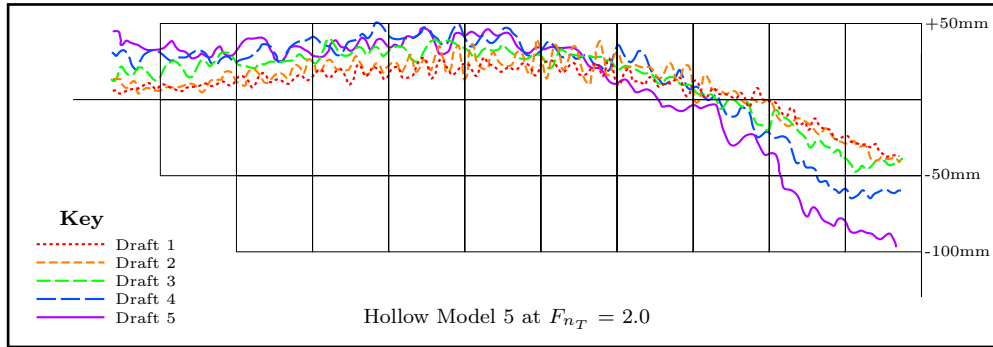


Figure 4.15: Influence of model draft on the transom hollow at $F_{nT} = 2.0$

As expected, the largest influence on the shape of the transom-hollow is the speed at which the vessel is travelling. Figure 4.17 shows the pronounced change in the measured hollow profile for Hollow Model 5 with change in speed.

The plots of all the hollow profiles recorded by the movable wave-probe are presented in Appendix C.

Hydrodynamic Draft

The hydrodynamic draft (T_H), as discussed in Section 4.1.3, is the wetted depth of the transom which, for the purpose of analysis, was non-dimensionalised by the

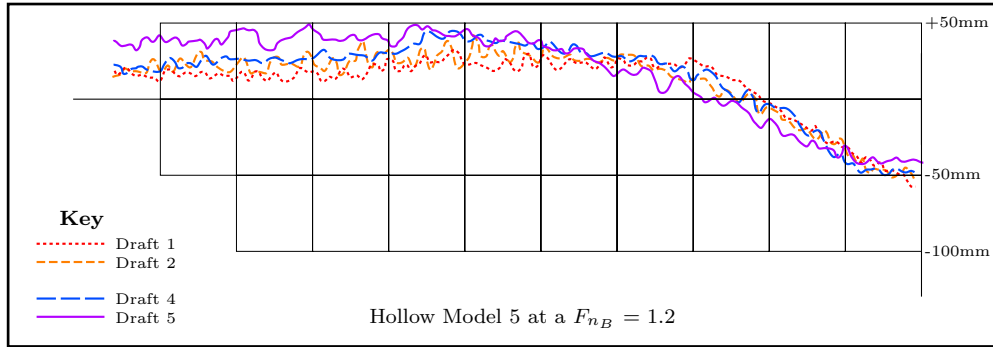


Figure 4.16: Influence of model draft on the transom hollow at $F_{n_B} = 1.2$

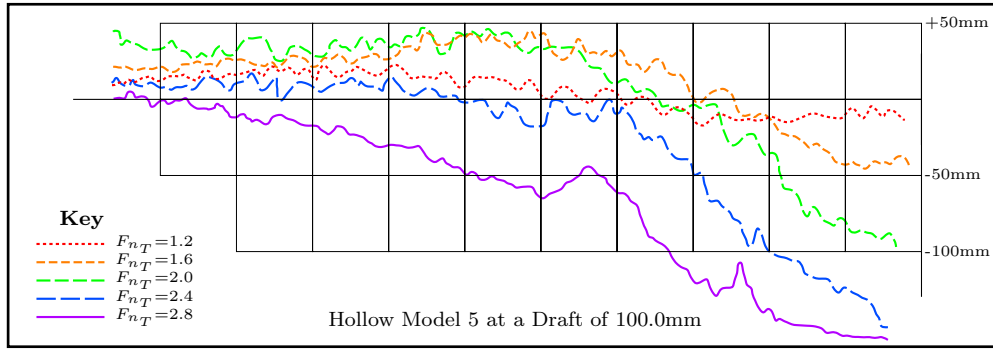


Figure 4.17: Influence of model speed on the transom hollow.

static draft (T). Therefore, when the model was stationary, (T_H/T) was equal to unity, and when the model was at a sufficiently-high speed that the flow past the transom was fully separating, (T_H/T) was equal to zero.

It was found with many of the high-speed runs that the probe measured a hollow profile which finished underneath the lowest point of the transom (i.e. a negative hydrodynamic draft). Logically, the flow must separate at the lowest point of the transom, meaning that the hydrodynamic draft must always be greater than or equal to zero. These errors are discussed in Section 4.4, and the methods for addressing these errors are presented in Chapter 5.

In the initial analysis, all values of hydrodynamic draft less than zero were taken

to be equal to zero, so the hydrodynamic drafts measured for the entire dataset are as shown in Figure 4.18. From the recorded measurements, a draft Froude number of approximately 2.5 is the point at which full separation of the flow from the transom first occurs.

By separating the data into the individual conditions of testing, further insight into the influences of the geometric properties of the vessel can be gained. Figures 4.19 to 4.23 show the non-dimensionalised hydrodynamic draft measured for each model plotted against the draft Froude number. In each condition, after an initial decrease in magnitude, the measured hydrodynamic draft has a period of increasing with increase in speed. Each of the curves of hydrodynamic draft in Figures 4.19 to 4.23 exhibit this “hump” in the data, with the draft Froude number at which this “hump” occurs increasing with increase in beam-to-draft (B/T) ratio. The influence of the beam-to-draft ratio on the speed at which this “hump” occurs is confirmed in Figure 4.24 where the five conditions at which $B/T=2$ are plotted against one another, with the “hump” occurring at the same draft Froude number.

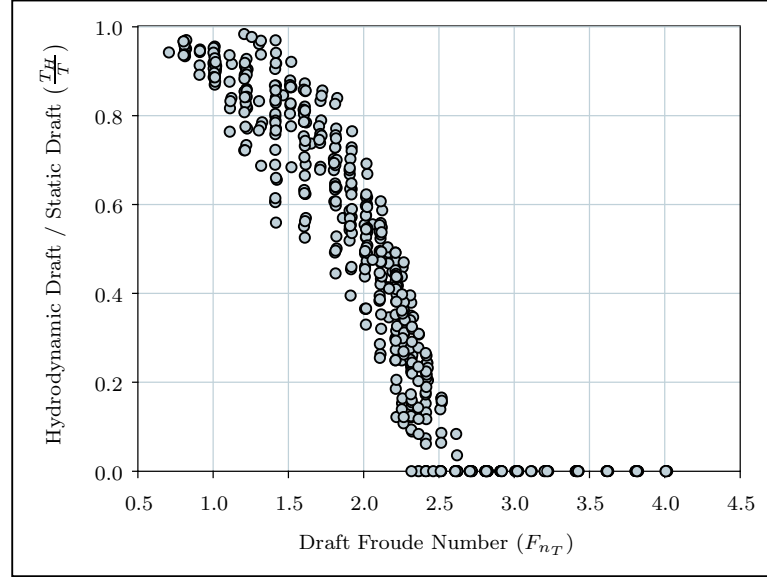


Figure 4.18: Non-Dimensionalised Hydrodynamic Draft (T_H) plotted against Draft Froude Number (F_{n_T}) for the entire dataset, with negative values assumed equal to zero.

Hollow Length

The hollow length was determined by fitting a parabola through the hollow profile and measuring the distance from the transom to the intersection of the parabola with the static waterline. Figure 4.25 shows the measured hollow length (L_H) for all the free-trimming test cases. As with the hydrodynamic draft, the hollow length has been non-dimensionalised by dividing by the static draft, and this has been plotted against the draft Froude number. There is a definite upward turn in the data at a draft Froude number of 2.5, after which the hollow length increases far more rapidly (Figure 4.13). A draft Froude number of 2.5 corresponds to the F_{n_T} at which full separation of the flow from the transom was observed (Figure 4.12). At speeds lower than the separation Froude number the transom hollow was observed to be filled with aerated circulating water (Figure 4.11).

The “hump” in the curve of hydrodynamic draft at the lower Froude range is also present in the curves of hollow length (Figures 4.26 to 4.30). As with the

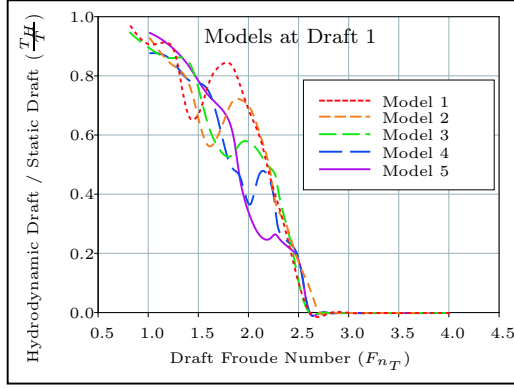


Figure 4.19: T_H measured at Draft 1

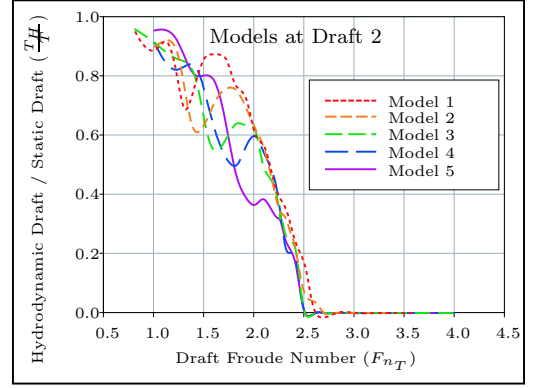


Figure 4.20: T_H measured at Draft 2

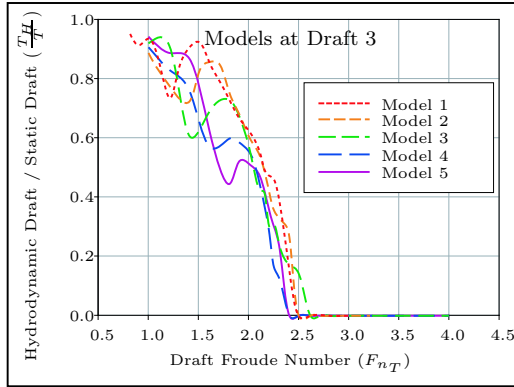


Figure 4.21: T_H measured at Draft 3

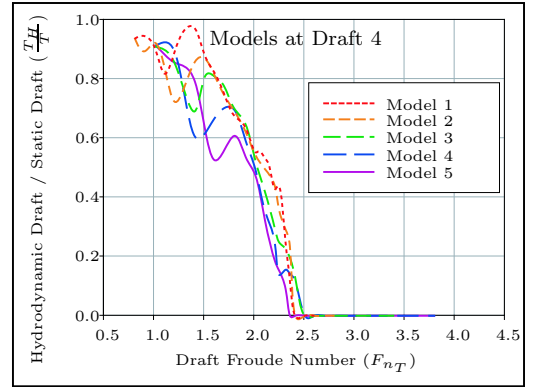


Figure 4.22: T_H measured at Draft 4

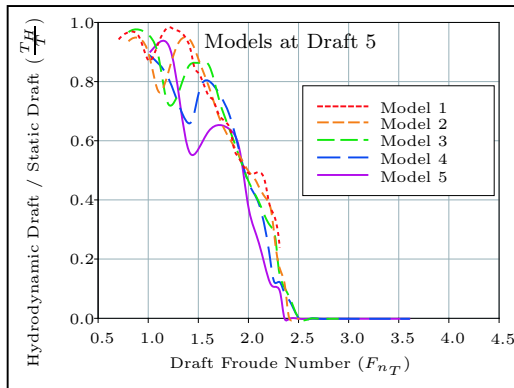


Figure 4.23: T_H measured at Draft 5

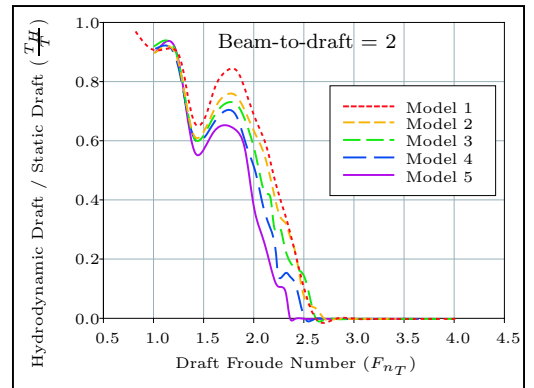


Figure 4.24: T_H for $B/T=2$ conditions

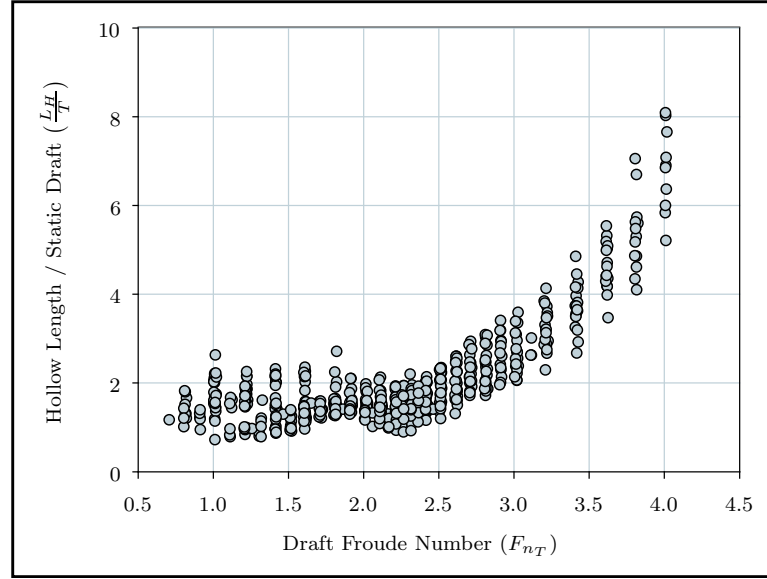


Figure 4.25: Non-Dimensionalised Hollow Length (L_H) plotted against Draft Froude Number (F_{n_T}) for entire dataset

hydrodynamic draft, the speed at which this hump occurs appears to be governed by the B/T ratio of the model. Figure 4.31 is a plot of the measured hollow length for Geosim 5 (Table 4.2) where $B/T = 2$, and parity between the speed at which the humps in each curve occur has been achieved. The hump is clearly visible at a $F_T = 1.7$ in Figure 4.30 for Hollow Model 1 where, at draft 5, the $B/T = 1$. The maximum speed was often restricted (especially for the smaller models) due to the wall-sided nature of the models increasing the threat of taking on “greenwater”. The maximum speed tested in Condition 5 (Appendix B) was 2.292 m/s, equating to a draft Froude number of 2.31. This was just at the point of full separation and this is reflected in the curve of measured hollow length. One possible explanation for the period of shortening and shallowing of the hollow with increase in speed could have been the trim experienced by the vessel in this speed range. However, the fixed-trim tests that were later conducted on Hollow Model 3 dispel this notion with the same “hump” occurring in the fixed-trim results.

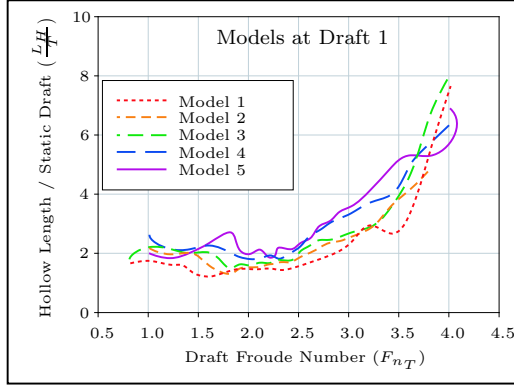


Figure 4.26: L_H measured at Draft 1

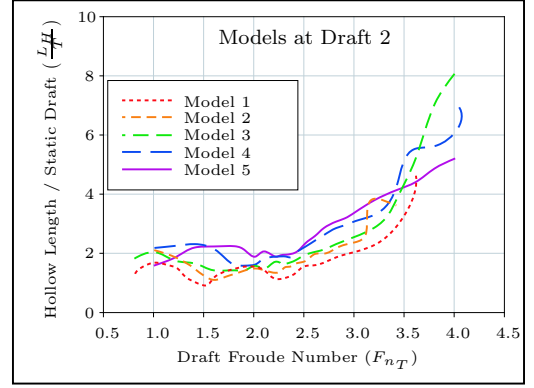


Figure 4.27: L_H measured at Draft 2

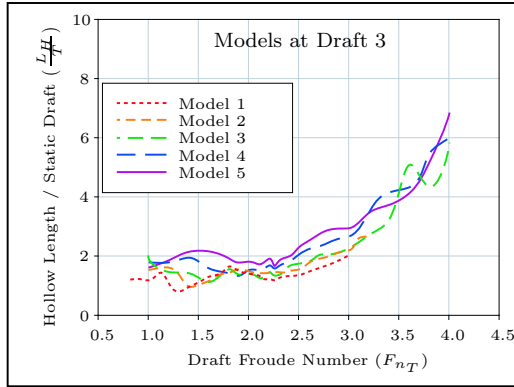


Figure 4.28: L_H measured at Draft 3

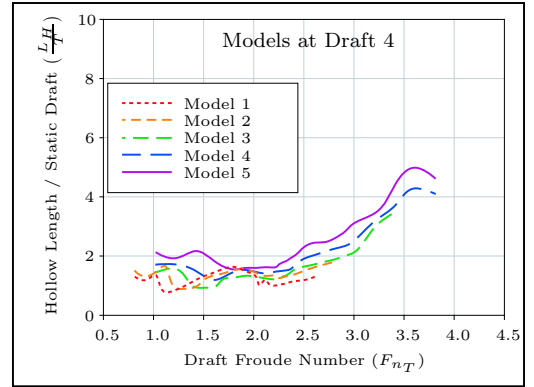


Figure 4.29: L_H measured at Draft 4

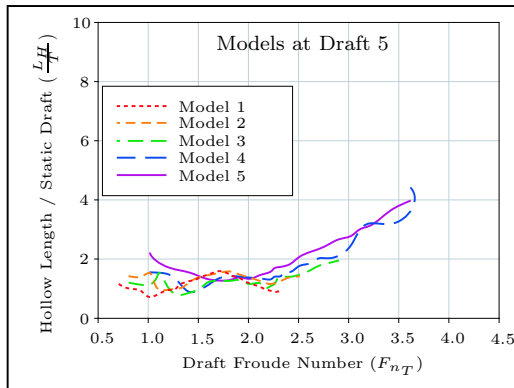


Figure 4.30: L_H measured at Draft 5

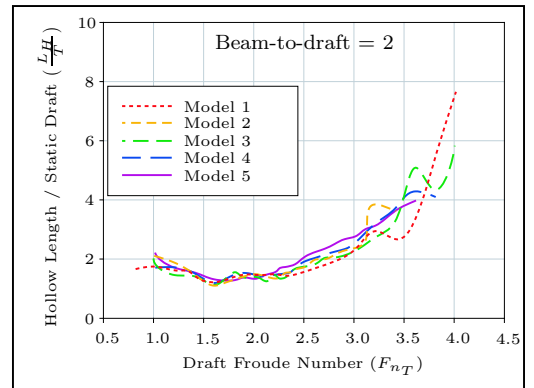


Figure 4.31: L_H for $B/T=2$ conditions

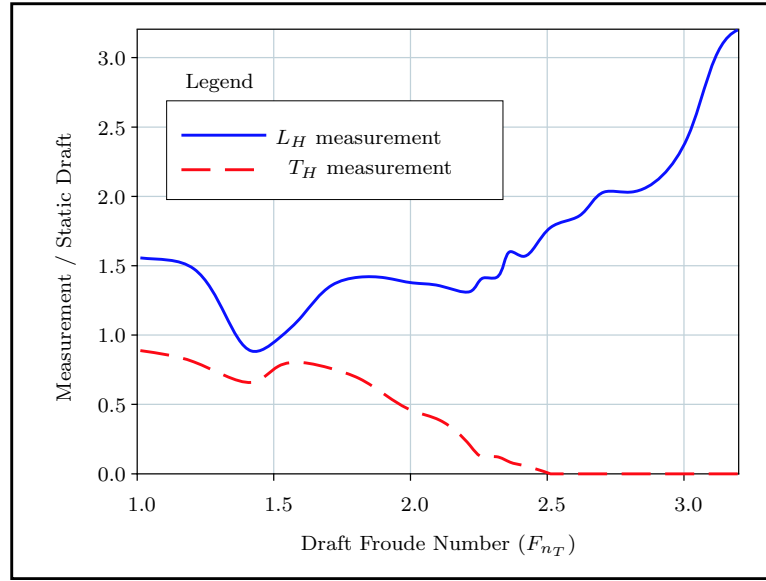


Figure 4.32: Comparison of the “Humps” in the curves of Hollow Length (L_H) and Hydrodynamic Draft (T_H) for Hollow Model 4 at Draft 5

Figure 4.32 shows the measured hollow length and hydrodynamic draft as measured for Hollow model 4 at draft 5 on the same chart where the alignment of the “hump” in each curve is observed. The dramatic increase in the hollow length after the point of full separation is also most evident.

The “hump” present in the curves of non-dimensionalised hollow length and hydrodynamic draft at low draft Froude numbers is not a result produced by the affects of squat or trim of the model, as confirmed by the existence of a similar hump in the data obtained in the fixed-trim experiments. Additionally, the “hump” in the data is not associated with the experimental errors obtained with the movable wave-probe (discussed in Section 4.4). This is confirmed by the existence of the same “hump” in the experimental data as measured by the wave probe attached to the transom during the fixed-trim tests. The “hump” appears to be a purely hydrodynamic phenomenon and is reflected in the hollow length predictions made by Couser *et al.* (1998), see Figure 3.1. Figure 4.33 shows the comparison between the proposed method for prediction of the re-attachment (or hollow) length by Couser

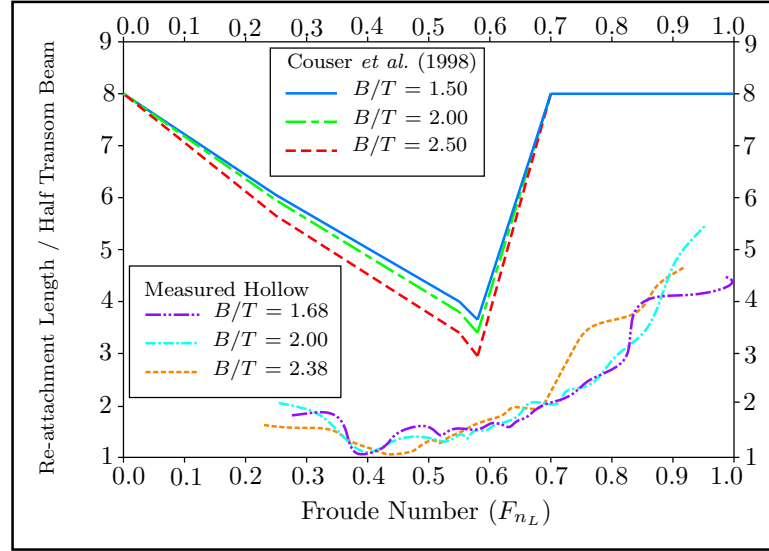


Figure 4.33: Comparison of Re-attachment Length Proposed by Couser *et al.* (1998) and Measured Hollow Length

et al. (1998) and the measured hollow length from the research presented here. Overall, the hollow length as proposed by Couser *et al.* (1998) is larger than that measured in the hollow experiments; however, the same initial decrease in hollow length is evident before a dramatic increase in hollow length occurring at a similar Froude number.

Geosim Comparisons

As discussed in Section 4.1.1, the arrangement of the hollow model series presented a number of geosim conditions, thereby providing a means for performing a dimensional check on the results. Ideally, once non-dimensionalised, the recorded hollow profiles for the geosim cases would correspond. Figures 4.34 and 4.35 show the non-dimensionalised hollow profiles, at draft Froude numbers of 1.4 and 2.4, for Geosim 5 (refer to Table 4.2). The non-dimensionalised profiles correlate well, especially at the lower speed.

The disparity in the profiles at the higher speed is most likely due to the dif-

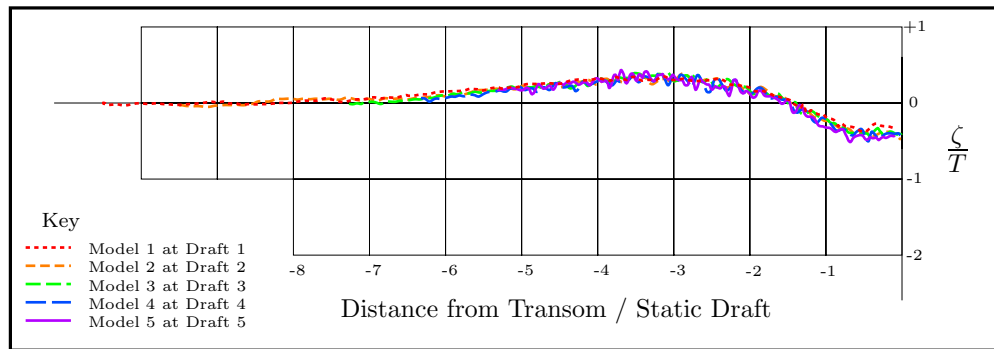


Figure 4.34: Comparison of Geosimilar Conditions for Each Model at a Draft Froude Number of 1.4

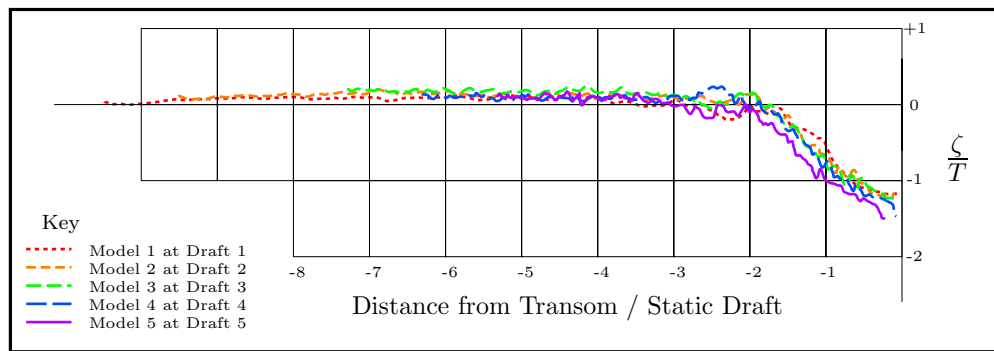


Figure 4.35: Comparison of Geosimilar Conditions for Each Model at a Draft Froude Number of 2.4

ferences in trim experienced by the five models at that draft Froude number. Figure 4.38 shows the difference in trim experienced by the Geosim models as speed increases. The effect which the trim of the vessel has on the measured hollow profile is apparent in the comparison of the fixed-trim results and the free-trim results for Hollow Model 3, shown in Figures 4.36 and 4.37. At the lower Froude numbers where the trim would be small there is little effect; however, at the higher Froude numbers the point of separation of the flow from the transom is clearly lower for the free-trim vessel (as expected) with the associated “rooster tail” more prominent.

4.3.2 Creation of Algorithms

Algorithms for the prediction of hollow length and hydrodynamic draft were developed using the experimentally-recorded hollow data. The algorithms were developed as functions of the speed, beam, and draft of the model using the DATAPLOT[®] regression analysis program.

As a first approximation, the complete datasets for both L_H and T_H were fitted with the cubic equations 4.7 and 4.8. The resulting root-mean-square (RMS) error for the dimensionless hollow length from Equation 4.7 is 0.4187 or 5.2% of the maximum value, and the RMS error for the dimensionless hydrodynamic draft from Equation 4.8 is 0.08736 or 8.7% of the maximum value (Robards and Doctors, 2003).

$$\frac{L_H}{T} = 0.3265F_{n_T}^3 - 1.7216F_{n_T}^2 + 2.7593F_{n_T} \quad (4.7)$$

$$\frac{T_H}{T} = -0.0774F_{n_T}^3 + 0.0895F_{n_T}^2 - 0.1042F_{n_T} + 1 \quad (4.8)$$

To improve on the cubic equations, and in an effort to encompass the prediction of both L_H and T_H with the one form of equation, the polynomial algorithm given in Equation 4.9 was developed. Non-linear least-squares regression was used to fit this higher-order polynomial to the experimental data. To more closely approximate

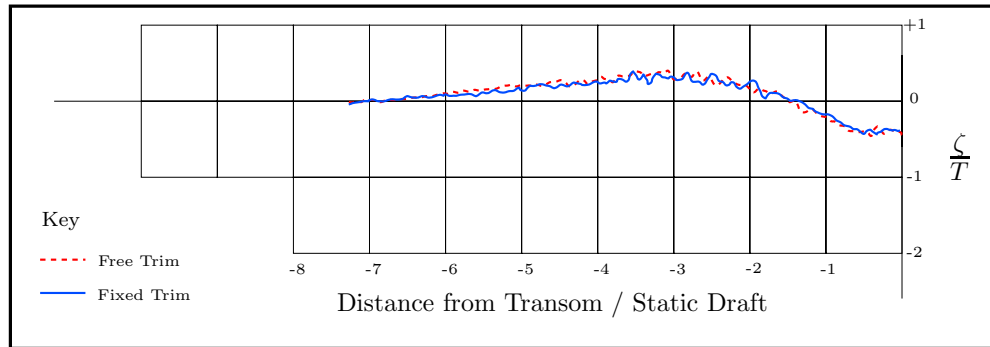


Figure 4.36: Comparison of the Fixed-Trim and Free-Trim Results of the Measured Hollow Profile for Hollow Model 3 at a Draft of 70.7 mm and Draft Froude Number of 1.4

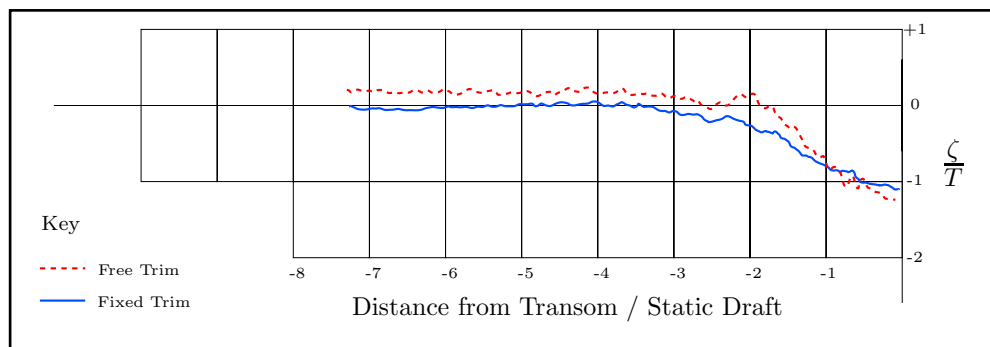


Figure 4.37: Comparison of the Fixed-Trim and Free-Trim Results of the Measured Hollow Profile for Hollow Model 3 at a Draft of 70.7 mm and Draft Froude Number of 2.4. Note that the Above Figure Represents Approximately 500 mm of Measured Wave Profile, and that the Wave Profile for the Free-Trim Case Tends to the Calm Water Level Further Down-Stream from the Transom.

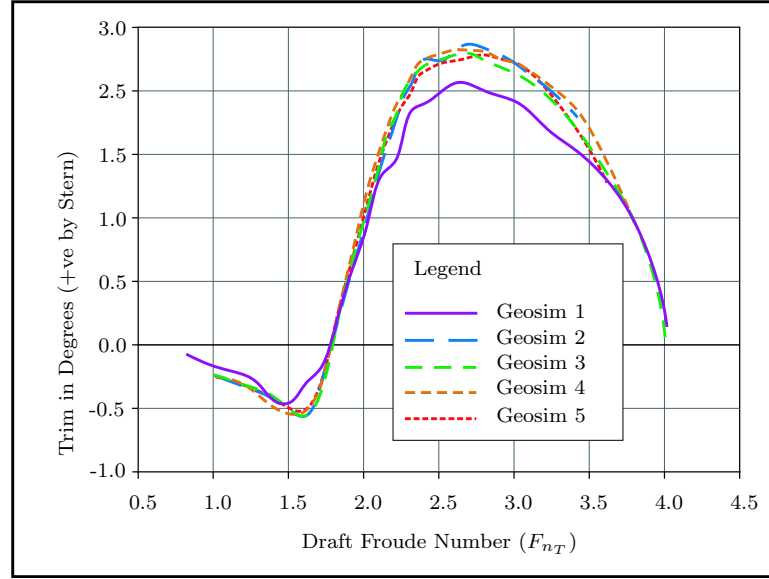


Figure 4.38: Comparison of Trim for Geosimilar conditions

the hollow length and hydrodynamic draft, the beam-to-length ratio was introduced into these polynomials. The coefficients a_i are dependent on whether L_H or T_H is to be determined, and these values are given in Table 4.5.

$$\left. \begin{array}{l} \frac{T_H}{T} \\ \frac{L_H}{T} \end{array} \right\} = a_0 + a_1 F_{n_T} + a_2 F_{n_T}^2 + a_3 \left(\frac{B}{T} \right) F_{n_T} + a_4 F_{n_T}^3 + \\
 + a_5 \left(\frac{B}{T} \right) F_{n_T}^2 + a_6 \left(\frac{B}{T} \right)^2 F_{n_T} + a_7 F_{n_T}^4 + a_8 F_{n_T}^5 + \\
 + F_{n_B} \left[a_9 + a_{10} F_{n_T} + a_{11} \left(\frac{B}{T} \right) + a_{12} F_{n_T}^2 + a_{13} \left(\frac{B}{T} \right)^2 + \right. \\
 + a_{14} \left(\frac{B}{T} \right) F_{n_T} + a_{15} F_{n_T}^3 + a_{16} \left(\frac{B}{T} \right)^3 + a_{17} \left(\frac{B}{T} \right) F_{n_T}^2 + \\
 \left. + a_{18} \left(\frac{B}{T} \right)^2 F_{n_T} + a_{19} F_{n_T}^4 + a_{20} \left(\frac{B}{T} \right)^4 + a_{21} F_{n_T}^5 \right] \quad (4.9)$$

Table 4.5: Polynomial Coefficients

Coefficient	L_H	T_H
a_0	0	1
a_1	-3.205×10^2	3.930×10^0
a_2	1.967×10^1	-3.495×10^1
a_3	-4.536×10^2	-1.323×10^0
a_4	7.526×10^0	-8.863×10^{-1}
a_5	1.094×10^1	-2.247×10^0
a_6	-6.909×10^0	-7.666×10^{-2}
a_7	-3.338×10^{-1}	-1.354×10^{-1}
a_8	-9.228×10^{-3}	-3.705×10^{-2}
a_9	7.133×10^1	-1.864×10^0
a_{10}	3.567×10^0	1.698×10^0
a_{11}	5.490×10^2	-2.397×10^0
a_{12}	-1.010×10^1	-3.565×10^0
a_{13}	1.712×10^2	1.508×10^0
a_{14}	-3.050×10^1	2.311×10^0
a_{15}	2.504×10^0	3.216×10^0
a_{16}	-1.036×10^1	-7.339×10^{-2}
a_{17}	-1.284×10^0	9.196×10^{-1}
a_{18}	-1.007×10^0	3.008×10^{-1}
a_{19}	-5.559×10^{-1}	-1.182×10^0
a_{20}	6.204×10^{-1}	8.341×10^{-6}
a_{21}	5.438×10^{-2}	1.760×10^{-1}

4.4 Discussion

Following the ideas of Doctors and Day (1997) whereby, for the purposes of numerical discretization, the hollow in the water behind a transom stern is meshed as a geometrically-smooth addition to the vessel, a large experimental programme was undertaken. The experiments were designed to enable measurement of the length and depth of the transom hollow and to determine the influence of the vessel's speed and transom dimensions upon the length and depth of the hollow.

A systematic series of transom-stern models was developed for this research along with a wave-probe experimental rig which was designed to provide a longitudinal cut through the transom hollow enabling measurement of the length and depth of the hollow. A large number of test runs was performed, and the hollow profiles that were recorded show definite trends in the influence of speed, beam and draft. The speed of the vessel has by far the greatest influence on the hollow, which changes dramatically with increase in speed. At very high speeds the transom becomes fully aerated, with the flow completely separating from the transom. Beyond these speeds the hollow length was observed to increase rapidly.

The change in beam appeared to have little effect on the depth of the hollow, and only a slight effect on the length of the hollow. However, the increase in beam appeared to have a dramatic effect on the size of the wake behind the re-attachment point, indicating the benefit of slender hulls in low-wash applications.

The affects of the draft at the transom were also far less pronounced than the vessel's speed. Observations made during the experiments, backed up by video-screen captures (Figure 4.12) and experimental measurements, indicated that the point of full aeration of the transom occurs at a draft Froude number of around 2.5, which is less than the draft Froude number for full aeration of 4 or 5 surmised by Saunders (1957a). It was discovered that errors were being obtained with the movable wave-probe which may have affected the separation Froude number; however, in later experiments an additional stationary wave probe was positioned on the transom of

the models, and the same value of 2.5 was observed for the separation Froude number. Further experiments on transom-stern vessels of a more-conventional nature, with some rise in the keel forward of the transom and more conventional cross-section, may produce greater correlation with Saunders value for the separation Froude number.

Indeed, the wall-sided flat-bottomed vessels tested were chosen so as to eliminate influences other than the beam, draft and speed. However, further work in this area could look at the effects of length-to-beam ratio, deadrise, rocker, bilge radius, narrowing of beam from midships to transom and rise of keel forward of the transom. Future work could also encompass validation of the calculated algorithms through computational fluid dynamics (CFD) work or through repetition of the experiments conducted here for a more conventional high-speed hullform.

The capacitance wave probe used in the experiments was found to produce inaccuracies in the hollow measurements due to the flow separating from the probe wires at high speeds. The methods by which these errors were detected and corrected for are discussed in detail in Chapter 5; however, future experiments would benefit from more non-obtrusive methods, such as laser measurement.

Chapter 5

Transom-wake Analysis

5.1 Introduction

5.1.1 Wave-probe errors

The results obtained from the transom-stern experiments described in Chapter 4 showed clearly the resulting change in the depth and length of the hollow corresponding to changes in the beam, draft or speed of the model. However, initial analysis of the results revealed anomalies in the experimental data. Specifically, for many of the experimental runs made at the higher draft-Froude numbers, the measured hollow profile did not correlate with the measured attitude of the profile of the model. In reality, the flow of water along the hull of the model always separates from the model tangentially at the base of the transom. As can be seen in Figure 5.2, however, the hollow profile measured for Run 340 suggests that the flow separated at a point well below the lowest point of the transom. This is not hydrodynamically plausible, and further experimentation was conducted to determine the cause of this error and make appropriate corrections.

Figure 5.1(a) shows the initial assumption that all values of hydrodynamic draft less than zero were assumed equal to zero. The polynomial algorithm (Equation 4.9) for the prediction of hydrodynamic draft was based on this assumption, where only

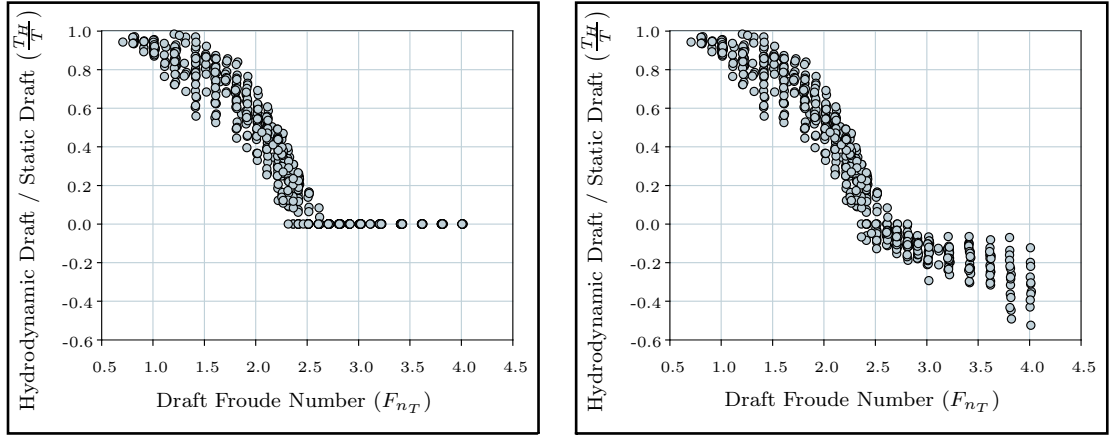


Figure 5.1: a) Initial Assumption b) Actual Measured Hydrodynamic Draft

the data up to the point of full separation were utilised in the production of the polynomial equation. However the actual measurements for hydrodynamic draft are shown in Figure 5.1 (b) where the values recorded for hydrodynamic draft become increasingly negative with increase in speed.

The most likely explanation for the errors observed is that there were miscalculations during the initial analysis. However, checks confirmed the initial analysis and the observed “gap” between the base of the transom and the measured hollow profile. Therefore, the source of the error was either a fault in the recording of the heave of the towing posts, or an inaccuracy in the measurement of the hollow profile using the capacitance wave probe.

To test the measurements made by the wave probe, runs were made in the tank at a range of speeds with the wave probe in isolation (that is, tested without a model). Section 5.2 of this Chapter details the results obtained from running the wave probe in isolation and the methods used to correct for the errors obtained.

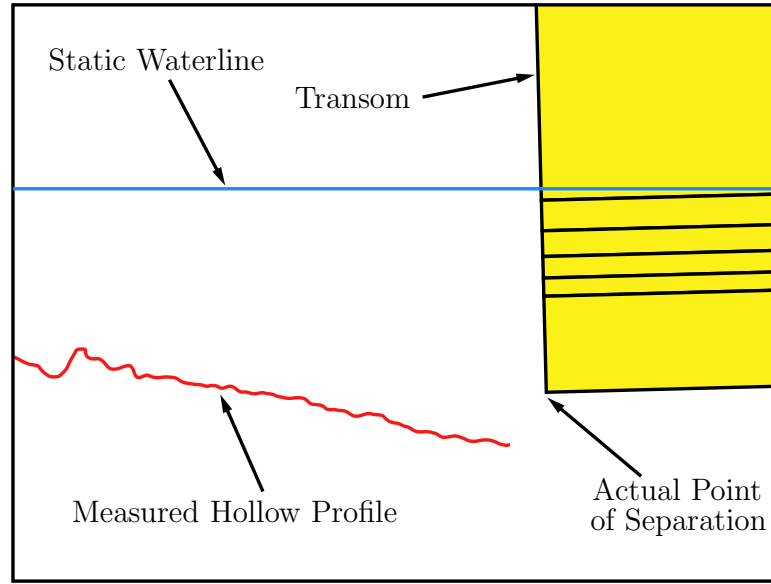


Figure 5.2: Hollow Profile Measured for Run 340 Shown *in situ* with Trimmed Vessel Profile Showing the Experimental Error Obtained at some of the Higher Draft Froude Numbers

5.1.2 Improved Algorithms

In developing the prediction algorithms presented in Section 4.3.2, only data up to the point of full separation were used. This was due in part to the errors observed at speeds beyond the point of full separation. Discovery and correction of these errors enabled re-calculation of these algorithms using the entire speed range. Due to the re-calculation of these prediction algorithms, shortcomings inherent in their polynomial nature were identified. New prediction algorithms, developed to circumvent these inadequacies are presented in Section 5.3.



Figure 5.3: Flow Separation from Probe Wires at $F_{PR}=22.04$ (2.673 m/s)

5.2 Wave Probe Correction

5.2.1 Wave probe in isolation

The accuracy of the measurements made by the wave probe was investigated by testing the wave probe in isolation. Theoretically, with the wave probe measuring an undisturbed free surface, the recorded elevation should be zero.

The wave-probe was calibrated using the methods detailed in Section 4.2.4. The probe rig was then towed along the tank at various speeds and the recorded water elevation computed. This process confirmed that the errors observed were due to inaccuracies in the measurements made by the wave probe. As the speed of the carriage was increased, instead of the expected zero reading, the probe recorded negative water elevations. This is due to the separation of the water from the wave-probe wires at high speed as shown in Figure 5.3, causing the reading from the capacitance wave probe to be lower than that of the actual free surface.

Many runs were made over a considerable speed range in an effort to establish

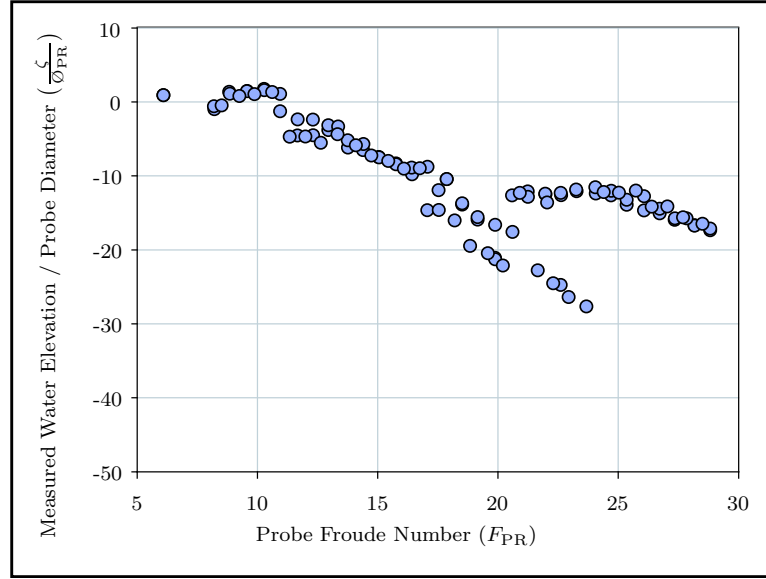


Figure 5.4: Measured water elevation of undisturbed free-surface with probe in isolation

a relationship between the set speed and the recorded water elevation. As can be seen in Figure 5.4, as the speed was increased the magnitude of the apparent water depression measured by the wave-probe increased. At the highest speeds the depth measured at each speed was not unique. That is, there was a “bifurcation” in the data where, for the same speed, the probe would record two very different results. The junction in the divergent results first occurs at a probe Froude number¹ of approximately 20. Above this speed the majority of the runs resulted in a measurement along the upper branch of the “bifurcation”. However, the runs were not entirely repeatable, and the cause of the deeper measurements (or lower branch of results) needed investigation.

Possibly, for some of these runs, imperfections in the undisturbed free surface

¹For Figures 5.4 and 5.6 the water elevation measured by the wave probe in isolation is non-dimensionalised by dividing by the diameter of the probe wires (1.5 mm). The non-dimensionalised water elevation is then plotted against the Froude number based on the probe wire diameter (that is, $F_{PR} = U/\sqrt{g \times O_{PR}}$).

were causing eddies around the wave-probe wires, thereby increasing the amount of separation observed. Alternatively, the high speeds at which the probe was being tested induced some degree of vibration in the wires, and for some runs a resonant frequency may have been reached, causing increased separation.

To test the theory that the results in the lower branch were caused by imperfections in the free surface, the wave-probe was tested in isolation with the water surface “roughened”. A plastic film was affixed to the guard at the forward end of the towing carriage so that the film just touched the water surface. The guard was approximately 3 m forward of the position of the wave-probe, and the film touching the water surface provided a disturbed free-surface without creating a major depression in the water. Upon testing the wave-probe in this arrangement it was found that all the measurements recorded by the wave-probe now correlated with the deeper measurements (or lower arm of the “fork”) made by the wave-probe in undisturbed water (see Figure 5.4).

Therefore, the misalignment of the plotted model and hollow profiles, identified in the initial analysis, was due to inaccuracies of the wave-probe at high speeds. However, the increase in wave-probe error was directly related to the increase in towing speed. This enabled the introduction of a speed correction for the measured hollow profile.



Figure 5.5: A Plastic Sheet Placed Just Touching the Water Surface was used to Roughen up the Previously Undisturbed Free Surface Without Creating a Major Depression in the Water.

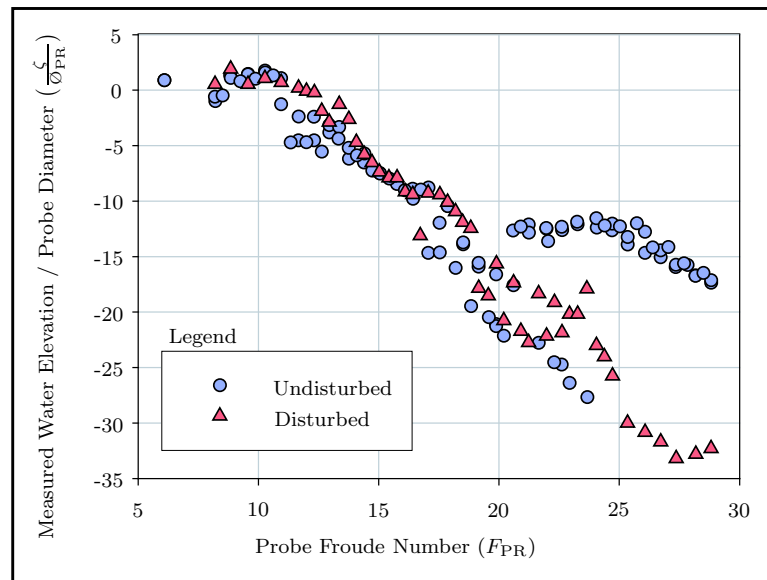


Figure 5.6: Measured Water Elevation of Disturbed Free Surface with Probe in Isolation.

5.2.2 Wave-probe speed correction

To correct for the errors obtained from the wave probe at high speeds, trend lines were fitted using least-squares regression. Initially, a polynomial of degree four was fitted exclusively to the experimental runs involving a disturbed free surface. This resulted in a Type A correction

$$\begin{aligned} Corr_A = & -5.577 \times 10^{-4} F_{PR}^4 + 4.473 \times 10^{-2} F_{PR}^3 \\ & - 1.308 F_{PR}^2 + 1.451 \times 10^1 F_{PR} - 5.214 \times 10^1 \end{aligned} \quad (5.1)$$

For the slow speed runs where full separation of the flow from the transom had not occurred, the transom hollow would be filled with circulating water which varied in speed (relative to the moveable wave-probe) along the length of the hollow. For this reason an exponential term (C_{DH}) and a hyperbolic tangent function (C_{HL}) were introduced to adjust the overall correction. The exponential term (C_{DH}) adjusted the correction depending on the ratio of the hollow depth (D_{Ho}) to transom draft (T_T). If the transom was fully ventilated (including the runs where the measured hollow profile finished under the bottom of the transom), C_{DH} would be equal to one meaning that C_{HL} would also be equal to one resulting in the full correction being applied. That is the exponential and hyperbolic tangent adjustments were only made for the non-separated runs where there was slow circulating water in the transom hollow. In applying this correction to the measured hollow profiles presented in Appendix C, the following approach was adopted:

- a) Due to the fact that the probe error was directly associated with high speed and that the speed range below full separation was accompanied with a hollow filled with stagnant water, the full correction was only applied to runs where the measured hollow depth² was greater than the measured dynamic draft (i.e. where there was a negative hydrodynamic draft.

²Not to be confused with the hydrodynamic draft, the hollow depth is the distance from the static waterline to the bottom of the hollow.

- b) To help take account of the change in velocity of the water flow past the transom, an exponential term (C_{DH}) was introduced to determine the magnitude of the correction factor to be applied based on the ratio of hollow depth to dynamic draft.
- c) In addition to the exponential term taking account of the original measured depth of the hollow, a hyperbolic tangent function was introduced to help take account of the distance of each data point from the transom compared with the original measured hollow length.

Therefore the correction made to point i on one of the original measured profiles becomes

$$\delta\zeta_i = Corr_A \times C_{DH} \times \frac{1}{C_{HL}} \quad (5.2)$$

where C_{DH} is the exponential term discussed above, given by

$$C_{DH} = \begin{cases} 0.05 \times \exp\left(\frac{7 \times D_{Ho}}{3 \times T_T}\right) & \text{if } D_{Ho} \leq T_T \\ 1 & \text{if } D_{Ho} > T_T \end{cases} \quad (5.3)$$

where D_{Ho} is the original measured hollow depth and T_T the measured draft at the transom. The hyperbolic tangent function C_{HL} , taking account of the distance of point i from the transom, is then given by

$$C_{HL} = 1 + 0.5 \left[\left(\frac{1}{C_{DH}} \right) - 1 \right] \times \left[1 - \tanh \left(\frac{-x \times \pi}{L_{Ho}} + \frac{\pi^2}{2} \right) \right] \quad (5.4)$$

where x is the distance of point i from the transom and L_{Ho} is the original measured hollow length.

The correction $\delta\zeta_i$ given by Equation 5.2 was applied to each of the 1024 points along each of the 625 hollow profiles for which the measured hollow depth was greater

than the dynamic draft. However, this was found to over correct for the wave-probe errors observed, as seen in Figure 5.8.

Using the same method of correction, but using the undisturbed data fitted by the “Correction B” line shown in Figure 5.7, yielded a far more realistic correction for the probe errors (Figure 5.9). The polynomial equation (C_B) for the “Correction B” line is

$$\begin{aligned} Corr_B = & -8.365 \times 10^{-4} F_{PR}^4 + 5.955 \times 10^{-2} F_{PR}^3 \\ & - 1.469 F_{PR}^2 + 1.369 \times 10^1 F_{PR} - 41.16 \end{aligned} \quad (5.5)$$

Therefore, the final correction for each point i in the fully-separated hollow profiles is given by

$$\delta\zeta_i = Corr_B \times C_{DH} \times C_{HL} \quad (5.6)$$

where C_{DH} is the exponential term given in Equation 5.3, and C_{HL} is the hyperbolic tangent function given in Equation 5.4.

5.2.3 Adjusted transom-hollow profiles

In order to apply the probe correction given in Equation 5.6 to each of the 625 hollow profiles, macros were developed in Microsoft[®] Excel[©]. The corrected hydrodynamic draft and hollow length for each run was then determined.

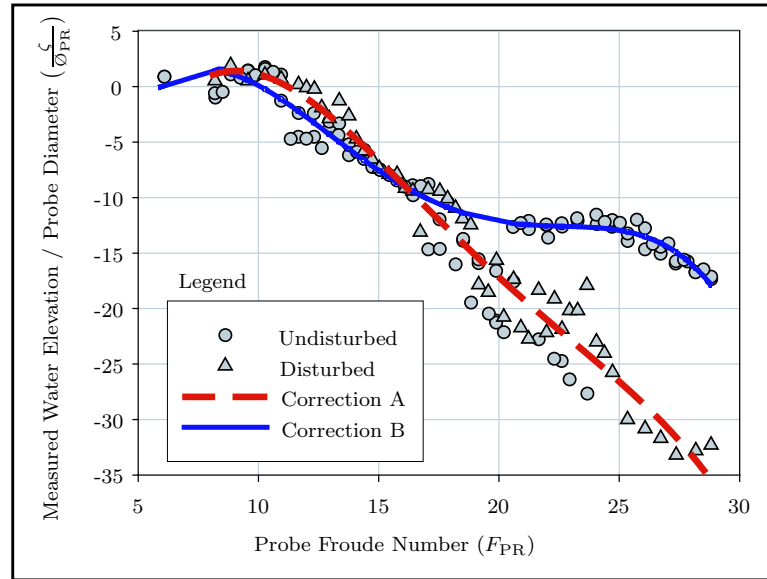


Figure 5.7: Algorithms Fitted to Correct for Wave-Probe Errors with Increasing Speed

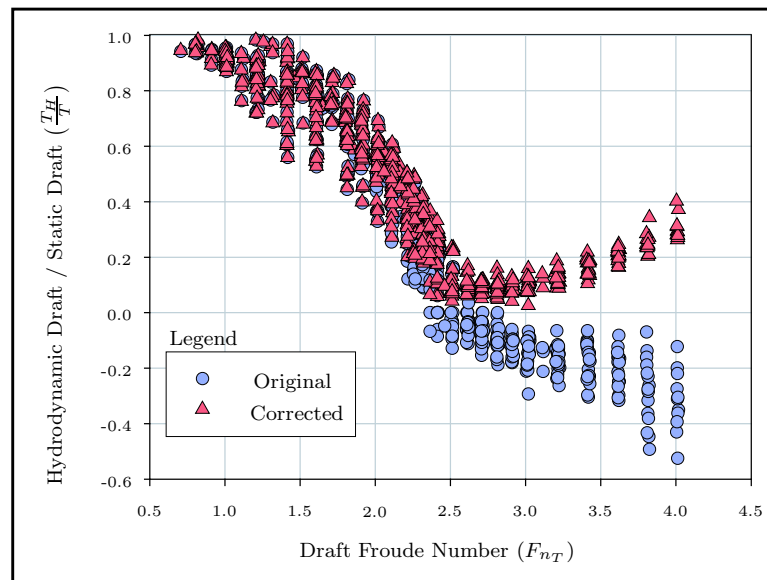


Figure 5.8: Over-Correction Made on Hydrodynamic Draft Based on Measurements of the Wave Probe in Isolation in Disturbed Free Surface

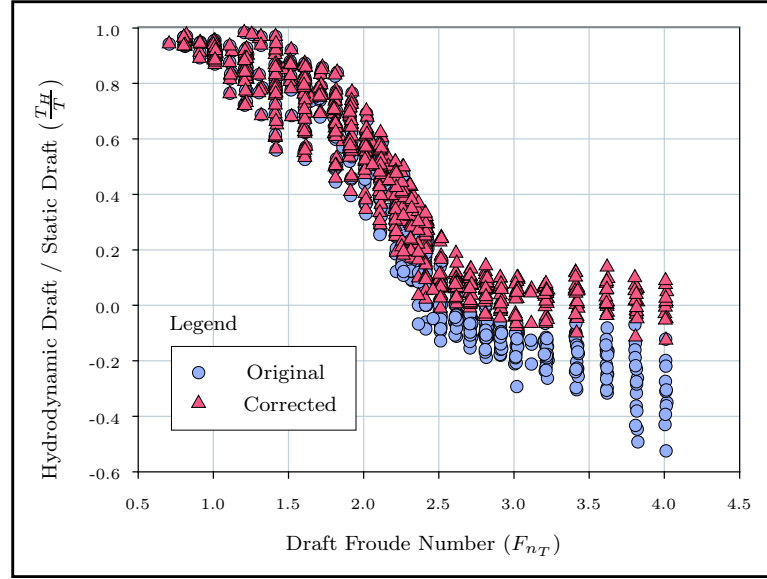


Figure 5.9: Hydrodynamic Draft Measurements after Correction Based on Measurements of the Wave Probe in Isolation in Undisturbed Free Surface

5.3 Improved Prediction Algorithms

Chapter 4 presented algorithms, of polynomial form, developed for the prediction of the hydrodynamic draft and hollow length. As discussed in Section 4.3.1, the hydrodynamic draft was taken to be equal to zero whenever the probe measured a hollow profile which finished underneath the lowest point of the transom. Hence, the algorithms were developed from regression of the lower-speed runs where full separation had not occurred. The identification of the cause of the probe errors, and the corrections for these errors presented in Section 5.2.2, enabled reproduction of the prediction algorithms using the entire database of experimental results. The reproduction of the prediction algorithms presented an opportunity to reassess the suitability of the algorithms originally developed.

5.3.1 Prediction Algorithms

Original Polynomial Algorithm for Hydrodynamic Draft

One of the disadvantages of the polynomial algorithms developed was the number of coefficients used. Furthermore, despite the number of terms used in the polynomial equations, these algorithms failed to predict the “humps” evident in the experimental results. However, the major shortcoming associated with polynomial algorithms is the limited range of applicability. As mentioned, the polynomials presented in Equation 4.9 were developed from regression of the experimental data up to full separation. Application of these algorithms beyond this speed range quickly results in large errors in prediction. This is illustrated in Figure 5.10 where the polynomial algorithm is extended beyond $F_{nT} = 2.5$ at which full separation occurs. Rapidly the polynomial gives totally unrealistic predictions and is not bounded by the physical upper limit of $T_H/T=1$. This is due to the draft Froude terms in the polynomial, raised to the third or fourth power, causing the resulting non-dimensionalised hydrodynamic draft to dramatically increase with increase in speed beyond the end of the data range from which the algorithm was developed. Clearly, a more appropriate form for the hydrodynamic draft prediction algorithm is required.

Hyperbolic Sinusoid Algorithm

The two major problems with the polynomial algorithm were that the function was not bounded by the physical limits for non-dimensionalised hydrodynamic draft of zero and one, and that the polynomial algorithm did not predict, with any deal of accuracy, the “humps” in the data for hydrodynamic draft. To address these deficiencies in the original algorithm, a new algorithm was proposed utilising a hyperbolic tangent function together with a damped sinusoid function. As shown in Figure 5.11 the hyperbolic tangent function predicts the general trend in the variation of non-dimensionalised hydrodynamic draft from one to zero, and the damped sinusoid function predicts the “humps” in the curve inherent at the lower

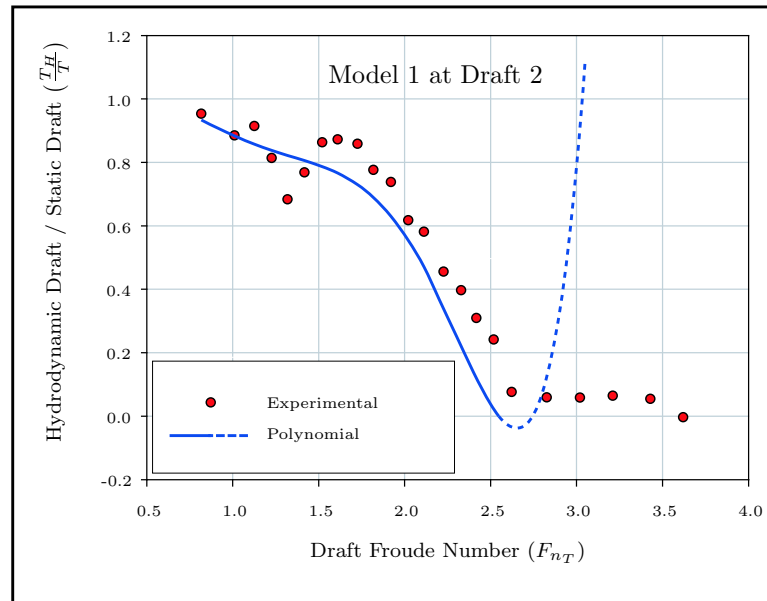


Figure 5.10: Unrealistic Predictions made by Original Polynomial when Applied at Speeds Greater than the Separation Froude Number

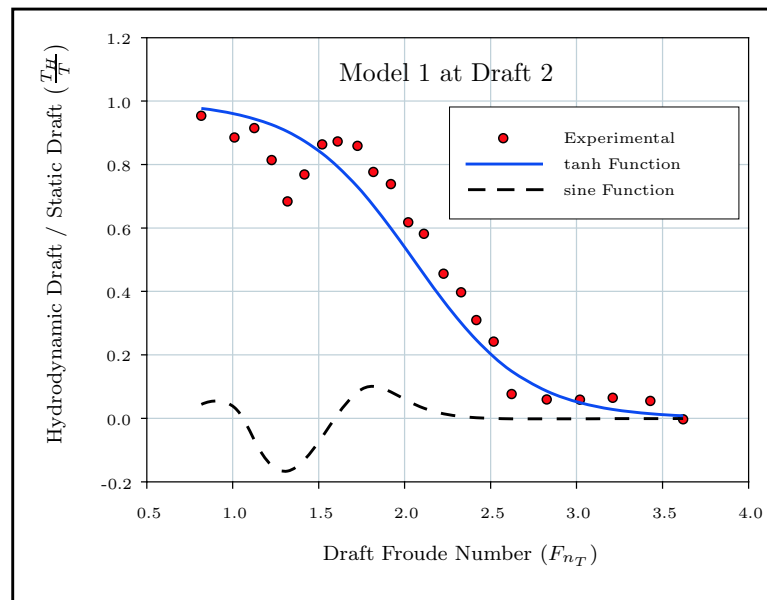


Figure 5.11: The Hyperbolic Tangent and Damped Sinusoid Components of the New T_H Prediction Algorithm.

speed range.

$$\begin{aligned} \frac{T_H}{T} = & \frac{1}{2} \left\{ 1 + \tanh \left[3.765 + \frac{B}{T} \left(0.145 F_{n_T} - 0.377 \right) - 1.770 F_{n_T} \right] \right\} + \\ & + \frac{B}{T} \left(\frac{a_0 \sin(a_1 F_{n_B} + a_2 \sqrt{F_{n_T}})}{a_3 + (a_4 - F_{n_T})^4} \right) \end{aligned} \quad (5.7)$$

where

$$\begin{aligned} a_0 &= -0.0002444 (B/T)^3 + 0.003303 (B/T)^2 - 0.01494 (B/T) + 0.02260 \\ a_1 &= -3.381 (B/T) - 2.609 \\ a_2 &= 0.7594 (B/T)^4 - 5.981 (B/T)^3 + 19.10 (B/T)^2 - 29.35 (B/T) + 45.70 \\ a_3 &= -0.002399 (B/T)^3 + 0.03279 (B/T)^2 - 0.1486 (B/T) + 0.2251 \\ a_4 &= -0.1111 (B/T)^2 + 0.9967 (B/T) + 0.07370 \end{aligned}$$

When superimposed, the hyperbolic tangent function and the damped sinusoid produce a great improvement in prediction over the original polynomial function as shown in Figure 5.12. A further improvement was made by introducing a third term to take account of any Reynolds number effects as shown in Equation 5.8.

The algorithm was developed using the DATAPLOT[®] program in association with Microsoft[®] Excel[®]. Firstly the hyperbolic tangent was fitted to the experimental data. The difference between the experimental data and the prediction made by the hyperbolic tangent function was then determined and the damped sinusoid fitted to this data. The variation in the coefficients a_i were determined by optimising the fit with the experiment data. The relationship between this variation and the beam-to-draft ratio was established and polynomials (a_0 to a_4) fitted using the trendline functions of Microsoft[®] Excel[®].

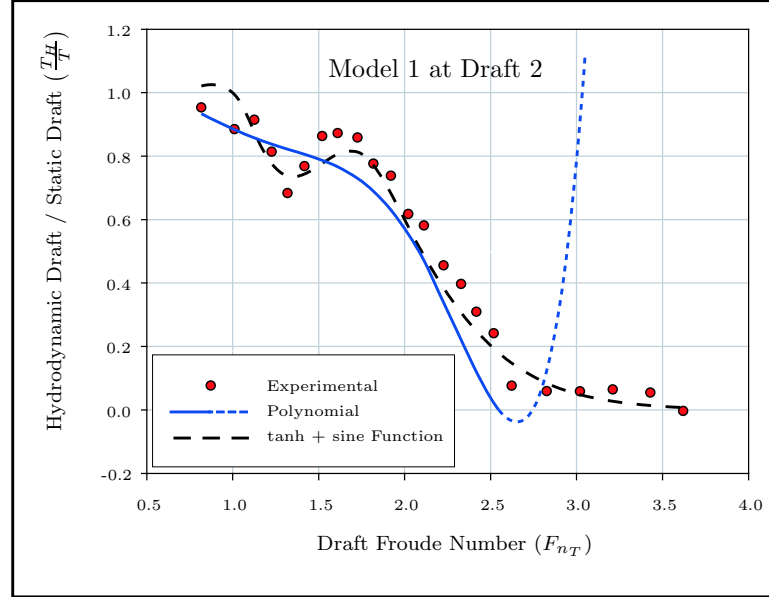


Figure 5.12: Comparison of the Predictions Made by the New T_H Algorithm Versus the Old Polynomial Algorithm

$$\begin{aligned}
 \frac{T_H}{T} = & \frac{1}{2} \left\{ 1 + \tanh \left[3.765 + \frac{B}{T} \left(0.145 F_{n_T} - 0.377 \right) - 1.770 F_{n_T} \right] \right\} + \\
 & + \frac{B}{T} \left(\frac{a_0 \sin(a_1 F_{n_B} + a_2 \sqrt{F_{n_T}})}{a_3 + (a_4 - F_{n_T})^4} \right) - \\
 & - \frac{0.008 (R_{n_T}/50000 - F_{n_T})}{0.1 (B/T)^{1/3} + (1.5 (B/T)^{1/3} - F_{n_T})^4}
 \end{aligned} \tag{5.8}$$

Original Polynomial Algorithm for Hollow Length

As with the hydrodynamic draft (T_H) prediction where the polynomial for prediction of T_H was only valid up to a draft Froude number of 2.5, the polynomial developed in Chapter 4 for the prediction of hollow length is only really applicable up to speeds equivalent to the top speed tested in the hollow experiments. Beyond these speeds

the polynomial becomes unstable, with the higher order terms rapidly producing unrealistic results. Therefore, in a similar manner to the revision of the hydrodynamic draft algorithm, a revision to the hollow length algorithm to a more appropriate and stable form is required.

Exponential Sinusoid Algorithm

As with the hydrodynamic draft, the shortcomings of the polynomial algorithm were that it did not predict the “humps” in the data, nor was it very reliable at high speeds. To improve the prediction of the hollow length a new algorithm was developed, consisting of an exponential term coupled with a damped sinusoidal term to take account of the “humps” as shown in Figure 5.13. The resulting improvement in correlation with the experimental data over the original polynomial is shown in Figure 5.14.

$$\begin{aligned} \frac{L_H}{T} = & 0.0113 \times \exp(1.9 \times F_{n_T} - 1.1223) + 1.2 + \\ & + \frac{B}{T} \times 0.03 \times \frac{\sin(b_0 \times F_{n_T} + b_1)}{0.08 + (b_2 - F_{n_T})^4} \end{aligned} \quad (5.9)$$

where

$$b_0 = -0.4574(B/T)^3 + 3.377(B/T)^2 - 8.585(B/T) + 11.51$$

$$b_1 = -0.5960(B/T)^4 + 6.174(B/T)^3 - 21.77(B/T)^2 + 30.17(B/T) + 9.929$$

$$b_2 = -0.03840(B/T)^3 + 0.3986(B/T)^2 - 1.420(B/T) + 2.529$$

As with the new hydrodynamic draft algorithm, the hollow length algorithm was developed using the DATAPLOT[®] program in association with Microsoft[®] Excel[©]. The same methodology was used in the development of the algorithm whereby the exponential function was first fitted to the experimental data with the difference

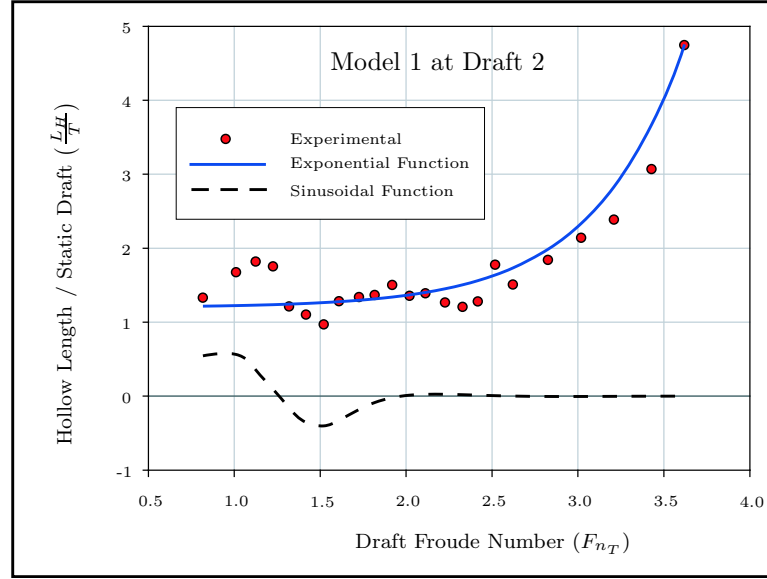


Figure 5.13: The Exponential and Damped Sinusoid Components of the New L_H Prediction Algorithm.

between the experimental data and the prediction made by the exponential function determined. The damped sinusoid was then fitted to the calculated difference with the variation in the coefficients b_i determined by optimising the fit with the experiment data. The polynomials b_0 to b_2 were fitted using the trendline functions of Microsoft[®] Excel[©].

5.3.2 Improvements in Resistance Prediction

The experimental programme detailed in this Chapter and Chapter 4 were undertaken to establish an understanding of the major influences on the hydrodynamics of the transom hollow. The primary reason for the investigation was due to the fact that, commonly in resistance prediction of transom-stern vessels, the hollow behind the transom is discretised as a geometrically-smooth addition to the vessel. Hence, greater knowledge of the hydrodynamics of the transom hollow and, specifically, the change in length and depth of the transom hollow with changes in

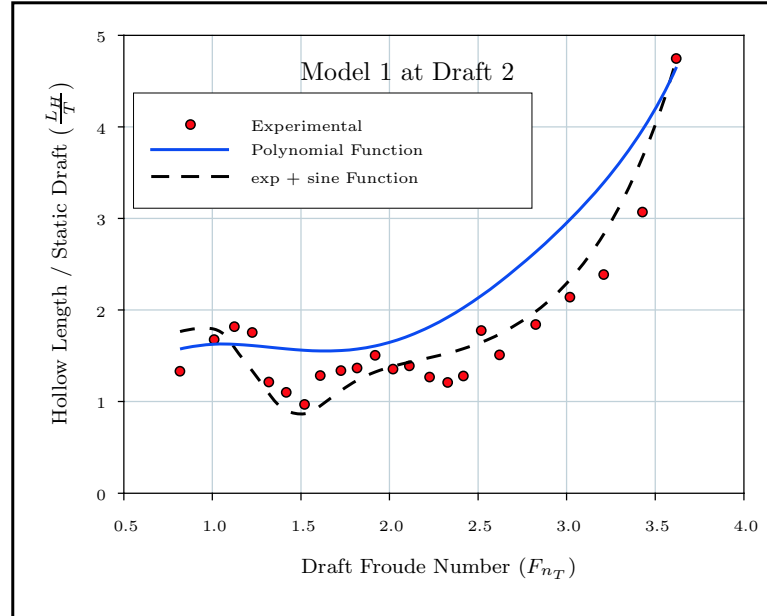


Figure 5.14: Comparison of the Predictions Made by the New L_H Algorithm Versus the Old Polynomial Algorithm

beam, draft and speed will lead to more-accurate predictions of vessel resistance. As discussed in Section 3.5, one of the major inaccuracies in modelling the hollow as a geometrically-smooth addition to the vessel is that the hollow tends to fill in at low speeds, so the current method greatly overestimates the total resistance of the vessel (Figure 5.15).

By incorporating the prediction algorithms into the HYDROS code, the transom hollow dimensions can be more closely estimated and improvements in resistance prediction made. Figure 5.16 shows the marked improvement in prediction at low speeds made by using the cubic prediction algorithms for hydrodynamic draft when applied to the parent model of the University of Southampton model series. However the wave-making resistance suffers at the highest speeds due to the prediction of hollow length using the cubic algorithm. Figure 5.16 exhibits a similar result when using the polynomial algorithm for the prediction of the hydrodynamic draft and hollow length.

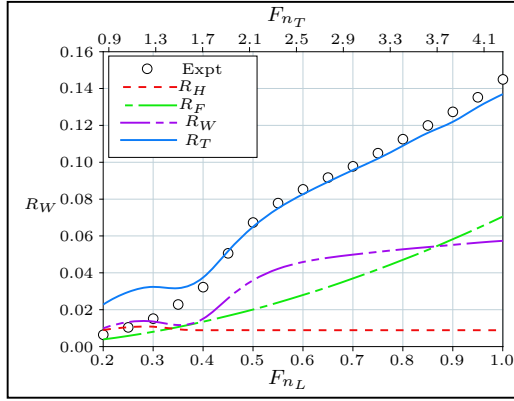


Figure 5.15: Methods of Doctors and Day
(1997)

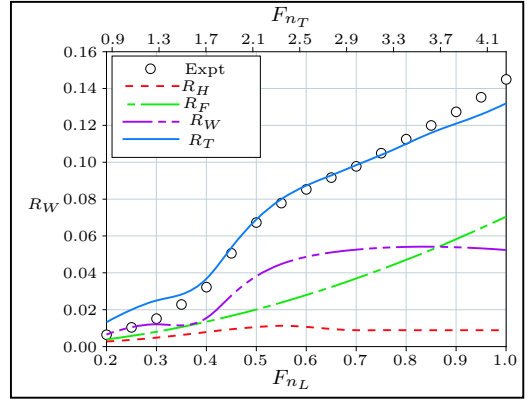


Figure 5.16: Cubic Algorithms for L_H and T_H

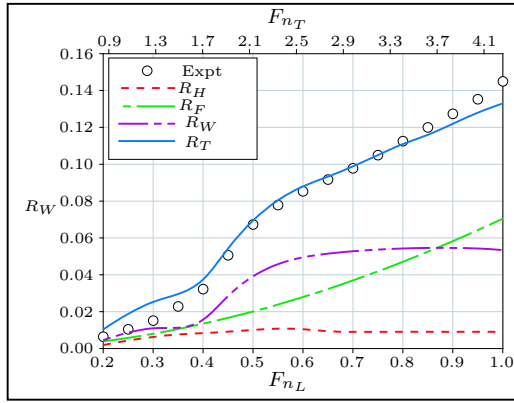


Figure 5.17: Polynomial Algorithms for L_H and
 T_H

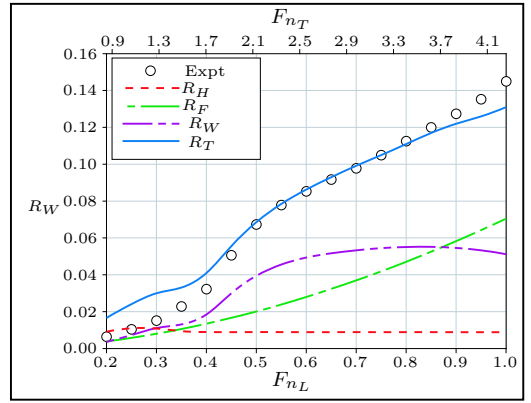


Figure 5.18: Exponential Algorithm for L_H

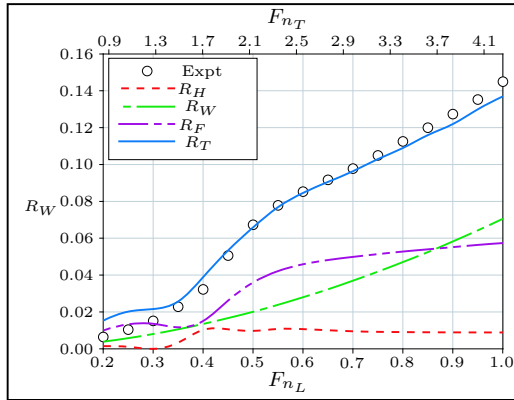


Figure 5.19: Hyperbolic Tangent Algorithm for
prediction of T_H

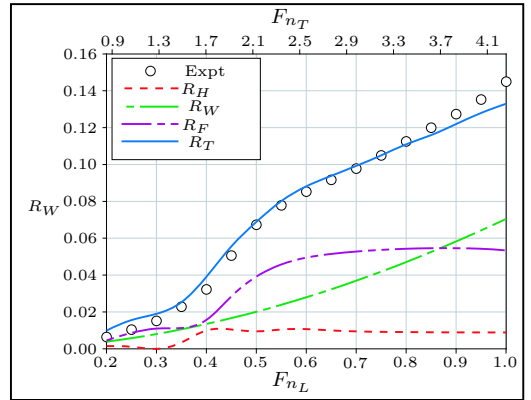


Figure 5.20: Hyperbolic Tangent Algorithm for
 T_H and Polynomial for L_H

Figure 5.18 shows the result of utilising the exponential function for the prediction of hollow length while using the original method for the hollow depth. The exponential function provides improvements in prediction at the low speeds but, like the cubic equation, produces negative effects on theoretical and experimental correlation at very high speeds.

By far the biggest improvement in correlation in the low speed range is produced by using the hyperbolic tangent algorithm for the prediction of hollow depth (Figure 5.19), especially when combined with the polynomial function for prediction of hollow length (Figure 5.20). Figure 5.21 compares the total resistance curves for the parent model from the University of Southampton series using the different hollow prediction methods. The figure clearly shows the improvement made over the original methods of Doctors and Day (1997) at the low speeds by incorporating the hyperbolic tangent function for the prediction of hollow depth and the further improvement made by incorporating the polynomial function for the prediction of hollow length. The original methods of Doctors and Day (1997) continue to provide better predictions at the highest speeds; however, in the lower speed range the new algorithms provide far better correlation.

The resulting reduction in root-mean-square error for specific resistance (R_T/W) through utilisation of the hollow prediction algorithms in the resistance formulation is shown in Table 5.1. The use of the hyperbolic tangent function for the prediction of the hydrodynamic draft coupled with the use of the polynomial function for the prediction of the hollow length produced an overall reduction in root-mean-square error between theory and experiment of 42.28%. Significant improvements in resistance prediction were realised with all of the prediction algorithms. Although excellent in the low-speed range, the overall improvement afforded by utilisation of the exponential function in the prediction of the hollow length is diminished due to the poor prediction at high speed. The exponential form, however, does provide a more-stable form of equation over the polynomial and, potentially, revision to the

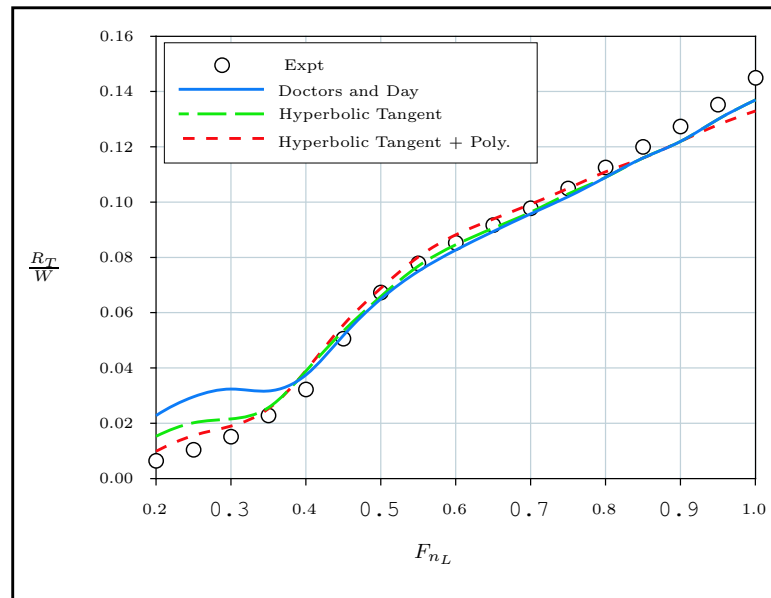


Figure 5.21: Comparison of Total Resistance for the Uni. of Southampton Model 3b Using Different Methods for Prediction of the Hollow Length and Hollow Depth

Hydrodynamic Draft Method	Hollow Length Method	RMS Error in Specific Resistance	Percentage Reduction in RMS Error
Original	Original	8.532×10^{-3}	—
Cubic	Cubic	6.081×10^{-3}	28.73
Poly	Poly	5.664×10^{-3}	33.62
Original	Exponential	7.911×10^{-3}	7.29
Hypebolic Tangent	Original	5.106×10^{-3}	40.15
Hypebolic Tangent	Polynomial	4.924×10^{-3}	42.28

Table 5.1: Reduction in Error Obtained Between Theory and Experiment for the University of Southampton Parent Model Depending on Hollow Prediction Method Employed

exponential algorithm could provide both reliability and better predictions.

5.4 Discussion

Analysis of the initial hollow experiments revealed obvious errors in the measurements made by the movable wave-probe, indicated by the hollow profile terminating under the measured position of the transom at high speeds. The cause of these errors was experimentally determined to be the flow separating from the probe wires affecting the measurements recorded. It was found that there was a direct relationship between the speed of the run and the magnitude of the separation. This enabled a correction factor to be applied to all of the experimental data which provided better correlation between the measured location of the bottom of the transom and the measured hollow profiles at high speeds where full separation from the transom was occurring.

The corrected experimental data were used to produce new hollow prediction

algorithms and the opportunity was taken to improve the form of these algorithms from the original polynomials to increase accuracy and reliability. The accuracy of prediction of the hydrodynamic draft was greatly improved by the new hyperbolic tangent function. The improvement in prediction of hollow length made by the new exponential function was significant at low speeds, but the accuracy of prediction made by the exponential function at high speeds was inferior. However, both new algorithms provide a robust and reliable method for predicting the shape of the transom hollow for use in resistance prediction. Further work on developing a more-superior prediction algorithm for the hollow length will no doubt provide greater improvements in resistance prediction.

Although utilisation for accurate resistance prediction of transom-stern vessels is the primary function, and the reason for which the hollow prediction algorithms were developed, there would be other possible uses by industry. Figure 5.22 shows an extract from a general arrangement drawing for a container vessel produced by Blue Water Designs Pty Ltd. The naval architects at Blue Water Designs Pty Ltd used the hollow length prediction algorithm (Equation 5.9) to calculate the minimum length of run required to avoid flow separation in the tunnel while maximising the cargo-carrying capacity of the vessel.

The hollow experiments detailed in Chapters 4 and 5 provide not only a greater understanding of the major influences affecting the transom hollow, but have been used to produce prediction algorithms for estimating the hollow length and hydrodynamic draft. Problems were experienced with the movable wave-probe rig, but these errors were detected and corrected. Improvements in accuracy may be achieved by repeating the experiments using non-intrusive techniques such as laser measurement. Additionally, the research program could be expanded to take into account the effects of more-complex transom geometry on the transom hollow.

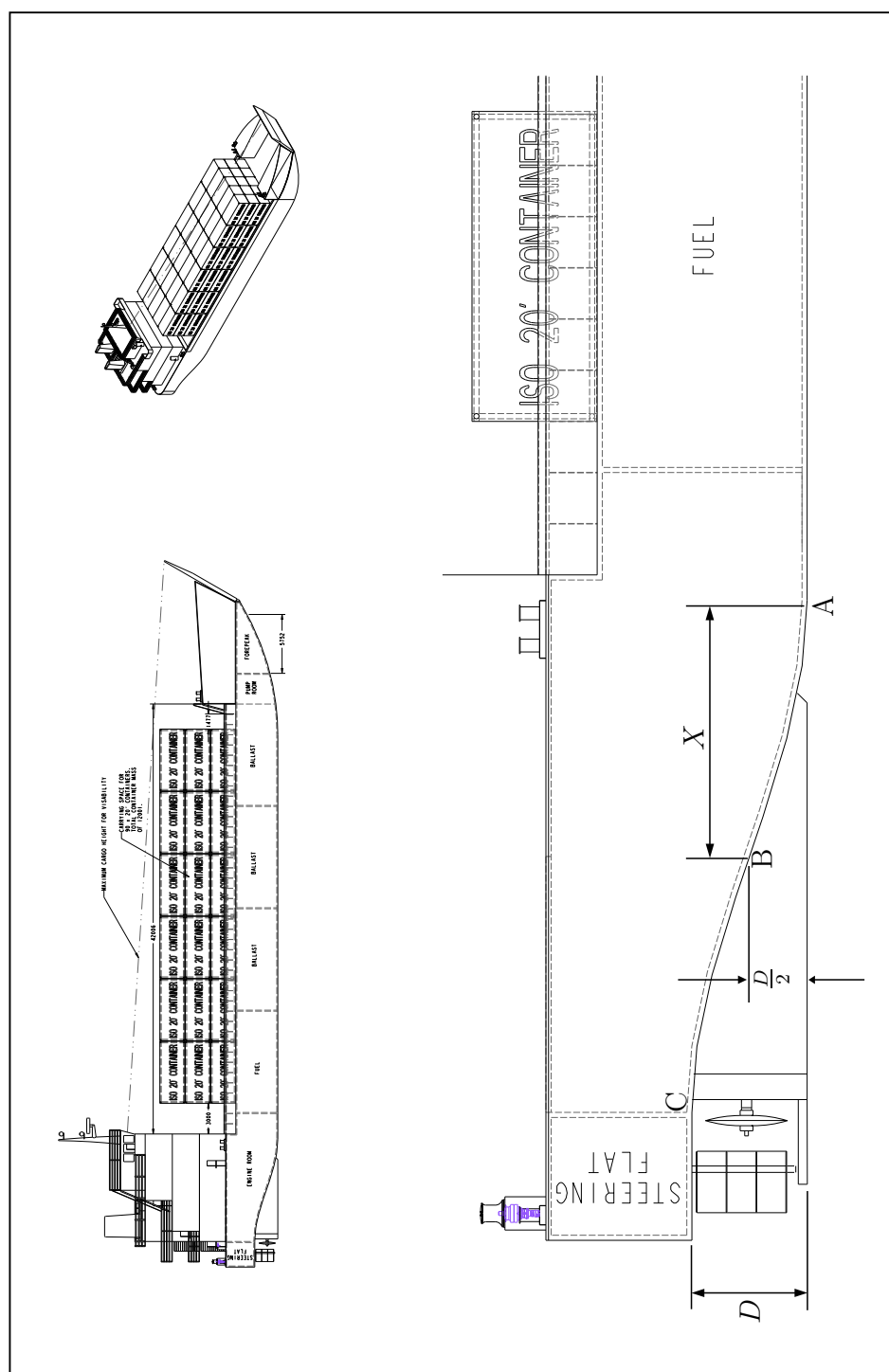


Figure 5.22: Calculation of Minimum Length of Run Required to Avoid Cavitation whilst Maximizing the Cargo Carrying Capacity (*Excerpt from General Arrangement of 65m Container Vessel, Courtesy of Blue Water Designs*)

Chapter 6

Reformatting HYDROS code

6.1 Introduction

To conduct the research into form factors presented in Chapter 7, whereby the accuracy of resistance prediction was improved through the application of form factors generated by regression of a large database of model test data, the HYDROS suite of programs was utilised. HYDROS was used to generate the hullforms, collate the towing-tank test results, calculate the theoretical resistance for each hullform and perform the regression analysis to establish the form-factors. The HYDROS suite of programs was developed by Doctors (1999b) in the Fortran77 programming language for use on a VMS operating system. To enable operation of these programs on a standard 32-bit personal computer (PC), major reformatting and restructuring of the applicable pieces of code was required before the form-factor research could commence. For the form-factor research to be undertaken, over 90 subroutines containing over 20 000 lines of code were required from the library of HYDROS programs. The function of the major subroutines are detailed in this Chapter, along with an account of the reformatting required to operate the programs on a Windows[®] operated PC.

6.1.1 The HYDROS Suite

The HYDROS suite of programs was designed and written for the calculation of hydrostatics and hydrodynamics of different types of vessels. The capabilities and functions that HYDROS possesses, are continually being augmented and updated by Doctors. However, at the time of the research reported here, HYDROS consisted of over 30 user-accessible program modules, primarily designed for the calculation of hydrostatics, stability, flooding, launching and other geometric characteristics of a vessel (Doctors, 1999b). In addition to the functions relating to static equilibrium, modules for the estimation of a vessel's hydrodynamic characteristics are available. These include modules for the computation of vessel motions and sea loads, as well as the calculation of a vessel's resistance by a variety of published methods. For the purposes of the work reported here, not all of HYDROS's modules were required.

6.1.2 HYDROS Programs Used

The principal purpose in using HYDROS was to further the ideas of Doctors (1998c) with regard to applying geometrically-based form-factors to the resistance formulation. Therefore, the HYDROS module of primary interest was program GENCAT. For this reason, the reformatting of the HYDROS code was limited to that required to run program GENCAT.

Program HULLIN is one of the HYDROS modules for input of the main geometric data for the description of a vessel, and was the module used for hull input in the form-factor research. Program MERGER was then utilised for the modification of hullforms generated using program HULLIN. MERGER can be used to form new hullforms by "merging" or "blending" however in the current work the module was utilised to modify parent hullforms to generate systematic series.

Once input and merged, the hullforms were discretised using Program MESHES. The module makes a series of calls to subroutine CUBICS, where cubic splines are placed through the original mesh points, both longitudinally and in the girthwise

direction. The hull is then represented by this new set of points.

Program **LOADER** computes the equilibrium condition of a vessel loaded and/or restrained in various ways and was used to check the principal particulars of the models input against published values. Subroutine **THRDEE** is called upon by both program **LOADER** and program **GENCAT** to compute the geometric properties of the immersed part of the vessel at a known condition.

Program **GENCAT** calculates a vessel's resistance by the methods of Doctors and Day (1997), Doctors (1998b), and Doctors (1998d), and was used extensively in the form-factor research presented in Chapter 7.

One of the subroutines used by program **GENCAT** is subroutine **HOLLOW** which is used to generate the hollow behind the transom stern of a vessel, where such a stern exists. The procedure, as detailed in Section 3.5, is based on creating the hollow as a smooth extension to the hull. Major modifications to the coding of this subroutine were made to incorporate the algorithms for the prediction of the hollow length as presented in Chapter 5. Whilst subroutine **DROPER** estimates the suction at the bottom of a transom stern in order to determine the drop in the water level in the pre-planing or low-Froude-number régime. The transom-stern resistance acting on the vessel, or the hydrostatic resistance (as calculated in Equation 3.1), is assumed to be equivalent to the lack of the force due to the hydrostatic pressure on the “dry” portion of the transom-stern. The details of the analysis were presented by Doctors (1998c). Major modifications to the coding of this subroutine were made to incorporate the algorithms for the prediction of the hollow depth developed in Chapter 5.

Program **GENCAT** calls subroutine **FRICTN** to compute the frictional resistance of a vessel according to one of a number of standard methods. In the current work, the frictional resistance was calculated using the ITTC-1957 ship-model correlation line. However, the different formulas available for calculation of the friction coefficient, using subroutine **FRICTN**, are:

$$C_F = \left\{ \begin{array}{ll} 0.455/(\log R_{n_L})^{2.58} & \text{Prandtl-Schlichting law} \\ 0.075/(\log R_{n_L} - 2)^2 & \text{ITTC-1957 line} \\ 0.074/R_{n_L}^{1/5} & \text{One-seventh-power law} \\ 0.0450/R_{n_L}^{1/6} & \text{One-ninth-power law} \\ 1/[4.13 \log(R_{n_L} C_F)]^2 & \text{ATTC-1947 line, Schoenherr (1932)} \\ 0.066/(\log R_{n_L} - 2.03)^2 & \text{Hughes line (1954)} \\ 0.07776/(\log R_{n_L} - 1.88)^2 + 60/R & \text{Granville line (1977)} \\ 0.0012 + 0.340/R_{n_L}^{1/3} & \text{Telfer line (1927)} \\ 0.0012 + 0.300/R_{n_L}^{1/3} & \text{Telfer-2 line} \\ 0.0113/(\log R_{n_L} - 3.7)^{1.15} & \text{Gadd line} \\ 0.427/(\log R_{n_L} - 0.407)^{2.64} & \text{Schultz-Grunow line} \\ 0.0718/(\log R_{n_L} - 2)^2 & \text{Hughes-2 line, Joubert and Hoffmann (1979)} \\ 0.0661/(\log R_{n_L} - 2.18)^2 & \text{Hughes-3 line, Joubert and Hoffmann (1979)} \\ 1/\{1.7063[\ln(R_{n_L} \sqrt{C_F}) - 2.311]\}^2 & \text{Lap-Troost line} \\ 0.523/\ln^2(0.06 R_{n_L}) & \text{Frank White line (1974)} \\ f_{Grigson} \times 0.075/(\log R_{n_L} - 2)^2 & \text{Grigson line (1993)} \\ 1/[4.06 \log(R_{n_L} C_F) - 0.729]^2 & \text{Date-Turnock line (2000)} \end{array} \right.$$

These formulas were presented by Duncan *et al.* (1970), Lewis (1988), Joubert and Matheson (1970), and Saunders (1957b).

Subroutine **FITTER** is employed to improve the correlation of the standard wave-resistance theory programmed in subroutine **GENRES**, by means of form factors for the wave resistance and the frictional resistance, as outlined in Section 2.3. The subroutine is called on each occasion that the resistance of the vessel is estimated. In this manner, the program can accumulate the sums defined in Equations 7.3 and 7.4. The subroutine also computes the resistance on the basis of the user-supplied form factors. In the form-factor research conducted here, subroutine **FITTER** was first utilised to determine the optimal form factors for the entire database of models, and

then used to calculate the effect on the resistance calculation when the optimal form factors were applied in the resistance formulation.

6.2 Methods

HYDROS was written in Fortran77 for use on a VMS system, and was not compatible with operation on a PC running Microsoft® Windows® as its operating system. Significant restructuring was necessary for the HYDROS code to run on a standard 32-bit PC, and the remainder of this Chapter is devoted to the reformatting and validation process involved.

6.2.1 Compiler

The compiler used in the reformatting process was LaheyED® for Windows® Version 3.80. LaheyED® supports 32 different programming languages including Assembler, C/C++, Clipper, Cobol, Delphi, Fortran90, Forth, HTML, Java, Perl, Progress, SQL, Verilog and VHDL. As HYDROS was originally developed in Fortran77 the natural choice was to reformat the code to the Fortran90 language.

6.2.2 Reformatting

There were many changes which needed to be made to the original code for it to compile and run in the Fortran90 language. The main difference between the Fortran77 and Fortran90 languages lies in the declaration of variables and the passing of variables from one subroutine to another. In the original Fortran77 code, variables used solely within a subroutine did not have to be declared at the beginning of the subroutine; however, with Fortran90 every single variable used had to be declared as to whether it was a string, integer, complex number, logical switch, real number or array as well as its intent (that is if the variable was being passed into the subroutine or being passed out). As an example of the differences in the variable declaration re-

quired at the start of a program, Table 6.1 shows the difference between the original Fortran77 code and the final Fortran90 code, for subroutine `GENRES`. It can be seen in Table 6.1 that calls made to other modules from within the subroutine have to be declared at the beginning of the subroutine with the `USE` command. An additional coding requirement of Fortran90 compared to Fortran77 is that all variables being passed in or out of the subroutine have to be declared as to their intent.

Many other formatting changes were necessary to compile the code in Fortran90, contributing to the reformatting becoming a considerable task and reinforcing the need to properly validate the conversion process as presented in Section 6.3.

6.2.3 Changes to Code

Over and above the numerous basic formatting changes required to convert the code to the FORTRAN90 structure, new subroutines were introduced and major changes were made to selected subroutines. New subroutines `NAMES` and `GNames` were used to enable batch files to be created for initiating multiple successive runs in both program `LOADER` and program `GENCAT`. A new subroutine `TIMEDAT` was required to enable the program to communicate with the central-processing-unit (CPU) clock on a standard PC.

Subroutine `FITTER` was modified to provide the user with more flexibility in the geometric functions to be used in a regression analysis. The original set of geometric functions proposed by Doctors (Table 7.1) were retained in the code; however, several more sets of geometric functions were coded, with a new input variable allowing the user to chose which set of geometric functions were to be used in a given regression analysis. The final set of geometric functions used in the research presented in Chapter 7 are given in Table 7.21, resulting from optimisation of the root-mean-square error obtained in the regression analysis of the model data collated.

Subroutine `DROPER` and subroutine `HOLLOW` were modified to incorporate the hollow-prediction algorithms developed in Chapters 4 and 5. The cubic equa-

Table 6.1: Original and Reformatted Code for Preamble to Subroutine GENRES

Line	Original Code	Reformatted Code
1		MODULE m_genres
2		IMPLICIT NONE
3		CONTAINS
4	subroutine genres (g, rho, q, d, width,	SUBROUTINE genres (g, rho, q, d, width,&
5	1 x1, x2, z1, z2, bb, space, kxmax, kymax,	x1, x2, z1, z2, bb, space, kxmax, kymax,&
6	2 itmax, nnmax, npmax, nbxmax, nx, nz, nbb,	itmax, nnmax, npmax, nbxmax, nx, nz, nbb,&
7	3 lp, lp1, lp2, rw, ier)	lp, lp1, lp2, rw, ier)
8		USE m_iounit
9		USE m_rconst
10		USE m_rcheck
11		USE m_ichack
12		USE m_genoch
13		USE m_flowier
14		USE m_waveno
15		USE m_locate
16		IMPLICIT NONE
17	parameter (mrmax= 80)	INTEGER, PARAMETER :: mrmax= 80
18	implicit logical (l)	LOGICAL, INTENT(IN) :: lp, lp1, lp2
19		LOGICAL :: la, lt, lkx
20		INTEGER, INTENT(IN) :: itmax, nnmax, npmax, nbxmax, nx, nz, nbb
21		REAL(KIND=8), INTENT(IN) :: g, rho, q, d, width, kymax, kxmax
22		REAL(KIND=8), INTENT(OUT) :: rw
23		INTEGER, INTENT(OUT) :: ier
24	dimension	
25	1 space (nbxmax), x1 (nbxmax), x2 (nbxmax),	REAL(KIND=8), DIMENSION(nbxmax), INTENT(IN) :: x1, x2, space
26	2 z1 (nnmax, nbxmax), z2 (nnmax, nbxmax),	REAL(KIND=8), DIMENSION(nnmax, nbxmax), INTENT(IN) :: z1, z2
27	3 bb (npmax, nbxmax)	REAL(KIND=8), DIMENSION(npmax, nbxmax), INTENT(IN) :: bb
28	real k, kx, kx2, kxmax, ky, kymax, k0, k0d, m	REAL(KIND=8) :: k, kx, kx2, ky, k0, k0d, m
29	complex ccocch	COMPLEX(KIND=8) :: ccocch
30	character*(mrmax) place	CHARACTER(mrmax) :: place
31	character*(*) module	
32	parameter (module= 'GENRES')	CHARACTER(*), PARAMETER :: MODULE= 'GENRES'
33		INTEGER :: ic6, np, key, nky, iflow, iky, it
34		REAL(KIND=8) :: rdiver, pi, dky, fac, weight, dgdm, dfdk, grand,&
35		cochin, swr, swr1, swr2, swr3, swr4, swr5

Table 6.2: Original and Reformatted Code for Passing Array Variables

Line	Original Code	Reformatted Code
1		genci(1)=genc
2		stabi(1)=stab
3		tanki(1)=tank
4		dati(1)=dat
5	call length (genc, 1, m1)	call length (genci, 1, m1i)
6	call length (stab, 1, m2)	call length (stabi, 1, m2i)
7	call length (mesh, nbbmax, m3)	call length (mesh, nbbmax, m3)
8	call length (sagg, nbbmax, m4)	call length (sagg, nbbmax, m4)
9	call length (tank, 1, m5)	call length (tanki, 1, m5i)
10	call length (dat, 1, m6)	call length (dati, 1, m6i)
11	call length (i_mesh, nbbmax, m7)	call length (i_mesh, nbbmax, m7)
12		m1=m1i(1)
13		m2=m2i(1)
14		m5=m5i(1)
15		m6=m6i(1)

tion (4.7), polynomial equation (4.9) and exponential equation (5.9) for prediction of hollow length were programmed into subroutine `HOLLOW` with a variable fed back to the input file for user control as to which hollow length prediction method was to be utilised. Similarly, the cubic equation (4.8), polynomial equation (4.9) and hyperbolic tangent equation (5.8) for the prediction of hydrodynamic draft were programmed into subroutine `DROPER` with a variable fed back to the input file for user control as to which hydrodynamic draft prediction method was to be utilised.

6.3 Results

To verify the conversion process of the `HYDROS` code to a FORTRAN90 PC compatible version, Professor Doctors provided access to the VMS version of `HYDROS` such that the same regression analysis could be processed on each version of `HYDROS` for means of comparison. A group of 28 models from the original three series tested by Doctors and Day (1997) were randomly selected. Hull input files (`HULLIN`) as well as `MERGER`, `MESHES`, `LOADER`, and `GENCAT` files were formatted for input into both `HYDROS` versions for each of the 28 models. The set of models were then run through

each version of the programs using a variety of regression analyses and the results compared.

The initial approach was to systematically increase the number of geometric functions used in the form factor regression analysis and compare the resulting reduction in root-mean-square error calculated by both versions of HYDROS. Figure 6.1 shows the reduction in root-mean-square error, for total resistance (R_T) divided by weight force (W), as the number of geometric functions used in the regression is increased from 1 to 9. It can be seen that the two versions of HYDROS produce exactly the same results to within expected machine accuracies.

The second approach was to apply each of the geometric functions individually to the group of 28 models and compare the resulting coefficient obtained by each version of HYDROS. Figure 6.2 shows the coefficients obtained for each geometric function and clearly shows that the two versions produced practically the same coefficient in each case. The slight differences obtained in the coefficients obtained by each version are as would be expected taking into account the differences in machine accuracy between the 32-bit PC and the 64-bit VMS system.

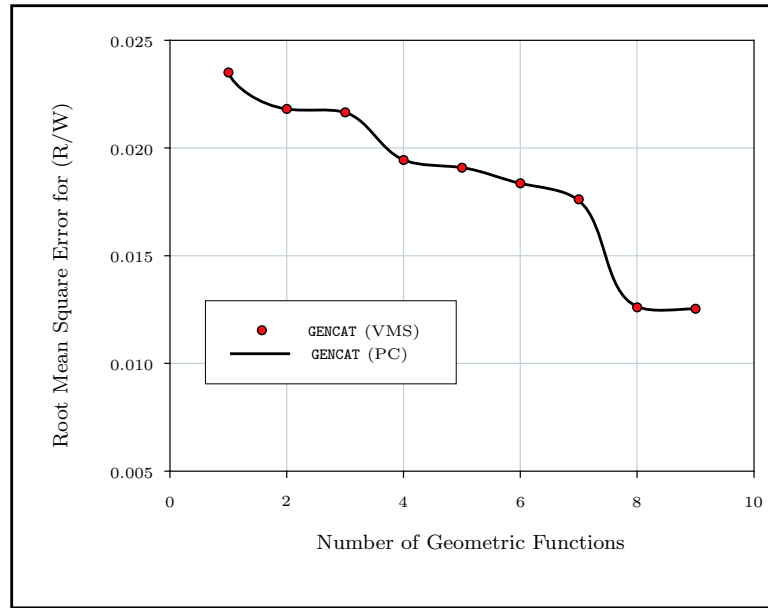


Figure 6.1: Comparison of the Root-Mean-Square Error of Total Resistance Divided by Weight Plotted Against the Number of Geometric Functions used in the Regression Analysis

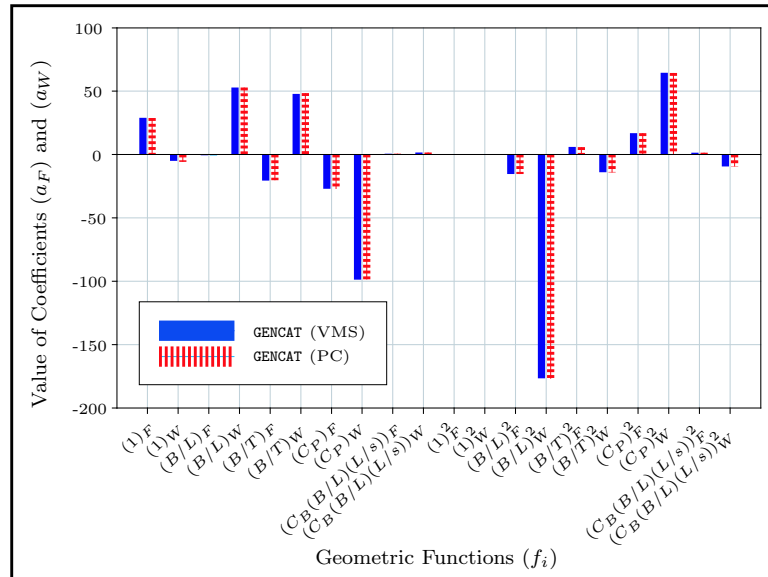


Figure 6.2: Comparison of the Individual Coefficients Calculated Using Both the VMS and PC Versions of Program GENCAT

6.4 Discussion

The reformatting of the *HYDROS* suite of programs from FORTRAN77 code for operation on a VMS system to FORTRAN90 code for operation on a PC was undertaken due to the very large demand that the form-factor research (presented in Chapter 7) was going to place on the VMS server. The magnitude of the changes required for successful conversion was not envisaged at the commencement of the reformatting process; however, the results presented in Section 6.3 show that successful conversion of the code was achieved. In addition to the reformatting, some of the subroutines were altered and some further subroutines added, firstly to improve efficiency through the ability to run batch files and, secondly, to add flexibility with regard to the geometric functions to be used in form-factor regression analysis.

The *HYDROS* suite is a powerful and highly-efficient set of programs which provide the user with a great deal of flexibility and control. However, this flexibility and control adds a great deal of complexity in successfully running the programs. In this regard the *HYDROS* suite would benefit greatly from a graphical user interface (GUI) to assist the operator in the formatting and control measures available. The development of a graphical user interface for the *HYDROS* suite presents a challenging yet valuable area of future development of the *HYDROS* suite.

Chapter 7

Form-factor Calculation

7.1 Introduction

7.1.1 Previous Research

As discussed in Chapter 2, one of the best methods of predicting the full scale resistance of a vessel is through model testing. The problem associated with scaling the model test results to full size is that the components of resistance scale according to different laws. Froude first proposed in 1868 (Froude, 1955) that the total resistance of a vessel could be divided into two components, the frictional resistance and the remainder (referred to as the residuary resistance). Based on the experiments of Froude (1872, 1874) and Hughes (1952) amongst others, equations were produced for the prediction of the frictional resistance for a vessel. These experiments were conducted largely on flat plates, planks and pontoons, and are referred to as two-dimensional, or flat-plate, skin friction lines. In order to take account of the three-dimensional shape of vessels, form factors are now often applied to the frictional resistance determined using these ship-model correlation lines. Indeed, a study carried out by the ITTC Performance Committee showed that use of form factors has led to considerable improvements in model-ship correlation (ITTC, 1978).

Hughes suggested that the total resistance for the model C_{TM} should be divided


$$1+k = \frac{C_{T_M}(R_{n_O})}{C_{F_O}(R_{n_O})} \quad (7.1)$$

Using the same assumption as Hughes, i.e. that the wave-making resistance becomes small at low Froude numbers, Prohaska (1966) proposed that the wave-making resistance at these low speeds could be approximated as $c F_{n_L}^n$, yielding the following equation:

$$\frac{C_{T_M}}{C_{F_O}} = (1+k) + \frac{c F_{n_L}^n}{C_{F_O}} \quad (7.2)$$

Therefore, by plotting C_{T_M}/C_{F_O} against $F_{n_L}^n/C_{F_O}$ (where the gradient c and the constant n are chosen so as to minimize the least-squares fit with the measured C_{T_M}), the form factor $(1 + k)$ is determined as the intercept on the C_{T_M}/C_{F_O} axis, and is assumed to be invariant with R_n (Lewis, 1988).

Another method used by Tanaka *et al.* (1990) for determining the form factor is to test a number of geosim models at the same Froude number. For a given Froude number the values obtained for C_T , when plotted against the Reynolds number, approximately follow the slope of the ITTC'57 ship-model correlation line. Therefore, upon plotting C_T against C_F for each model at the same Froude number, the gradient of the line fitted between these points is the form factor $(1 + k)$.

7.1.2 Geometry-based Form Factors

As discussed in Chapter 2, the wave-resistance theory of Michell is based on the assumption of a thin hullform. So, in addition to the frictional resistance form factor, Doctors and Day (1997) applied a single constant wave-making resistance form factor to the computed linearised wave resistance. The method was applied to a catamaran in several conditions, and the application of a single constant wave-making resistance form factor improved the correlation between theory and experiment. Doctors (1998c) then extended this research by proposing that both the frictional and wave-making resistance form factors could be approximated in the following manner:

$$f_W = \sum_{i=1}^N a_{W,i} f_i \quad (7.3)$$

$$f_F = \sum_{i=1}^N a_{F,i} f_i \quad (7.4)$$

where $a_{W,i}$ and $a_{F,i}$ are constants to be found by regression analysis, and f_i are functions of the hull geometry such as those listed in Table 7.1.

Index (i)	Function (f_i)
1	1
2	B/L
3	B/T
4	C_P
5	$C_B(B/L)(L/s)$
6	$(1)^2$
7	$(B/L)^2$
8	$(B/T)^2$
9	$(C_P)^2$
10	$[C_B(B/L)(L/s)]^2$
11	F_{n_L}
12	$(B/L) \cdot F_{n_L}$
13	$(B/T) \cdot F_{n_L}$
14	$C_P \cdot F_{n_L}$
15	$C_B(B/L)(L/s) \cdot F_{n_L}$

Table 7.1: Geometric Functions (*Doctors, 1998c*)

The method of least squares was used to minimize the error in the fit of the functions given by Equations (7.3) and (7.4). The application of this procedure over the M experimental points leads to the following set of equations in solving for the optimal form-factors

$$\sum_{k=1}^M \sum_{j=1}^{2N} F_i F_j a_j = \sum_{k=1}^M F_i (R_{T,E} - R_H - R_A - R_{AA} - \sum_{j=1}^{2N} F_j a_j) \quad (7.5)$$

$$F_{2l-1} = R_W f_l \quad (7.6)$$

$$F_{2l} = R_F f_l \quad (7.7)$$

$$a_{2l-1} = a_{W,l} \quad (7.8)$$

$$a_{2l} = a_{F,l} \quad (7.9)$$

There are up to $2N$ coefficients to be determined, N coefficients for the wave-making resistance factor and N coefficients for the frictional-resistance factor. Using the 15 geometrical functions listed in Table 7.1, Doctors applied the method separately to three different model series, and the results were shown to be most favourable in increasing the accuracy of correlation between theory and experiment. The limitation of the form factors calculated in this way is that they only apply, with any deal of confidence, to the three model series from which they were derived.

This chapter details the collection, analysis, and regression of a large database of model test results. From this database the methods of Doctors (1998c) were applied such that a set of form factors for both frictional and wave-making resistance could be determined which would be more widely applicable to a large range of high-speed semi-displacement vessels.

7.2 Model Data Utilised

A vast amount of model test data was collected, incorporating both monohull and catamaran configurations. The array of models collected was limited to model series

possessing transom-stern configurations. Model series are generally developed from a single parent model of known favourable resistance characteristics. The geometric parameters defining the parent model are then systematically altered to form the model series. The processing time associated with defining a model's hull shape can be considerable. Therefore model series data was beneficial in this respect, as the parent hullform could be easily modified using Program **MERGER** (see Section ??) to form the complete series.

Primarily the model data collected is for high-speed semi-displacement¹ pre-planing models. The model data collected has been tested in experimental facilities throughout the world and published in transactions, proceedings and laboratory reports.

7.2.1 Lego Model Series

The Lego model series was utilised in the form factor research of Doctors and Day (1997) and consisted of a series of model segments tested in various combinations. The model series consisted of twelve models comprising various combinations of seven base segments. Figure 7.2 provides details of the hull segments from which the Lego series was formed. The bow and stern segments (1, 5, 6, and 7) possessed parabolic waterplanes, and all seven segments had parabolic cross-sections beneath the waterline. Each model had a beam B of 0.150 m and a draft T of 0.09375 m. Table 7.2 lists the elements constituting the twelve Lego models. The body plans of the twelve Lego models are displayed in Appendix A. The parabolic nature of the Lego model series enabled the model offsets to be calculated mathematically. Program **HULLIN** (see Section 6.1.2) was then utilized to process these offsets for use in Program **GENCAT**.

¹Various figures are quoted for the speed at which a vessel is classed as “high speed”, and the speed at which planing commences; however, high-speed semi-displacement vessels are generally considered to operate in the speed range $0.3 \leq F_{n_L} \leq 1.2$.

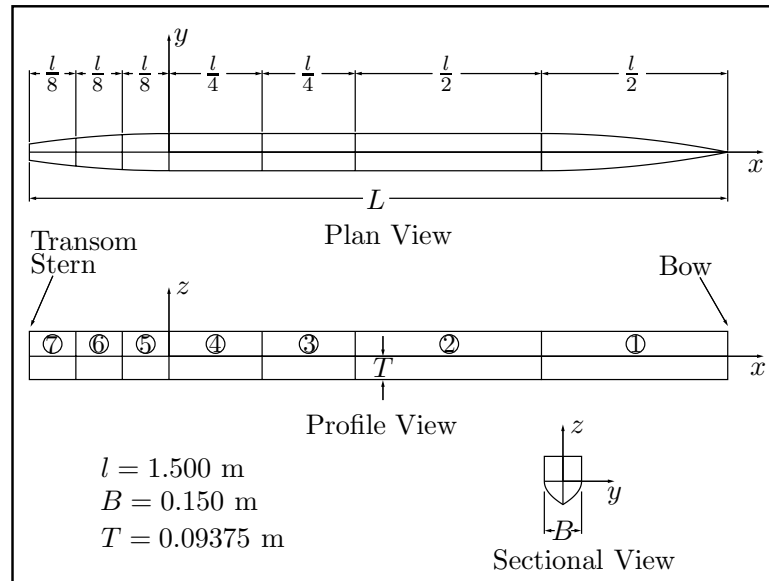


Figure 7.2: Segmentation of The Lego Model Series (*Doctors, 1998c*)

The models were tested by towing them over a range of steady speeds in the towing tank at the Australian Maritime College. The towing tank had a width of 3.5 m and was filled to a water depth of 1.5 m representing a full-scale deep water condition. A total of 409 experimental runs was performed. The results from these experimental runs (courtesy of Doctors) were compiled into an experimental data file for use by Program GENCAT in the regression process.

7.2.2 National Physical Laboratory (NPL) Model Series

Due to the lack of design data available in the 1960s for fast round-bilge displacement hulls, the Ship Division of the National Physical Laboratory undertook resistance tests on a systematic series of such hullforms, the results of which were reported by Marwood and Bailey (1969) and Bailey (1976). A parent hullform was chosen for its known favourable resistance characteristics (Model 100A, see Table 7.3), which was then systematically scaled to form the complete series. The range of length-to-beam ratios was represented by the five models 100Z, 100A, 100B, 100C, and 100D.

Lego Model Number	Segments	Length L (m)	Prismatic Coefficient C_P
1	1	0.7500	0.6666
2	15	0.9375	0.7290
3	156	1.1250	0.7499
4	1567	1.3125	0.7290
5	12	1.5000	0.8332
6	125	1.6875	0.8494
7	1256	1.8750	0.8499
8	12567	2.0625	0.8275
9	1234	2.2500	0.8888
10	12345	2.4375	0.8957
11	123456	2.6250	0.8928
12	1234567	2.8125	0.8735

Table 7.2: The Lego Model Series (*Doctors and Day, 1997*)

As the beam was increased for these models, the draft was decreased to maintain the displacement of the parent model. From these five models, the remainder of the model series was created by maintaining the beam but varying the draft in proportion the change in displacement.

For the purpose of current analysis, the body plan of the parent hullform published by Bailey (1976) (see Appendix A) was digitised and the offsets entered into Program HULLIN. The other models in the NPL series were derived by scaling the parent model using Program MERGER in accordance with the particulars detailed in Table 7.4.

The NPL models were of timber construction, with turbulence stimulation studs fitted approximately 25 mm aft of the bow profile. The models were tested in the No. 3 tank of the Ship Division at the National Physical Laboratory. The tank was 396.2 m long, 14.6 m wide and 7.6 m deep. The ratio of model draft to tank depth was very small, circumventing any shallow water effects. The towing point for all models was at the longitudinal centre of gravity on the waterline.

The experimental results were presented by Bailey (1976) in the form of a series of charts of residuary resistance (non-dimensionalised by displacement) plotted against the Froude-length-constant² \mathbb{M} for the various length-to-beam ratio group of models. Charts of the total resistance coefficient (C_T) were also presented, plotted against the Froude number for each length-to-beam ratio group of models. Charts were also presented by Bailey (1976) for three of the NPL models (80A, 100A, 150A) tested at a range of displacements. In these charts, C_T was plotted against displacement as a percentage of the design displacement for a range of Froude numbers. To run these cases through HYDROS, the three models in question were run through Program LOADER at the desired displacement in order to determine the corresponding nominal draft (see Table 7.5). The models were then run through Program GENCAT at these

²The Froude-length-constant \mathbb{M} is not to be confused with the Froude number F_{nL} . The Froude-Length-Constant is a non-dimensional geometrical property, also called the slenderness ratio, and is of the form $\mathbb{M} = \frac{L}{\nabla^{1/3}}$

Particular	Symbol	Value	Unit
Length on Designed Waterline	L_{WL}	2.54	m
Beam on Designed Waterline	B_{WL}	0.4064	m
Draught of Designed Waterline	T	0.140	m
Displacement	Δ	57.33	kg
Block Coefficient	C_B	0.397	
Prismatic Coefficient	C_P	0.693	
Maximum-Section Area Coefficient	C_M	0.573	
Location of Maximum Section	40% L_{WL} from transom		
Longitudinal Centre of Buoyancy	LCB	6.4% L_{WL} aft of \mathcal{O}	

Table 7.3: Principal Particulars of the NPL Parent Model 100A (*Marwood and Bailey, 1969*)

calculated drafts and the resistance results compared with the experimental data interpolated from the published charts.

The results for the NPL models were interpolated from these charts and compiled along with the running trim data (also presented in graphical form) into a towing-tank data file ready for use by Program **GENCAT** in the regression process.

7.2.3 University of Southampton Catamaran Model Series

An investigation of the components of catamaran resistance and the influence of hull separation was undertaken by Molland *et al.* (1994a). The effect on resistance of changes in length-to-displacement ratio and length-to-beam ratio were also considered in this study. The model series was developed from the NPL model series (see Section 7.2.2) and the principal particulars of the model series are presented in Table 7.6. The study was an extension of the work by Insel (1990) and Insel and Molland (1992), where models 3b, 4b, and 5b were tested.

NPL Model Number	Length on DWL (m)	Beam on DWL (m)	Draught on DWL (m)	Model Displacement (kg)
50Z	2.540	0.338	0.084	28.67
50A	2.540	0.406	0.070	28.67
80Z	2.540	0.338	0.134	45.86
80A	2.540	0.406	0.112	45.86
80B	2.540	0.470	0.097	45.86
80C	2.540	0.559	0.081	45.86
100Z	2.540	0.338	0.168	57.33
100A	2.540	0.406	0.140	57.33
100B	2.540	0.470	0.121	57.33
100C	2.540	0.559	0.102	57.33
100D	2.540	0.762	0.075	57.33
150A	2.540	0.406	0.210	86.00
150B	2.540	0.470	0.181	86.00
150C	2.540	0.559	0.152	86.00
150D	2.540	0.762	0.112	86.00
200B	2.540	0.470	0.242	114.66
200C	2.540	0.559	0.204	114.66
200D	2.540	0.762	0.149	114.66
250C	2.540	0.559	0.254	143.33
250D	2.540	0.762	0.187	143.33
320C	2.540	0.559	0.326	183.46
320D	2.540	0.762	0.239	183.46

Table 7.4: The National Physical Laboratory (NPL) Model Series with Model 100A being the Parent Model of the Series (*Bailey, 1976*)

Δ_i % of Δ_{DWL}	Draft T_i (m) corresponding to Displacement Δ_i for NPL Models		
	80A	100A	150A
60	-	-	0.1641
70	-	-	0.1762
80	-	0.1252	0.1878
90	-	0.1328	0.1992
100	0.1120	0.1400	0.2100
110	0.1186	0.1475	0.2212
120	0.1237	0.1546	0.2319
130	0.1293	0.1616	0.2425
140	0.1349	0.1686	0.2529
150	0.1403	0.1754	-
160	0.1458	0.1822	-
170	0.1511	0.1889	-
180	0.1564	0.1955	-
190	0.1616	-	-
200	0.1668	-	-
210	0.1719	-	-
220	0.1769	-	-
230	0.1819	-	-
240	0.1869	-	-

Table 7.5: Additional Towing Tank Results from Three of the NPL Models
Tested at Varying Displacements (*Bailey, 1976*)

The model hullforms were replicated by scaling the NPL parent form using Program **MERGER**, and the demihull spacing for each run was set in the input file for Program **GENCAT**.

The ten models presented in Table 7.6 were tested as monohulls and as catamarans with separation-to-length ratios (s/L) of 0.2, 0.3, 0.4, and 0.5. The model experiments were conducted at the Southampton Institute of Higher Education test tank which has a length of 60 m, breadth of 3.7 m and water depth of 1.85 m. The models were towed from a point at the longitudinal centre of gravity and at an effective height of one-third of the draft above the keel. Calm water total resistance, sinkage and trim were recorded along with wave pattern analysis.

Both the total resistance coefficient (C_T) and the residuary resistance coefficient (C_R) were presented, with C_R calculated based on C_F being obtained from the ITTC'57 ship-model correlation line. A towing-tank data file, for use in Program **GENCAT**, containing the resistance, sinkage and trim data was obtained courtesy of Doctors.

7.2.4 D-Series Models

Due to the lack of design data available for shorter broader vessels, and due to the problems associated with extrapolating existing experimental data for resistance and power predictions of these vessels, Kracht and Jacobsen (1992) tested a series of seven twin-screw round-bilge hullforms. The model series, called the D-Series, covered a range of beam-to-draft ratios from 3.5 to 4.0, volumetric coefficients of 0.003 and 0.0035, and longitudinal prismatic coefficients of 0.620 and 0.646. The details of the complete series of models is presented in Table 7.7. Model D5 was developed from the parent model D1 by alteration of the sectional area curve, such that the longitudinal centre of buoyancy remained unchanged, and the prismatic coefficient was increased by 0.026. The body plans for the two parent forms D1 and D5 are presented in Appendix A. The remaining models were developed by linear

Model	L_{WL} (m)	L/B	B/T	$L/\nabla^{1/3}$	C_B	C_P	C_M	S (m ²)	LCB % fwd of ∇
3b	1.6	7.0	2.0	6.27	0.397	0.693	0.565	0.434	-6.4
4a	1.6	10.4	1.5	7.40	0.397	0.693	0.565	0.348	-6.4
4b	1.6	9.0	2.0	7.41	0.397	0.693	0.565	0.338	-6.4
4c	1.6	8.0	2.5	7.39	0.397	0.693	0.565	0.340	-6.4
5a	1.6	12.8	1.5	8.51	0.397	0.693	0.565	0.282	-6.4
5b	1.6	11.0	2.0	8.50	0.397	0.693	0.565	0.276	-6.4
5c	1.6	9.9	2.5	8.49	0.397	0.693	0.565	0.277	-6.4
6a	1.6	15.1	1.5	9.50	0.397	0.693	0.565	0.240	-6.4
6b	1.6	13.1	2.0	9.50	0.397	0.693	0.565	0.233	-6.4
6c	1.6	11.7	2.5	9.50	0.397	0.693	0.565	0.234	-6.4

Table 7.6: Principal Particulars of the University of Southampton Catamaran
Model Series (*Molland et al., 1995*)

Model	$L_{PP}(\text{m})$	B/T	C_P	$10^3 C_V$	L/B	C_B	S/L^2
D1	6.0	3.75	0.620	3.0	6.67	0.500	0.150
D2	6.0	3.75	0.620	3.5	6.17	0.500	0.162
D3	6.0	4.00	0.620	3.0	6.45	0.500	0.152
D4	6.0	3.50	0.620	3.0	6.90	0.500	0.148
D5	6.0	3.75	0.646	3.0	6.81	0.521	0.149
D6	6.0	3.75	0.646	3.5	6.30	0.521	0.161
D7	6.0	4.00	0.646	3.0	6.59	0.521	0.151

Table 7.7: Principal Particulars of the D-Series Models tested at the Berlin Model Basin (*from Harries and Schulze, 1997*)

scaling of transverse and vertical coordinates of these two models using Program MERGER.

The models were tested in the towing tank at the Berlin Model Basin which was 250 m long, 8 m wide, and 4.8 m deep. The models were fitted with turbulence stimulation studs set 83 mm back from the line of the bow, and all models were towed from the position of the longitudinal centre of gravity in line with the propeller shafts.

Kracht and Jacobsen (1992) presented the resistance results in the form of charts where the residuary resistance coefficient (C_R) was plotted against the Froude number. The residuary resistance coefficient C_R was calculated based on C_F being obtained from the ITTC'57 ship-model correlation line. The resistance curves presented by Kracht and Jacobsen (1992) were digitised with the resistance data formatted into a towing-tank data file for use in Program GENCAT.

7.2.5 Catamaran Model Series with Modified Prismatic Coefficient

Following the experimental investigation into catamaran resistance by Molland *et al.* (1994a), an extension was made to the series to investigate the effect of change in the prismatic coefficient (C_P). Molland and Lee (1997) tested further models based on the NPL parent model (100A), one with a substantial decrease in C_P and one with a substantial increase in C_P . The two new hullforms were tested both as monohulls and in catamaran configurations with demihull separation-to-length ratios (s/L) of 0.2, 0.3, 0.4, and 0.5. The principal particulars of the two models are presented in Table 7.8.

The model body plans were digitised, and the offsets formatted for input into Program HULLIN. The body plans of these two models are presented in Appendix A. The demihull spacing for each run was set in the input file for Program GENCAT.

The models were tested in the Southampton Institute test tank which had a length of 60 m, a breadth of 3.7 m and a water depth of 1.85 m. The models were fitted with turbulence stimulation studs 37.5 mm aft of the bow and the models were towed from a point situated at the longitudinal centre of gravity at a height of one-third of the draft above the keel. The resistance results were presented in charts as well as tabulated values for residuary resistance based on the ITTC 1957 ship-model correlation line. These tabulated values were formatted into a towing-tank data file for use by Program GENCAT in the regression analysis.

7.2.6 SKLAD Models

The SKLAD series is a series of semi-displacement ships that were tested by Gamulin (1996) at the Brodarski Institute in Zagreb, Croatia. The series, developed at the Brodarski Institute between 1972 and 1980, consists of 27 models covering three block coefficients C_B , three L/B ratios and three B/T ratios. A parent hullform was chosen for its known resistance characteristics (M-741). Three base hulls (including

Model	5d	5e	Units
L	1.6	1.6	m
$\frac{L}{B}$	11	11	
$\frac{B}{T}$	2	2	
$\frac{L}{\nabla^{1/3}}$	8.48	8.48	
C_P	0.653	0.733	
C_B	0.397	0.397	
C_X	0.608	0.542	
C_M	0.607	0.530	
C_W	0.756	0.770	
LCB	-6.4	-6.4	% fwd of ∇
S	0.272	0.270	m ²
$\frac{L}{S^{1/2}}$	3.07	3.08	
$\frac{S}{\nabla^{2/3}}$	7.63	7.58	
$\frac{TransomArea}{MidshipArea}$	0.472	0.597	

Table 7.8: An Extension of the University of Southampton Catamaran Model Series to Investigate the Effect of the Prismatic Coefficient (*Molland and Lee, 1997*)

the parent hull) were then used to form the remaining 24 hulls in the series. The derivation of the other hullforms is displayed in Table 7.9, where the scaling factors a_i are given below:

$$a_1 = 0.7631428$$

$$a_2 = 1.2114137$$

$$a_3 = 0.8254818$$

$$a_4 = 1.1603972$$

The body plans of the three parent hullforms, shown in Appendix A, were digitised and the offsets formatted for input into Program `HULLIN`. The remaining models in the series were then formed by scaling the parent hullforms using Program `MERGER`. The principal particulars of the whole series are shown in Table 7.10.

The resistance results were presented by Gamulin in the form of contours of the residuary resistance coefficient (C_R) plotted over grids of the length-to-beam ratio versus the block coefficient. These plots were produced at various beam-to-draft ratios and volumetric Froude numbers. The arrangement of the resistance data defied simple digitising and required manual interpolation of the residuary resistance coefficient at each intersection of the length-to-beam ratio and the block coefficient. The interpolated data was then sorted, converted to total resistance using the 1957 ITTC ship-model correlation line utilised by Gamulin in producing the published charts, and formatted for use in Program `GENCAT`.

7.2.7 de Groot Models

The resistance and propulsion of motor boats was investigated by de Groot (1955) at the Delft Institute of Technology. Motor boats are characterised as possessing lengths smaller than most seagoing merchant vessels and, hence, higher speed-length

Models		M742	M743	M744	M745	M746	M747	M748	M749
		M752	M753	M754	M755	M756	M757	M758	M759
		M762	M763	M764	M765	M766	M767	M768	M769
M741	L_{WL}	a_1	a_2	$a_3^{1/2}$	$a_4^{1/2}$				
M751	B_{WL}	$a_1^{-1/2}$	$a_2^{-1/2}$	$a_3^{1/2}$	$a_4^{1/2}$				
M761	T	$a_1^{-1/2}$	$a_2^{-1/2}$	a_3^{-1}	a_4^{-1}				
M742	L_{WL}					$a_3^{1/2}$	$a_4^{1/2}$		
M752	B_{WL}					$a_3^{1/2}$	$a_4^{1/2}$		
M762	T					a_3^{-1}	a_4^{-1}		
M743	L_{WL}							$a_3^{1/2}$	$a_4^{1/2}$
M753	B_{WL}							$a_3^{1/2}$	$a_4^{1/2}$
M753	B_{WL}							a_3^{-1}	a_4^{-1}

Table 7.9: Derivation of the SKLAD Model Series (*Gamulin, 1996*)

Note: The dimensions of the models in the columns were obtained by multiplying the particular characteristic of the model in the row by the appropriate coefficient. That is; L_{WL} for Model M742 was obtained by multiplying L_{WL} for Model M741 by the coefficient a_1 .

Model	L/B	B/T	C_B	$L/\nabla^{1/3}$	$S/\nabla^{2/3}$	L (m)	B (m)	T (m)
M741	6	4	0.45	6.844	7.260	4.196	0.699	0.174
M742	4	4	0.45	5.223	6.343	3.202	0.800	0.200
M743	8	4	0.45	8.291	7.991	5.083	0.635	0.158
M744	6	3	0.45	6.218	6.580	3.812	0.635	0.211
M745	6	5	0.45	7.373	7.983	4.520	0.753	0.150
M746	4	3	0.45	4.745	5.748	2.909	0.727	0.242
M747	4	5	0.45	5.626	6.974	3.449	0.862	0.172
M748	8	3	0.45	7.533	7.243	4.619	0.577	0.192
M749	8	5	0.45	8.932	8.787	5.475	0.684	0.136
M751	6	4	0.35	7.438	8.035	4.557	0.759	0.189
M752	4	4	0.35	5.676	7.019	3.477	0.869	0.217
M753	8	4	0.35	9.012	8.844	5.520	0.690	0.172
M754	6	3	0.35	6.758	7.288	4.140	0.690	0.230
M755	6	5	0.35	8.012	8.821	4.909	0.818	0.163
M756	4	3	0.35	5.157	6.366	3.159	0.789	0.263
M757	4	5	0.35	6.115	7.706	3.746	0.936	0.187
M758	8	3	0.35	8.187	8.021	5.015	0.626	0.208
M759	8	5	0.35	9.706	8.706	5.946	0.743	0.148
M761	6	4	0.55	6.392	6.784	3.919	0.653	0.163
M762	4	4	0.55	4.875	5.920	2.991	0.747	0.187
M763	8	4	0.55	7.739	7.459	4.748	0.593	0.148
M764	6	3	0.55	5.804	6.163	3.561	0.593	0.197
M765	6	5	0.55	6.882	7.432	4.222	0.703	0.140
M766	4	3	0.55	4.429	5.384	2.717	0.679	0.226
M767	4	5	0.55	5.252	6.493	3.222	0.805	0.161
M768	8	3	0.55	7.032	6.783	4.314	0.539	0.179
M769	8	3	0.55	8.337	8.180	5.114	0.639	0.127

Table 7.10: The Principal Particulars of the SKLAD Model Series Tested at the Brodarski Institute (*Gamulin, 1996*)

ratios (V/\sqrt{L}) or Froude numbers (F_{n_L}). In addition to collating resistance data for several V-form (planing) and U-form (displacement) motor boats, de Groot presented the resistance results of four models which he tested in the small model basin at the Delft Institute of Technology³ which, at the time of testing, had an overall length of 97 m⁴, a width of 4.2 m and a depth of 2.5 m.

The four models had a length of 4 ft (1.2192 m) and were tested at four different drafts (I, II, III, and IV). Some tests at the lightest displacement (draft IV) possessed trim by the bow and were disregarded in the research presented here. The principal particulars of the four models are presented in Table 7.11. The models were tested without turbulence stimulation with the towing force applied at point A (Figure 7.3). To investigate the influence of the point of application, de Groot conducted further tests with the towing force applied at point B (55 mm below A) and point C (160 mm above A). de Groot showed that, for speed-length ratios less than 2.5, the point of application of the towing force can be moved within the given limits without affecting the measured model resistance. For very fast models, when the speed-length ratio exceeds 2.5, it becomes necessary to apply the towing force as closely as possible to the corresponding position of the thrust block on the full scale vessel. de Groot calculated the frictional resistance using Schoenherr's (ATTC'47) ship-model correlation line with the wetted surface area estimated by means of the following formula:

$$S = 2.75\sqrt{\Delta \cdot L}$$

The body plan for the parent model 6-I (shown in Appendix A, Figure A.21) was digitised using the Seismic Solutions' Pocket Digitiser software which saves

³Test cases 4-I, 5-I, 6-I, and 7-I (Refer to Table 7.11) were conducted at the towing tank at the Netherlands Ship Model Basin which has an overall length of 253 m, width of 10.5 m and depth of 5.5 m.

⁴The length has since been extended to 142 m

Model	$\frac{\nabla}{(L/10)^3}$	C_{WP}	C_M	C_B	C_P	L/B	B/T	LCG/L_{BP} % fwd of \mathbb{O}
4-I	2.15	0.787	0.648	0.421	0.650	7.39	3.57	1.60
4-II	2.47	0.790	0.661	0.437	0.661	7.27	3.34	2.15
4-III	2.81	0.796	0.674	0.457	0.677	7.18	3.16	2.64
5-I	3.23	0.787	0.648	0.421	0.650	6.04	3.57	1.60
5-II	3.71	0.790	0.661	0.437	0.661	5.93	3.34	2.15
5-III	4.21	0.796	0.674	0.457	0.677	5.87	3.16	2.64
6-I	4.31	0.787	0.648	0.421	0.650	5.22	3.57	1.60
6-II	4.94	0.790	0.661	0.437	0.661	5.15	3.34	2.15
6-III	5.60	0.796	0.674	0.457	0.677	5.09	3.16	2.64
7-I	5.39	0.787	0.648	0.421	0.650	4.67	3.57	1.60
7-II	6.17	0.790	0.661	0.437	0.661	4.60	3.34	2.15
7-III	6.98	0.796	0.674	0.457	0.677	4.55	3.16	2.64

Table 7.11: The Principal Particulars of the de Groot Model Series Tested at the Delft Institute of Technology (*de Groot, 1956*)

the digitised points in spreadsheet format. The model offsets were then formatted for input into program **HULLIN**. The remaining three models were prepared using program **MERGER**. de Groot published the resistance results in the form of curves of the wave-making resistance; however, instead of digitising these charts to produced the towing-tank data file, the resistance results to be utilised by program **GENCAT** were collated from tabular data presented by Mercier and Savitsky (1973).

7.2.8 Series 63 Models

The calm-water performance of five round-bottom utility boats was tested in the towing tank at the Stevens Institute of Technology. The parent hullform (model

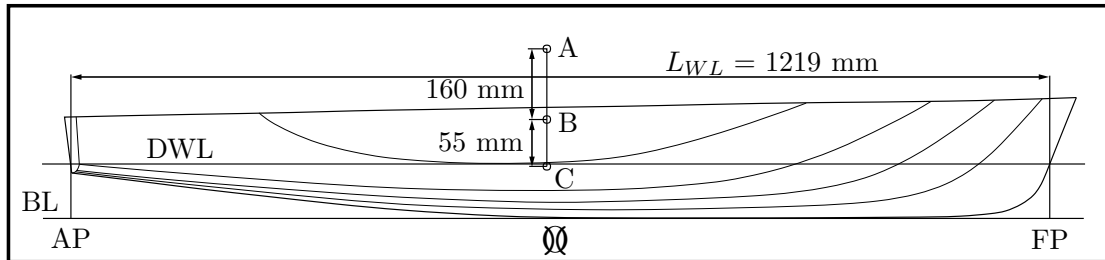


Figure 7.3: Profile of de Groot Model 6-I Showing the Towing Point A, and the Alternative Towing Points B and C (*de Groot, 1956*)

4777) was a 1/16 scale model of a 50 ft United States Navy utility-boat design which had a nominal length-to-beam ratio $(L/B)^5$ of 4. The other four models in the series had length-to-beam ratios of 2.5, 3.0, 5.0, and 6.0 for models 4778, 4779, 4780, and 4781 respectively. All of the five models were constructed to the same overall length, with each of the models in the series derived from the parent form by multiplying the waterline and buttock spacing of the parent by a constant. Accordingly, the body plans of the five models were all geometrically similar. Each of the five models was tested at various displacements corresponding to values of slenderness ratio $(L/\nabla^{1/3})$ equal to 4.5, 4.8, 5.15, 5.6 and 6.4. The principal particulars of the five models and the different conditions under which they were tested is presented in Table 7.12.

All the tests were run in Tank No.1 at the Davidson Laboratory which was 100 ft long, 9 ft wide and 4.5 ft deep. To induce turbulence stimulation, a wire strut (approximately 1 mm in diameter) was placed 127 mm forward of the forward perpendicular and to a depth equal to the draft of the model. Resistance results were presented by Beys (1963) with the frictional resistance calculated from Schoenherr's (ATTC'47) ship-model correlation line.

For use in the form-factor research, the body plan presented by Beys (1963) for

⁵Here the term L represents the length between perpendiculars and B the breadth to the No. 6 buttock line situated 84% of the distance from the centreline to the extreme beam at the gunwale.

Model	L_{BP} (m)	$10^3 \nabla$ (m ³)	$\frac{L_{WL}}{\nabla^{1/3}}$	$\frac{L_{WL}}{B_{WL}}$	$\frac{B_{WL}}{T}$	$\frac{S}{\nabla^{2/3}}$	C_B	C_P	LCG/L_{BP} % fwd of ∇
4781-I	3.0	3.087	6.40	5.75	4.34	7.02	0.549	0.740	5.43
4781-II	3.0	4.672	5.60	5.59	3.36	6.21	0.594	0.745	5.33
4781-III	3.0	6.116	5.15	5.48	2.89	5.83	0.636	0.774	5.80
4780-I	3.0	3.030	6.40	4.92	5.59	7.39	0.512	0.690	3.55
4780-II	3.0	4.616	5.60	4.78	4.39	6.38	0.571	0.701	4.22
4780-III	3.0	6.003	5.15	4.70	3.69	5.92	0.597	0.735	5.05
4780-IV	3.0	7.504	4.80	4.62	3.21	5.63	0.623	0.764	4.94
4777-I	3.0	3.002	6.40	4.10	7.14	8.21	0.462	0.647	3.11
4777-II	3.0	4.531	5.60	3.98	5.66	7.05	0.508	0.677	4.21
4777-III	3.0	5.862	5.15	3.86	4.88	6.43	0.530	0.695	4.65
4777-IV	3.0	7.362	4.80	3.81	4.24	5.95	0.560	0.712	4.31
4777-V	3.0	8.976	4.50	3.76	3.76	5.59	0.584	0.734	4.95
4779-I	3.0	2.917	6.40	3.31	9.50	9.64	0.393	0.591	0.00
4779-II	3.0	4.446	5.60	3.14	7.66	8.08	0.430	0.620	2.39
4779-III	3.0	5.748	5.15	3.05	6.84	7.23	0.466	0.639	3.34
4779-IV	3.0	7.136	4.80	2.99	6.18	6.64	0.499	0.659	4.38
4779-V	3.0	8.750	4.50	2.95	5.44	6.17	0.520	0.690	4.63
4778-II	3.0	4.276	5.60	2.70	9.20	8.66	0.383	0.577	-0.30
4778-III	3.0	5.635	5.15	2.63	8.19	7.92	0.412	0.601	2.39
4778-IV	3.0	7.051	4.80	2.57	7.33	7.35	0.435	0.613	2.75
4778-V	3.0	8.637	4.50	2.52	6.64	6.80	0.464	0.642	3.40

Table 7.12: The Principal Particulars of the Series 63 Model Series Tested at the Davidson Laboratory (*Beys, 1963*)

the parent model was digitised using the Seismic Solutions' Pocket Digitiser software, with the model offsets formatted for input into program `HULLIN`. The remaining four models in the series were prepared using program `MERGER`. The resistance curves presented were also digitised for utilisation by program `GENCAT` in the form-factor regression.

7.2.9 Series 64 Models

In the interest of providing the United States Navy with resistance data for conventional hullforms with speed-length ratios greater than 2.0, a series of 27 models were tested at the David Taylor Model Basin (DTMB). The models in the series possessed a block coefficient of either 0.35, 0.45, or 0.55. The body plans of the three parent hullforms are presented in Appendix A with the principal particulars of the 27 models given in Table 7.13. All of the models were constructed to be 10 ft long at the design waterline. The tests were conducted in the DTMB deep water basin⁶ with each of the models towed from the centre of flotation (Yeh, 1965). The models were free to pitch, heave, and roll but were restricted in yaw with the resistance tests conducted without turbulence stimulation. The resistance results were presented in the form of residuary resistance with the frictional resistance calculated using Schoenherr's (ATTC'47) ship-model correlation line.

The three parent models were digitised using the Seismic Solutions' Pocket Digitiser software, with the parent hullforms modified in program `MERGER` to produce the remainder of the model series. The resistance curves presented were also digitised for utilisation by program `GENCAT` in the form-factor regression.

⁶The deep water basin at the David Taylor Model Basin has a length of 1886 ft, width of 51 ft and depth of 22 ft.

Model	$\frac{\Delta}{(0.01L_{WL})^3}$	$\frac{L_{WL}}{B_{WL}}$	$\frac{B_{WL}}{T}$	B_{WL} (m)	T (m)	$10^3 S$ (m ²)	C_B	C_M
4787	55	11.956	2	0.2549	0.1275	7.315	0.55	0.873
4788	40	14.020	2	0.2174	0.1087	6.265	0.55	0.873
4789	25	17.734	2	0.1719	0.0860	4.954	0.55	0.873
4790	55	9.762	3	0.3122	0.1041	7.421	0.55	0.873
4791	40	11.447	3	0.2663	0.0888	6.328	0.55	0.873
4792	25	14.479	3	0.2105	0.0702	5.003	0.55	0.873
4793	55	8.454	4	0.3605	0.0901	7.679	0.55	0.873
4794	40	9.914	4	0.3074	0.0769	6.549	0.55	0.873
4795	25	12.540	4	0.2431	0.0608	5.177	0.55	0.873
4796	45	11.956	2	0.2549	0.1275	6.717	0.45	0.714
4797	32.5	14.069	2	0.2166	0.1083	5.708	0.45	0.714
4798	20	17.934	2	0.1700	0.0850	4.478	0.45	0.714
4799	45	9.762	3	0.3122	0.1041	6.849	0.45	0.714
4800	32.5	11.487	3	0.2653	0.0885	5.821	0.45	0.714
4801	20	14.643	3	0.2082	0.0694	4.566	0.45	0.714
4802	45	8.454	4	0.3605	0.0901	7.167	0.45	0.714
4803	32.5	9.948	4	0.3064	0.0766	6.091	0.45	0.714
4804	20	12.682	4	0.2403	0.0601	4.778	0.45	0.714
4805	35	11.956	2	0.2549	0.1275	6.392	0.35	0.556
4806	25	14.146	2	0.2155	0.1077	5.402	0.35	0.556
4807	15	18.264	2	0.1669	0.0834	4.185	0.35	0.556
4808	35	9.762	3	0.3122	0.1041	6.509	0.35	0.556
4809	25	11.551	3	0.2639	0.0880	5.501	0.35	0.556
4810	15	14.913	3	0.2044	0.0681	4.261	0.35	0.556
4811	35	8.454	4	0.3605	0.0901	6.867	0.35	0.556
4812	25	10.004	4	0.3047	0.0762	5.804	0.35	0.556
4813	15	12.915	4	0.2360	0.0590	4.495	0.35	0.556

Table 7.13: The Principal Particulars of the Series 64 Model Series Tested at the David Taylor Model Basin (*Yeh, 1965*)

Model	$\frac{L_{WL}}{\nabla^{1/3}}$	$\frac{B_{WL}}{T}$	$\frac{L_{BP}}{(\text{m})}$	$B_{WL} \text{ (m)}$	$T \text{ (m)}$	$\frac{S}{\sqrt{\nabla \cdot L_{BP}}}$
1209-A	6	4.0	3.306	0.7152	0.1788	3.00
1210-A	7	4.0	3.857	0.6621	0.1655	3.00
1211-A	8	4.0	4.408	0.6193	0.1548	3.00
1212-A	6	3.5	3.306	0.6690	0.1911	2.94
1213-A	7	3.5	3.857	0.6194	0.1770	2.94
1214-A	8	3.5	4.408	0.5794	0.1655	2.94
1215-A	6	3.0	3.306	0.6194	0.2065	2.90
1216-A	7	3.0	3.857	0.5734	0.1911	2.90
1217-A	8	3.0	4.408	0.5367	0.1788	2.90

Table 7.14: The Principal Particulars of the SSPA Model Series Tested at the Swedish State Shipbuilding Experimental Tank in Göteborg (*Lindgren and Williams, 1968*)

7.2.10 SSPA Models

In connection with design studies for fast naval vessels of 150 to 200 tons displacement, a series of models were developed at the Swedish State Shipbuilding experimental tank (SSPA) in close cooperation with the Royal Swedish Naval Administration (Lindgren and Williams, 1968). To investigate the influence of beam-to-draft ratio and length-to-displacement ratio, nine hullforms were designed with the block coefficient, maximum sectional area coefficient and longitudinal centre of buoyancy kept constant. The principal particulars of the model series are presented in Table 7.14.

All of the models were constructed in paraffin wax with timber decks located so that the freeboard corresponding to that of the full-scale ship was realised. A tripwire 1 mm in diameter was attached to the models around station 9 (see Appendix A for the body plan of the parent model) to ensure turbulent flow along the hull surface.

The tests were carried out at the SSPA towing tank which was 240 m long and had a width and depth of 10 m and 5 m respectively. The towing force for all test cases was applied horizontally to the models. The resistance results, which were collated for use in the form-factor regression analysis, were presented by Lindgren and Williams (1968) in the form of charts of the residuary resistance coefficient as a function of the Froude number. Extrapolation to the full-scale ship was performed by use of the ITTC 1957 ship-model correlation line.

7.2.11 AMECRC Models

To provide a comparative study on resistance of high-speed round-bilge hull forms using computational fluid dynamics (CFD) techniques, theoretical analysis and experimental results, Sahoo *et al.* (1999) conducted calm water resistance tests on a systematic series of 14 high-speed round-bilge displacement hullforms. The body plans of all 14 models in the AMECRC model series are presented in Appendix A

Model	L/B	B/T	C_B	Δ (kg)	$L/\nabla^{1/3}$
1	8	4	0.396	6.321	8.653
2	6.512	3.51	0.395	11.455	7.098
3	8	2.5	0.447	11.454	7.098
4	8	4	0.447	7.158	8.302
5	4	4	0.395	25.344	5.447
6	8	2.5	0.395	10.123	7.396
7	4	2.5	0.396	40.523	4.658
8	4	2.5	0.5	51.197	4.308
9	8	2.5	0.5	12.804	6.839
10	8	4	0.5	8.002	7.998
11	4	4	0.5	32.006	5.039
12	8	3.25	0.497	9.846	7.464
13	6	3.25	0.45	15.784	6.379
14	6	4	0.5	14.204	6.606

Table 7.15: Principal Particulars of the AMECRC Model Series Tested at the Australian Maritime College in Launceston (*Sahoo et al., 1999*)

with the principal particulars of the models listed in Table 7.15.

The towing-tank data file, for use in Program **GENCAT**, containing the resistance, sinkage and trim results from the AMECRC experiments was obtained courtesy of Doctors.

7.2.12 Nova Models

To supplement an existing systematic series of transom-stern models, five systematic hullforms⁷ suited to operation in the shallow Finnish archipelago were designed and tested at the VTT Ship Laboratory Technology Research Centre on Finland (Lahtiharju *et al.*, 1991). The NOVA series of models were developed based on the NPL parent model. The principal particulars of the four round-bilge models are presented in Table 7.16 with the body plan of the parent model given in Appendix A.

The wooden models were fitted with turbulence stimulation studs in the bow to ensure turbulent flow over the hull surface. Each of the four models were tested at various displacements with the draft corresponding to each of these test cases presented in Table 7.17. Lahtiharju *et al.* (1991) published the resistance results in the form of curves of the total resistance coefficient; however, instead of digitising these charts to produced the towing-tank data file, the resistance results were collated from the tabular data presented by Mercier and Savitsky (1973).

7.2.13 Compton Models

As a contribution to the Naval Sea Systems Command Norfolk Detachmen the staff of the Naval Academy Hydromechanics Laboratory (NAHL) performed a series of experiments involving a systematically varied set of hullforms representing medium-speed, transom-stern, high displacement-length ratio, low length-beam ratio, coastal patrol craft (Compton, 1986). The body plans of the three models tested are presented in Appendix A with the principal particulars of the three models presented in Table 7.18. The models were tested at three different displacement-length ratios with the drafts corresponding to these conditions presented in Table 7.19.

⁷As the form-factor regression utilises the geometric parameters of the vessels, planing hulls (whose waterline length changes throughout the speed range) could not be used. Hence, only the four round-bilge NOVA models were utilized in the research presented here.

Model	NOVA-I	NOVA-II	NOVA-III	NOVA-IV	Units
$L/\nabla^{1/3}$	6.586	6.586	6.586	6.586	
L_{WL}/B_{WL}	5.41	4.55	5.41	6.25	
B_{WL}/T	4.39	6.90	5.37	4.39	
L_{WL}	0.28	0.28	0.28	0.28	m
B_{WL}	0.5176	0.6154	0.5176	0.4480	m
T	0.1178	0.0892	0.0964	0.1021	m
$10^2 \nabla$	7.683	7.683	7.683	7.683	m ³
S	1.343	1.492	1.365	1.279	m ²
C_B	0.45	0.50	0.55	0.60	
C_M	0.6494	0.7214	0.7937	0.8658	

Table 7.16: The Principal Particulars of the NOVA Model Series Tested at the VTT Ship Laboratory Technology Research Center of Finland (*Lahtiharju et al., 1991*)

Δ_i % of Δ_{DWL}	Draft T_i (m) corresponding to Displacement Δ_i for NOVA Models			
	NOVA-I	NOVA-II	NOVA-III	NOVA-IV
75	0.1002	0.07591	0.08204	0.08689
80	0.1039	0.07865	0.08500	0.09002
85	0.1074	0.08135	0.08792	0.09311
90	0.1109	0.08401	0.09079	0.09616
95	0.1144	0.08664	0.09364	0.09917
100	0.1178	0.08920	0.09640	0.1021
105	0.1212	0.09181	0.09922	0.1051
110	0.1246	0.09435	0.1020	0.1080
115	0.1279	0.09687	0.1047	0.1109
120	0.1312	0.09937	0.1074	0.1137
125	0.1345	0.1018	0.1101	0.1166
130	0.1377	0.1043	0.1127	0.1194
135	0.1410	0.1067	0.1154	0.1222
140	0.1442	0.1092	0.1180	0.1249
145	0.1473	0.1116	0.1206	0.1277

Table 7.17: Drafts T_i Corresponding to the Displacement Δ_i as a Percentage of the Displacement of the Nova Models at their Design Draft Δ_{DWL}

Model	$\frac{L_{PP}}{B_{REF}}$	$\frac{B_{REF}}{T}$	L_{PP} (m)	$\frac{S}{\sqrt{\nabla} \cdot L_{BP}}$	$\frac{\Delta_i}{(0.01L_{BP})^3}$	C_B	C_P
YP81-1	4.59	3.84	1.524	6.695	154.7	0.437	0.720
YP81-2	3.97	5.05	1.524	7.222	155.2	0.432	0.724
YP81-3	5.17	3.06	1.524	6.412	151.0	0.432	0.716

Table 7.18: The Principal Particulars of the Systematic Series of Semiplaning Transom-Stern Hulls Tested by Compton at the U.S. Naval Academy Hydromechanics Laboratory (*Compton, 1986*)

The resistance results of the model series were presented by Compton (1986) in the form of residuary resistance curves as a function of the Froude number. The presented resistance curves were digitised and collated into a towing-tank data file for use in the form-factor regression analysis.

Draft No.	Δ_i $(0.01L_{BP})^3$	Draft T_i corresponding to Displacement-Length Ratio for Compton Models		
		YP81-1	YP81-2	YP81-3
1	104.2	0.079	-	-
2	125.2	0.059	-	-
3	145.9	0.039	-	-
1	102.7	-	0.069	-
2	124.2	-	0.049	-
3	146.6	-	0.029	-
1	110	-	-	0.089
2	130	-	-	0.069
3	150	-	-	0.049

Table 7.19: Drafts T_i Corresponding to the Displacement-Length Ratio Tested for each of the Compton (1986) Models

7.3 Methods

The large database of collated model resistance results were formatted for use in program **GENCAT**. This required digitising the parent hullforms and arranging the digitised offsets in the correct format for use by program **HULLIN**. Before using program **GENCAT** to perform any regression analysis, program **LOADER** was used to verify the principal particulars of each of the entered models against the published values.

The main objective of the regression analysis was to produce a set of form factors for both wave-making resistance and frictional resistance that pertain to a wide range of high-speed transom-stern vessels. Hence, the initial approach in the regression analysis was to run the whole database of 325 models together in a single run. The resulting output file from program **GENCAT** presents the calculated resistance results based on the underlying theory with no form factors applied for each of the 325 models. Also presented are the overall form coefficients calculated from the regression of the entire database. To obtain the resistance results with the form coefficients applied and, hence, determine the reduction in root-mean-square error between theory and experiment, the database of models needed to be run through **GENCAT** a second time with the form coefficients entered as additional input. One of the alterations made to the original coding in the **HYDROS** suite of programs (Section 6.2.3) enabled the user to change the geometric functions to be used in the regression. Up to 16 geometric functions can be used in the one regression, resulting in a large matrix of possible combinations.

The methodology chosen in optimising or maximising the reduction in root-mean-square error was to start by applying each of the geometric functions individually in a regression analysis to establish which geometric functions produced the largest reduction in root-mean-square error. Forty geometric functions were used in this approach all of which are shown in Table 7.20. The geometric function producing the most favourable result was then systematically paired with each of the other geo-

1	B/L	C_P	$S/\nabla^{2/3}$	F
C_B	$(B/L)^2$	$(C_P)^2$	$(S/\nabla^{2/3})^2$	F^2
$(C_B)^2$	$(B/L) \cdot F$	$C_P \cdot F$	$S/\nabla^{2/3} \cdot F$	$L/\nabla^{1/3}$
$C_B \cdot F$	$(B/L)^2 \cdot F$	$(C_P)^2 \cdot F$	$(S/\nabla^{2/3})^2 \cdot F$	$(L/\nabla^{1/3})^2$
$(C_B)^2 \cdot F$	B/T	C_{VP}	C_M	$L/\nabla^{1/3} \cdot F$
$C_B(B/L)(L/s)$	$(B/T)^2$	C_{VP}^2	C_M^2	$[L/\nabla^{1/3}]^2 \cdot F$
$[C_B(B/L)(L/s)]^2$	$B/T \cdot F$	$C_{VP} \cdot F$	$C_M \cdot F$	$L/\nabla^{1/3} \cdot B/T$
$[C_B(B/L)(L/s)] \cdot F$	$(B/T)^2 \cdot F$	$C_{VP}^2 \cdot F$	$C_M^2 \cdot F$	$[L/\nabla^{1/3} \cdot B/T]^2$

Table 7.20: Summary of all the Geometric Functions Investigated in the Optimisation Process with the Final 15 Highlighted and Presented in Table 7.21

metric functions in further regression analyses. Then the pair of functions producing the most favourable result were systematically combined with each of the other geometric functions in further regression analyses and so on until the combination of 15 functions giving the most favourable result was determined. As well as detailing the overall root-mean-square error, **GENCAT** details the minimum, mean and maximum form factors obtained from the database when the form coefficients are applied to each model. Ideally, the range between the minimum and maximum values of form factors would be small, so at the end of each successive series of regression analyses the results were compared to find the combination of geometric functions producing not only the largest reduction in root-mean-square error but also the smallest range of form factors. Using this methodology, the overall improvement in resistance prediction was maximised through systematic optimisation of the geometric functions used in the regression.

7.4 Results

In optimising the reduction in root-mean-square error regression analyses were conducted where the geometric functions were applied to the database of models individually. This was to establish which geometric functions produced the largest reduction in root-mean-square error. From these initial regression analyses it became apparent that the geometric functions having the most benefit in reduction of root-mean-square error were the prismatic coefficient, the beam-to-length ratio and the spacing-to-length ratio which provided significant improvements due to the fact that it took account of the catamaran models in the database.

Using the methodology described in Section 7.3 the geometric function providing the greatest benefit was then systematically applied in combination with a second geometric function until the best combination of two geometric functions was determined. In this way the optimum combination of 15 geometric functions⁸ was established. Over 1000 batch runs were performed in optimizing the improvements in root-mean-square error, the results of which are the final form factors presented in Table 7.21. When applied retrospectively to the entire database of 325 models, the root-mean-square error of specific resistance between theory and experiment was reduced by an average of 35.7% over linear thin-ship theory. This is a considerable reduction in error and indicates the value in applying form factors in the manner proposed by Doctors and Day (1997).

Further regression analyses were performed where, instead of running the entire database through program **GENCAT**, each of the series were processed individually. Hence, for the model series possessing a form quite different to the majority of models in the database and, where the benefit from the overall form factors was marginal or no benefit was experienced, the individual series form factors provide a valuable alternative.

⁸Of the final 15 functions presented in Table 7.21 14 are geometric functions with the first being a constant represented in the Table by a 1.

f_i	$a_{W,i}$	$a_{F,i}$
1	-3.609	5.166
B/L	11.080	-0.532
B/T	-0.136	-0.005
$C_B^2 \cdot F_{n_L}$	-1.035	2.301
$C_B(B/L)(L/s)$	-1.925	3.394
C_{VP}	-4.158	2.140
C_M	2.084	-2.129
$S/\nabla^{2/3}$	0.660	-0.633
$(S/\nabla^{2/3})^2$	-0.036	0.041
$(B/L)^2$	-15.920	0.059
C_P^2	0.846	-1.594
$[C_B(B/L)(L/s)]^2$	15.420	-16.590
$(L/\nabla^{1/3})^2$	0.007	-0.004
C_{VP}^2	3.171	-0.704
$C_M \cdot F_{n_L}$	-0.187	-0.553
f_W	0.711	
f_F		1.360

Table 7.21: Final Form Factor Coefficients $a_{F,i}$ and $a_{W,i}$ and the final form factors f_F and f_W

Table 7.22 presents the form coefficients for frictional resistance, series by series, with the frictional resistance form factor f_F also given. The form coefficients and form factor for wave-making resistance are given in Table 7.23. The resulting reduction in root-mean-square error achieved, when the series form factors are applied retrospectively to the models in that series, is presented in Table 7.24 along with the root-mean-square error when no form factors are applied, and when the overall form factors presented in Table 7.21 are applied to each series individually. Table 7.24 provides an excellent reference for designers whose vessel's form is very similar to any of the individual series. The benefit of the overall form-factors over using no form factors at all can be seen series-by-series and, where the benefit is little or none, the individual series form factors can be utilised instead should the vessel's form be similar.

	1	$\frac{B}{L}$	$\frac{B}{T}$	C_P	C_B	F_{nL}	$\frac{L}{\nabla^{1/3}}$	C_{VP}	$C_B(\frac{B}{L})(\frac{L}{s})$	$(\frac{B}{L})^2$	$(\frac{B}{T})^2$	F_{nL}^2	$(\frac{L}{\nabla^{1/3}})^2$	f_F
Lego	-15.39	40.48	-	1.71	-	-	-5.70	2.71	-	-27.28	-	-0.12	4.01	1.068
Cat. ¹	2.99	-12.86	-0.38	-	0.67	-	-2.69	0.01	-	53.44	0.12	-	1.951	1.347
NPL	-80.36	-2.63	0.02	163.10	-	-13.12	0.69	0.16	-51.57	-	-	-	-	0.112
D-Series	97.10	-382.60	7.48	78.45	-	-220.40	-2.63	-12.74	130.10	-	-	-	-	0.798
Cat. ²	-0.01	-40.63	1.22	1.32	0.80	0.93	0.13	-0.03	2.62	-	-	-	-	1.229
SKLAD	201.40	22.37	-0.42	-232.70	-	908.80	0.18	0.47	-784.20	-	-	-	-	1.832
de Groot	167.40	-66.43	-	-106.30	-	-	-19.10	-17.97	-	-177.70	-	0.97	15.49	1.491
Series 63	-201.30	-17.73	7.06	215.90	-	-33.17	-1.14	-0.22	62.52	-	-	-	-	-0.129
Series 64	0.92	4.35	0.01	-	-	-	-0.51	0.03	-	-13.27	-0.01	-	0.22	1.218
SSPA	-15.27	98.09	-1.79	-	-	-	-2.19	1.45	-	-141.60	0.11	-	2.20	1.598
AMECRC	-1.92	3.18	-0.13	0.08	-	110.00	-0.40	0.23	-84.39	-	-	-	-	1.343
NOVA	14.22	-16.93	0.25	-4.01	-	11.53	-1.08	-0.49	-16.77	-	-	-	-	0.994
Compton	-8.61	27.21	-0.39	0.36	-	-13.69	0.88	0.67	10.45	-	-	-	-	0.415
¹ University of Southampton Catamaran Series														
² University of Southampton C_P Modified Catamaran Series														

Table 7.22: Frictional-Resistance Form-Coefficients ($a_{F,i}$) and Form Factor (f_F) for Each Model Series Generated by Regression of Each Model Series Individually

	1	$\frac{B}{L}$	$\frac{B}{T}$	C_P	C_B	F_{nL}	$\frac{L}{\nabla^{1/3}}$	$C_B(\frac{B}{L})(\frac{L}{s})$	$(\frac{B}{L})^2$	$(\frac{B}{T})^2$	F_{nL}^2	$(\frac{L}{\nabla^{1/3}})^2$	f_W
Lego	31.58	-123.60	-	-5.79	-	-	7.36	-	211.90	-	0.12	-4.55	0.833
Cat. ¹	-1.88	11.25	0.18	-	0.45	-	5.68	-	-42.47	-0.09	-	-4.08	0.801
NPL	29.44	-2.13	0.08	-53.86	-	16.15	0.43	4.61	-	-	-	-	1.305
D-Series	-45.71	167.90	-3.43	-31.03	-	96.08	1.60	-55.09	-	-	-	-	0.973
Cat. ²	-4.37	22.82	-0.43	1.84	-0.12	-13.16	0.14	12.64	-	-	-	-	0.773
SKLAD	-42.48	-3.35	-0.08	47.55	-	-199.30	-0.73	175.90	-	-	-	-	0.316
de Groot	-98.13	56.99	-	65.08	-	-	7.75	-	60.84	-	-0.53	-6.49	0.924
Series 63	38.24	-3.56	-1.63	-9.28	-	-40.88	1.05	2.15	-	-	-	-	1.155
Series 64	2.00	-12.95	-0.17	-	-	-	0.99	-	68.94	0.03	-	-0.02	0.746
SSPA	8.41	-46.64	0.16	-	-	-	4.90	-	80.26	0.02	-	-4.58	0.538
AMECRC	-21.94	-13.64	0.35	50.60	-	-196.00	0.33	150.70	-	-	-	-	0.631
NOVA	-23.96	5.40	-0.08	41.68	-	12.17	1.37	-25.30	-	-	-	-	1.151
Compton	14.38	-28.82	0.57	-18.65	-	28.90	1.50	-18.34	-	-	-	-	2.945
¹ University of Southampton Catamaran Series													
² University of Southampton C_P Modified Catamaran Series													

Table 7.23: Wave-Making-Resistance Form-Coefficients ($a_{W,i}$) and Form Factor (f_W) for Each Model Series Generated by Regression of Each Model Series Individually

Model Series	Average Root Mean Square Error in R_T/W Prediction		
	No Form Factors	Overall Form Factors	Series Form Factors
Lego Model Series	7.741×10^{-3}	8.032×10^{-3}	3.162×10^{-3}
Uni. of Southampton Catamaran Series	1.664×10^{-2}	4.623×10^{-3}	3.767×10^{-3}
National Physical Laboratory Series	1.477×10^{-2}	1.238×10^{-2}	7.738×10^{-3}
D-Series Models	4.607×10^{-3}	4.055×10^{-3}	2.594×10^{-3}
Uni. of Southampton C_P Modified	1.003×10^{-2}	5.739×10^{-3}	4.034×10^{-3}
SKLAD Model Series	1.609×10^{-2}	1.432×10^{-2}	8.383×10^{-3}
de Groot Model Series	5.601×10^{-3}	1.080×10^{-2}	2.161×10^{-3}
Series 63 Models	2.224×10^{-2}	1.097×10^{-2}	6.923×10^{-3}
Series 64 Models	2.868×10^{-2}	6.804×10^{-3}	4.403×10^{-3}
SSPA Model Series	1.738×10^{-3}	3.533×10^{-3}	8.254×10^{-4}
AMECRC Model Series	7.710×10^{-3}	6.699×10^{-3}	4.606×10^{-3}
NOVA Model Series	1.029×10^{-2}	1.048×10^{-2}	5.034×10^{-3}
Compton Model Series	3.048×10^{-2}	2.098×10^{-2}	3.666×10^{-3}

Table 7.24: Average Reduction in Root Mean Square Error Series-by-Series Using Overall Form Factors Detailed in Table 7.21 and Series Based Form Factors detailed in Table 7.22 and Table 7.23

7.5 Discussion

The aim of this research was to produce a set of form factors based on a large database of high-speed transom-stern models such that the form factors will have a wide range of applicability. With such a large database of models of varying forms there is no avoiding the calculated form factors producing a negative impact on root-mean-square error for some of the models in the database. The real attribute of the form-factor method proposed by Doctors and Day (1997) is the use of geometric particulars which greatly increases the number of models for which the form factors produce positive results. This is due to the fact that the final form-factors for each vessel differ according to the vessel's form. However, as discussed, a small minority of vessels in the database did experience slight increases in error due to the vessels' hullforms. For this reason, further regression analyses were performed where, instead of running the entire database through program *GENCAT*, each of the series were processed individually.

Overall the final form-factors produced in the research presented here provide significant improvements in correlation between theoretical and experimental predictions of total resistance for high-speed transom-stern vessels. The vessels for which the benefit of the overall form factors is not significant can easily be identified from the results presented and accordingly the individual form factors applied. The reduction in root-mean-square and associated improvements in correlation between theory and experiment ensure that the designer can use the theoretical methods presented with confidence early in the design process.

The form-factor method was applied here specifically to high-speed transom-stern vessels; however, future work could be invested, and similar benefit achieved, in application of these methods to a database of resistance data for other vessel hullforms. Indeed, the improvements in correlation between theory and experiment could be substantial when the form-factor method is applied to fuller form vessels such as tankers and bulk carriers.

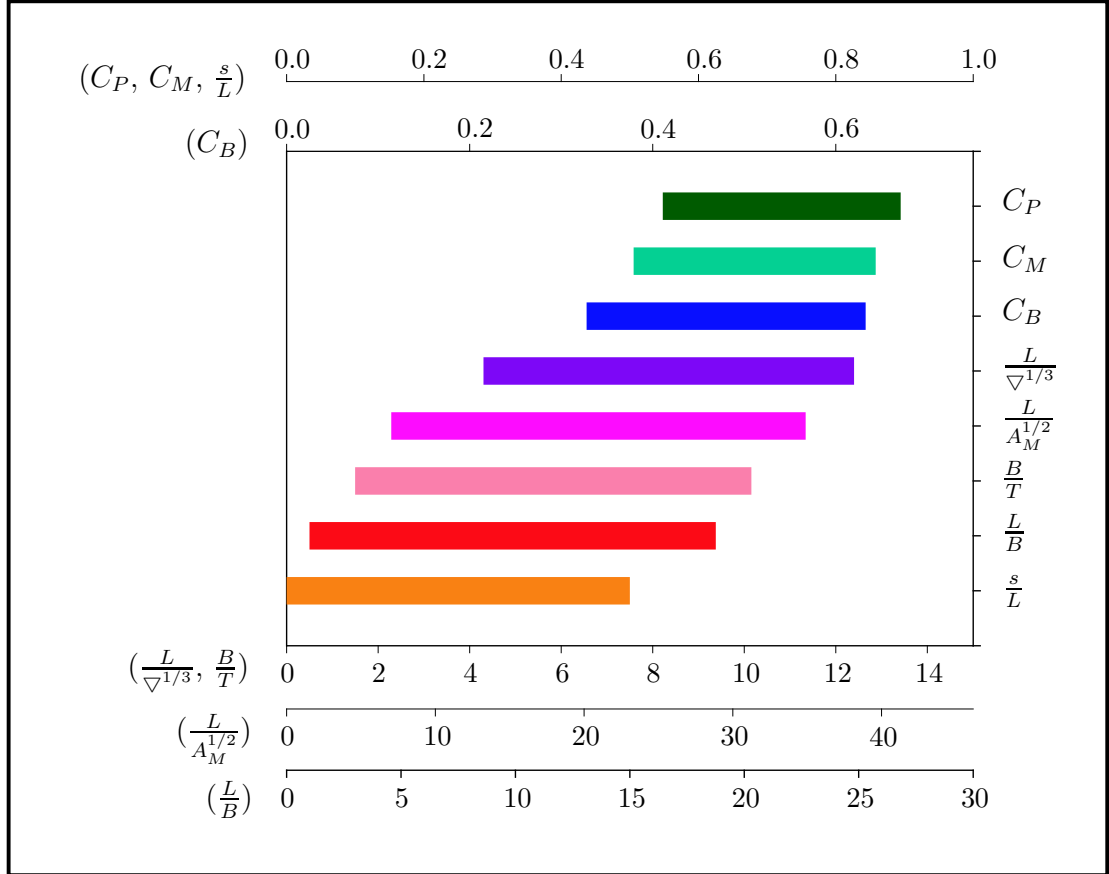


Figure 7.4: The Limits of Applicability of the Form Factors Presented in Table 7.21 Based on the Range of the Geometric Parameters of the Models used in the Regression Analyses. For Example of all the Models used in the Regression Analyses $0.328 \leq C_B \leq 0.633$ and $1.498 \leq B/T \leq 10.15$

Chapter 8

Concluding Remarks

To improve the accuracy of resistance prediction for high-speed transom-stern vessels using linearized theory, a two-fold approach was taken including experimental, computational analysis.

The major part of the research involved an investigation into the hydrodynamics governing the flow past a transom stern and, particularly, the geometric parameters of a vessel which have the greatest influence on the nature of this flow. The assumption was made that the beam and draft of the vessel would be the main geometric influences on the hydrodynamics of the transom stern, and it was ultimately desired to establish a relationship between the shape of the transom hollow and a vessel's speed, beam and draft. To this end, an extensive experimental programme was undertaken whereby a systematic series of transom-stern models was tank tested with a specially-manufactured experimental rig designed to measure the shape of the hollow in the water behind the transom. The systematic series of hollow models was tested at several drafts in such a way that the matrix of beam-to-draft ratios resulted in several test cases being exact geosims. This provided an additional means for checking the repeatability of the experimental results when the measured profiles for these geosim cases were non-dimensionalised by the static draft at a given draft Froude number. The close comparison of the non-dimensionalised geosim cases at

a given draft Froude number indicated that the Reynolds number is not a major driving factor influencing the hydrodynamics of the transom hollow.

Due to the fact that it is a common approach in numerical resistance prediction to discretize the transom hollow as a geometrically-smooth addition to the vessel, great value can be obtained through greater knowledge of the hydrodynamics of the transom hollow. To this end, the results from the transom-hollow experiments were used to produce prediction algorithms for the length of the hollow and the hydrodynamic draft, taking into account the beam, draft and speed of the vessel. These algorithms were then programmed back into the HYDROS suite of programs for prediction of the hollow shape in the discretisation of the model hullforms. As the hollow models from which the algorithms were generated were limited to a beam-to-draft ratio of 4, the new hollow-prediction algorithms were not used in the regression of the entire database of collected model data. However, the algorithms were applied in the prediction of resistance of the parent model from the University of Southampton series and the results indicated that the use of the hyperbolic tangent function for the prediction of hydrodynamic draft given in Equation 5.8, coupled with the polynomial algorithm for the prediction of hollow length given in Equation 4.9, produced a 42% reduction in root-mean-square error in specific resistance between theory and experiment.

The exponential hollow length algorithm given in Equation 5.9 has been shown to have other application to industry, with the naval architects at Blue Water Designs in Sydney using this algorithm to design a container ship for maximum cargo-carrying capacity without the flow in the tunnel separating.

Secondly, the ideas of Doctors and Day (1997) were investigated whereby the resistance prediction based on the traditional linearized wave-resistance theory was improved upon by the application of form factors. Doctors and Day proposed the idea of creating the form factors based on the major geometric particulars of the models used in the regression. The method had been applied to a single series of

model data with favourable results. However, as the form factors are dependant on the geometric parameters of the models from which they are calculated, their application is restricted to vessels of a very similar form. In the research presented here, the method was applied to a large database of various high-speed displacement transom-stern model data, resulting in a set of form factors providing improved resistance predictions but with a much wider application.

Initially, a study was undertaken to determine the most influential geometric parameters with respect to the magnitude of a vessel's total resistance. This study was conducted by calculating form factors for a random selection of models based on a single geometric parameter at a time. The resulting form factors were then used in correlating the theoretical and experimental results for the set of models used in the study and ranked according to the improvements made in correlation. The study revealed that the prismatic coefficient and the beam-to-length ratio are two of the more influential geometric parameters in the regression analysis. The final form factors determined from the entire database of models were based on 15 geometric parameters, and resulted in a root-mean-square error reduction in correlation between theory and experiment of 35.7% when applied to the 325 models in the database. Due to the assumptions made by the linearized theory and the fact that non-viscous effects are not accounted for, the linearized theory generally over predicts (depending on vessel form) the resistance calculated by experimental means. Therefore, the improved correlation provided by the application of the calculated form factors could represent significant savings in enabling better powering predictions early in the design stage.

The form factors determined from the presented research were determined from experimental data of high-speed displacement-type models, and are essentially restricted in their application to this form of vessel. However, the method could equally be applied to vessels of other forms such as bulk carriers, liners, container vessels and tankers. Theoretical resistance prediction is based on ship-model correlation

lines calculated from experiments on flat plates, and a linearized wave-resistance formulation which assumes a thin hull form. The form-factor approach takes account of these shortcomings in the basic theoretical approach. Therefore, arguably, even greater improvements could be realised in applying form factors to these fuller hullforms.

The large database of bodyplans, model particulars, and resistance results provide an excellent reference to the high-speed vessel designer. In addition, the hollow prediction algorithms, along with the geometric-based form-factors for frictional and wave-making resistance, provide great improvements in correlation between theory and experiment enabling the designer to use theoretical resistance prediction with greater confidence early in the design process.

Bibliography

- BAILEY, D. (1976), *The NPL High-Speed Round-Bilge Displacement Hull Series*, Technical Report, The Royal Institution of Naval Architects.
- BATCHELOR, G. (1959), “A proposal concerning wakes behind bluff bodies at large Reynolds numbers.”, *Journal of Fluid Mechanics*, Vol. 6, pp. 547–567.
- BERNOULLI, D. (1738), *Hydrodynamica, sive, De viribus et motibus fluidorum commentarii*, Sumptibus Johannis Reinholdi Dulseckeri, typis Joh. Henr. Deckeri, Typographi Basiliensis, Argentorati.
- BEYS, P.M. (1963), “Series 63: Round Bottom Boats”, *Davidson Laboratory Report No. 949*, Stephenson Institute of Technology, Hoboken, April.
- COMPTON, R. H. (1986), “Resistance of s Systematic Series of Semiplaning Transom-Stern Hulls”, *Marine Technology*, Vol. 23, No. 4, Society of Naval Architects and Marine Engineers, New York, October.
- CORDIER, S. AND DUMEZ, F.X. (1993), “Scale Effects on the Resistance Components of a High-Speed Semi-Displacement Craft”, *Proceedings of the Second International Conference on Fast Sea Transportation (FAST '93)*, Yokohama, Japan, December.
- COUSER, P. (1996), *An Investigation into the Performance of High-speed Catamarans in Calm Water and Waves*, PhD Thesis, Department of Ship Science, University of Southampton.

- COUSER, P.R., WELLICOME, J.F., AND MOLLAND, A.F. (1998), “An Improved Method for the Theoretical Prediction of the Wave Resistance of Transom-Stern Hulls using a Slender Body Approach”, *International Shipbuilding Progress*, Vol. 45, No. 444, pp. 331–349.
- DATE, J.C. AND TURNOCK, S.R. (2000), “Computational Fluid Dynamics Estimation of Skin Friction Experienced by a Plane Moving through Water”, *Transactions of the Royal Institution of Naval Architects*, Vol. 142, pp. 116–131, December, Discussion: 131-135.
- DAY, A. H. AND DOCTORS, L. J. (1997a), “Design of Fast Ships for Minimal Resistance and Motions”, *Proceedings of the Sixth International Marine Design Conference*, pp. 15+i, Newcastle-upon-Tyne, England, June.
- DAY, A. H. AND DOCTORS, L. J. (1997b), “Resistance Optimisation of Displacement Vessels on the Basis of Principal Parameters”, *Journal of Ship Research*, Vol. 41, No. 4, December, pp. 249-259.
- DE GROOT, D. (1955), “Resistance and Propulsion of Motorboats”, *International Shipbuilding Progress*, Vol. 2.
- DE GROOT, D. (1956), “Resistance and Propulsion of Motorboats”, *Netherlands Ship Model Basin Publication No. 93*, Wageningen, The Netherlands, (David Taylor Model Basin Translation 244, by W.B. Hinterthan, January 1956).
- DOCTORS, L. J. (1995a), “The influence of a Proboscidean Bow on Ship Motions”, *Proceedings of the Twelfth Australasian Fluid Mechanics Conference*, Vol. 1, University of Sydney, Australia, December, pp. 263-266.
- DOCTORS, L. J. (1995b), “A Versatile Hull Generator Program”, *Proceedings of the symposium on 21st Century Shipping*, University of New South Wales, Sydney, November, pp. 140-158, Discussion: pp. 158-159.

- DOCTORS, L. J. (1998a), “An Improved Theoretical Model for the Resistance of a Vessel with a Transom Stern”, *Proceedings of the Thirteenth Australasian Fluid Mechanics Conference*, Monash University, Melbourne, December, pp. 271-274.
- DOCTORS, L. J. (1998b), “Improvement of the Correlation of Michell’s Integral for Displacement Vessels”, *Proceedings of the Third Biennial Mathematics and Applications Conference*, Adelaide, July.
- DOCTORS, L. J. (1998c), “Intelligent Regression of Resistance Data for Hydrodynamics in Ship Design”, *Proceedings of the Twenty-second Symposium on Naval Hydrodynamics*, Washington DC, USA, August.
- DOCTORS, L. J. (1998d), “Modifications to the Michell Integral for Improved Prediction of Ship Resistance”, *Proceedings of the Twenty-seventh Israel Conference on Mechanical Engineering*, Technion City, Haifa, Israel, May, pp. 502-506.
- DOCTORS, L. J. (1998e), “An Improved Theoretical Model for the Resistance of a Vessel with a Transom Stern”, *Proceedings of the Thirteenth Australasian Fluid Mechanics Conference*, Vol. 1, Monash University, Melbourne, December, pp. 271-274.
- DOCTORS, L. J. (1998f), “Development of Low-Wash Vessels”, *Proceedings of the International Conference and Exhibition for the Commercial Marine Industry*, Fremantle, November.
- DOCTORS, L. J. (1999a), “The Foil-Stabilized Super-Slender Monohull”, *Proceedings of the International Conference on Hydrodynamics of High-speed Craft*, London, England, November.
- DOCTORS, L. J. (1999b), *The HYDROS/4.1 Programs: Description and Documentation*, The University of New South Wales, Sydney.

- DOCTORS, L. J. AND DAY, A. H. (1997), “Resistance Prediction for Transom-Stern Vessels”, *Proceedings of the Fourth International Conference on Fast Sea Transportation*, Sydney, July.
- DOCTORS, L.J. AND RENILSON, M.R. (1992), “Corrections for Finite-Water-Depth Effects on Ship Resistance”, *Proceedings of the Eleventh Australasian Fluid Mechanics Conference*, Vol. 1, University of Tasmania, Hobart, December, pp. 663-666.
- DUNCAN, W.J., THOM, A.S., AND YOUNG, A.D. (1970), *Mechanics of Fluids*, Edward Arnold Ltd., London.
- EGGERT, E.F. (1939), “Further Form Resistance Experiments”, *Transactions of the Society of Naval Architects of Marine Engineers*, Vol. 47.
- FROUDE, W. (1872, 1874), “Experiments on Surface Friction”, *British Association Reports*.
- FROUDE, W. (1955), “Observations and Suggestions on the Subject of Determining by Experiment the Resistance of Ships – The Papers of William Froude (1810–1879)”, *Transactions of the Institution of Naval Architects*.
- FUNG, C. (1991), “Resistance and Powering Prediction for Transom Stern Hull Forms During Early Stage Ship Design”, *Transactions of the Society of Naval Architects and Marine Engineers*, Vol. 99, pp. 29–84.
- GADD, G.E. AND HOGBEN, N. (1962), “An Appraisal of the Ship Resistance Problem in Light of Measurements of the Wave Pattern”, *NPL Ship Division Technical Report 36*.
- GAMULIN, A. (1996), “A Semi-displacement Series of Ships”, *International Ship-building Progress*, Vol. 43, No. 434, pp. 93–107.

- GRANVILLE, P.S. (1977), “Drag and Turbulent Boundary Layer of Flat Plates at Low Reynolds Numbers”, *Journal of Ship Research*, Vol. 21, No. 1.
- GRIGSON, C.W.B. (1993), “An Accurate Smooth Friction Line for Use in Performance Prediction”, *Transaction of the Royal Institution of Naval Architects*, Vol. 135, pp. 149–158, Discussion: 158–162.
- GRIGSON, C.W.B. (2000), “A Planar Friction Algorithm and its Use in Analysing Hull Resistance”, *Transactions of the Royal Institution of Naval Architects*, Vol. 142, pp. 76–102, December, Discussion: 102–115.
- HARRIES, S. AND SCHULZE, D. (1997), “Numerical Investigation of a Systematic Model Series for the Design of Fast Monohulls”, *Proceedings of the Fourth International Conference on Fast Sea Transportation*, pp. 339–347, December, Vol. 1.
- HAVELOCK, T. H. (1934), “The Calculation of Wave Resistance”, *Proceedings of the Royal Society*, Vol. 144, Series A, 514 pp.
- HELMORE, P. J. (1995), “Resistance Prediction: State of the Art”, *Proceedings of the Symposium on 21st Century Shipping*, Univeristy of New South Wales, Sydney.
- HIRANO, S., INATSU, S., AND HIMENO, Y. (1990), “Measurement of Spray Resistance for Prismatic Planing Hull Forms.”, *Proceedings of the Fourth International Symposium on Marine Engineering*, Kobe, Japan.
- HOLTROP, J. (1984), “A Statistical Re-analysis of Resistance and Propulsion Data”, *International Shipbuilding Progress*, Vol. 31, No. 363, November.
- HUGHES, G. (1930), “Model Experiments on the Wind Resistance of Ships”, *Transactions of the Institution of Naval Architects*, Vol. 72.

- HUGHES, G. (1952), “Frictional Resistance of Smooth Plane Surfaces in Turbulent Flow”, *Transactions of the Institution of Naval Architects*, Vol. 94.
- HUGHES, G. (1954), “Friction and Form Resistance in Turbulent Flow and a Proposed Formulation for Use in Model and Ship Correlation”, *Transactions of the Institution of Naval Architects*, Vol. 96.
- INSEL, M. (1990), *An Investigation into the Resistance Components of High Speed Displacement Catamarans*, PhD Thesis, Department of Ship Science, University of Southampton.
- INSEL, M. AND MOLLAND, A. F. (1992), “An Investigation into the Resistance Components of High Speed Displacement Catamarans”, *Transactions of the Royal Institution of Naval Architects*, Vol. 134.
- ITTC (1978), *Proceedings of the 15th International Towing Tank Congress*, Technical Report, The Hague, Netherlands Ship Model Basin.
- JOUBERT, P. N. AND HOFFMANN, P. H. (1979), “An Experimental Study of the Viscous Resistance of a 0.564 C_B Form”, *Journal of Ship Research*, Vol. 23, No. 2, June, pp. 140-156.
- JOUBERT, P.N. AND MATHESON, N. (1970), “Wind tunnel tests of two *Lucy Ashton* Reflex Geosims”, *Journal of Ship Research*, Vol. 14, No. 4, pp. 241–276, December.
- KELVIN, LORD (1887), “Ship Waves”, *Transactions of the Institute of Mechanical Engineers*, London.
- KRACHT, A.M. AND JACOBSEN, A. (1992), “D-Series Systematic Experiments with Models of Fast Twin Screw Displacement Ships”, *Transactions of the Society of Naval Architects and Marine Engineers*, Vol. 100, pp. 199–222.
- LAGRANGE, J.L. (1788), *Mechanique Analitique*, Desaint, Paris.

- LAHTIHARJU, E., KARPPINEN, T., HELLEVAARA, M., AND AITTA, T. (1991), "Resistance and Sea-keeping Characteristics of Fast Transom Stern Hulls with Systematically Varied Form", *Transactions of the Society of Naval Architects and Marine Engineers*, Vol. 99, pp. 85–118.
- LARSON, L. (1993), "Resistance and Flow Predictions using the Shipflow Code", *Proceedings of The Nineteenth WEGEMT School*, Nantes.
- LEWIS, E. V. Ed. (1988), *Principles of Naval Architecture*, Vol. 2, Society of Naval Architects and Marine Engineers, Jersey City, USA.
- LINDGREN, H. AND WILLIAMS, A. (1968), "Systematic Tests with Small, Fast Displacement Vessels, Including a Study of the Influence of Spray Strips", *Proceedings of the Diamond Jubilee International Meeting*, Society of Naval Architects and Marine Engineers, New York, June.
- LUNDE, J.K. (1951), "On the Linearized Theory of Wave Resistance for Displacement Ships in Steady and Accelerated Motion", *Transactions of the Society of Naval Architects and Marine Engineers*, Vol. 59, pp. 25–76, Discussion: pp. 76–85, December.
- MARWOOD, W.J. AND BAILEY, D (1969), "Design Data for High-Speed Displacement Hulls of Round-Bilge Form", *Ship Report No. 99* National Physical Laboratory, February.
- MERCIER, J.A. AND SAVITSKY, D. (1973), "Resistance of Transom-Stern Craft in the Pre-Planing Regime", *Davidson Laboratory Report No. 1667*, Stevens Institute of Technology, Hoboken, June.
- MICHELL, J. H. (1898), "The Wave Resistance of a Ship", *Philosophical Magazine*, Vol. 45, Series 5, pp. 106–123.
- MILGRAM, J.H. (1969), "The Effect of a Wake on the Wave Resistance of a Ship", *Journal of Ship Research*, Vol. 13, No. 1, pp. 69–71, March.

- MOLLAND, A.F. AND LEE, A.R. (1997), “An Investigation into the Effect of Prismatic Coefficient on Catamaran Resistance”, *Transactions of the Royal Institution of Naval Architects*, Vol. 140, pp. 157–165.
- MOLLAND, A.F., WELLCOME, J.F., AND COUSER, P.R. (1994a), “Resistance Experiments on a Systematic Series of High Speed Displacement Catamaran Forms: Variation of Length-Displacement Ratio and Breadth-Draught Ratio”, *Ship Science Report No. 71*, University of Southampton, pp. 82+i, March.
- MOLLAND, A.F., WELLCOME, J.F., AND COUSER, P.R. (1994b), “Theoretical Prediction of the Wave Resistance of Slender Hull Forms in Catamaran Configurations”, *Ship Science Report No. 72*, University of Southampton, March.
- MOLLAND, A.F., WELLCOME, J.F., AND COUSER, P.R. (1995), “Resistance Experiments on a Systematic Series of High Speed Displacement Catamaran Forms: Variation of Length-Displacement Ratio and Breadth-Draught Ratio”, *Transactions of the Royal Institution of Naval Architects*, Vol. 138, pp. 55–69.
- PHILLIPS-BIRT, D. (1970), *Ship Model Testing*, International Textbook Company Limited.
- PROHASKA, C.W. (1966), “A Simple Method for the Evaluation of the Form Factor and Low Speed Wave Resistance”, *Proceedings of the Eleventh International Towing Tank Congress*.
- RAVEN, H. (1992), “Practical Non-Linear Method for Calculating Ship Wave-Making and Wave Resistance”, *Proceedings of the Nineteenth Symposium on Naval Hydrodynamics*, Seoul, Korea.
- ROBARDS, S.W. AND DOCTORS, L.J. (2003), “Transom Hollow Prediction for High-Speed Displacement Vessels”, *Proceedings of the Seventh International Conference on Fast Sea Transportation*, Naples, Italy,

- SAHOO, P.K., DOCTORS, L.J., AND RENILSON, M.R. (1999), “Theoretical and Experimental Investigation of Resistance of High-Speed Round-Bilge Hull Forms”, *Proceedings of the Fifth Conference on Fast Sea Transportation*, Seattle, USA, August.
- SAUNDERS, H.E. (1957a), *Hydrodynamics in Ship Design* Vol. 1, Society of Naval Architects and Marine Engineers, New York.
- SAUNDERS, H.E. (1957b), *Hydrodynamics in Ship Design* Vol. 2, Society of Naval Architects and Marine Engineers, New York.
- SCHOENHERR, K.E. (1932), “Resistance of Flat Surfaces Moving Through a Fluid”, *Transactions of the Society of Naval Architects and Marine Engineers*, Vol. 40, New York.
- SINHA, S. (1981), “Backward facing step flow experiments.”, *AIAA Journal*, Vol. 19, pp. 1527–1530.
- SRETENSKY, L.N. (1936), “On the Wave-Making Resistance of a Ship Moving along a Canal”, *Philosophical Magazine*, Vol. 22, No. 150, November, Series 7, Supplement, pp. 1005–1013.
- TAGGART, R. Ed. (1980), *Ship Design and Construction*, Society of Naval Architects and Marine Engineers, New York, USA.
- TANAKA, H., NAKATAKE, K., ARAKI, S., NAKATO, M., AND UEDA, T. (1990), “Cooperative Resistance Tests with Geosim Models of a High-Speed Semi-Displacement Craft”, *Journal of the Society of Naval Architects of Japan*, Vol. 169.
- TELFER, E.V. (1927), “Ship Resistance Similarity”, *Transactions of the Institution of Naval Architects*, Vol. 69.

- TODD, F.H. (1966), "The Model-Ship Correlation Problem", *Marine Technology*, Society of Naval Architects and Marine Engineers, New York, pp. 152–157, April.
- TULIN, M.P. AND HSU, C.C. (1986), "Theory of High-Speed Displacement Ships with Transom Sterns", *Journal of Ship Research*, Vol. 30, No. 3, pp. 186–193, September.
- TURSINI, L. (1953), "Leonardo da Vinci and the Problems of Navigation and Naval Design", *Transactions of the Institution of Naval Architects*, Vol. 95.
- WARD, L.W. (1962), "A Method for the Direct Experimental Determination of Ship Wave Resistance", Stevens Institute of Technology, PhD thesis.
- WHITE, F.M. (1974), *Viscous Fluid Flow*, McGraw-Hill Inc., New York.
- YEH, H.J.H. (1965), "Series 64 resistance experiments on high-speed displacement forms", *Marine Technology*, Society of Naval Architects and Marine Engineers, New York, July. pp. 248–271,

Appendix A

Collected Model Data

This appendix contains the body plans of all parent models used in the form-factor regression presented in Chapter 7. Some model series utilised in the regression were designed such that a single parent hull did not exist and, for these model series, all models have been presented. The sections of each body plan have been labelled from 10 to 1 with the transom of each model labelled T. Section 10 represents the section at the intersection of the datum waterline with the vessel's stem. The body plans have not been presented at a set scale; however, the datum waterline is shown on each body plan at its correct location. For scaling purposes, reference should be made to Chapter 7 where the magnitude of the datum draft is listed for each model.

Lego Series

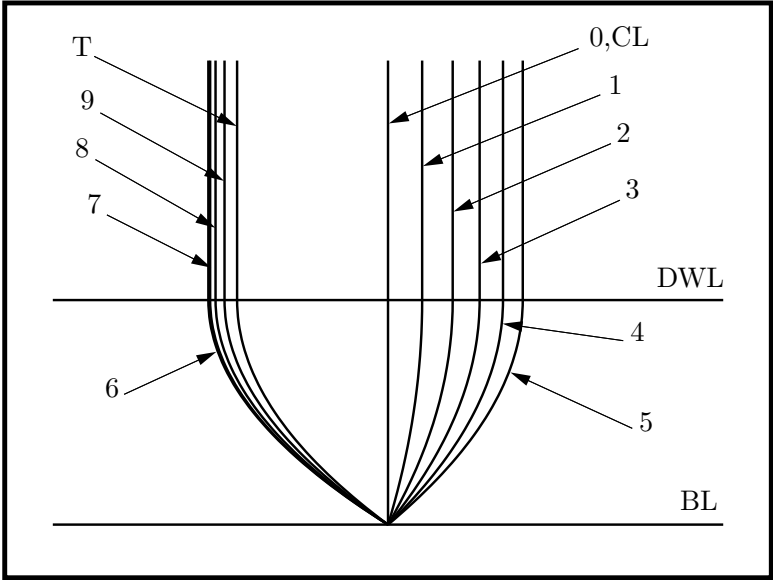


Figure A.1: Lego Model 1

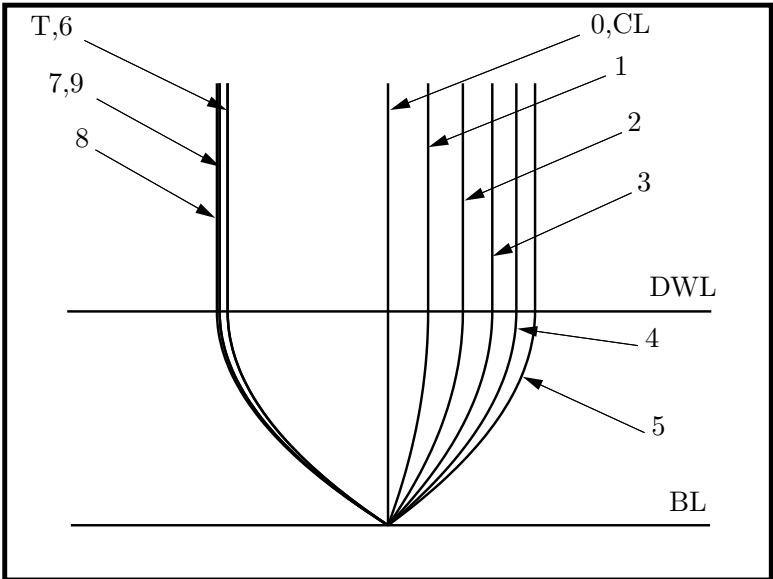


Figure A.2: Lego Model 2

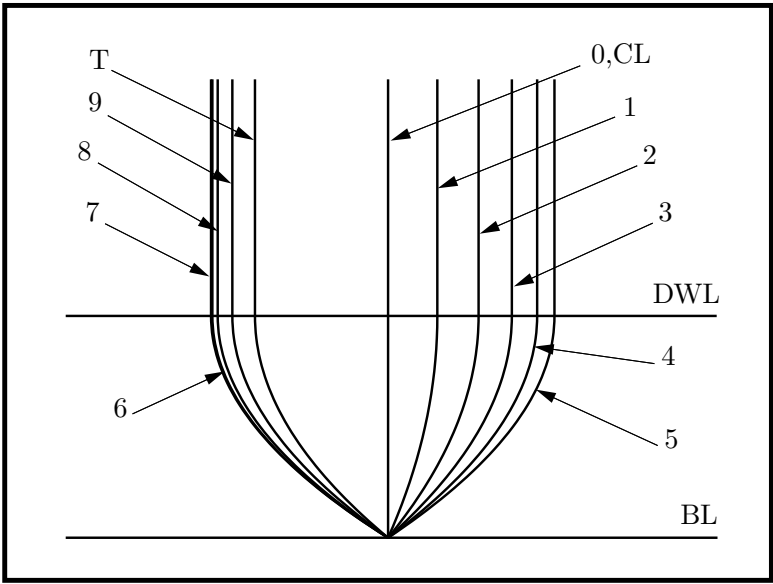


Figure A.3: Lego Model 3

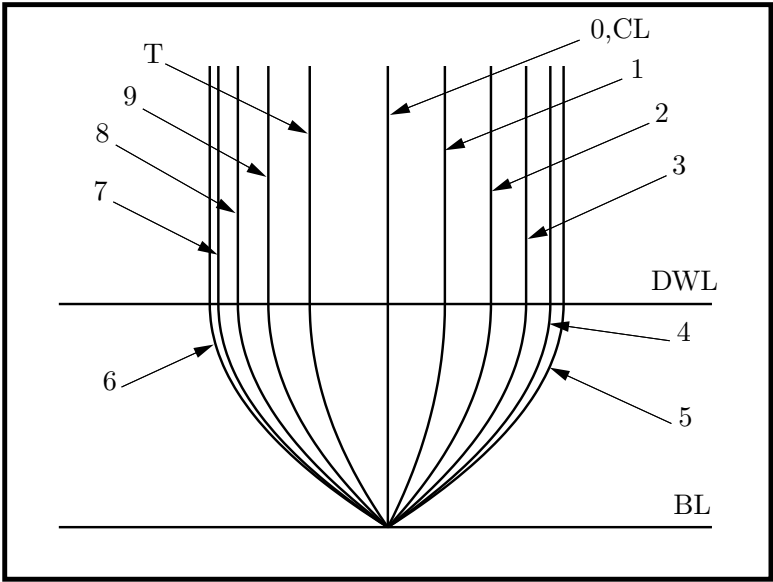


Figure A.4: Lego Model 4

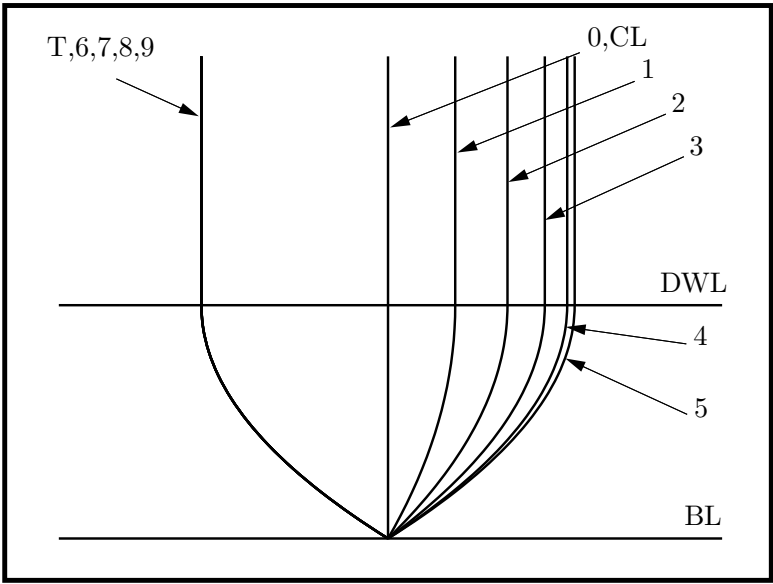


Figure A.5: Lego Model 5

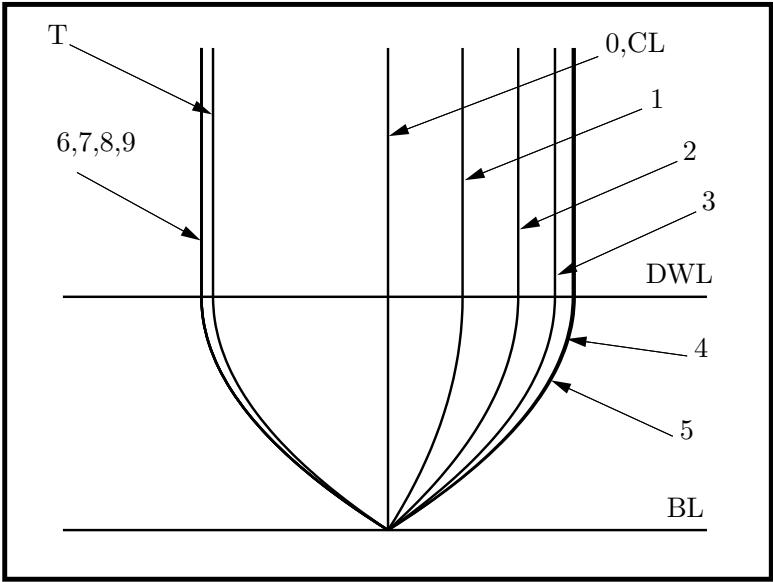


Figure A.6: Lego Model 6

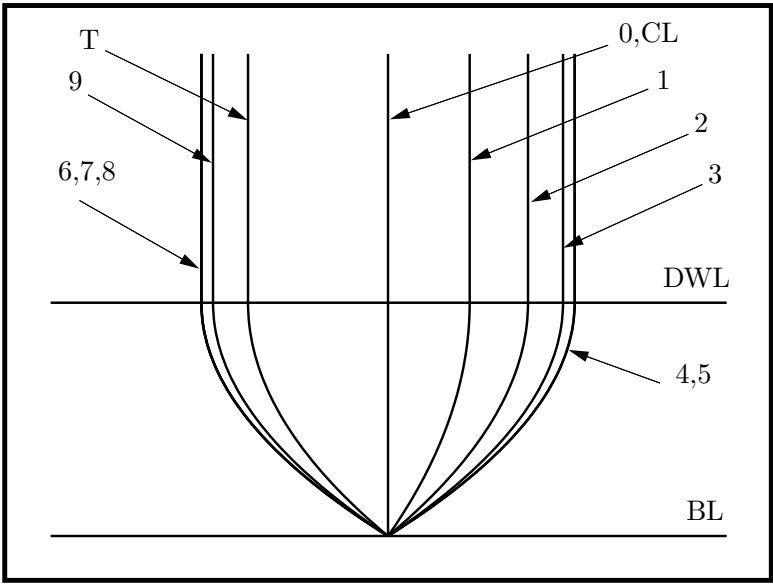


Figure A.7: Lego Model 7

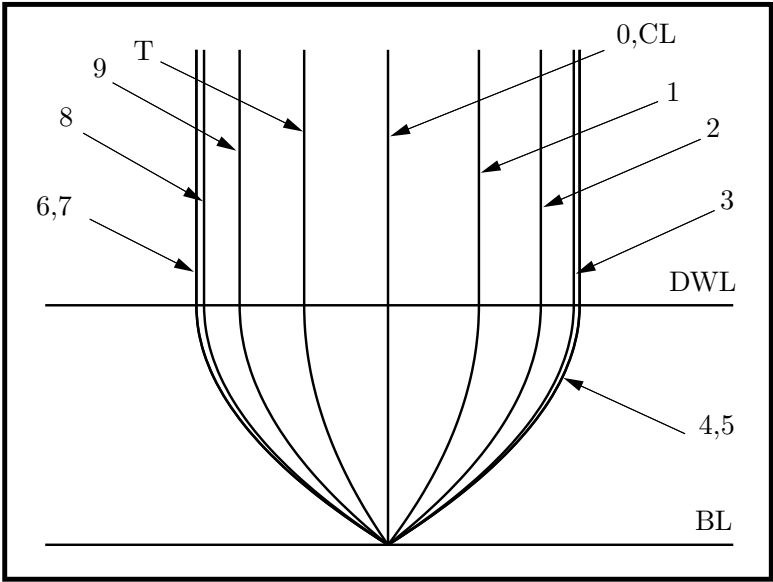


Figure A.8: Lego Model 8

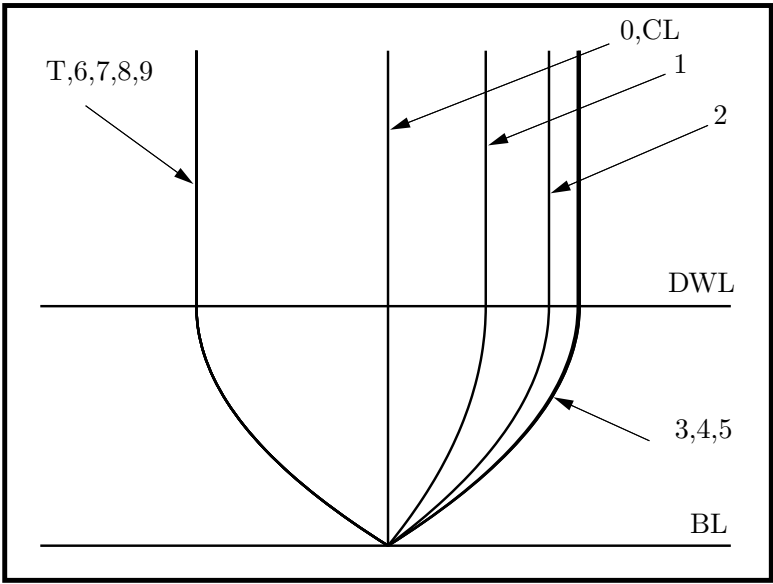


Figure A.9: Lego Model 9

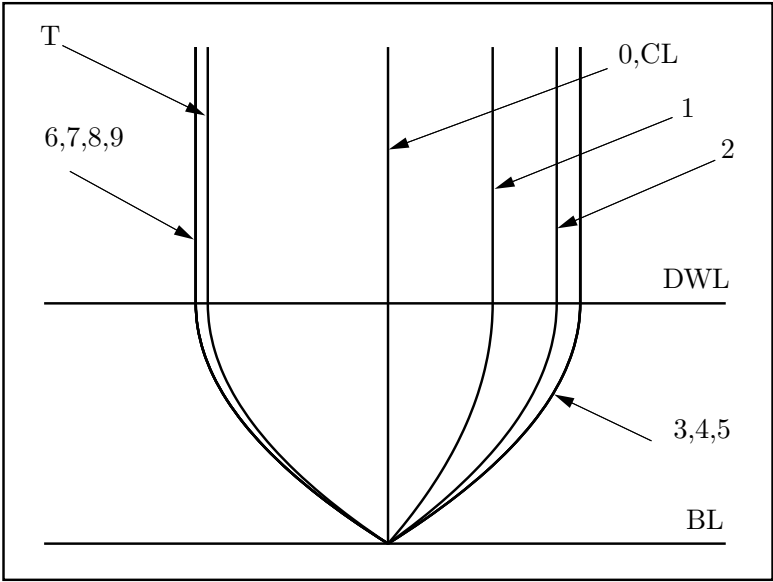


Figure A.10: Lego Model 10

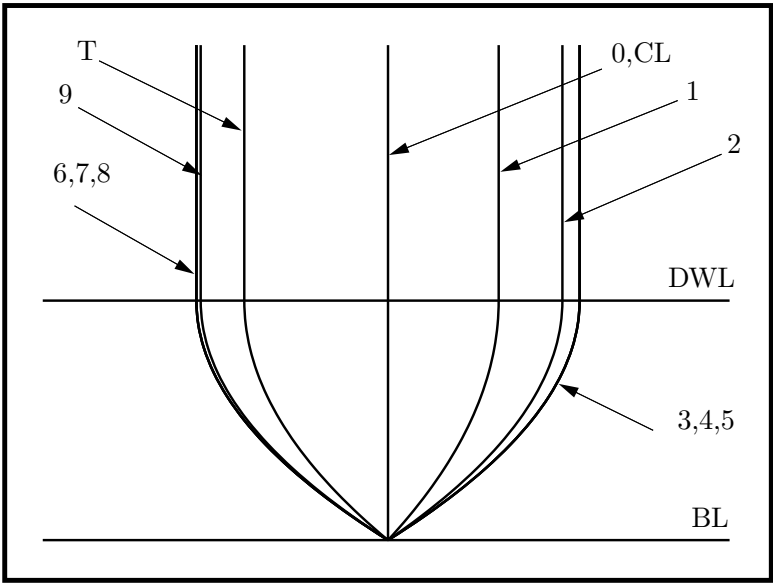


Figure A.11: Lego Model 11

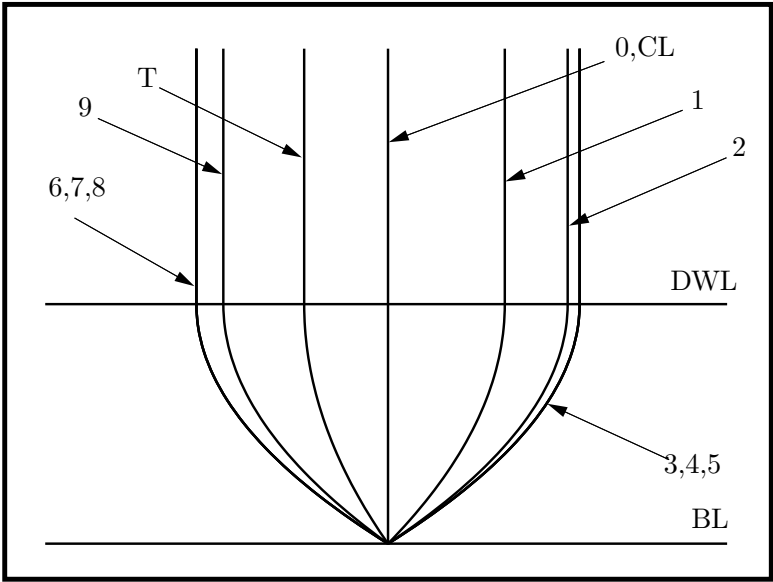


Figure A.12: Lego Model 12

NPL Series

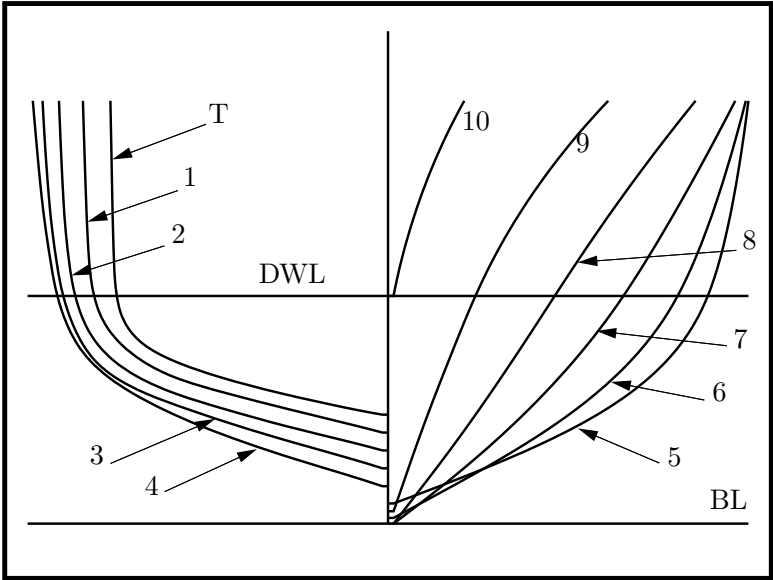


Figure A.13: NPL Parent Model

German Series

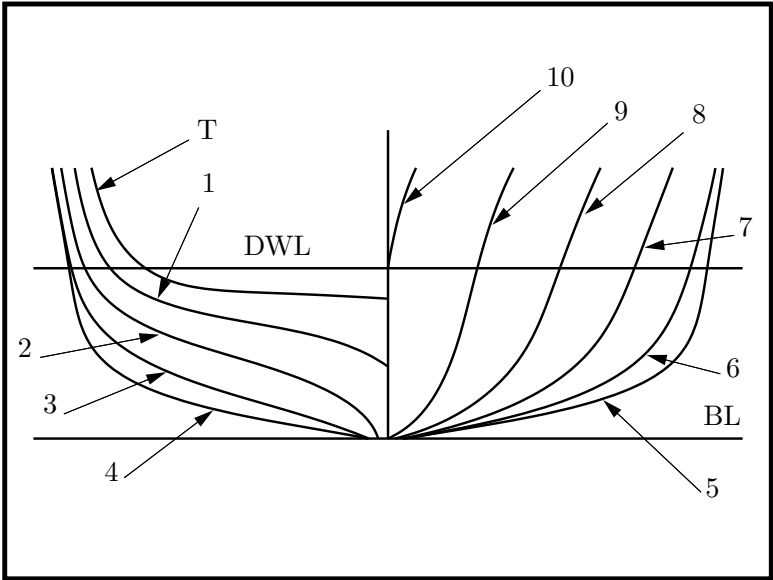


Figure A.14: D-Series Parent Model D1

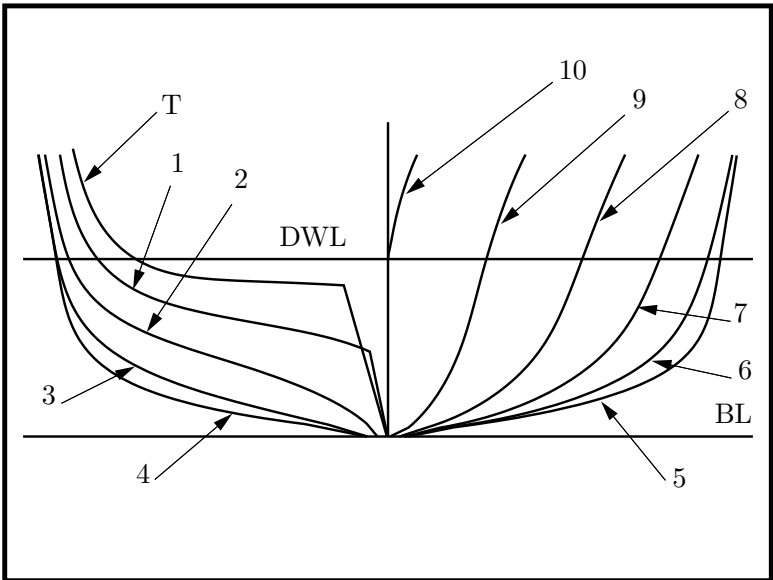


Figure A.15: D-Series Parent Model D5

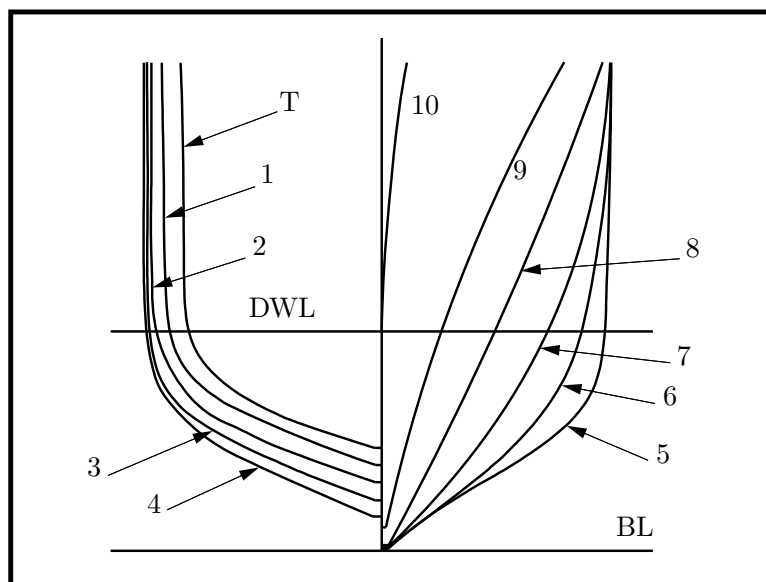
University of Southampton Models of Modified C_P 

Figure A.16: University of Southampton Model 5d

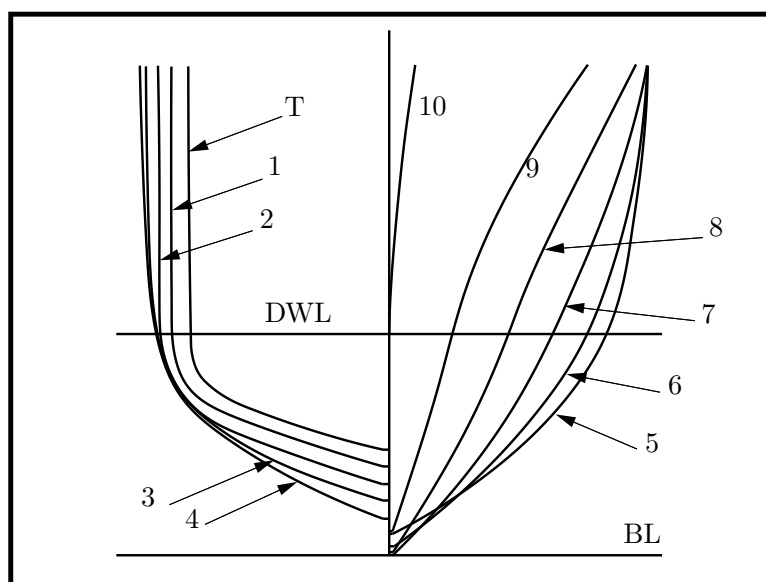


Figure A.17: University of Southampton Model 5e

SKLAD Series

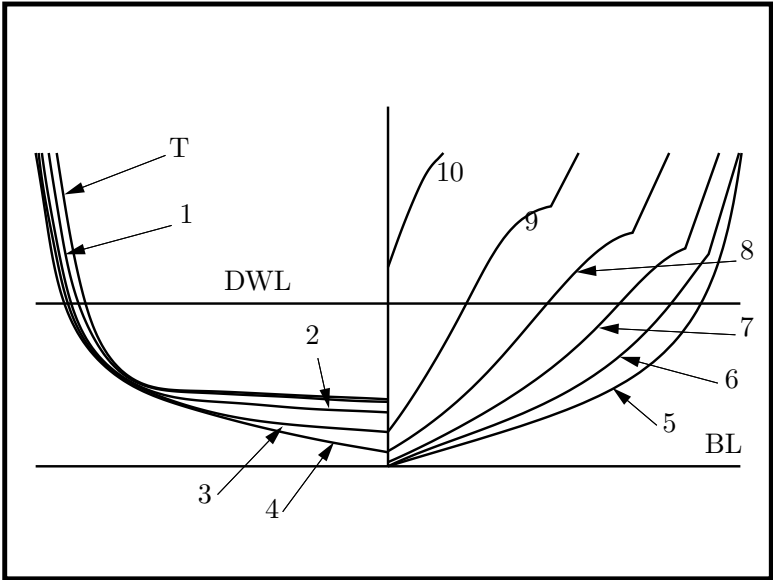


Figure A.18: SKLAD Parent Model M-741

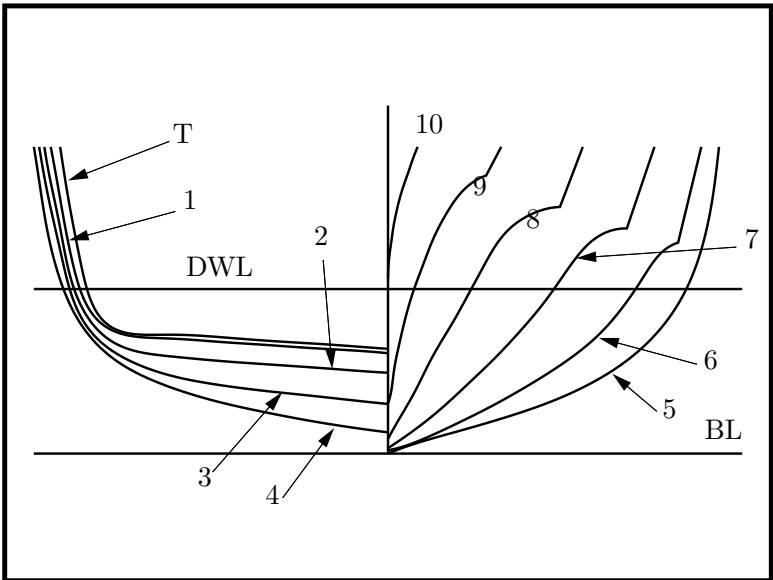


Figure A.19: SKLAD Parent Model M-751

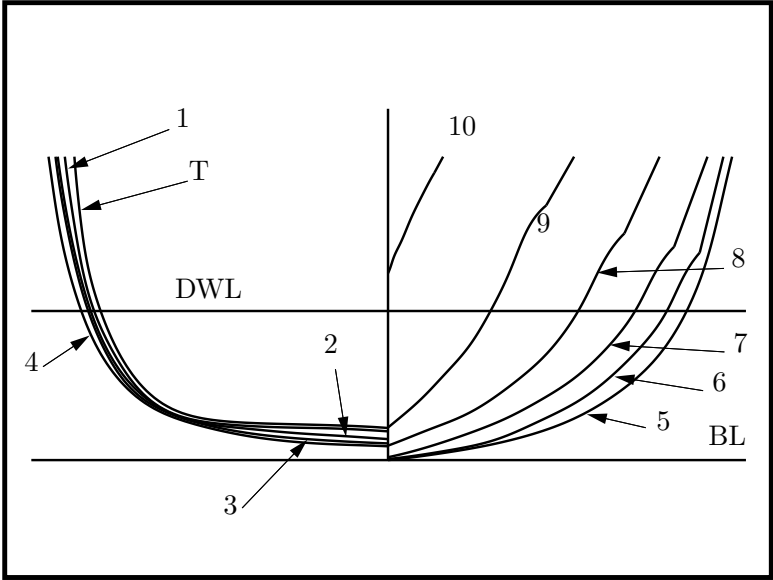


Figure A.20: SKLAD Parent Model M-761

DeGroot Series

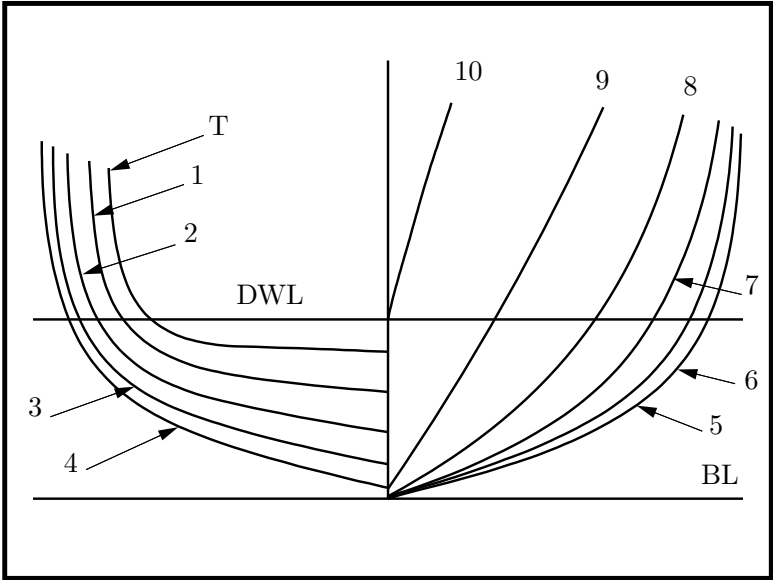


Figure A.21: Degroot Model 6-I

Series 63

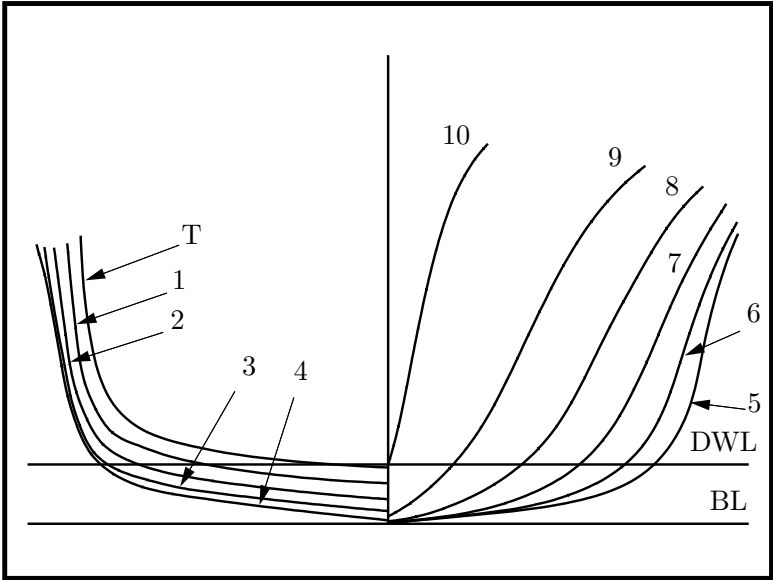


Figure A.22: Series 63 Parent Model

Series 64

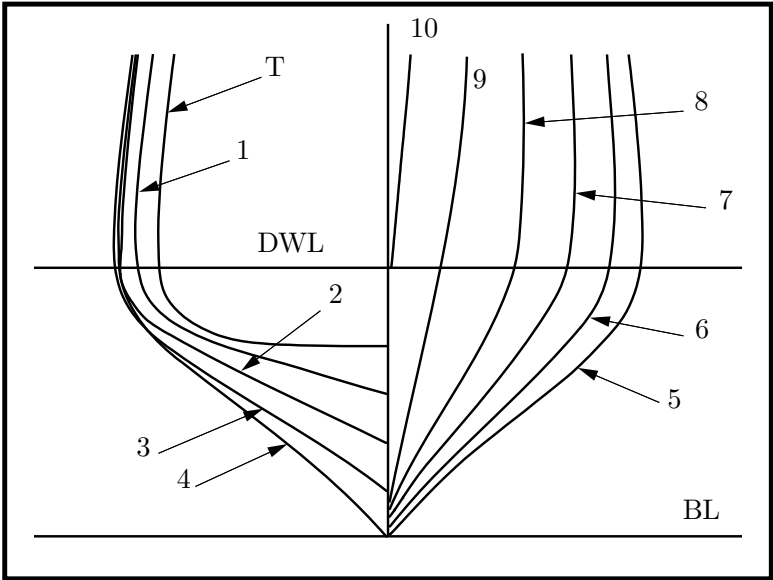


Figure A.23: Series 64 Model 4805

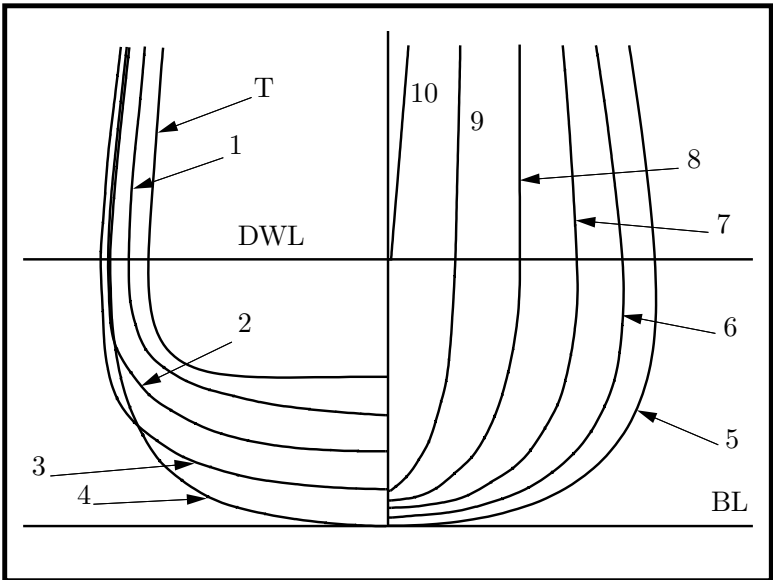


Figure A.24: Series 64 Model 4787

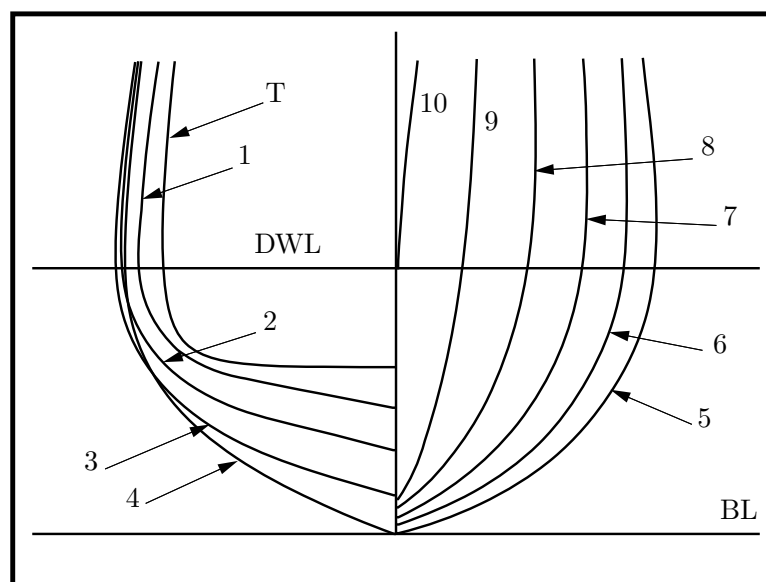


Figure A.25: Series 64 Model 4796

SSPA

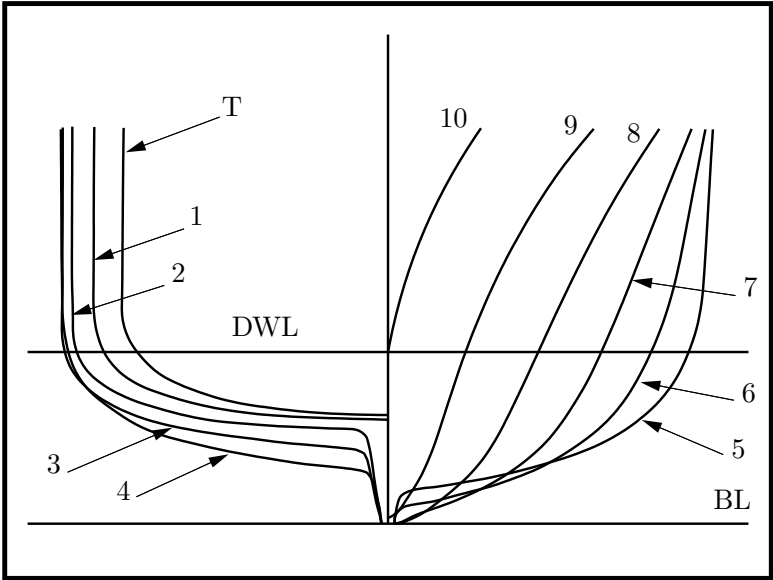


Figure A.26: SSPA Parent Model

AMECRC Series

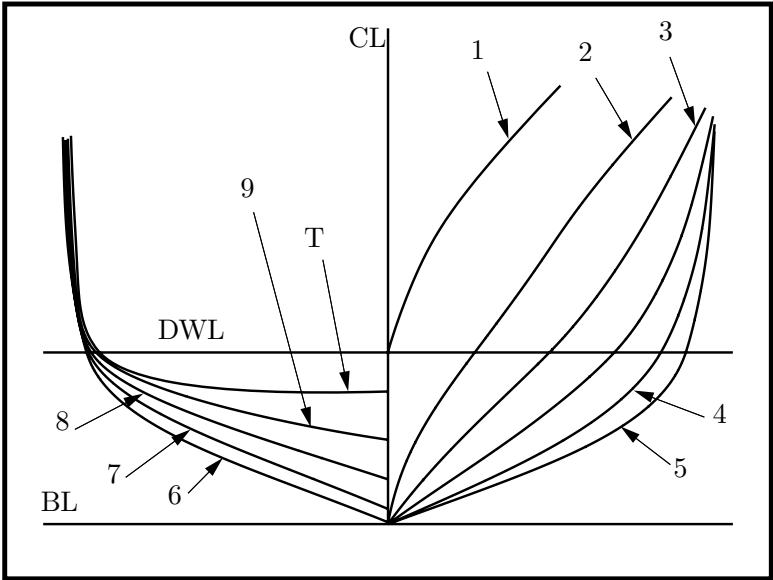


Figure A.27: AMECRC Model 1

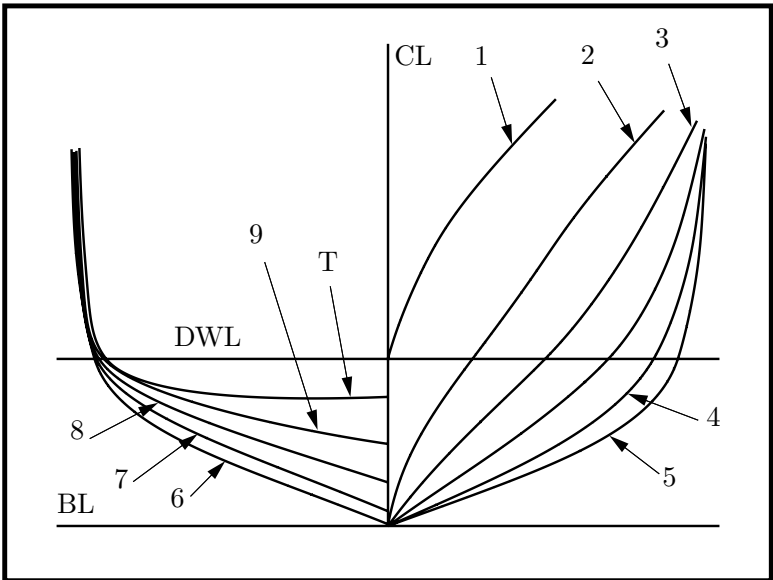


Figure A.28: AMECRC Model 2

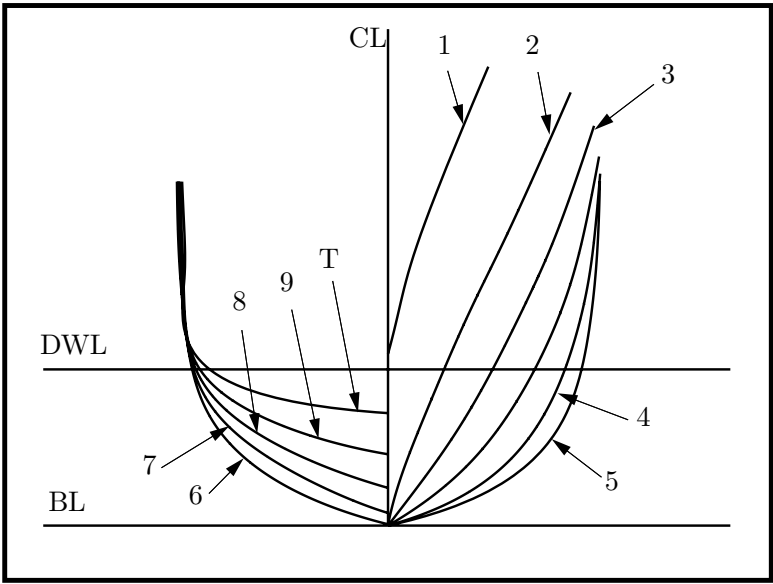


Figure A.29: AMECRC Model 3

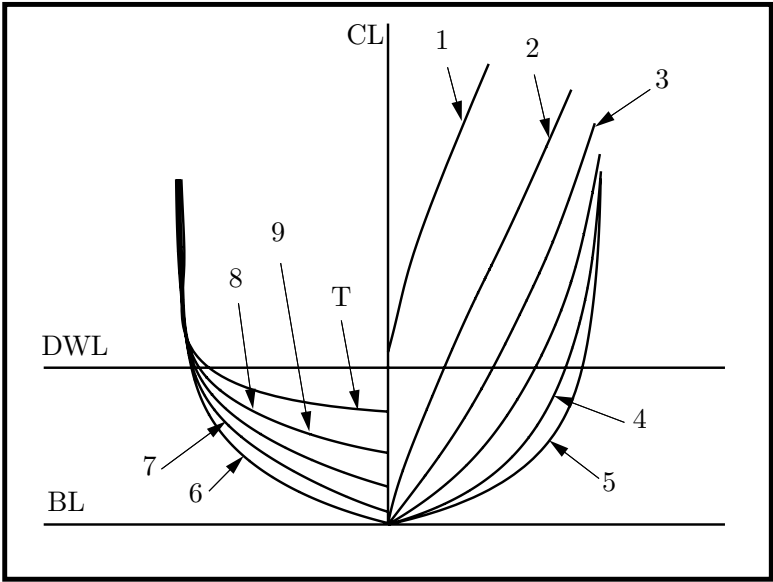


Figure A.30: AMECRC Model 4

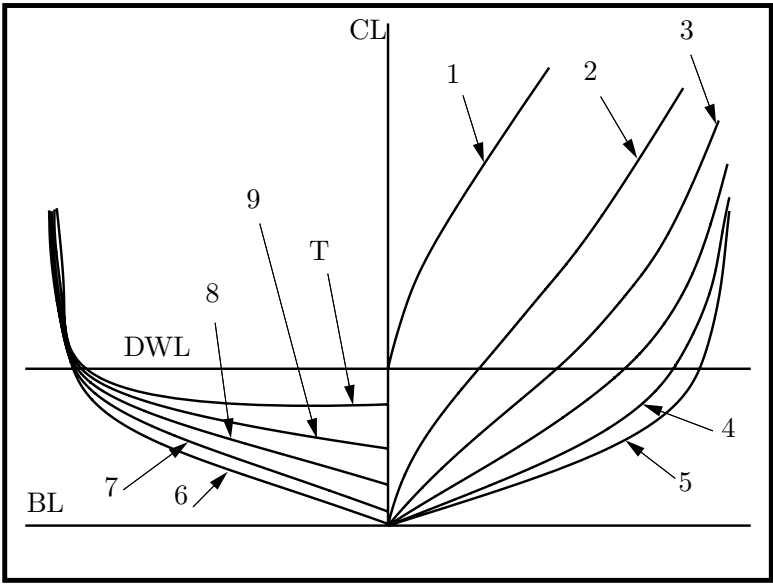


Figure A.31: AMECRC Model 5

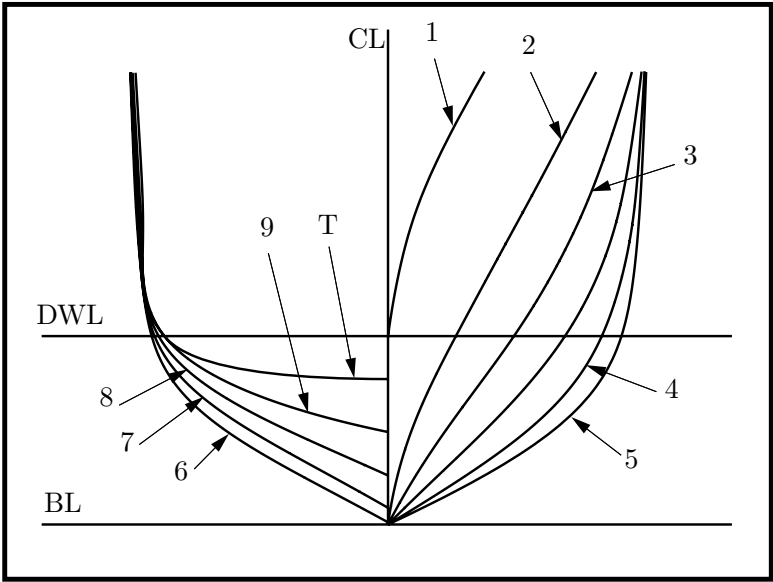


Figure A.32: AMECRC Model 6

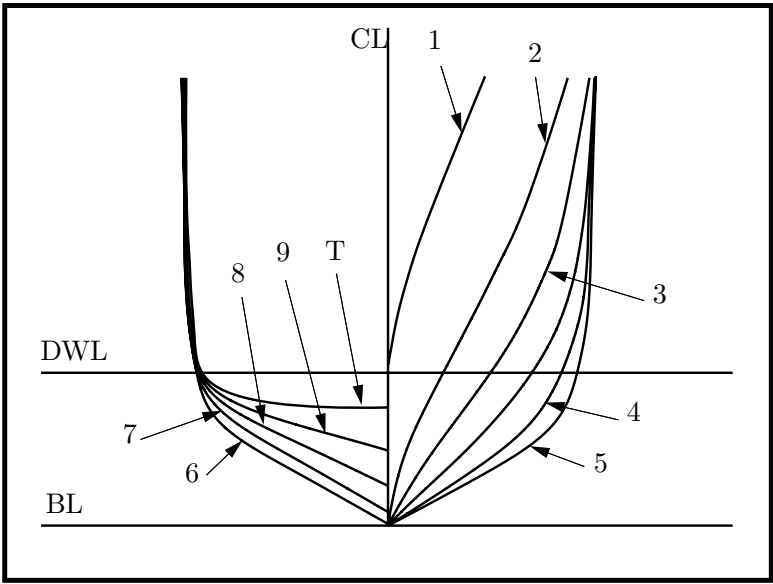


Figure A.33: AMECRC Model 7

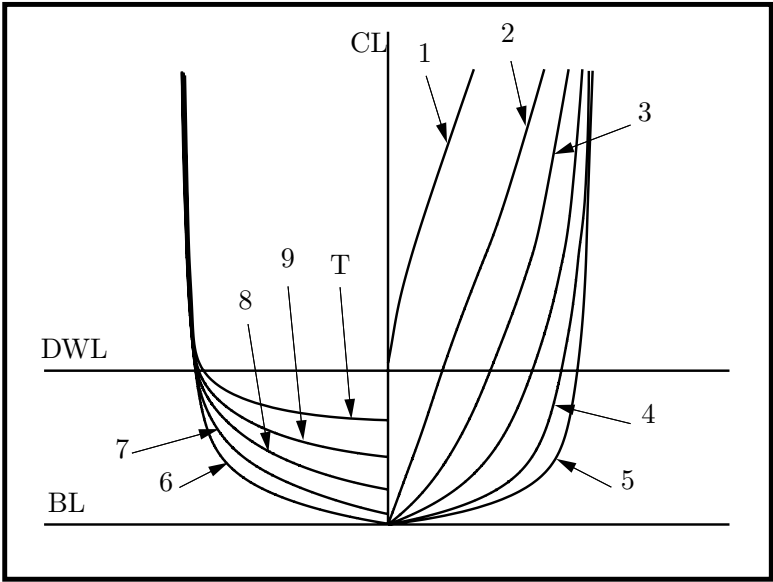


Figure A.34: AMECRC Model 8

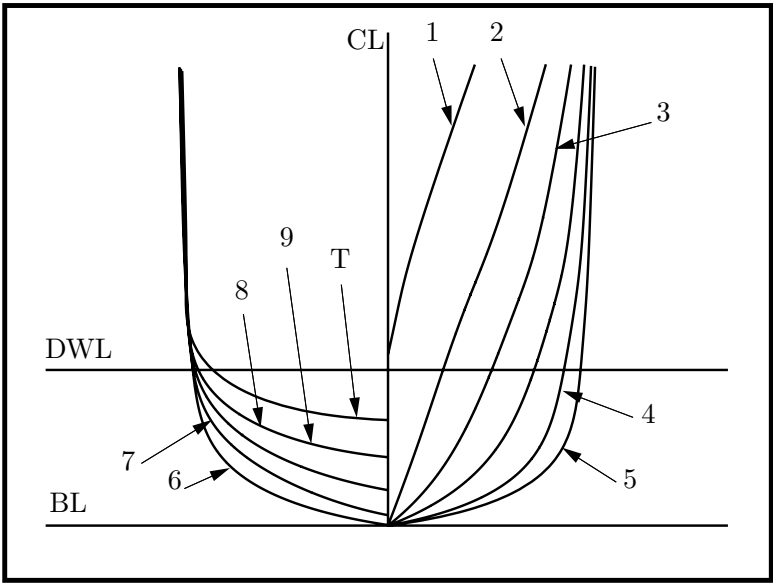


Figure A.35: AMECRC Model 9

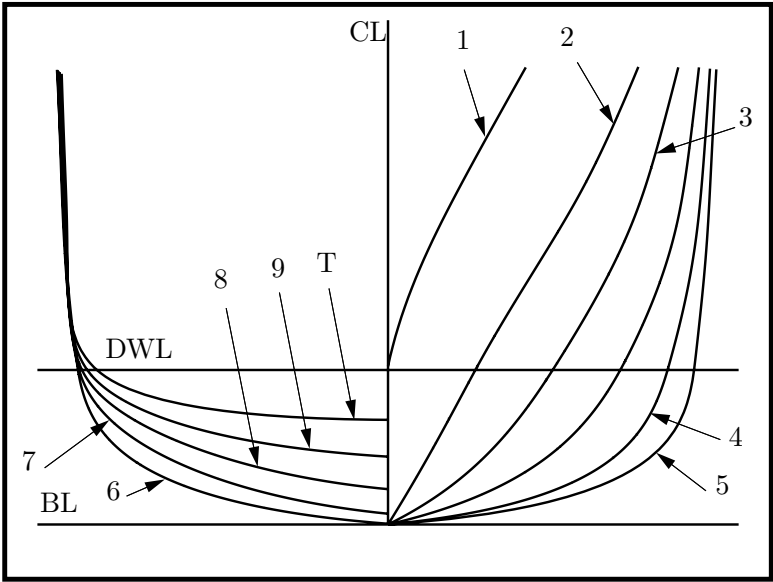


Figure A.36: AMECRC Model 10

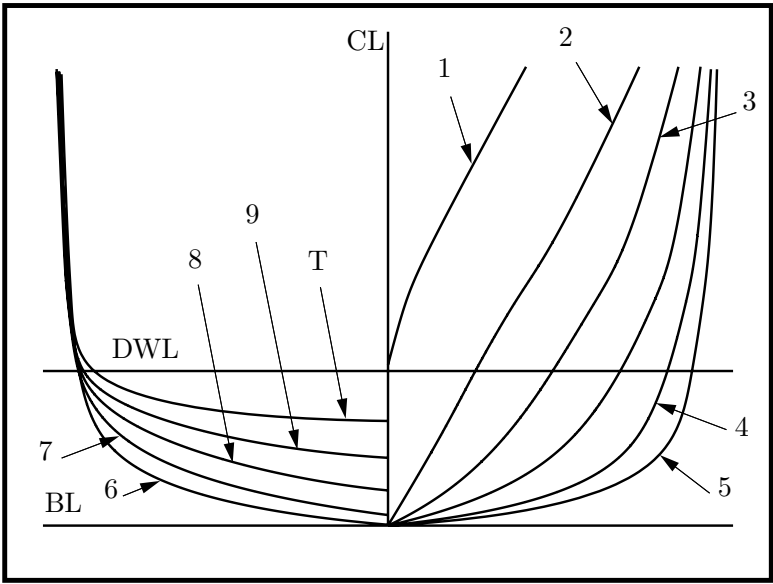


Figure A.37: AMECRC Model 11

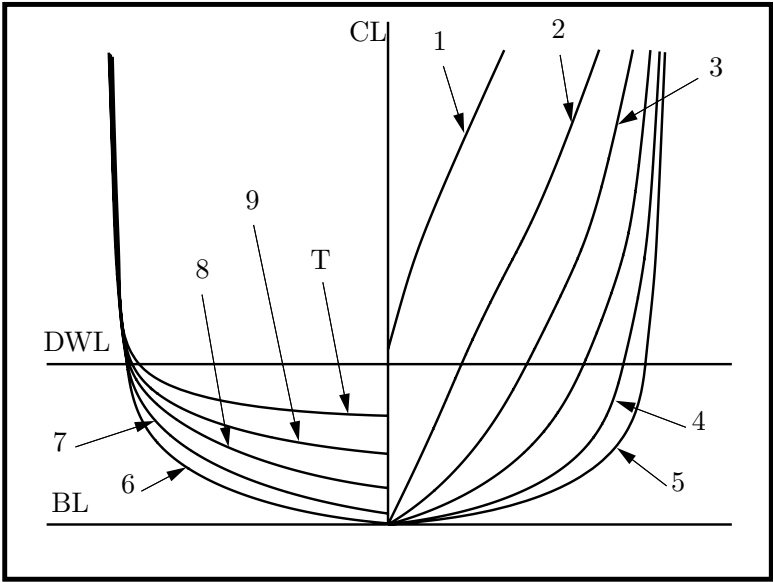


Figure A.38: AMECRC Model 12

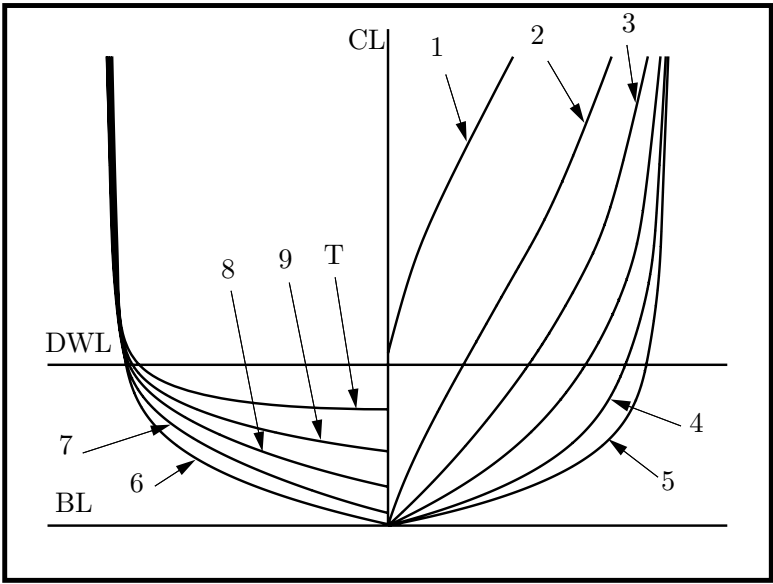


Figure A.39: AMECRC Model 13

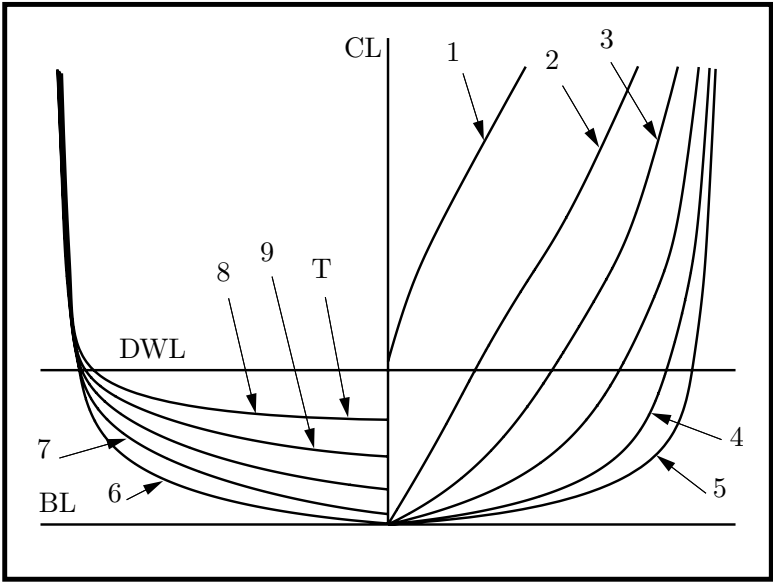


Figure A.40: AMECRC Model 14

NOVA Series

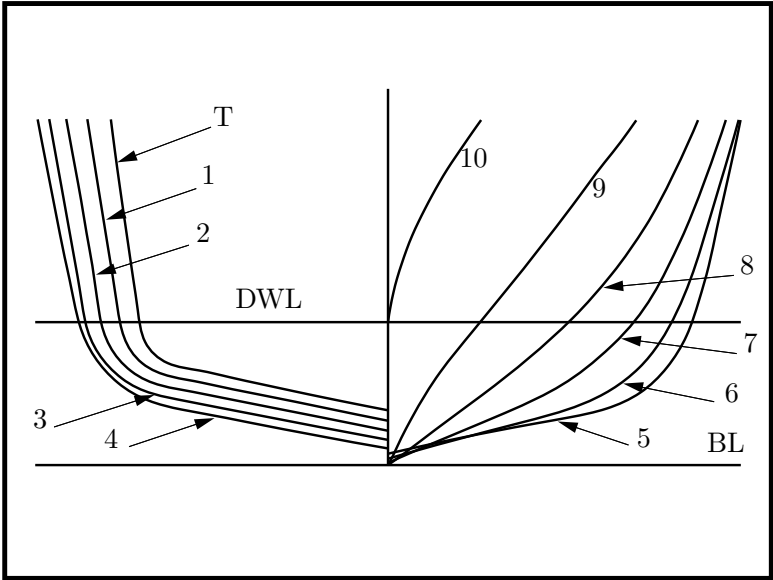


Figure A.41: NOVA Parent Model

Compton Series

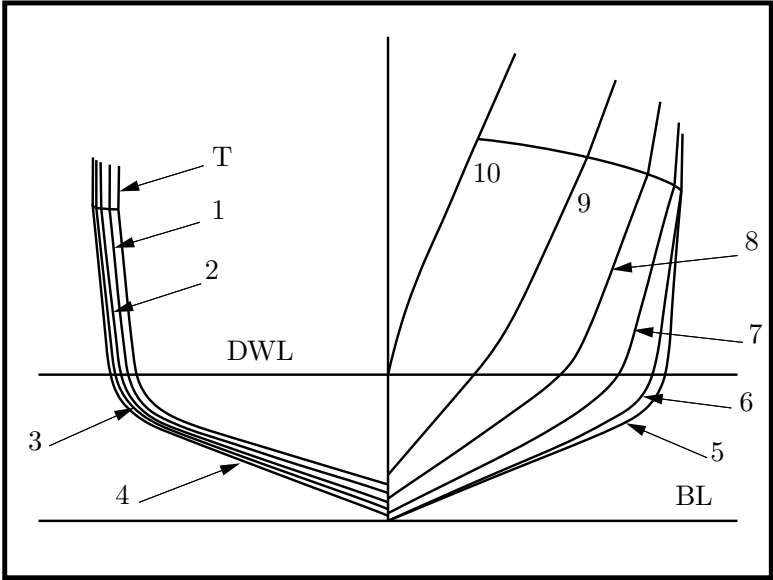


Figure A.42: Compton Model YP81.1

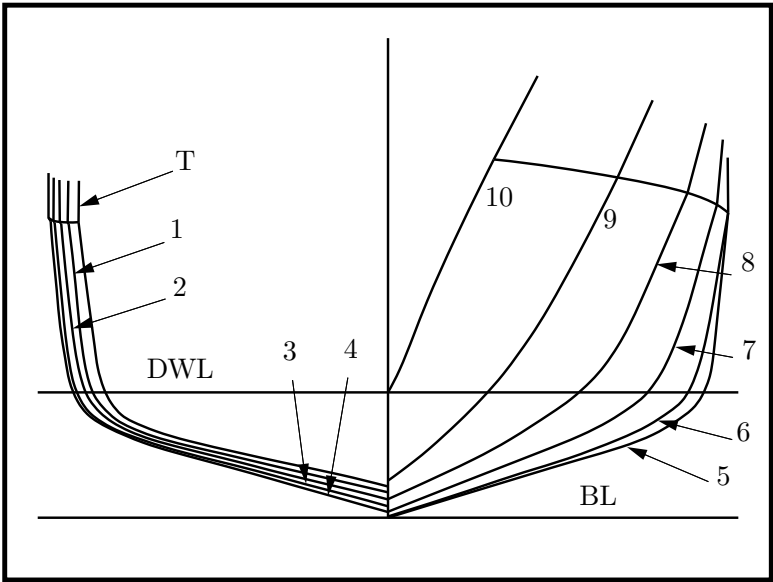


Figure A.43: Compton Model YP81.2

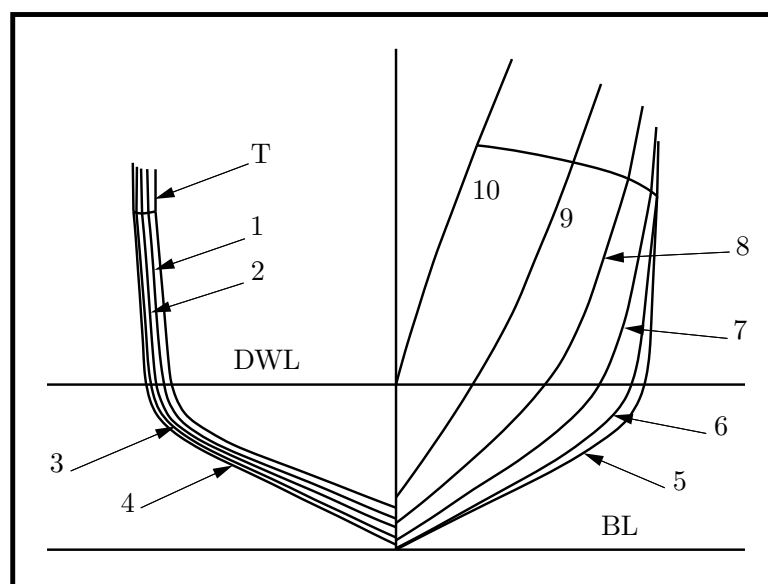


Figure A.44: Compton Model YP81L3

Appendix B

Transom Hollow Data

This appendix contains a complete record of the transom hollow experiments conducted at the Australian Maritime College in Launceston, Tasmania. Each table lists the model being tested, the condition of the model, the calibration factors recorded, the time of each run and the speed, total resistance (R_T), and heave recorded.

For some conditions, a calibration has been performed part way through the test procedure for that condition. In these instances, the stage at which the calibration was performed has been recorded in the comments column beside the run which immediately followed the calibration. Where a calibration has been performed part way through a condition, the calibration factors listed at the top of the Table represent the second set of calibration factors, with the first set already listed in the preceding table.

The calibration factors for the wave-probe and the rotary potentiometer measuring the location of the wave probe are also listed in these tables with the resulting measured hollow profiles exhibited in Appendix C.

Hollow Model 1**Condition 1:** 4th June 2002**Model Data:**

LWL=	800.0	mm
WSA=	0.1561	m ²
Draft=	50.0	mm
Δ =	3.550	kg
Water Temp=	16.0	degrees

Calibration Factors:

Data Channel	Calibration Factor	Gain	Filter	Channel Description
0	0.002329	1	1	Speed
1	0.037955	2	1	Fwd Heave
2	0.041361	2	1	Aft Heave
3	-0.647010	10	1	R_T
4	0.511958	1	5	Probe Position
5	0.067959	2	5	Water Elevation

Recorded Runs:

Run	Time	Speed m/s	R_T gf	Heave		Figure	Comments
				FWD Post	AFT Post		
				mm	mm		
1	15:35	1.131	201.9	-5.9	-3.4	C.2	Incomplete Run
2	15:45	1.132	197.1	-5.9	-2.6	C.3	Repeat of Run 1
3	15:55	1.277	235.3	-4.7	-6.3	C.5	
4	16:05	1.417	314.5	-2.5	-10.4	C.2	
5	16:20	1.552	395.9	-0.4	-12.6	C.4	
6	16:50	1.699	432.5	1.2	-14.8	C.1	
7	17:05	1.836	455.1	2.7	-14.6	C.2	
8	17:15	1.971	470.9	3.2	-13.5	C.3	
9	17:25	2.120	498.9	3.6	-12.4	C.4	
10	17:35	2.259	519.9	3.3	-10.9	C.5	
11	17:45	2.393	554.7	2.7	-10.1	C.1	
12	17:55	2.539	593.0	1.9	-8.9	C.2	
13	18:40	2.678	641.0	0.0	-8.1	C.3	
14	18:55	2.676	639.6	-0.2	-7.9	C.4	Repeat of Run 13
15	19:05	2.813	705.9	-5.6	-6.8	C.5	
16	19:15	0.996	171.6	-5.3	-1.6	C.5	
17	19:35	0.860	77.8	-3.3	-1.2	C.3	
18	19:45	0.713	44.5	-2.2	-0.7	C.2	
19	19:55	0.575	23.0	-1.2	-0.6	C.1	
20	20:05	1.064	182.2	-5.4	-1.7	C.1	
21	20:15	0.928	118.8	-4.1	-1.3	C.4	
22	20:25	1.200	205.3	-5.8	-4.2	C.4	
23	20:35	1.346	270.9	-3.7	-8.6	C.1	
24	20:45	1.486	364.7	-1.1	-12.4	C.3	
25	20:55	1.621	414.5	0.7	-14.7	C.5	

Hollow Model 1**Condition 2:** 4th and 5th June 2002**Model Data:**

LWL=	800.0	mm
WSA=	0.1722	m ²
Draft=	59.5	mm
Δ =	4.221	kg
Water Temp=	16.2	degrees

Calibration Factors:

Data Channel	Calibration Factor	Gain	Filter	Channel Description
0	0.002329	1	1	Speed
1	0.038206	2	1	Fwd Heave
2	0.041427	2	1	Aft Heave
3	-0.647903	10	1	R_T
4	0.507738	1	5	Probe Position
5	0.068638	2	5	Water Elevation

Recorded Runs:

Run	Time	Speed m/s	R_T gf	Heave		Figure	Comments
				FWD Post	AFT Post		
				mm	mm		
26	21:50	0.624	46.9	-2.2	-1.2	C.6	
27	22:00	0.771	74.9	-3.0	-0.8	C.7	
28	22:10	0.936	153.2	-4.6	-1.5	C.9	
29	22:20	1.082	224.6	-7.4	-2.7	C.9	
30	22:30	1.229	248.5	-6.3	-5.9	C.9	
31	10:10	1.388	339.6	-3.9	-11.5	C.6	Calibration 5/6/02
32	10:25	1.543	449.2	-1.0	-14.0	C.8	
33	10:35	1.700	531.3	1.0	-15.9	C.10	
34	10:55	1.846	578.3	2.7	-15.8	C.7	
35	11:05	2.002	593.6	3.6	-15.6	C.10	
36	11:15	2.158	622.8	3.7	-14.0	C.6	
37	11:25	2.306	654.6	3.3	-12.8	C.7	
38	11:40	2.451	693.0	2.5	-11.2	C.8	
39	11:50	2.618	747.0	0.0	-9.2	C.9	
40	12:05	2.764	804.3	-5.6	-7.8	C.10	
41	12:15	1.007	205.6	-7.6	-1.2	C.6	
42	12:25	1.161	218.6	-6.8	-3.1	C.8	
43	12:55	1.318	295.3	-4.8	-8.4	C.10	
44	13:05	1.466	399.4	-2.1	-12.4	C.7	
45	13:15	1.613	488.8	-0.1	-14.7	C.9	
46	13:25	1.778	562.4	2.1	-16.6	C.6	
47	13:35	0.859	87.0	-4.2	-0.9	C.8	
48	13:45	1.923	584.5	3.8	-16.0	C.9	
49	13:55	0.936	143.9	-5.0	-1.3	C.10	Repeat of Run 28
50	14:15	1.846	581.0	3.5	-16.9	C.8	Repeat of Run 34

Hollow Model 1**Condition 3:**5th June 2002**Model Data:**

LWL=	800.0	mm
WSA=	0.1913	m ²
Draft=	70.7	mm
Δ =	5.020	kg
Water Temp=	15.0	degrees

Calibration Factors:

Data Channel	Calibration Factor	Gain	Filter	Channel Description
0	0.002329	1	1	Speed
1	0.038206	2	1	Fwd Heave
2	0.041427	2	1	Aft Heave
3	-0.647903	10	1	R_T
4	0.507738	1	5	Probe Position
5	0.068638	2	5	Water Elevation

Recorded Runs:

Run	Time	Speed	R_T	Heave		Figure	Comments
				FWD Post	AFT Post		
		m/s	gf	mm	mm		
51	15:10	0.683	58.6	-3.4	-1.1	C.11	
52	15:20	0.840	96.2	-3.8	-1.1	C.13	
53	15:30	1.016	246.4	-6.1	-1.9	C.15	
54	15:40	1.181	257.9	-7.5	-4.0	C.12	
55	16:20	1.342	358.0	-5.2	-10.0	C.15	
56	16:30	1.509	482.0	-2.2	-14.0	C.12	
57	16:40	1.684	596.8	-0.2	-15.6	C.14	
58	16:50	1.843	701.7	2.0	-16.8	C.12	
59	17:00	2.008	758.2	3.7	-17.1	C.11	
60	17:10	2.184	783.2	3.6	-15.3	C.13	
61	17:20	2.340	815.2	2.5	-13.2	C.14	
62	17:30	2.513	864.6	0.2	-12.0	C.15	
63	17:40	0.758	83.5	-3.3	-0.8	C.12	
64	17:50	0.934	168.4	-5.0	-1.5	C.14	
65	18:35	1.087	257.2	-7.3	-2.2	C.11	
66	18:45	1.265	290.3	-6.6	-6.5	C.14	
67	18:55	1.430	431.4	-3.5	-12.2	C.11	
68	19:05	1.588	541.7	-1.1	-14.7	C.13	
69	19:15	1.765	646.7	0.8	-16.1	C.15	
70	19:25	1.928	745.9	3.3	-18.2	C.15	
71	19:35	2.084	770.4	3.9	-16.7	C.12	
72	19:45	1.802	674.4	1.2	-16.6	C.11	Partial Separation
73	19:55	1.881	728.7	2.5	-17.6	C.14	Full Separation
74	20:10	1.176	260.5	-7.7	-4.0	C.13	Repeat of Run 54
75	20:35	1.824	709.7	2.6	-17.7	C.13	Repeat of Run 58

Hollow Model 1**Condition 4:** 5th and 6th June 2002**Model Data:**

LWL=	800.0	mm
WSA=	0.2141	m ²
Draft=	84.1	mm
Δ =	5.970	kg
Water Temp=	16.4	degrees

Calibration Factors:

Data Channel	Calibration Factor	Gain	Filter	Channel Description
0	0.002329	1	1	Speed
1	0.038081	2	1	Fwd Heave
2	0.041336	2	1	Aft Heave
3	-0.647523	10	1	R_T
4	0.513777	1	5	Probe Position
5	0.067004	2	5	Water Elevation

Recorded Runs:

Run	Time	Speed m/s	R_T gf	Heave		Figure	Comments
				FWD Post	AFT Post		
				mm	mm		
76	21:05	0.738	94.3	-3.5	-1.6	C.16	
77	21:15	0.923	177.3	-5.0	-1.7	C.18	
78	21:25	1.099	295.7	-7.6	-2.6	C.20	
79	21:35	1.284	353.0	-6.6	-8.4	C.17	
80	21:45	1.461	537.6	-3.1	-14.0	C.19	
81	21:55	1.636	673.9	-1.0	-16.3	C.16	
82	22:05	1.831	779.0	0.6	-16.6	C.18	
83	22:15	2.009	956.7	2.9	-18.6	C.19	
84	22:25	2.193	992.2	2.9	-17.4	C.18	
85	22:35	0.828	110.5	-4.2	-1.3	C.17	
86	22:45	1.010	288.6	-6.2	-2.3	C.19	
87	10:25	1.185	296.6	-8.3	-5.6	C.16	Calibration 6/6/02
88	10:35	1.373	435.5	-4.8	-11.5	C.18	
89	10:45	1.549	604.2	-2.2	-15.2	C.20	
90	10:55	1.744	727.5	0.0	-16.5	C.17	
91	11:05	1.917	856.5	1.3	-16.9	C.16	
92	11:15	2.105	982.8	3.6	-18.8	C.16	
93	11:25	2.281	1008.1	2.7	-16.3	C.19	
94	11:35	1.960	894.1	2.0	-17.3	C.18	
95	11:50	2.046	968.0	3.3	-18.9	C.20	Full Separation
96	12:00	1.829	779.9	0.5	-16.3	C.19	Repeat of Run 82
97	12:10	1.919	854.8	1.4	-17.1	C.17	Repeat of Run 91
98	12:20	2.369	1029.9	2.0	-15.5	C.20	
99	12:30	1.870	815.2	0.6	-17.6	C.20	
100	12:40	2.145	986.6	3.3	-17.9	C.17	

Hollow Model 1**Condition 5:**6th June 2002**Model Data:**

LWL=	800.0	mm
WSA=	0.2411	m ²
Draft=	100.0	mm
Δ =	7.099	kg
Water Temp=	16.5	degrees

Calibration Factors:

Data Channel	Calibration Factor	Gain	Filter	Channel Description
0	0.002329	1	1	Speed
1	0.038081	2	1	Fwd Heave
2	0.041336	2	1	Aft Heave
3	-0.647523	10	1	R_T
4	0.513777	1	5	Probe Position
5	0.067004	2	5	Water Elevation

Recorded Runs:

Run	Time	Speed	R_T	Heave		Figure	Comments
				FWD Post	AFT Post		
		m/s	gf	mm	mm		
101	13:35	0.796	127.3	-3.6	-2.1	C.22	
102	13:45	1.001	333.6	-6.4	-2.7	C.24	
103	14:00	1.194	347.3	-8.1	-5.9	C.21	
104	14:15	1.402	565.3	-4.5	-13.2	C.24	
105	14:25	1.585	727.7	-1.7	-16.9	C.22	
106	14:35	1.793	882.4	0.0	-17.7	C.21	
107	14:45	1.986	1023.1	1.0	-16.7	C.24	
108	15:30	2.194	1290.8	1.3	-19.5	C.23	
109	16:50	0.699	83.0	-5.1	-0.9	C.21	
110	17:00	0.904	181.6	-4.7	-1.8	C.23	
111	17:15	1.098	333.6	-7.5	-3.4	C.25	
112	17:25	1.305	426.9	-6.7	-9.8	C.23	
113	17:35	1.499	684.5	-2.9	-15.7	C.21	
114	17:45	1.696	857.2	-0.7	-17.8	C.25	
115	18:00	1.888	965.7	0.8	-17.1	C.23	
116	18:45	2.085	1096.4	1.7	-16.9	C.21	
117	18:55	2.143	1241.5	2.4	-18.9	C.22	
118	19:10	1.843	948.3	0.5	-17.6	C.22	
119	19:20	1.635	815.6	-1.5	-17.6	C.24	
120	19:30	1.45	621.2	-4.0	-14.8	C.25	
121	19:45	1.244	369.3	-7.8	-7.5	C.22	
122	20:00	1.587	787.9	-1.6	-17.2	C.23	Repeat of Run 105
123	20:10	1.990	1035.1	0.6	-17.0	C.25	Repeat of Run 107
124	20:20	2.243	1267.6	2.3	-18.8	C.24	Full Separation
125	20:30	2.292	1269.5	2.1	-18.9	C.25	

Hollow Model 2**Condition 6:**15th July 2002**Model Data:**

LWL=	951.4	mm
WSA=	0.2016	m ²
Draft=	50.0	mm
Δ =	5.020	kg
Water Temp=	17.1	degrees

Calibration Factors:

Data Channel	Calibration Factor	Gain	Filter	Channel Description
0	0.002329	1	1	Speed
1	0.037059	2	1	Fwd Heave
2	0.039892	2	1	Aft Heave
3	-1.261672	5	1	R_T
4	0.507243	1	5	Probe Position
5	0.060597	2	5	Water Elevation

Recorded Runs:

Run	Time	Speed	R_T	Heave		Figure	Comments
				FWD Post	AFT Post		
		m/s	gf	mm	mm		
501	13:40	0.708	55.1	-2.0	-1.3	C.26	
502	13:50	0.856	103.8	-3.9	-1.2	C.27	
503	14:00	0.991	164.6	-5.2	-1.8	C.28	
504	14:10	1.128	264.3	-7.0	-2.0	C.29	
505	14:20	1.274	307.0	-5.2	-4.6	C.30	
506	14:30	1.413	382.9	-4.1	-8.7	C.27	
507	14:45	1.549	477.9	-2.4	-13.2	C.29	
508	14:55	1.693	547.2	0.8	-16.8	C.28	
509	15:05	1.831	580.4	2.7	-16.8	C.30	
510	15:15	1.970	607.0	4.4	-16.6	C.28	
511	15:25	2.117	637.2	5.7	-15.7	C.26	
512	15:40	2.252	665.8	6.4	-15.3	C.27	
513	15:50	2.390	701.5	6.3	-13.8	C.28	
514	16:00	2.534	740.8	5.8	-12.9	C.29	
515	16:10	2.671	787.4	4.9	-12.0	C.30	
516	16:20	1.344	341.1	-6.7	-6.5	C.26	
517	16:30	1.480	436.1	-3.6	-11.3	C.28	
518	16:45	1.617	519.6	-0.7	-15.5	C.26	Full Separation
519	16:55	1.764	566.3	1.8	-17.1	C.29	
520	17:05	1.901	595.4	3.6	-16.8	C.26	
521	17:15	2.037	624.4	5.0	-16.0	C.30	
522	17:25	1.588	509.3	-1.3	-14.9	C.30	
523	17:35	1.658	537.8	0.2	-16.4	C.27	
524	17:45	1.970	607.6	4.3	-16.5	C.29	Repeat of Run 510
525	18:00	1.898	594.8	3.8	-16.7	C.27	Repeat of Run 520

Hollow Model 2**Condition 7:** 15th and 16th July 2002**Model Data:**

LWL=	951.4	mm
WSA=	0.2208	m ²
Draft=	59.5	mm
Δ =	5.970	kg
Water Temp=	17.1	degrees

Calibration Factors:

Data Channel	Calibration Factor	Gain	Filter	Channel Description
0	0.002329	1	1	Speed
1	0.037079	2	1	Fwd Heave
2	0.039918	2	1	Aft Heave
3	-1.252261	5	1	R_T
4	0.507330	1	5	Probe Position
5	0.060670	2	5	Water Elevation

Recorded Runs:

Run	Time	Speed	R_T	Heave		Figure	Comments
				FWD Post	AFT Post		
		m/s	gf	mm	mm		
526	18:35	0.769	79.6	-3.3	-0.9	C.31	
527	19:20	0.934	143.2	-5.1	-1.8	C.32	
528	19:30	1.079	290.2	-6.7	-2.3	C.33	
529	19:40	1.226	336.9	-8.7	-3.1	C.34	
530	19:50	1.384	402.0	-6.9	-8.2	C.31	
531	20:00	1.540	546.3	-3.9	-13.6	C.34	
532	20:10	1.694	670.6	-0.1	-17.8	C.31	
533	20:25	1.844	731.0	2.9	-19.6	C.35	
534	20:35	2.001	763.4	4.5	-18.7	C.32	
535	20:45	2.154	793.4	5.4	-17.5	C.34	
536	20:55	2.300	829.4	5.7	-16.4	C.32	
537	21:25	2.445	866.2	5.3	-15.0	C.34	
538	21:35	2.614	920.6	4.2	-13.7	C.35	
539	21:50	1.313	361.9	-8.4	-5.4	C.35	
540	22:00	1.460	470.2	-5.5	-10.9	C.33	
541	22:15	1.608	616.1	-2.0	-15.7	C.35	
542	22:30	1.774	709.3	1.7	-18.9	C.33	
543	10:25	1.920	742.7	3.1	-19.2	C.31	Calibration 16/7/02
544	10:35	2.067	770.5	5.1	-18.5	C.33	
545	10:50	2.225	804.7	5.7	-17.1	C.31	
546	11:00	2.380	842.7	5.6	-15.5	C.33	
547	11:10	1.735	684.7	1.0	-18.6	C.32	
548	11:25	1.804	713.9	2.3	-19.6	C.34	Full Separation
549	11:35	1.382	401.9	-7.2	-8.2	C.32	Repeat of Run 530
550	11:45	2.155	792.0	5.6	-17.6	C.35	Repeat of Run 535

Hollow Model 2**Condition 8:**16th July 2002**Model Data:**

LWL=	951.4	mm
WSA=	0.2435	m ²
Draft=	70.7	mm
Δ =	7.099	kg
Water Temp=	15.0	degrees

Calibration Factors:

Data Channel	Calibration Factor	Gain	Filter	Channel Description
0	0.002329	1	1	Speed
1	0.037079	2	1	Fwd Heave
2	0.039918	2	1	Aft Heave
3	-1.252261	5	1	R_T
4	0.507330	1	5	Probe Position
5	0.060670	2	5	Water Elevation

Recorded Runs:

Run	Time	Speed	R_T	Heave		Figure	Comments
		m/s	gf	FWD Post	AFT Post		
				mm	mm		
551	12:20	0.836	133.3	-4.3	-1.8	C.36	
552	12:30	1.011	252.2	-5.8	-2.2	C.37	
553	12:40	1.177	381.4	-9.0	-2.5	C.38	
554	13:20	1.344	421.8	-8.4	-7.1	C.40	
555	13:30	1.512	571.3	-5.3	-13.3	C.37	
556	13:40	1.684	757.8	-1.5	-17.8	C.39	
557	13:50	1.844	892.2	1.9	-20.1	C.36	
558	14:00	2.008	963.3	5.1	-21.2	C.37	
559	14:10	2.183	995.6	5.9	-19.7	C.39	
560	14:20	2.341	1031.9	5.8	-17.9	C.36	
561	14:30	2.515	1083.8	4.9	-16.3	C.38	
562	14:45	2.68	1141.2	2.8	-14.6	C.40	
563	15:00	1.261	385.0	-9.1	-4.0	C.39	
564	15:10	1.432	487.8	-6.9	-10.4	C.36	
565	15:20	1.588	659.7	-3.5	-15.5	C.38	
566	15:30	1.764	837.9	0.4	-19.2	C.40	
567	15:40	1.929	941.9	3.8	-20.8	C.39	Full Separation
568	15:50	2.086	983.4	5.5	-20.6	C.38	
569	16:00	2.264	1018.0	6.1	-18.8	C.40	
570	16:10	2.429	1057.6	5.6	-17.0	C.37	
571	16:20	2.591	1112.7	4.0	-15.5	C.39	
572	16:35	1.881	921.5	2.9	-20.9	C.38	
573	16:45	1.970	959.7	4.8	-21.5	C.36	
574	16:55	1.844	894.2	2.1	-20.1	C.37	Repeat of Run 557
575	17:05	1.932	939.9	3.8	-20.9	C.40	Repeat of Run 567

Hollow Model 2**Condition 9:** 16th and 17th July 2002**Model Data:**

LWL=	951.4	mm
WSA=	0.2706	m ²
Draft=	84.1	mm
Δ =	8.443	kg
Water Temp=	17.3	degrees

Calibration Factors:

Data Channel	Calibration Factor	Gain	Filter	Channel Description
0	0.002329	1	1	Speed
1	0.037192	2	1	Fwd Heave
2	0.039776	2	1	Aft Heave
3	-1.264603	5	1	R_T
4	0.507616	1	5	Probe Position
5	0.120749	2	5	Water Elevation

Recorded Runs:

Run	Time	Speed	R_T	Heave		Figure	Comments
				FWD Post	AFT Post		
		m/s	gf	mm	mm		
576	18:30	0.737	87.0	-3.3	-1.3	C.41	
577	18:40	0.922	175.0	-5.8	-1.8	C.43	
578	18:50	1.100	423.6	-8.2	-2.5	C.45	
579	19:00	1.285	440.6	-9.5	-5.4	C.42	
580	19:10	1.462	590.1	-7.1	-12.1	C.44	
581	19:20	1.637	809.4	-3.2	-17.5	C.41	
582	19:30	1.831	1004.7	0.3	-20.2	C.43	
583	19:40	2.008	1179.7	3.7	-21.9	C.41	
584	19:50	2.195	1267.8	5.8	-22.2	C.41	
585	20:05	2.369	1307.1	5.5	-20.1	C.43	
586	20:15	2.555	1358.0	3.6	-18.4	C.45	
587	20:25	0.825	144.0	-4.5	-1.1	C.42	
588	20:35	1.012	264.4	-6.2	-2.0	C.44	
589	20:45	1.184	438.4	-9.3	-3.0	C.41	
590	20:55	1.372	496.1	-8.8	-8.7	C.43	
591	21:05	1.548	708.8	-4.8	-15.2	C.45	
592	21:15	1.742	925.4	-0.8	-19.4	C.42	
593	21:25	1.922	1098.6	1.9	-20.8	C.44	
594	21:35	2.107	1254.2	5.5	-23.1	C.44	
595	09:45	2.282	1302.5	4.7	-20.8	C.42	Calibration 17/7/02
596	09:55	2.457	1343.0	4.5	-18.9	C.44	
597	10:05	2.046	1225.2	4.2	-22.0	C.42	
598	10:20	2.146	1276.6	5.5	-22.5	C.45	Full Separation
599	10:30	1.919	1101.3	1.9	-20.7	C.45	Repeat of Run 593
600	10:45	2.047	1229.7	4.2	-22.2	C.43	Repeat of Run 597

Condition 10: 17th July 2002**Model Data:**

LWL=	951.4	mm
WSA=	0.3027	m ²
Draft=	100.0	mm
Δ =	10.040	kg
Water Temp=	17.3	degrees

Calibration Factors:

Data Channel	Calibration Factor	Gain	Filter	Channel Description
0	0.002329	1	1	Speed
1	0.037192	2	1	Fwd Heave
2	0.039776	2	1	Aft Heave
3	-1.264603	10	1	R_T
4	0.507616	1	5	Probe Position
5	0.120749	1	5	Water Elevation

Recorded Runs:

Run	Time	Speed m/s	R_T gf	Heave		Figure	Comments
				FWD Post	AFT Post		
				mm	mm		
601	11:30	0.796	153.3	-3.9	-1.9	C.46	
602	11:40	1.002	297.7	-6.7	-2.1	C.48	
603	11:50	1.198	488.6	-10.0	-3.7	C.50	
604	12:05	1.403	606.5	-8.6	-11.2	C.48	
605	12:15	1.588	907.6	-4.5	-17.2	C.50	
606	12:25	1.797	1153.5	-0.8	-20.4	C.47	
607	12:35	1.989	1312.4	1.7	-20.5	C.49	
608	13:45	2.196	1606.4	4.5	-22.5	C.48	
609	13:55	0.903	191.1	-5.7	-1.6	C.47	
610	14:05	1.100	494.7	-8.2	-3.1	C.49	
611	14:15	1.304	505.0	-10.2	-6.8	C.47	
612	14:25	1.892	1226.2	0.4	-21.0	C.49	
613	14:35	1.694	1042.9	-2.5	-19.4	C.46	
614	14:45	1.892	1226.2	0.4	-21.0	C.48	
615	15:00	2.085	1402.6	2.5	-20.6	C.46	
616	15:10	2.039	1345.9	2.1	-20.3	C.50	
617	15:20	2.147	1515.0	3.4	-21.3	C.47	
618	15:30	2.243	1641.4	5.2	-23.1	C.50	
619	15:45	2.290	1663.4	5.4	-23.2	C.46	Full Separation
620	16:00	1.196	496.3	-10.1	-3.6	C.46	Repeat of Run 603
621	16:10	2.195	1615.1	4.7	-22.7	C.49	Repeat of Run 608
622	16:20	2.341	1672.6	5.4	-22.7	C.47	
623	16:30	2.389	1684.3	5.0	-22.2	C.48	
624	16:40	2.438	1699.7	4.3	-21.9	C.49	
625	16:55	2.487	1715.8	4.3	-21.2	C.50	

Hollow Model 3**Condition 11:** 7th June 2002**Model Data:**

LWL=	1131.4	mm
WSA=	0.2624	m ²
Draft=	50.0	mm
Δ =	7.099	kg
Water Temp=	16.7	degrees

Calibration Factors:

Data Channel	Calibration Factor	Gain	Filter	Channel Description
0	0.002329	1	1	Speed
1	0.038089	2	1	Fwd Heave
2	0.039833	2	1	Aft Heave
3	-1.256528	5	1	R_T
4	0.508034	1	5	Probe Position
5	0.067531	2	5	Water Elevation

Recorded Runs:

Run	Time	Speed	R_T	Heave		Figure	Comments
				FWD Post	AFT Post		
		m/s	gf	mm	mm		
126	11:45	0.569	37.7	-2.0	-0.8	C.51	
127	11:55	0.707	58.1	-2.3	-0.9	C.52	
128	12:05	0.855	111.7	-3.4	-1.0	C.53	
129	12:15	0.992	154.6	-4.8	-1.6	C.54	
130	12:25	1.128	280.7	-5.9	-2.6	C.55	
131	12:35	1.273	361.8	-7.6	-2.4	C.51	
132	12:45	1.412	430.1	-7.9	-5.1	C.53	
133	12:55	1.548	550.3	-5.6	-10.6	C.51	
134	13:05	1.696	641.9	-2.1	-15.7	C.54	
135	13:45	1.831	706.5	0.3	-17.3	C.51	
136	13:55	1.968	745.2	2.0	-17.3	C.53	
137	14:05	2.115	783.7	3.8	-17.1	C.54	
138	14:15	2.251	824.7	4.8	-16.4	C.55	
139	14:25	2.388	873.0	5.5	-15.9	C.51	
140	14:35	2.535	918.8	5.7	-15.0	C.53	
141	14:45	2.671	964.6	5.5	-14.5	C.54	
142	14:55	2.807	1031.8	5.3	-13.7	C.55	
143	15:05	1.344	406.2	-8.3	-3.6	C.52	
144	15:15	1.479	486.0	-6.8	-7.8	C.55	
145	15:25	1.617	605.8	-3.5	-13.5	C.53	Full Separation
146	15:40	1.762	681.9	-0.8	-16.7	C.55	
147	15:50	1.899	729.2	1.2	-17.2	C.52	
148	16:00	1.587	590.5	-4.3	-12.5	C.52	
149	16:10	1.411	435.0	-7.9	-5.2	C.54	Repeat of Run 132
150	16:20	2.389	869.3	5.6	-15.8	C.52	Repeat of Run 139

Hollow Model 3**Condition 12:**7th June 2002**Model Data:**

LWL=	1131.4	mm
WSA=	0.2852	m ²
Draft=	59.5	mm
Δ =	8.443	kg
Water Temp=	16.9	degrees

Calibration Factors:

Data Channel	Calibration Factor	Gain	Filter	Channel Description
0	0.002329	1	1	Speed
1	0.038089	2	1	Fwd Heave
2	0.039833	2	1	Aft Heave
3	-1.256528	5	1	R_T
4	0.508034	1	5	Probe Position
5	0.067531	2	5	Water Elevation

Recorded Runs:

Run	Time	Speed	R_T	Heave		Figure	Comments
		m/s	gf	FWD Post	AFT Post		
				mm	mm		
151	16:50	0.618	58.5	-1.8	-1.0	C.56	
152	17:00	0.767	79.8	-3.0	-0.9	C.57	
153	17:15	0.933	169.3	-4.7	-1.4	C.58	
154	17:25	1.079	264.4	-6.1	-2.1	C.59	
155	17:40	1.224	414.5	-7.9	-2.3	C.60	
156	18:40	1.382	482.8	-8.8	-4.6	C.56	
157	18:50	1.539	634.2	-6.6	-10.7	C.58	
158	19:05	1.694	801.8	-2.8	-16.7	C.60	
159	19:15	1.843	889.9	0.5	-19.8	C.59	
160	19:25	1.998	945.8	2.7	-20	C.56	
161	19:35	2.156	1002.5	4.5	-19.5	C.58	
162	19:45	2.445	1083.8	6	-17.5	C.59	
163	19:55	2.445	1083.8	6	-17.5	C.60	
164	20:05	2.614	1144.6	5.8	-16.4	C.56	
165	20:15	2.760	1220.5	5.2	-15.5	C.57	
166	20:25	2.907	1291.8	4.2	-14.1	C.59	
167	20:35	3.061	1380.6	2.3	-12.8	C.60	
168	20:45	1.459	556.5	-8.4	-7.5	C.57	
169	20:55	1.608	716.6	-5.1	-13.4	C.59	
170	21:05	1.774	870.7	-0.8	-19.0	C.58	Full Separation
171	21:15	1.919	925.2	2.0	-19.9	C.60	
172	21:25	2.065	980.5	3.7	-20.0	C.57	
173	21:35	1.735	843.5	-1.6	-18.1	C.56	
174	21:45	2.760	1215.4	5.4	-15.5	C.58	Repeat of Run 165
175	21:55	1.734	843.5	-1.5	-18.0	C.57	Repeat of Run 173

Hollow Model 3**Condition 13:** 7th and 8th June 2002**Model Data:**

LWL=	1131.4	mm
WSA=	0.3122	m ²
Draft=	70.7	mm
Δ =	10.040	kg
Water Temp=	17.0	degrees

Calibration Factors:

Data Channel	Calibration Factor	Gain	Filter	Channel Description
0	0.002329	1	1	Speed
1	0.038072	2	1	Fwd Heave
2	0.039868	2	1	Aft Heave
3	-1.262450	5	1	R_T
4	0.507879	1	5	Probe Position
5	0.070332	2	5	Water Elevation

Recorded Runs:

Run	Time	Speed	R_T	Heave		Figure	Comments
				FWD Post	AFT Post		
		m/s	gf	mm	mm		
176	22:25	0.835	130.0	-4.0	-1.2	C.61	
177	22:35	1.009	219.5	-5.8	-2.0	C.62	
178	22:45	1.176	472.4	-7.7	-2.8	C.63	
179	10:05	1.344	559.7	-10.3	-3.7	C.64	Calibration 8/6/02
180	10:15	1.508	672.1	-8.7	-9.7	C.65	
181	10:25	1.685	929.6	-4.1	-16.7	C.62	
182	10:40	1.842	1118.6	0.1	-21.2	C.61	
183	10:50	2.008	1213.9	3.3	-22.8	C.64	
184	11:00	2.183	1268.3	5.1	-22.0	C.61	
185	11:10	2.340	1308.7	5.6	-20.9	C.63	
186	11:20	2.514	1362.8	6.0	-19.3	C.64	
187	11:30	2.680	1436.6	5.6	-17.7	C.65	
188	11:40	2.837	1511.7	4.1	-16.2	C.62	
189	11:50	3.016	1618.1	1.9	-14.0	C.63	
190	12:00	3.168	1717.3	-0.9	-12.4	C.64	
191	12:15	3.335	1882.3	-8.5	-9.2	C.65	
192	12:25	1.587	785.7	-6.4	-13.2	C.61	
193	12:35	1.762	1053.2	-1.8	-19.3	C.64	
194	14:10	1.928	1184.2	2.2	-22.6	C.63	
195	14:20	2.089	1237.1	4.0	-22.6	C.65	
196	14:30	2.262	1291.7	5.8	-21.4	C.62	
197	14:45	1.879	1162.1	1.1	-22.2	C.62	Full Separation
198	14:55	1.801	1089.4	-0.8	-20.8	C.65	
199	15:05	1.685	940.6	-4.1	-16.8	C.63	Repeat of Run 181
200	15:15	2.677	1435.2	5.5	-17.7	C.61	Repeat of Run 187

Hollow Model 3**Condition 14:**8th June 2002**Model Data:**

LWL=	1131.4	mm
WSA=	0.3444	m ²
Draft=	84.1	mm
Δ =	11.940	kg
Water Temp=	17.2	degrees

Calibration Factors:

Data Channel	Calibration Factor	Gain	Filter	Channel Description
0	0.002329	1	1	Speed
1	0.038072	2	1	Fwd Heave
2	0.039868	2	1	Aft Heave
3	-1.262450	5	1	R_T
4	0.507879	1	5	Probe Position
5	0.070332	2	5	Water Elevation

Recorded Runs:

Run	Time	Speed	R_T	Heave		Figure	Comments
				FWD Post	AFT Post		
		m/s	gf	mm	mm		
201	15:50	0.921	224.0	-5.0	-1.6	C.66	
202	16:00	1.098	378.4	-7.2	-2.5	C.67	
203	16:10	1.282	642.4	-10.2	-3.2	C.68	
204	16:25	1.460	677.0	-10.3	-7.9	C.70	
205	16:35	1.636	942.7	-6.5	-15.2	C.67	
206	16:45	1.831	1298.6	-1.2	-21.4	C.69	
207	17:00	2.008	1515.3	2.7	-24.3	C.68	
208	17:10	2.193	1608.4	5.7	-24.3	C.66	
209	17:20	2.368	1667.7	6.1	-23.6	C.68	
210	17:30	2.554	1723.8	5.7	-21.4	C.66	
211	17:40	2.729	1803.9	4.6	-19.8	C.68	
212	17:50	2.913	1887.5	2.5	-17.3	C.69	
213	18:00	3.098	1995.8	-1.2	-14.3	C.70	
214	18:20	1.372	639.9	-10.9	-4.9	C.69	
215	18:40	1.547	784.5	-8.5	-11.4	C.66	
216	18:50	1.742	1131.9	-3.6	-18.9	C.68	
217	19:00	1.920	1414.3	0.8	-23.0	C.70	
218	19:10	2.105	1583.7	4.7	-25.0	C.70	Full Separation
219	19:20	2.280	1640.6	6.0	-24.2	C.67	
220	19:30	2.458	1681.9	6.1	-22.9	C.70	
221	19:50	2.643	1756.7	5.0	-20.6	C.67	
222	20:00	1.959	1472.1	1.6	-23.5	C.67	
223	20:10	2.046	1533.9	3.4	-24.3	C.69	
224	20:20	2.367	1658.7	6.0	-23.4	C.69	Repeat of Run 209
225	20:30	1.918	1426.8	0.7	-23.2	C.66	Repeat of Run 217

Hollow Model 3**Condition 15:** 8th and 9th June 2002**Model Data:**

LWL=	1131.4	mm
WSA=	0.3826	m ²
Draft=	100.0	mm
Δ =	14.199	kg
Water Temp=	15.0	degrees

Calibration Factors:

Data Channel	Calibration Factor	Gain	Filter	Channel Description
0	0.002329	1	1	Speed
1	0.038032	2	1	Fwd Heave
2	0.039813	2	1	Aft Heave
3	-1.263796	5	1	R_T
4	0.507566	1	5	Probe Position
5	0.070610	2	5	Water Elevation

Recorded Runs:

Run	Time	Speed	R_T	Heave		Figure	Comments
				FWD Post	AFT Post		
		m/s	gf	mm	mm		
226	21:30	0.796	149.2	-3.7	-1.6	C.71	
227	21:40	1.001	274.4	-6.3	-2.2	C.72	
228	21:50	1.195	704.0	-9.1	-3.4	C.74	
229	22:00	1.403	730.3	-11.3	-6.4	C.71	
230	22:10	1.586	992.6	-8.0	-14.2	C.74	
231	22:20	1.793	1376.7	-3.1	-21.1	C.71	
232	22:30	1.989	1695.3	0.8	-24.0	C.73	
233	11:00	2.193	1999.4	3.7	-25.5	C.71	Calibration 9/6/02
234	11:10	2.388	2117.7	5.9	-26.2	C.75	
235	11:20	2.592	2173.8	5.6	-23.9	C.72	
236	11:30	2.777	2259.8	3.8	-21.6	C.74	
237	11:40	1.098	429.7	-7.9	-2.6	C.73	
238	11:50	1.304	709.3	-11.2	-3.7	C.75	
239	12:00	1.499	823.4	-10.2	-10.5	C.73	
240	12:10	1.693	1202.8	-5.5	-18.6	C.75	
241	12:20	1.889	1552.0	-1.1	-23.1	C.72	
242	12:30	2.086	1832.3	2.5	-24.6	C.74	
243	13:35	2.292	2092.2	5.8	-26.8	C.74	
244	13:45	2.486	2144.8	6.4	-25.2	C.71	
245	13:55	2.679	2214.5	5.0	-22.9	C.73	
246	14:05	2.146	1942.5	3.9	-25.2	C.75	
247	14:15	2.244	2053.5	5.0	-26.3	C.73	Full Separation
248	14:25	1.402	738.3	-11.7	-6.4	C.72	Repeat of Run 229
249	14:35	2.194	2009.4	4.6	-25.9	C.72	Repeat of Run 233
250	14:45	2.876	2304.7	2.8	-20.1	C.75	

Hollow Model 4**Condition 16:**12th July 2002**Model Data:**

LWL=	1345.4	mm
WSA=	0.3441	m ²
Draft=	50.0	mm
Δ =	10.040	kg
Water Temp=	15.0	degrees

Calibration Factors:

Data Channel	Calibration Factor	Gain	Filter	Channel Description
0	0.002329	1	1	Speed
1	0.037139	2	1	Fwd Heave
2	0.039918	2	1	Aft Heave
3	-3.188714	2	1	R_T
4	0.506919	1	5	Probe Position
5	0.061642	2	5	Water Elevation

Recorded Runs:

Run	Time	Speed	R_T	Heave		Figure	Comments
		m/s	gf	FWD Post	AFT Post		
				mm	mm		
376	16:20	0.709	87.2	-2.1	-0.9	C.76	
377	16:30	0.856	135.2	-3.2	-1.1	C.77	
378	16:40	0.990	216.1	-4.5	-1.4	C.78	
379	16:50	1.129	292.4	-5.5	-2.3	C.79	
380	17:00	1.274	449.8	-6.9	-2.9	C.80	
381	17:10	1.412	539.3	-8.5	-3.3	C.77	
382	17:20	1.549	645.8	-8.0	-6.8	C.79	
383	17:30	1.695	785.2	-4.9	-12.7	C.77	Full Separation
384	17:40	1.832	876.5	-1.9	-16.0	C.80	
385	17:50	1.969	943.1	0.4	-17.4	C.77	
386	18:00	2.117	998.4	2.4	-17.7	C.79	
387	18:35	2.254	1047.9	3.7	-17.6	C.80	
388	18:45	2.390	1098.9	4.9	-17.2	C.76	
389	18:55	2.535	1159.1	5.6	-17.1	C.77	
390	19:05	2.673	1215.9	6.3	-16.7	C.78	
391	19:15	2.810	1285.8	6.5	-16.5	C.80	
392	19:25	1.343	507.5	-7.8	-3.2	C.76	
393	19:35	1.480	589.5	-8.6	-4.5	C.78	
394	19:45	1.617	722.3	-6.4	-9.9	C.76	
395	19:55	1.763	835.3	-3.1	-14.9	C.79	
396	20:05	1.901	915.8	-0.6	-16.9	C.76	
397	20:15	2.038	973.7	1.5	-17.7	C.78	
398	20:25	1.588	698.9	-7.2	-9.0	C.80	
399	20:35	2.675	1218.5	6.0	-16.8	C.79	Repeat of Run 390
400	20:45	1.698	792.1	-4.5	-13.2	C.78	Repeat of Run 383

Hollow Model 4**Condition 17:**13th July 2002**Model Data:**

LWL=	1354.4	mm
WSA=	0.3711	m ²
Draft=	59.5	mm
Δ =	11.940	kg
Water Temp=	17.1	degrees

Calibration Factors:

Data Channel	Calibration Factor	Gain	Filter	Channel Description
0	0.002329	1	1	Speed
1	0.037108	2	1	Fwd Heave
2	0.040010	2	1	Aft Heave
3	-3.183555	2	1	R_T
4	0.507233	1	5	Probe Position
5	0.060809	2	5	Water Elevation

Recorded Runs:

Run	Time	Speed	R_T	Heave		Figure	Comments
				FWD Post	AFT Post		
		m/s	gf	mm	mm		
401	10:05	0.771	117.7	-2.7	-1.1	C.81	
402	10:15	0.933	196.6	-4.3	-1.4	C.82	
403	10:25	1.079	285.2	-5.7	-2.2	C.83	
404	10:35	1.227	478.3	-7.0	-3.2	C.84	
405	10:45	1.384	618.7	-9.3	-2.9	C.85	
406	11:00	1.538	733.7	-9.4	-6.5	C.82	
407	11:10	1.697	950.2	-5.9	-13.8	C.84	
408	11:20	1.845	1100.4	-1.5	-18.8	C.82	
409	11:30	2.001	1188.0	1.3	-20.5	C.84	
410	11:40	2.154	1249.4	3.2	-20.6	C.81	
411	11:50	2.302	1315.0	4.9	-20.4	C.84	
412	12:00	2.449	1371.5	6.0	-20.0	C.85	
413	12:10	2.617	1445.3	6.7	-19.5	C.81	
414	12:25	2.761	1518.7	6.8	-19.0	C.82	
415	13:00	2.908	1599.0	7.5	-18.1	C.83	
416	13:10	3.062	1697.9	7.1	-16.8	C.84	
417	13:20	1.462	666.7	-9.9	-4.3	C.81	
418	13:30	1.608	819.6	-8.2	-9.4	C.83	
419	13:40	1.773	1047.5	-3.4	-16.7	C.85	Full Separation
420	13:50	1.920	1147.2	0.0	-19.9	C.83	
421	14:00	2.067	1218.0	2.3	-20.8	C.85	
422	14:10	2.225	1282.2	4.2	-20.7	C.82	
423	14:25	1.804	1069.0	-1.4	-17.7	C.81	
424	14:35	3.064	1696.2	6.9	-16.5	C.85	Repeat of Run 416
425	14:50	2.225	1281.9	0.7	-20.7	C.83	Repeat of Run 422

Hollow Model 4**Condition 18:**13th July 2002**Model Data:**

LWL=	1345.4	mm
WSA=	0.4033	m ²
Draft=	70.7	mm
Δ =	14.199	kg
Water Temp=	17.0	degrees

Calibration Factors:

Data Channel	Calibration Factor	Gain	Filter	Channel Description
0	0.002329	1	1	Speed
1	0.037108	2	1	Fwd Heave
2	0.040010	2	1	Aft Heave
3	-3.183555	2	1	R_T
4	0.507233	1	5	Probe Position
5	0.060809	2	5	Water Elevation

Recorded Runs:

Run	Time	Speed	R_T	Heave		Figure	Comments
				FWD Post	AFT Post		
		m/s	gf	mm	mm		
426	15:20	0.836	154.9	-3.5	-1.3	C.86	
427	15:30	1.012	286.2	-5.5	-1.5	C.87	
428	15:40	1.177	465.7	-7.1	-2.8	C.89	
429	15:50	1.345	715.7	-9.7	-3.0	C.89	
430	16:00	1.511	849.1	-10.7	-6.1	C.90	
431	16:10	1.686	1095.6	-7.2	-13.7	C.87	
432	16:20	1.843	1354.4	-2.4	-20.2	C.89	
433	16:30	2.009	1495.9	1.8	-23.6	C.88	
434	16:45	2.183	1579.2	4.4	-23.8	C.90	
435	16:55	2.341	1649.2	6.1	-23.4	C.87	
436	17:15	2.516	1724.5	7.1	-22.8	C.89	
437	17:25	2.682	1799.1	7.3	-22.0	C.90	
438	17:35	2.838	1889.2	7.5	-20.7	C.87	
439	17:45	3.017	2001.6	7.5	-18.6	C.88	
440	18:00	3.171	2113.9	7.0	-16.7	C.89	
441	18:10	3.337	2242.3	5.3	-14.4	C.90	
442	18:20	1.587	930.8	-9.7	-9.0	C.86	
443	18:35	1.765	1226.5	-4.9	-17.0	C.88	
444	18:50	1.928	1440.4	0.3	-22.8	C.87	
445	19:05	2.087	1533.7	2.9	-23.8	C.89	
446	19:35	2.264	1616.8	5.3	-23.7	C.86	
447	19:45	2.430	1683.8	6.7	-22.9	C.88	
448	20:05	1.880	1404.1	-1.0	-21.5	C.86	Full Separation
449	20:15	1.843	1362.1	-2.2	-20.5	C.90	Repeat of Run 432
450	20:30	2.683	1805.0	7.2	-21.9	C.86	Repeat of Run 437

Hollow Model 4**Condition 19:** 13th and 14th June 2002**Model Data:**

LWL=	1345.4	mm
WSA=	0.4415	m ²
Draft=	84.1	mm
Δ =	16.885	kg
Water Temp=	17.1	degrees

Calibration Factors:

Data Channel	Calibration Factor	Gain	Filter	Channel Description
0	0.002329	1	1	Speed
1	0.037247	2	1	Fwd Heave
2	0.040009	2	1	Aft Heave
3	-3.187615	2	1	R_T
4	0.507104	1	5	Probe Position
5	0.122720	1	5	Water Elevation

Recorded Runs:

Run	Time	Speed	R_T	Heave		Figure	Comments
				FWD Post	AFT Post		
		m/s	gf	mm	mm		
451	21:15	0.924	229.7	-4.8	-1.3	C.91	
452	21:30	1.099	369.3	-6.9	-2.4	C.92	
453	10:25	1.283	796.4	-10.1	-3.1	C.93	Calibration 14/7/02
454	10:40	1.461	930.8	-12.1	-4.7	C.94	
455	10:50	1.639	1124.0	-10.2	-11.8	C.95	
456	11:00	1.835	1569.3	-4.1	-20.3	C.92	
457	11:10	2.008	1864.3	1.1	-25.4	C.95	
458	12:00	2.194	2005.9	4.7	-27.1	C.95	
459	12:15	2.368	2085.9	6.5	-26.3	C.92	
460	12:25	2.556	2167.2	7.1	-25.4	C.94	
461	12:40	2.733	2254.7	7.3	-24.0	C.91	
462	13:35	2.917	2370.0	7.2	-21.9	C.92	
463	13:45	3.102	2500.1	7.1	-19.0	C.93	
464	13:55	3.279	2626.1	4.9	-15.7	C.94	
465	14:10	3.465	2808.5	0.1	-12.7	C.95	
466	14:25	1.745	1367.3	-6.9	-16.8	C.91	
467	14:35	1.921	1758.6	-1.4	-23.5	C.94	
468	14:45	2.106	1954.4	3.2	-26.7	C.92	Full Separation
469	14:55	2.282	2048.3	5.6	-26.8	C.91	
470	15:05	2.457	2120.0	6.9	-25.8	C.93	
471	15:20	2.644	2205.2	7.0	-24.7	C.95	
472	15:35	2.046	1889.4	1.8	-25.9	C.91	
473	15:55	2.145	1982.8	4.0	-27.1	C.94	
474	16:05	2.106	1950.9	3.2	-26.6	C.93	Repeat of Run 468
475	16:20	1.833	1590.3	-3.9	-20.7	C.93	Repeat of Run 456

Hollow Model 4**Condition 20:**14th July 2002**Model Data:**

LWL=	1345.4	mm
WSA=	0.4870	m ²
Draft=	100.0	mm
Δ =	20.080	kg
Water Temp=	15.0	degrees

Calibration Factors:

Data Channel	Calibration Factor	Gain	Filter	Channel Description
0	0.002329	1	1	Speed
1	0.037247	2	1	Fwd Heave
2	0.040009	2	1	Aft Heave
3	-3.187615	2	1	R_T
4	0.507104	1	5	Probe Position
5	0.122720	1	5	Water Elevation

Recorded Runs:

Run	Time	Speed	R_T	Heave		Figure	Comments
				FWD Post	AFT Post		
		m/s	gf	mm	mm		
476	16:40	1.002	372.3	-6.0	-2.1	C.96	
477	16:50	1.196	692.8	-8.6	-3.3	C.97	
478	17:00	1.404	1054.0	-12.4	-4.0	C.98	
479	17:15	1.588	1148.8	-12.1	-9.9	C.100	
480	17:25	1.794	1643.2	-6.4	-19.6	C.97	
481	17:35	1.988	2152.0	-0.6	-25.5	C.99	
482	17:45	2.196	2514.1	4.1	-28.8	C.97	
483	17:55	2.389	2665.4	7.1	-29.6	C.96	
484	18:35	2.592	2749.4	7.4	-28.3	C.98	
485	18:45	2.781	2852.5	7.0	-27.0	C.96	
486	18:55	2.984	2983.7	7.5	-23.7	C.97	
487	19:10	3.182	3117.5	6.0	-19.3	C.98	
488	19:25	3.388	3277.0	1.7	-14.8	C.99	
489	19:40	3.58	3502.9	-9.7	-9.4	C.100	
490	20:00	1.502	1060.9	-12.5	-6.6	C.99	
491	20:20	1.695	1368.9	-9.3	-15.2	C.96	
492	20:40	1.890	1892.6	-3.5	-22.7	C.98	
493	21:00	2.087	2375.3	1.4	-27.5	C.96	
494	21:15	2.292	2603.1	5.9	-30.0	C.99	
495	21:30	2.488	2711.5	7.5	-29.1	C.97	
496	21:45	2.682	2813.9	7.4	-27.9	C.99	
497	22:00	2.244	2549.4	4.8	-29.1	C.98	
498	22:15	2.342	2646.8	6.5	-30.0	C.100	Full Separation
499	22:30	1.989	2169.2	-0.7	-25.5	C.100	Repeat of Run 481
500	22:45	2.683	2804.5	7.2	-27.8	C.100	Repeat of Run 496

Hollow Model 5**Condition 21:** 9th and 10th June 2002**Model Data:**

LWL=	1600.0	mm
WSA=	0.4544	m ²
Draft=	50.0	mm
Δ =	14.199	kg
Water Temp=	17.2	degrees

Calibration Factors:

Data Channel	Calibration Factor	Gain	Filter	Channel Description
0	0.002329	1	1	Speed
1	0.038026	2	1	Fwd Heave
2	0.039802	2	1	Aft Heave
3	-3.189169	2	1	R_T
4	0.507364	1	5	Probe Position
5	0.069968	2	5	Water Elevation

Recorded Runs:

Run	Time	Speed m/s	R_T gf	Heave		Figure	Comments
				FWD Post	AFT Post		
				mm	mm		
251	19:50	0.706	107.6	-1.8	-1.1	C.101	
252	20:00	0.854	175.7	-2.5	-1.4	C.102	
253	20:10	0.991	239.6	-3.9	-1.6	C.103	
254	20:20	1.127	341.3	-5.0	-1.8	C.104	
255	20:30	1.274	480.8	-6.1	-3.3	C.105	
256	20:40	1.411	654.1	-7.2	-3.9	C.102	
257	20:50	1.548	768.8	-8.5	-4.5	C.104	
258	21:00	1.694	918.2	-7.6	-8.4	C.103	
259	21:05	1.830	1044.9	-5.2	-12.9	C.105	
260	21:15	1.967	1152.3	-2.9	-15.5	C.102	
261	21:25	2.119	1243.4	-0.4	-17.3	C.104	
262	21:35	2.250	1316.4	1.2	-17.7	C.101	
263	21:45	2.388	1398.3	2.4	-17.8	C.102	
264	22:05	2.533	1469.4	3.3	-17.9	C.103	
265	22:15	2.670	1546.3	4.0	-18.1	C.104	
266	22:25	2.808	1623.3	4.4	-18.2	C.105	
267	22:35	1.342	593.3	-6.5	-3.8	C.101	
268	22:45	1.479	718.9	-7.8	-4.3	C.103	
269	22:55	1.617	834.2	-8.4	-6.1	C.102	
270	23:05	1.762	988.4	-6.3	-11.1	C.104	
271	11:40	1.899	1106.6	-4.0	-14.3	C.101	Calibration 10/6/02
272	11:50	2.038	1203.7	-2.0	-16.4	C.103	
273	12:00	1.587	811.6	-8.6	-5.3	C.105	Full Separation
274	12:10	2.116	1244.7	-0.8	-17.2	C.105	Repeat of Run 261
275	12:20	1.587	810.0	-8.5	-4.5	C.101	Repeat of Run 273

Hollow Model 5**Condition 22:**10th June 2002**Model Data:**

LWL=	1600.0	mm
WSA=	0.4866	m ²
Draft=	59.5	mm
Δ =	16.885	kg
Water Temp=	17.2	degrees

Calibration Factors:

Data Channel	Calibration Factor	Gain	Filter	Channel Description
0	0.002329	1	1	Speed
1	0.038026	2	1	Fwd Heave
2	0.039802	2	1	Aft Heave
3	-3.189169	2	1	R_T
4	0.507364	1	5	Probe Position
5	0.069968	2	5	Water Elevation

Recorded Runs:

Run	Time	Speed	R_T	Heave		Figure	Comments
				FWD Post	AFT Post		
		m/s	gf	mm	mm		
276	13:20	0.766	143.7	-2.3	-1.1	C.106	
277	13:30	0.933	227.1	-3.7	-1.1	C.107	
278	13:40	1.079	360.8	-5.2	-1.8	C.108	
279	13:50	1.224	487.2	-6.4	-3.0	C.109	
280	14:00	1.381	752.7	-8.0	-3.7	C.110	
281	14:10	1.538	925.0	-9.7	-4.7	C.107	
282	14:20	1.696	1107.2	-9.2	-8.8	C.109	
283	14:30	1.842	1302.6	-5.9	-14.7	C.108	
284	14:40	1.997	1447.0	-2.7	-18.4	C.110	
285	14:50	2.155	1556.8	-0.2	-20.2	C.108	
286	15:00	2.299	1642.4	1.8	-20.6	C.110	
287	15:10	2.448	1732.0	3.6	-20.1	C.106	
288	15:20	2.615	1829.3	4.2	-21.2	C.107	
289	15:30	2.760	1918.2	4.7	-21.2	C.108	
290	15:40	2.905	2015.4	6.2	-20.4	C.109	
291	15:50	3.063	2134.5	8.1	-18.6	C.110	
292	16:00	1.461	852.7	-9.0	-4.0	C.106	
293	16:10	1.607	976.1	-10.1	-5.8	C.108	
294	16:20	1.773	1206.1	-7.7	-11.9	C.107	
295	16:30	1.921	1373.5	-4.2	-16.9	C.109	
296	16:40	2.063	1497.9	-1.6	-19.4	C.107	
297	16:50	2.221	1598.7	0.7	-20.5	C.109	
298	17:00	1.734	1162.1	-8.4	-10.2	C.110	Full Separation
299	17:10	1.997	1450.4	-2.6	-18.4	C.106	Repeat of Run 284
300	17:20	1.732	1166.8	-8.4	-10.4	C.106	Repeat of Run 298

Hollow Model 5**Condition 23:**10th June 2002**Model Data:**

LWL=	1600.0	mm
WSA=	0.4866	m ²
Draft=	70.7	mm
Δ =	20.080	kg
Water Temp=	17.2	degrees

Calibration Factors:

Data Channel	Calibration Factor	Gain	Filter	Channel Description
0	0.002329	1	1	Speed
1	0.038026	2	1	Fwd Heave
2	0.039802	2	1	Aft Heave
3	-3.189169	2	1	R_T
4	0.507364	1	5	Probe Position
5	0.069968	2	5	Water Elevation

Recorded Runs:

Run	Time	Speed	R_T	Heave		Figure	Comments
				FWD Post	AFT Post		
		m/s	gf	mm	mm		
301	18:20	0.835	193.4	-3.3	-1.4	C.111	
302	18:30	1.010	323.9	-4.9	-1.6	C.112	
303	18:40	1.175	487.8	-6.6	-2.6	C.113	
304	18:50	1.343	796.2	-8.3	-3.6	C.114	
305	19:00	1.510	1036.7	-11.0	-7.5	C.115	
306	19:10	1.685	1234.1	-11.1	-7.5	C.112	
307	19:20	1.842	1537.2	-7.6	-15.2	C.114	
308	19:30	2.008	1817.0	-2.6	-21.5	C.112	
309	19:40	2.181	1960.0	0.8	-23.5	C.115	
310	19:50	2.339	2066.9	2.7	-24.1	C.112	
311	20:00	2.514	2169.8	4.3	-24.2	C.114	
312	20:10	2.683	2278.9	5.2	-24.5	C.115	
313	20:20	2.837	2392.5	7.1	-23.8	C.112	
314	20:30	3.014	2527.9	8.5	-21.5	C.113	
315	20:40	3.169	2657.2	9.5	-19.4	C.114	
316	20:50	3.337	2800.4	9.5	-16.7	C.115	
317	21:00	1.587	1115.0	-11.5	-4.8	C.111	
318	21:10	1.762	1370.1	-9.7	-11.0	C.113	
319	21:20	1.928	1717.8	-4.8	-19.0	C.111	Full Separation
320	21:30	2.085	1882.1	-1.2	-22.7	C.114	
321	21:40	2.263	2019.3	1.7	-24.0	C.111	
322	21:50	2.427	2120.6	4.1	-23.4	C.113	
323	22:00	1.881	1640.3	-6.1	-16.9	C.115	
324	22:10	2.681	2281.6	5.3	-24.3	C.111	Repeat of Run 312
325	22:20	2.008	1821.2	-2.6	-21.5	C.113	Repeat of Run 308

Hollow Model 5**Condition 24:**11th June 2002**Model Data:**

LWL=	1600.0	mm
WSA=	0.5703	m ²
Draft=	84.1	mm
Δ =	23.879	kg
Water Temp=	17.0	degrees

Calibration Factors:

Data Channel	Calibration Factor	Gain	Filter	Channel Description
0	0.002329	1	1	Speed
1	0.037075	2	1	Fwd Heave
2	0.039981	2	1	Aft Heave
3	-3.180626	2	1	R_T
4	0.507500	1	5	Probe Position
5	0.122041	1	5	Water Elevation

Recorded Runs:

Run	Time	Speed	R_T	Heave		Figure	Comments
				FWD Post	AFT Post		
		m/s	gf	mm	mm		
326	14:40	0.927	266.1	-4.3	-1.4	C.116	
327	14:50	1.099	484.2	-6.5	-2.0	C.117	
328	15:00	1.285	772.6	-8.7	-3.6	C.118	
329	15:15	1.461	1199.7	-11.4	-3.7	C.119	
330	15:25	1.639	1374.3	-12.9	-6.4	C.120	
331	15:35	1.834	1780.5	-9.2	-15.2	C.117	
332	15:45	2.010	2228.2	-3.2	-23.3	C.119	
333	15:55	2.196	2470.8	1.2	-27.1	C.118	
334	18:30	2.372	2603.1	3.9	-27.6	C.120	
335	18:40	2.557	2723.6	5.4	-27.4	C.118	
336	18:50	2.732	2844.2	6.7	-27.1	C.116	
337	19:00	2.920	2991.9	8.0	-25.6	C.117	
338	19:10	3.103	3129.9	10.1	-22.0	C.118	
339	19:20	3.282	3291.9	10.5	-19.2	C.119	
340	19:35	3.464	3469.5	9.6	-15.4	C.120	
341	19:45	1.745	1580.0	-11.1	-11.2	C.116	
342	19:55	1.921	2032.9	-6.3	-19.3	C.118	
343	20:05	2.108	2386.0	-0.5	-26.2	C.116	
344	20:15	2.280	2542.4	2.6	-27.5	C.119	
345	20:25	2.458	2667.9	4.7	-27.5	C.116	
346	20:35	2.644	2785.2	5.8	-27.6	C.119	
347	20:45	2.048	2306.6	-2.4	-24.8	C.120	Full Separation
348	20:55	2.147	2435.5	0.3	-26.6	C.117	
349	21:05	2.459	2661.8	4.6	-27.7	C.117	Repeat of Run 345
350	21:15	2.645	2785.0	6.2	-27.5	C.120	Repeat of Run 346

Hollow Model 5**Condition 25:**11th and 12th June 2002**Model Data:**

LWL=	1600.0	mm
WSA=	0.6244	m ²
Draft=	100.0	mm
Δ =	28.397	kg
Water Temp=	17.0	degrees

Calibration Factors:

Data Channel	Calibration Factor	Gain	Filter	Channel Description
0	0.002329	1	1	Speed
1	0.037139	2	1	Fwd Heave
2	0.039918	2	1	Aft Heave
3	-3.188714	2	1	R_T
4	0.506919	1	5	Probe Position
5	0.122429	1	5	Water Elevation

Recorded Runs:

Run	Time	Speed	R_T	Heave		Figure	Comments
				FWD Post	AFT Post		
		m/s	gf	mm	mm		
351	21:55	1.006	374.7	-5.7	-1.5	C.121	
352	22:05	1.198	611.4	-8.2	-2.9	C.122	
353	22:15	1.403	1366.4	-11.2	-3.9	C.123	
354	22:25	1.589	1553.4	-14.2	-5.6	C.124	
355	22:35	1.795	1909.0	-11.6	-14.2	C.125	
356	9:55	1.989	2576.3	-5.8	-23.3	C.122	
357	10:05	2.196	3090.3	0.6	-29.4	C.125	
358	10:15	2.389	3318.0	4.5	-31.7	C.124	
359	10:25	2.595	3470.2	5.9	-31.6	C.121	
360	10:35	2.781	3609.1	7.8	-30.5	C.123	
361	10:50	2.985	3768.9	10.0	-27.2	C.125	
362	11:00	3.181	3921.7	11.2	-22.6	C.122	
363	11:10	3.386	4109.1	10.8	-18.0	C.123	
364	11:20	3.584	4325.5	7.8	-13.6	C.125	
365	11:35	1.889	2211.1	-8.8	-18.8	C.121	
366	11:45	2.087	2880.1	-2.4	-26.8	C.123	
367	11:55	2.293	3222.9	2.6	-30.7	C.122	Full Separation
368	12:05	2.487	3399.6	5.8	-31.4	C.125	
369	12:15	2.682	3528.6	6.9	-31.1	C.122	
370	12:25	2.879	3696.8	8.2	-29.6	C.124	
371	12:35	3.085	3848.0	10.6	-25.2	C.121	
372	12:45	2.243	3165.2	1.9	-30.0	C.121	
373	13:30	2.341	3281.1	3.9	-31.6	C.123	
374	13:40	3.387	4112.3	10.5	-17.8	C.124	Repeat of Run 363
375	13:55	2.087	2881.6	-2.2	-26.7	C.124	Repeat of Run 366

Probe in Isolation with Undisturbed Water Surface

Condition 26: 1st September 2003

Model Data:

LWL=	N/A	mm
WSA=	N/A	m ²
Draft=	N/A	mm
Δ =	N/A	kg
Water Temp=	17.0	degrees

Calibration Factors:

Data Channel	Calibration Factor	Gain	Filter	Channel Description
0	0.002329	1	1	Speed
1	0.000000	-	-	Fwd Heave
2	0.000000	-	-	Aft Heave
3	0.000000	-	-	R_T
4	0.507110	1	5	Probe Position
5	0.059155	1	5	Water Elevation

Recorded Runs:

Run	Time	Speed	Probe Reading	Comments
		m/s	mm	
626	13:35	0.739	1.33	
627	13:55	0.955	-1.48	
628	14:15	1.246	2.62	
629	14:25	1.493	-6.79	
630	14:35	1.745	-9.77	
631	14:45	1.992	-14.69	
632	14:50	2.245	-20.85	
633	15:00	2.499	-26.37	
634	15:10	2.744	-18.93	
635	15:20	2.995	-18.97	
636	15:20	3.241	-22.61	
637	15:30	3.495	-26.05	
638	15:40	0.739	1.33	
639	15:47	0.993	-0.89	
640	15:55	1.247	2.37	
641	16:05	1.492	-3.60	
642	16:15	1.747	-8.57	
643	16:25	1.990	-13.33	
644	16:35	2.245	-20.60	
645	16:45	2.497	-18.97	
646	16:55	2.742	-37.11	
647	17:05	2.997	-18.06	
648	17:15	3.241	-21.67	
649	17:25	3.496	-25.72	
650	17:35	2.742	-18.48	

Probe in Isolation with Undisturbed Water Surface

Condition 26 (continued): 2nd September 2003

Model Data:

LWL=	N/A	mm
WSA=	N/A	m ²
Draft=	N/A	mm
Δ =	N/A	kg
Water Temp=	17.0	degrees

Calibration Factors:

Data Channel	Calibration Factor	Gain	Filter	Channel Description
0	0.002329	1	1	Speed
1	0.000000	-	-	Fwd Heave
2	0.000000	-	-	Aft Heave
3	0.000000	-	-	R_T
4	0.506994	1	5	Probe Position
5	0.059351	1	5	Water Elevation

Recorded Runs:

Run	Time	Speed	Probe Reading	Comments
		m/s	mm	
651	09:20	1.070	2.02	
652	09:28	1.327	1.60	
653	09:36	1.570	-5.73	
654	09:45	1.824	-11.20	
655	09:55	2.069	-21.99	
656	10:03	2.323	-23.88	
657	10:11	2.576	-18.17	
658	10:20	2.822	-18.14	
659	10:29	3.074	-20.88	
660	10:39	3.317	-23.92	
661	10:47	1.073	1.65	
662	10:55	1.327	-1.90	
663	11:14	1.570	-4.745	
664	11:22	1.826	-11.27	
665	11:30	2.070	-13.18	
666	11:40	2.323	-23.36	
667	11:51	2.577	-19.27	
668	12:01	2.820	-17.80	
669	12:11	3.074	-19.87	
670	12:25	3.318	-23.62	
671	13:05	1.161	2.18	
672	13:15	1.415	-3.574	
673	13:25	1.669	-9.272	
674	13:35	1.911	-12.50	
675	13:43	2.167	-15.67	

Probe in Isolation with Undisturbed Water Surface

Condition 26 (continued): 2nd September 2003

Model Data:

LWL=	N/A	mm
WSA=	N/A	m ²
Draft=	N/A	mm
Δ =	N/A	kg
Water Temp=	17.0	degrees

Calibration Factors:

Data Channel	Calibration Factor	Gain	Filter	Channel Description
0	0.002329	1	1	Speed
1	0.000000	-	-	Fwd Heave
2	0.000000	-	-	Aft Heave
3	0.000000	-	-	R_T
4	0.506994	1	5	Probe Position
5	0.059351	1	5	Water Elevation

Recorded Runs:

Run	Time	Speed	Probe Reading	Comments
		m/s	mm	
676	13:52	2.411	-24.93	
677	14:00	2.665	-18.74	
678	14:09	2.919	-18.58	
679	14:18	3.162	-22.01	
680	14:28	3.417	-25.04	
681	14:38	1.160	2.14	
682	14:48	1.414	-6.81	
683	14:57	1.668	-7.81	
684	15:06	1.911	-12.68	
685	15:17	2.167	-15.69	
686	15:25	2.410	-31.64	
687	15:35	2.411	-31.92	
688	15:43	2.664	-18.65	
689	15:51	2.917	-17.32	
690	16:00	3.162	-19.15	
691	16:10	3.417	-25.11	
692	16:18	1.032	-0.73	
693	16:29	1.287	1.98	
694	16:40	1.532	-8.32	
695	16:48	1.787	-10.88	
696	16:56	2.031	-13.45	
697	17:09	2.285	-29.21	
698	17:28	2.535	-18.46	
699	17:38	2.782	-39.59	
700	17:47	3.036	-18.41	

Probe in Isolation with Undisturbed Water Surface

Condition 26 (continued): 2nd and 3rd September 2003

Model Data:

LWL=	N/A	mm
WSA=	N/A	m ²
Draft=	N/A	mm
Δ =	N/A	kg
Water Temp=	17.0	degrees

Calibration Factors:

Data Channel	Calibration Factor	Gain	Filter	Channel Description
0	0.002329	1	1	Speed
1	0.000000	-	-	Fwd Heave
2	0.000000	-	-	Aft Heave
3	0.000000	-	-	R_T
4	0.506930	1	5	Probe Position
5	0.059021	1	5	Water Elevation

Recorded Runs:

Run	Time	Speed	Probe Reading	Comments
		m/s	mm	
701	17:55	3.280	-21.23	
702	18:03	1.122	1.20	
703	09:50	1.375	-7.09	
704	10:00	1.620	-4.98	
705	10:08	1.872	-11.97	
706	10:16	2.127	-21.95	
707	10:24	2.374	-30.69	
708	10:32	2.626	-34.17	
709	10:40	2.871	-41.51	
710	10:48	3.121	-18.00	
711	10:56	3.377	-23.65	
712	11:04	1.198	1.55	
713	11:15	1.454	-7.04	
714	11:23	1.709	-8.83	
715	11:31	1.951	-13.55	
716	11:39	2.207	-24.04	
717	11:47	2.450	-33.21	
718	11:55	2.704	-36.78	
719	12:04	2.959	-18.30	
720	12:15	3.201	-21.26	
721	12:30	3.457	-24.72	
722	13:05	1.617	-6.58	
723	13:16	2.126	-17.93	
724	13:25	2.673	-20.42	
725	13:35	3.359	-23.41	

Hollow Model 3**Condition 27:**3rd and 4th September 2003**Model Data:**

LWL=	1131.4	mm
WSA=	0.2624	m ²
Draft=	50.0	mm
Δ =	7.099	kg
Water Temp=	16.5	degrees

Calibration Factors:

Data Channel	Calibration Factor	Gain	Filter	Channel Description
0	0.002329	1	1	Speed
1	0.000000	-	-	Fwd Heave (Fixed)
2	0.000000	-	-	Aft Heave (Fixed)
3	-1.438304	5	1	R_T
4	0.507283	1	5	Probe Position
5	0.058719	2	5	Water Elevation
6	0.050022	2	5	Transom Water Elevation

Recorded Runs:

Run	Time	Speed	R_T	Water Elevation at Transom	Figure	Comments
		m/s	gf	mm		
726	17:10	0.571	44.6	-3.132	C.126	
727	17:20	0.710	72.3	-3.684	C.127	
728	17:32	0.856	120.8	-6.343	C.128	
729	17:43	0.993	172.4	-7.801	C.129	
730	17:55	1.129	278.1	-20.499	C.130	
731	9:43	1.275	352.4	-26.543	C.126	Calibration 4/9/03
732	9:55	1.413	399.7	-33.009	C.128	
733	10:05	1.550	467.4	-50.965	C.130	
734	10:20	1.696	514.4	-51.147	C.128	
735	10:32	1.831	556.2	-51.173	C.126	
736	10:45	1.969	600.2	-51.281	C.128	
737	11:00	2.116	647.4	-51.406	C.129	
738	11:12	2.253	694.4	-51.461	C.126	
739	11:25	2.390	746.5	-51.506	C.127	
740	11:37	2.534	803.4	-51.557	C.128	
741	11:48	2.671	866.4	-51.549	C.129	
742	12:00	2.810	936.1	-51.614	C.130	
743	12:12	1.345	368.6	-27.777	C.127	
744	12:25	1.482	442.0	-42.274	C.129	
745	12:37	1.616	489.0	-51.139	C.127	
746	12:52	1.765	538.6	-51.231	C.130	
747	13:04	1.900	580.3	-51.301	C.127	
748	13:16	1.588	481.9	-50.988	C.126	
749	13:30	1.696	517.2	-51.180	C.129	
750	13:42	2.118	651.3	-51.353	C.130	

Hollow Model 3**Condition 28:**4rd and 5th September 2003**Model Data:**

LWL=	1131.4	mm
WSA=	0.2624	m ²
Draft=	70.7	mm
Δ =	10.040	kg
Water Temp=	16.5	degrees

Calibration Factors:

Data Channel	Calibration Factor	Gain	Filter	Channel Description
0	0.002329	1	1	Speed
1	0.000000	-	-	Fwd Heave (Fixed)
2	0.000000	-	-	Aft Heave (Fixed)
3	-1.437922	5	1	R_T
4	0.507411	1	5	Probe Position
5	0.059917	2	5	Water Elevation
6	0.049139	2	5	Transom Water Elevation

Recorded Runs:

Run	Time	Speed	R_T	Water Elevation at Transom	Figure	Comments
		m/s	gf	mm		
751	14:42	0.835	128.4	-5.450	C.131	
752	14:55	1.012	217.0	-7.016	C.132	
753	15:08	1.178	452.8	-26.980	C.133	
754	15:22	1.343	518.2	-26.667	C.134	
755	15:38	1.510	643.5	-34.616	C.132	
756	15:50	1.686	797.5	-71.010	C.134	
757	16:13	1.840	855.6	-72.391	C.132	
758	16:25	2.007	919.7	-72.369	C.131	
759	16:40	2.185	988.3	-72.497	C.133	
760	16:55	2.340	1051.6	-72.614	C.135	
761	17:12	2.514	1124.7	-72.567	C.132	
762	17:28	2.682	1213.2	-73.125	C.133	
763	17:40	2.837	1306.1	-73.197	C.134	
764	17:52	3.014	1421.9	-73.130	C.135	
765	18:04	1.431	564.7	-28.178	C.131	
766	10:15	2.428	1078.9	-71.931	C.131	Calibration 5/9/03
767	10:28	1.587	712.0	-44.858	C.133	
768	10:40	1.764	824.3	-71.775	C.135	
769	10:57	1.930	884.0	-71.915	C.135	
770	11:08	2.088	941.7	-71.878	C.132	
771	11:20	2.262	1012.9	-71.960	C.134	
772	11:32	1.882	869.6	-71.742	C.134	
773	11:43	1.801	841.7	-71.775	C.131	
774	11:56	1.344	523.9	-27.092	C.135	
775	12:10	1.881	870.9	-71.775	C.133	

Hollow Model 3**Condition 29:**5rd and 6th September 2003**Model Data:**

LWL=	1131.4	mm
WSA=	0.3826	m ²
Draft=	100.0	mm
Δ =	14.199	kg
Water Temp=	16.5	degrees

Calibration Factors:

Data Channel	Calibration Factor	Gain	Filter	Channel Description
0	0.002329	1	1	Speed
1	0.000000	-	-	Fwd Heave (Fixed)
2	0.000000	-	-	Aft Heave (Fixed)
3	-1.442448	5	1	R_T
4	0.507397	1	5	Probe Position
5	0.059541	2	5	Water Elevation
6	0.048974	2	5	Transom Water Elevation

Recorded Runs:

Run	Time	Speed	R_T	Water Elevation at Transom	Figure	Comments
		m/s	gf	mm		
776	13:20	0.795	140.6	-2.713	C.136	
777	13:33	1.002	280.8	-5.077	C.137	
778	13:47	1.196	667.4	-26.878	C.139	
779	14:00	1.402	693.8	-15.889	C.136	
780	14:11	1.587	914	-29.188	C.139	
781	14:21	1.792	1313.7	-77.984	C.136	
782	14:32	1.987	1435.6	-100.604	C.138	
783	14:44	2.194	1531.5	-100.832	C.136	
784	14:55	2.388	1624.8	-100.873	C.140	
785	15:08	2.596	1727.1	-100.940	C.138	
786	15:21	2.779	1848.4	-101.157	C.140	
787	16:00	1.099	442.3	-14.416	C.138	
788	16:12	1.303	680.9	-20.294	C.140	
789	16:23	1.499	786.5	-20.405	C.137	
790	16:35	1.696	1146.5	-51.620	C.140	
791	16:47	1.889	1392.8	-100.540	C.137	
792	17:01	2.087	1485.2	-100.372	C.139	
793	17:14	2.292	1582.1	-100.573	C.138	
794	17:27	2.487	1672.5	-101.013	C.137	
795	17:42	2.683	1782.4	-101.256	C.139	
796	17:55	2.145	1509.5	-100.570	C.140	
797	10:30	2.241	1550.4	-99.620	C.137	Calibration 6/9/03
798	10:42	2.341	1593.3	-100.458	C.139	
799	10:58	2.390	1617.3	-100.491	C.136	Repeat of Run 784
800	11:12	1.501	777.4	-6.232	C.138	Repeat of Run 789

Probe in Isolation with Water Surface Disturbed**Condition 30:** 8th September 2003**Model Data:**

LWL=	N/A	mm
WSA=	N/A	m ²
Draft=	N/A	mm
Δ =	N/A	kg
Water Temp=	17.0	degrees

Calibration Factors:

Data Channel	Calibration Factor	Gain	Filter	Channel Description
0	0.002329	1	1	Speed
1	0.000000	-	-	Fwd Heave
2	0.000000	-	-	Aft Heave
3	0.000000	-	-	R_T
4	0.507397	1	5	Probe Position
5	0.059541	1	5	Water Elevation

Recorded Runs:

Run	Time	Speed	Probe Reading	Comments
		m/s	mm	
801	13:55	0.994	0.79	
802	14:00	1.073	2.85	
803	14:05	1.161	0.80	
804	14:10	1.246	1.58	
805	14:17	1.328	1.06	
806	14:23	1.416	0.28	
807	14:30	1.455	-0.14	
808	14:43	1.495	-0.33	
809	14:55	1.532	-2.84	
810	14:58	1.570	-4.32	
811	15:01	1.621	-1.90	
812	15:05	1.669	-3.93	
813	15:10	1.707	-7.04	
814	15:14	1.747	-8.67	
815	15:19	1.786	-9.78	
816	15:23	1.823	-11.06	
817	15:26	1.871	-11.86	
818	15:30	1.912	-11.86	
819	15:33	1.953	-13.73	
820	15:37	1.991	-14.11	
821	15:40	2.029	-19.68	
822	15:44	2.069	-13.91	
823	15:47	2.128	-14.14	
824	15:51	2.167	-15.15	
825	15:55	2.207	-16.42	

Probe in Isolation with Water Surface Disturbed

Condition 30 (continued): 8th September 2003

Model Data:

LWL=	N/A	mm
WSA=	N/A	m ²
Draft=	N/A	mm
Δ =	N/A	kg
Water Temp=	17.0	degrees

Calibration Factors:

Data Channel	Calibration Factor	Gain	Filter	Channel Description
0	0.002329	1	1	Speed
1	0.000000	-	-	Fwd Heave
2	0.000000	-	-	Aft Heave
3	0.000000	-	-	R_T
4	0.507397	1	5	Probe Position
5	0.059541	1	5	Water Elevation

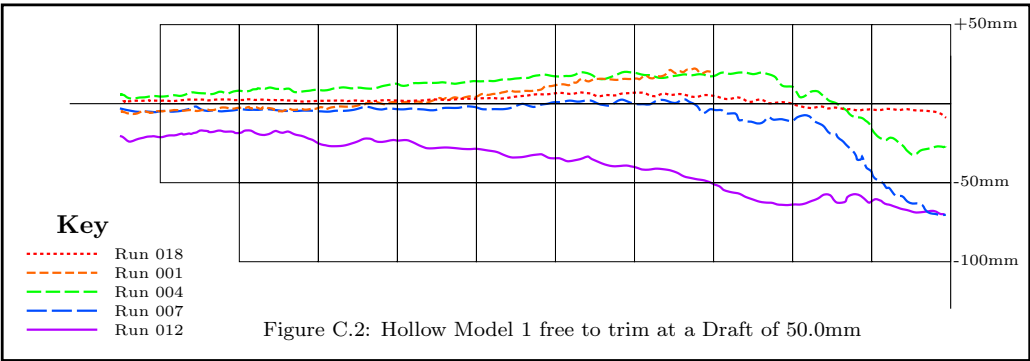
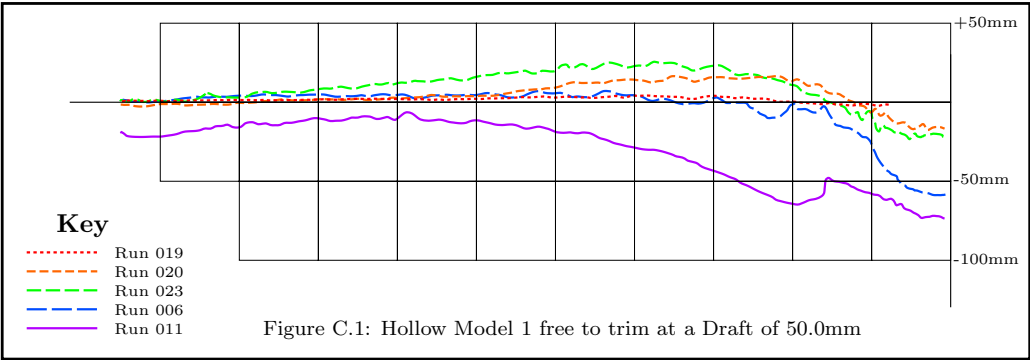
Recorded Runs:

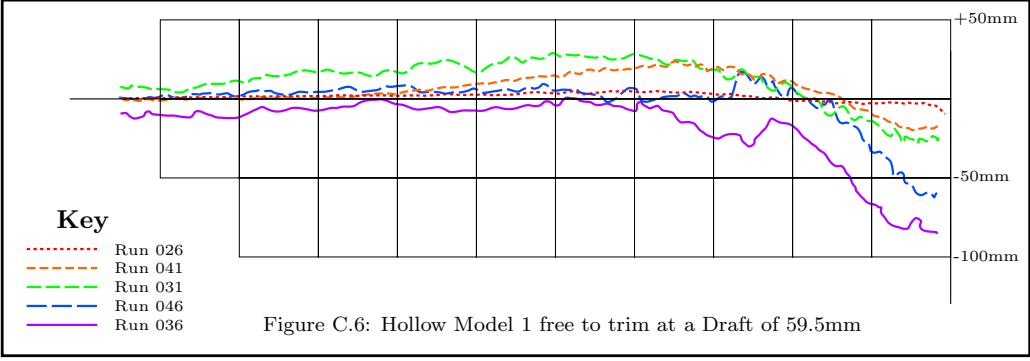
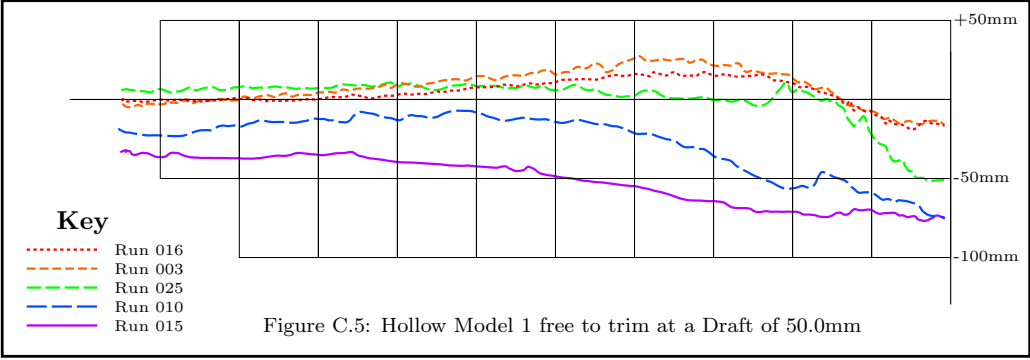
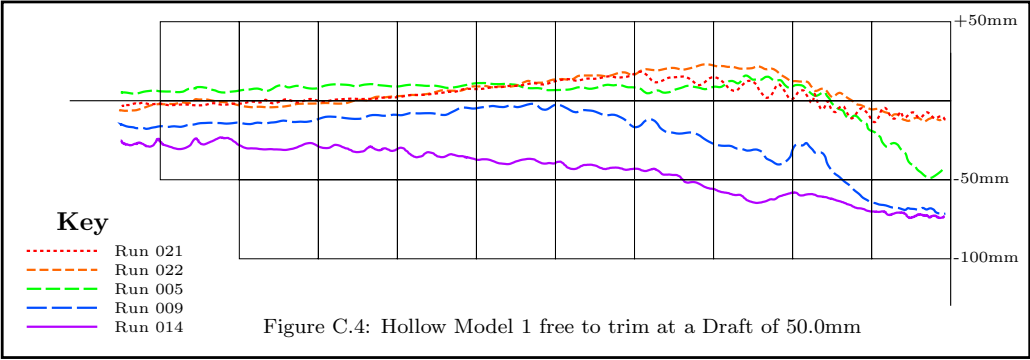
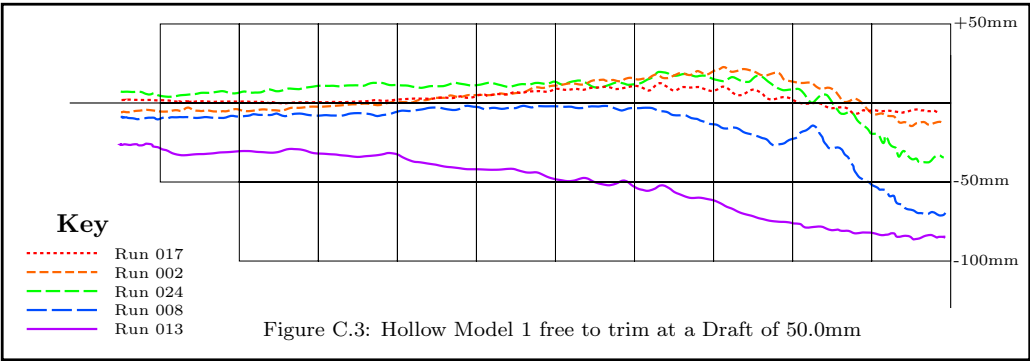
Run	Time	Speed	Probe Reading	Comments
		m/s	mm	
826	16:01	2.243	-17.85	
827	16:04	2.284	-18.67	
828	16:07	2.324	-26.78	
829	16:10	2.372	-27.80	
830	16:14	2.413	-23.49	
831	16:17	2.450	-31.16	
832	16:20	2.500	-26.05	
833	16:24	2.537	-32.59	
834	16:28	2.576	-34.10	
835	16:32	2.626	-27.52	
836	16:36	2.666	-33.25	
837	16:41	2.706	-28.68	
838	16:45	2.744	-32.78	
839	16:49	2.782	-30.28	
840	16:53	2.823	-30.27	
841	16:56	2.869	-26.86	
842	16:59	2.918	-34.51	
843	17:04	2.958	-36.03	
844	17:08	2.999	-38.63	
845	17:11	3.074	-45.01	
846	17:14	3.163	-46.25	
847	17:18	3.242	-47.56	
848	17:25	3.320	-49.81	
849	17:29	3.419	-49.22	
850	17:32	3.495	-48.45	

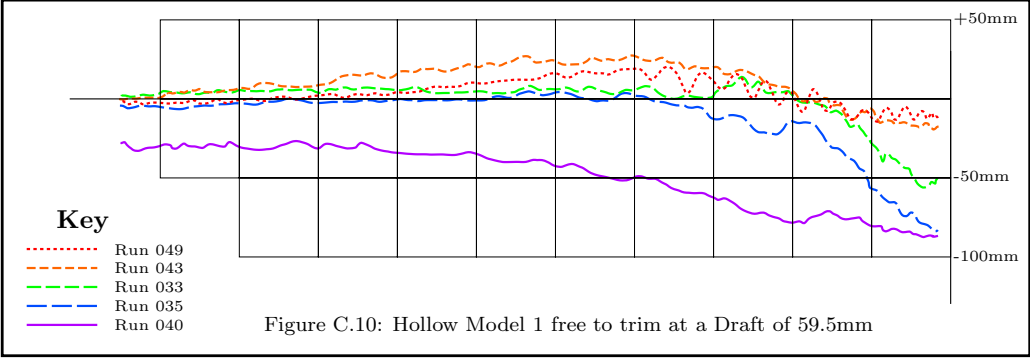
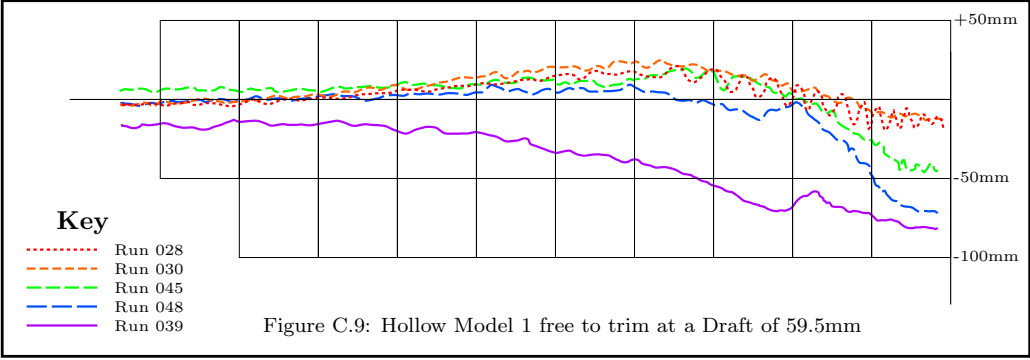
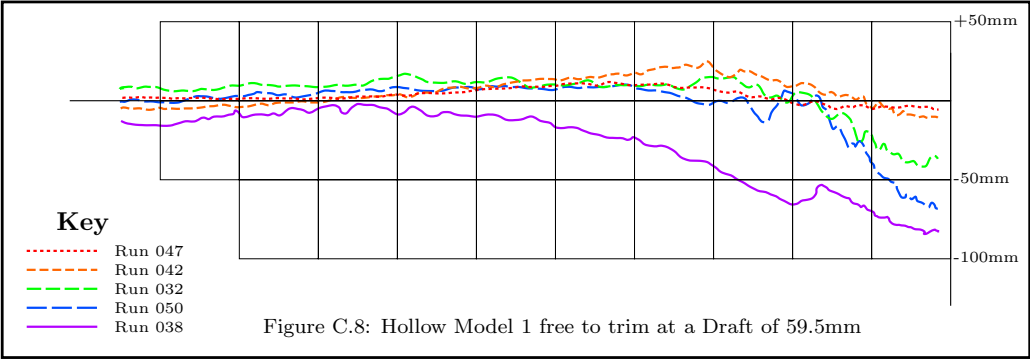
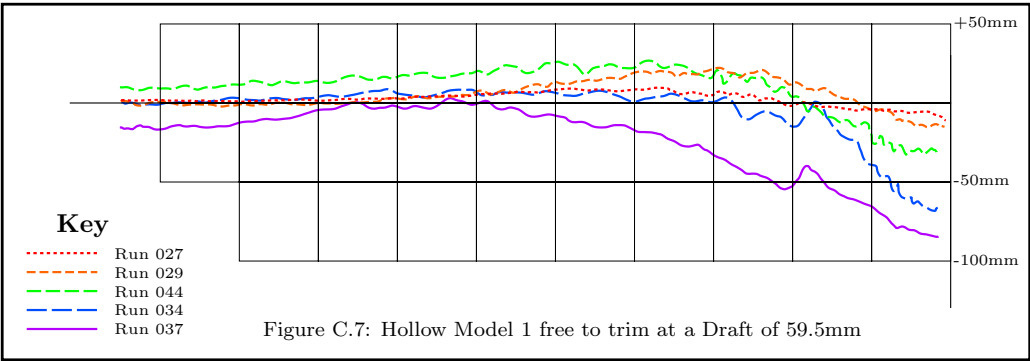
Appendix C

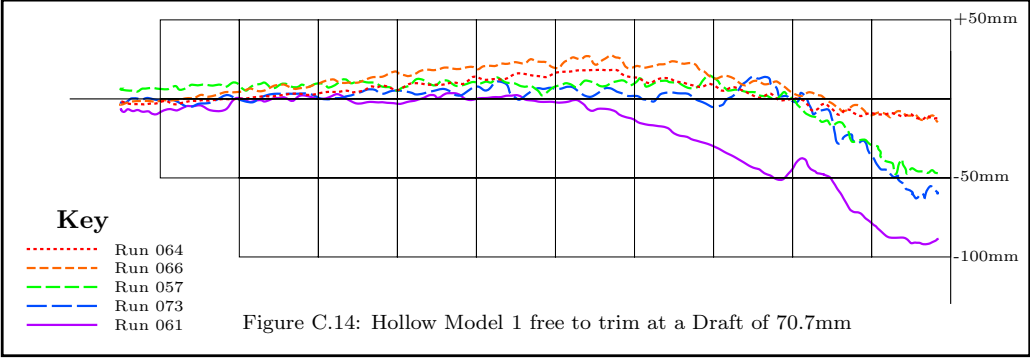
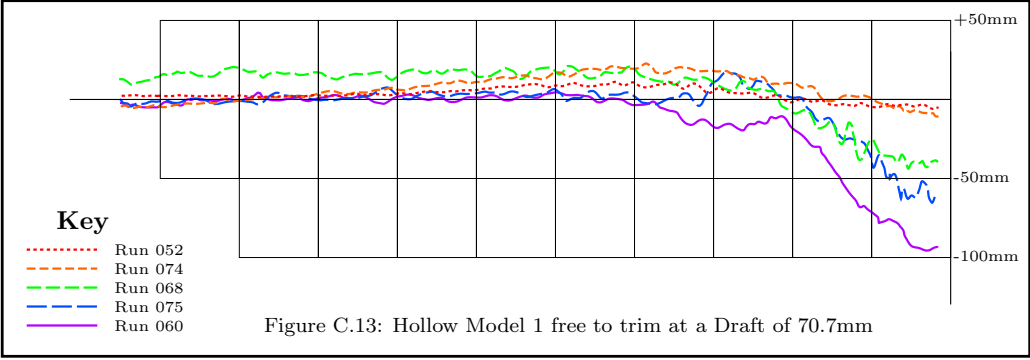
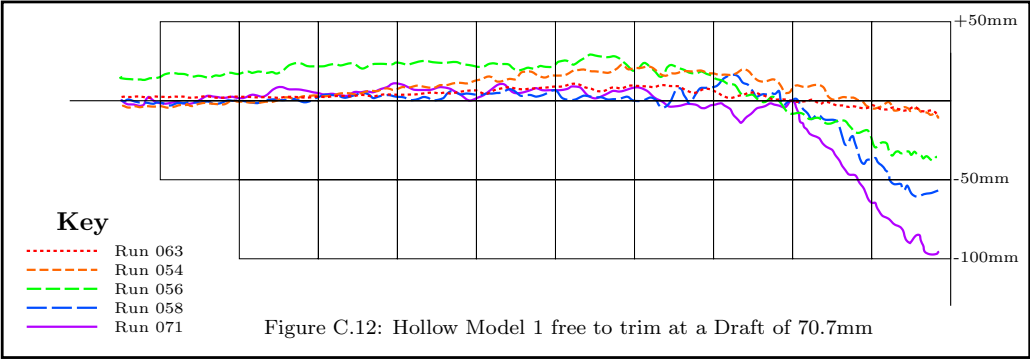
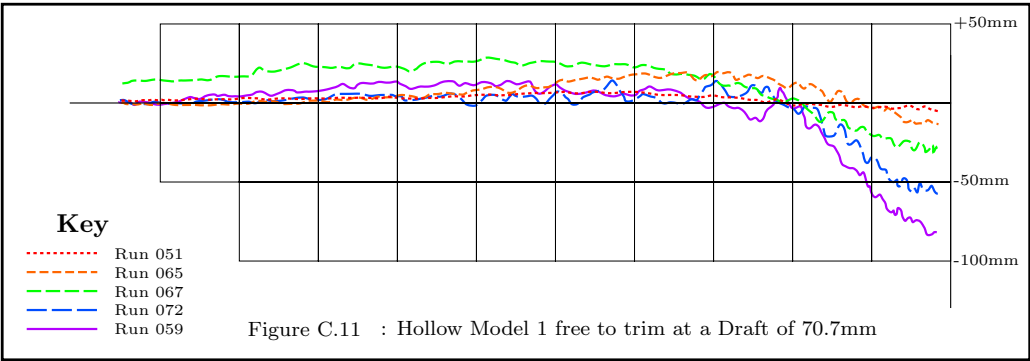
Measured Hollow Profiles

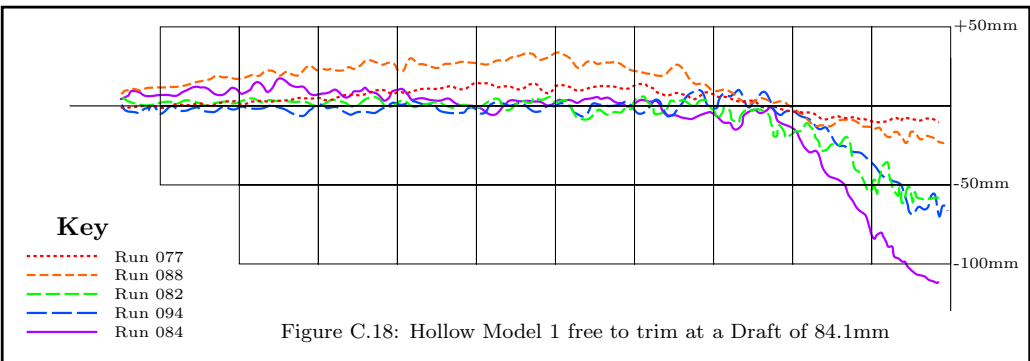
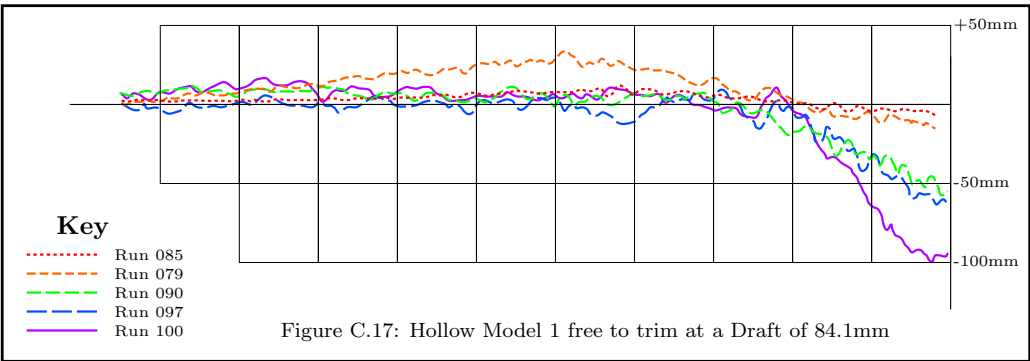
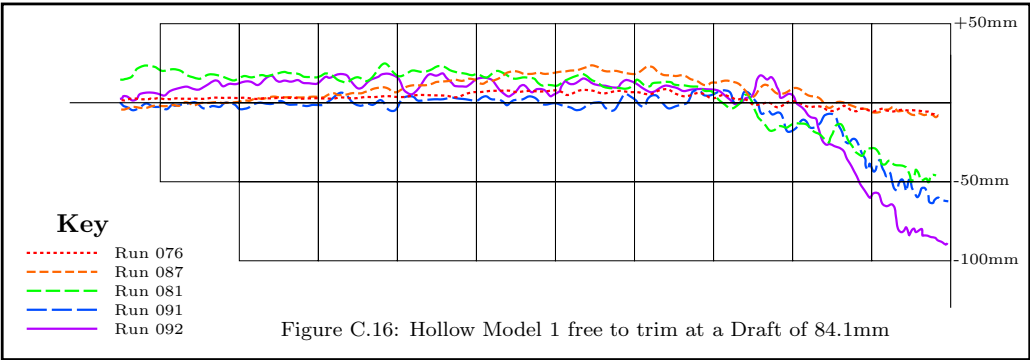
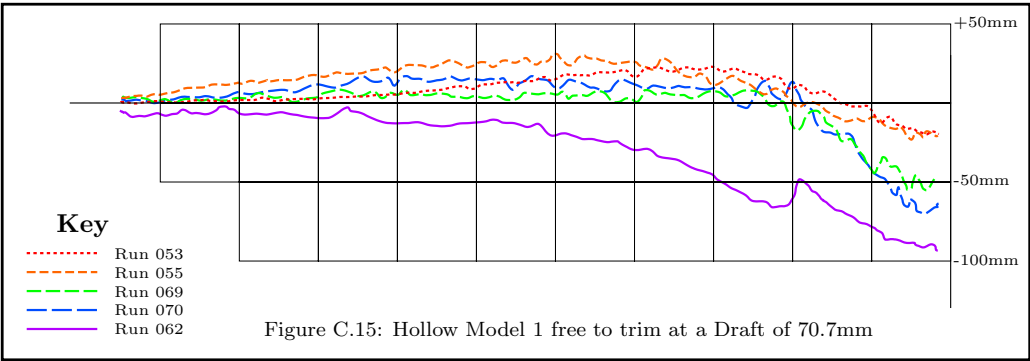
This appendix contains all the measured hollow profiles for both the fixed trim and free trim experiments without the probe correction factor applied (Chapter 5). Each figure contains five measured profiles at a set draft and reference should be made to Appendix B for the speed associated with each run.

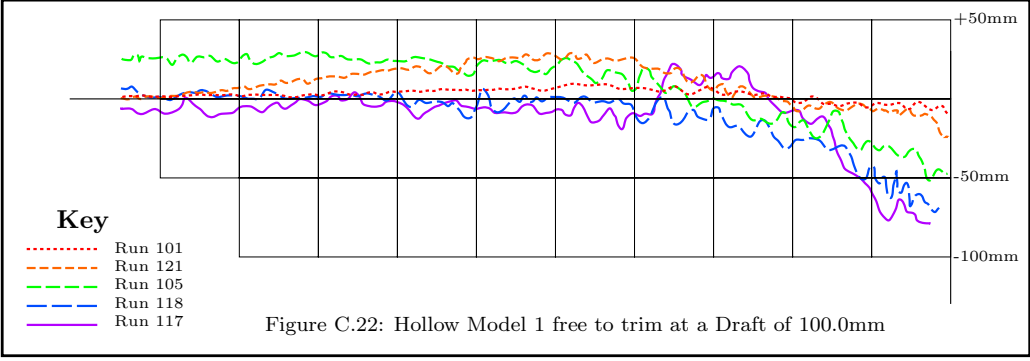
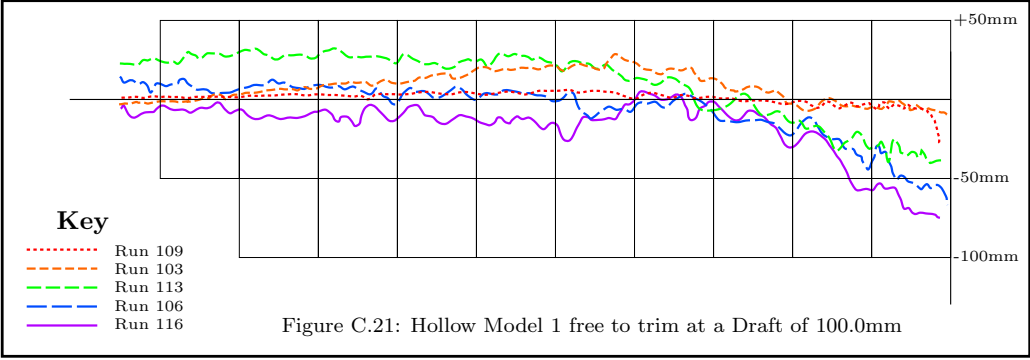
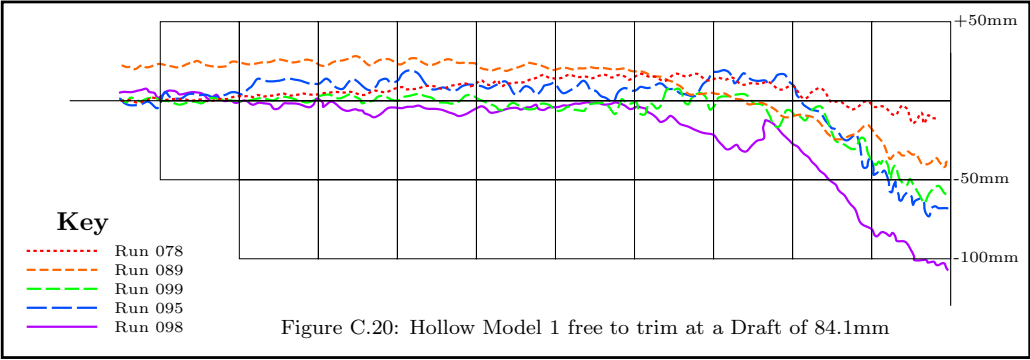
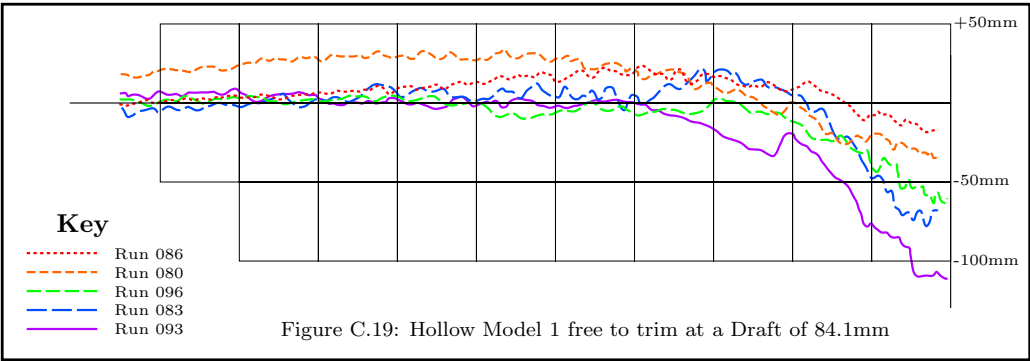


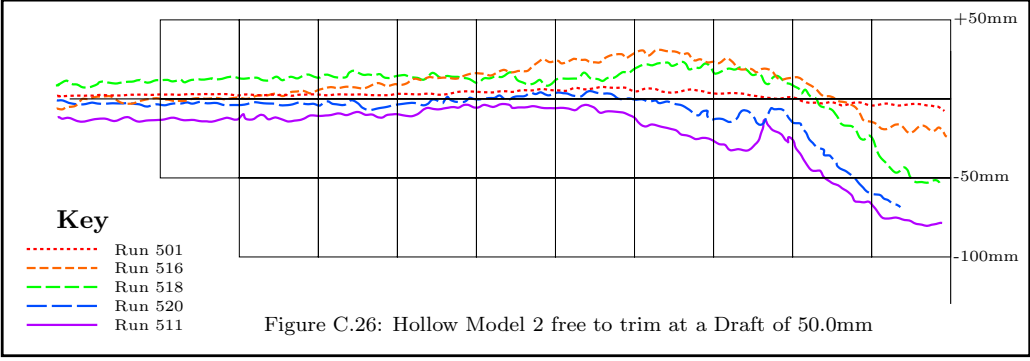
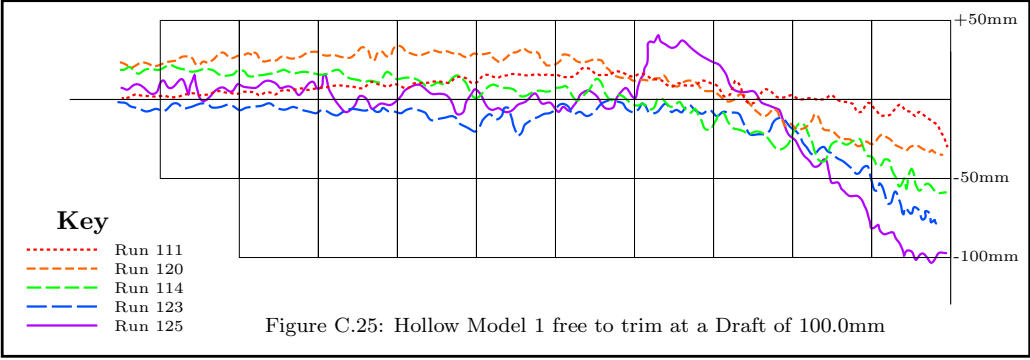
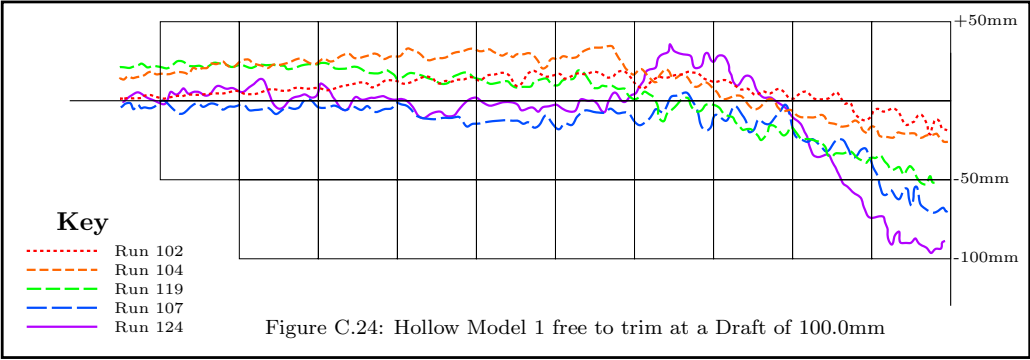
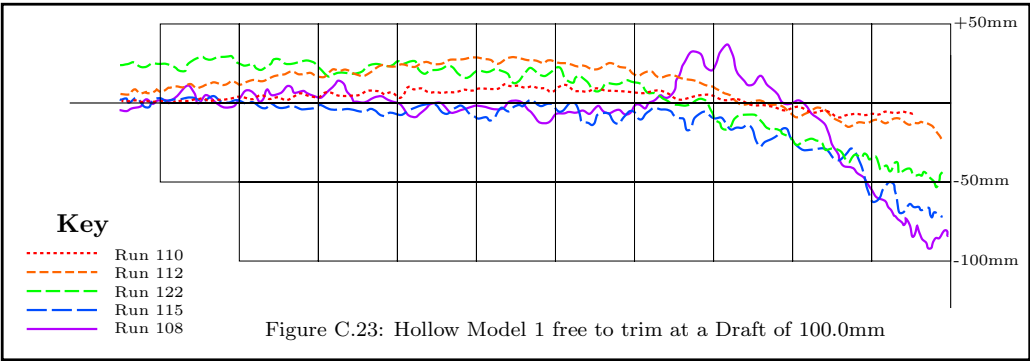


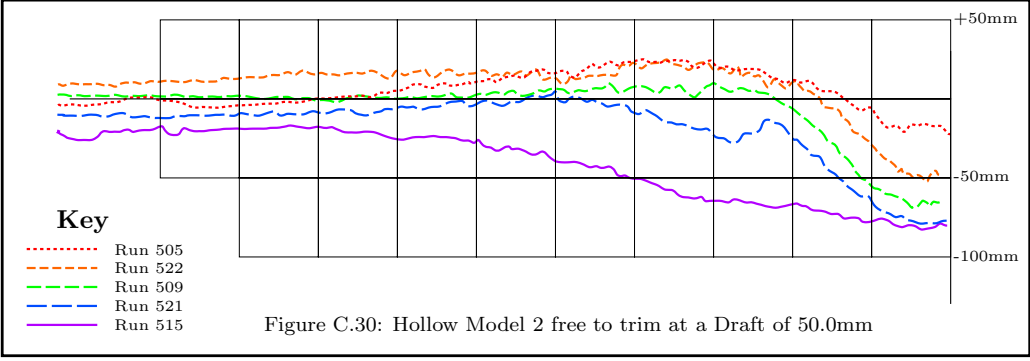
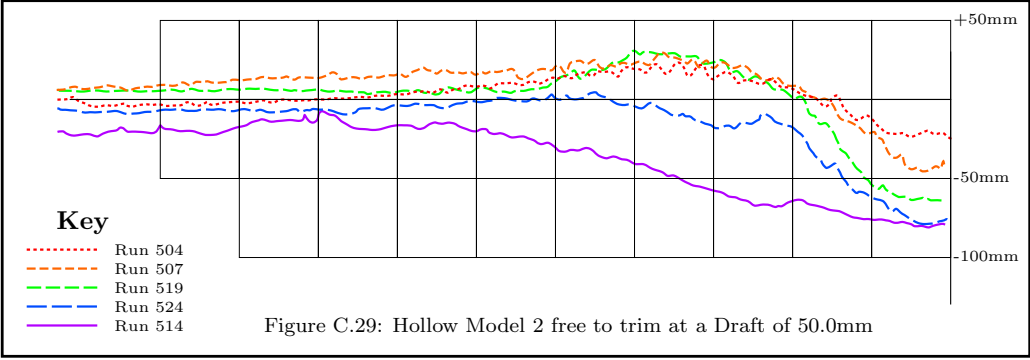
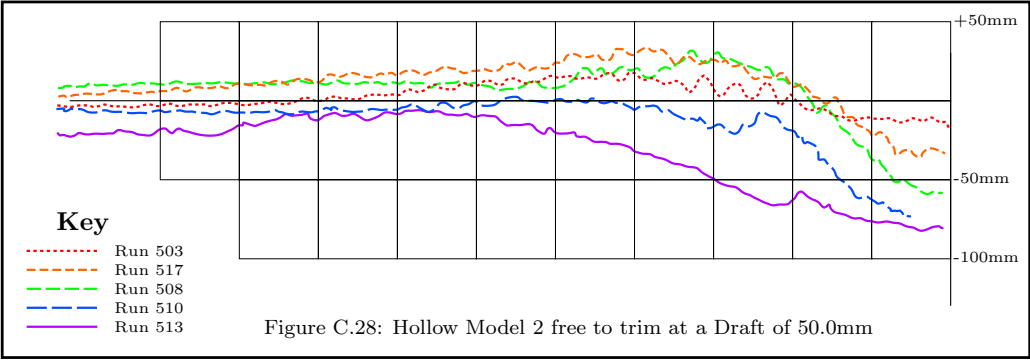
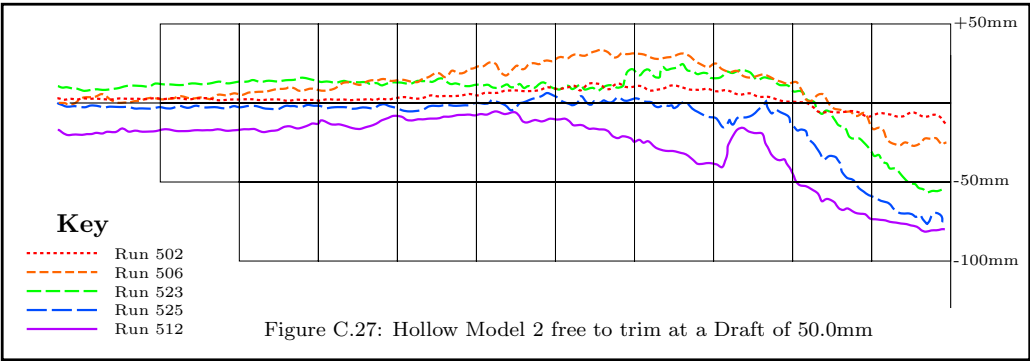


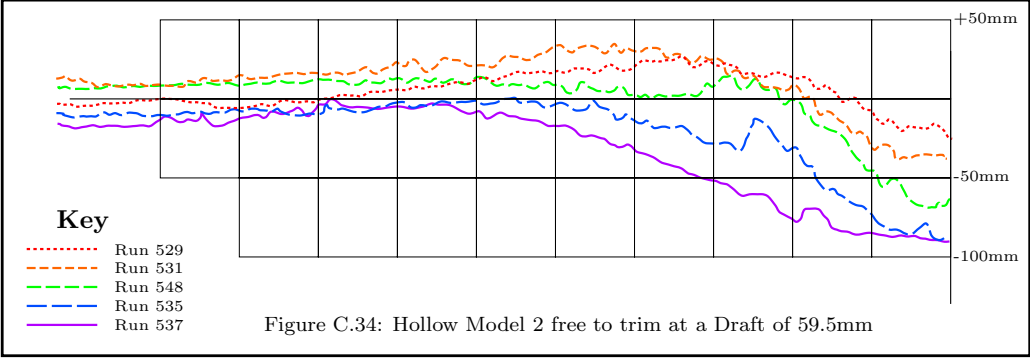
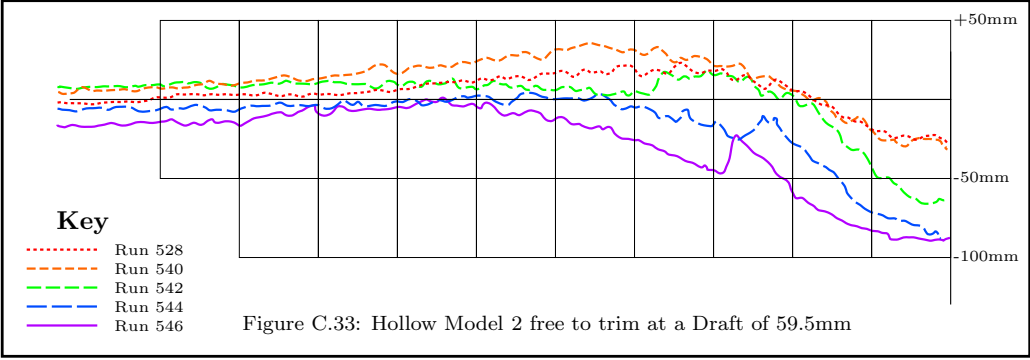
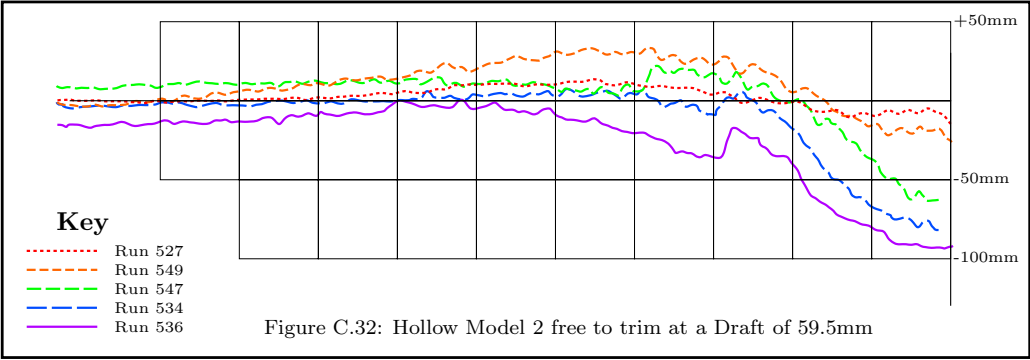
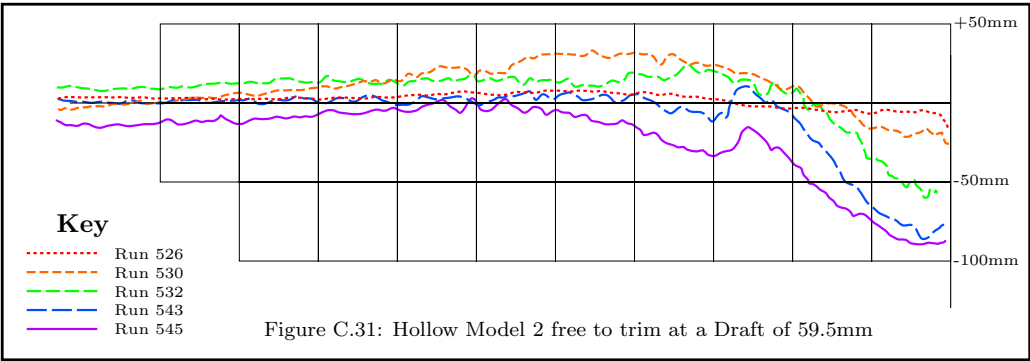


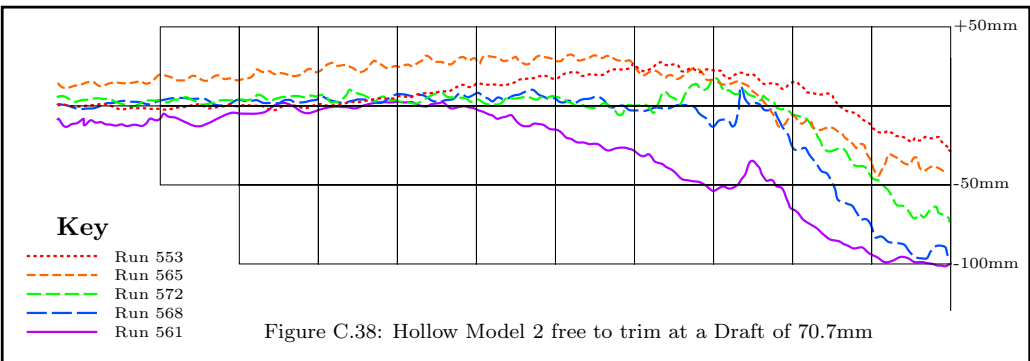
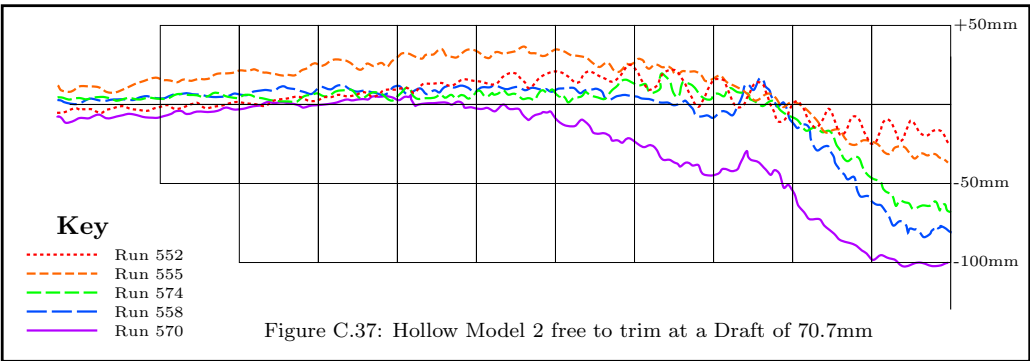
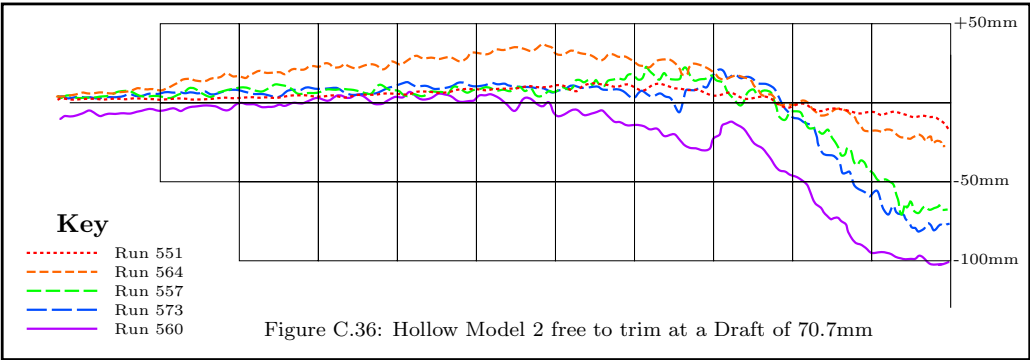
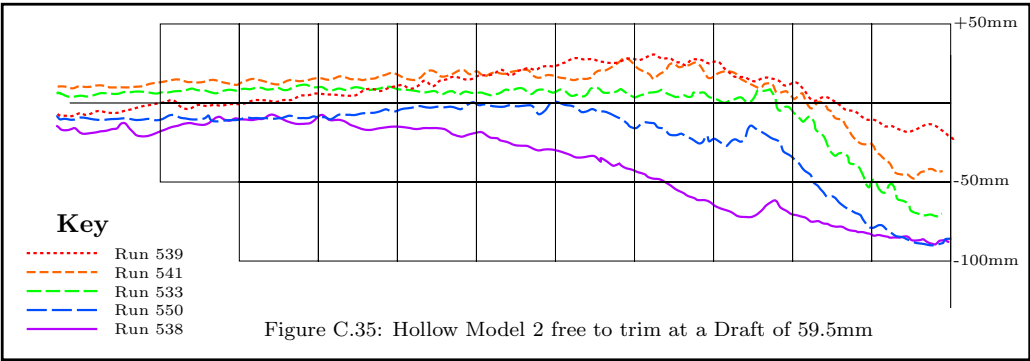


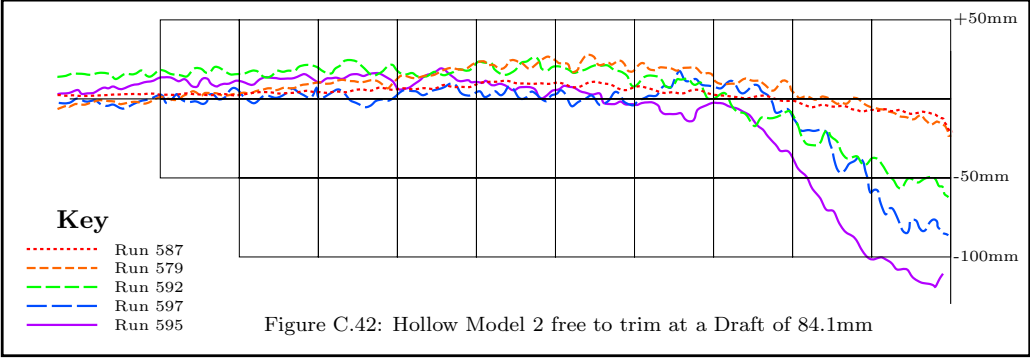
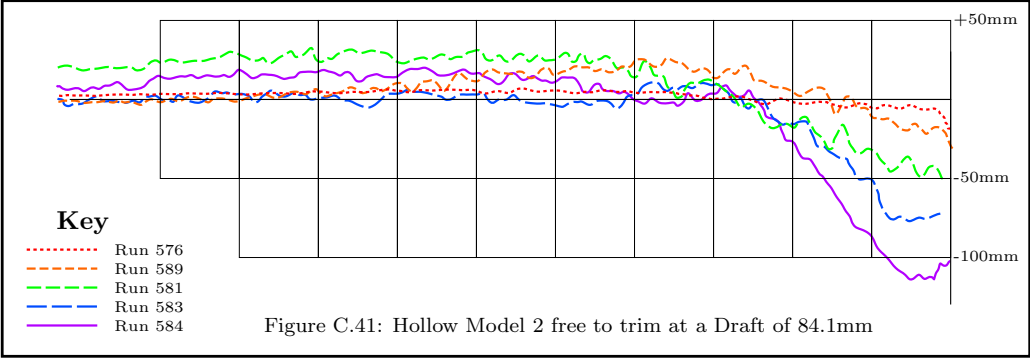
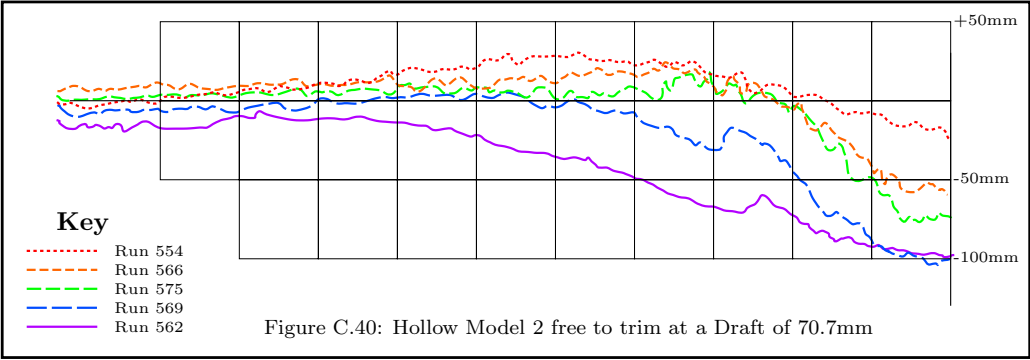
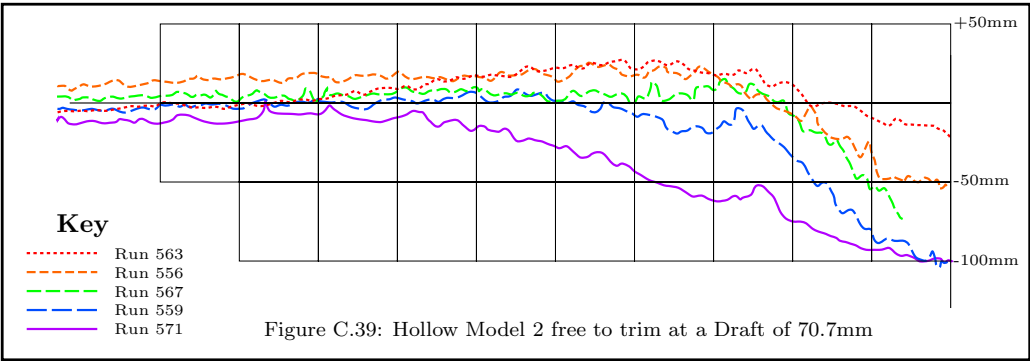


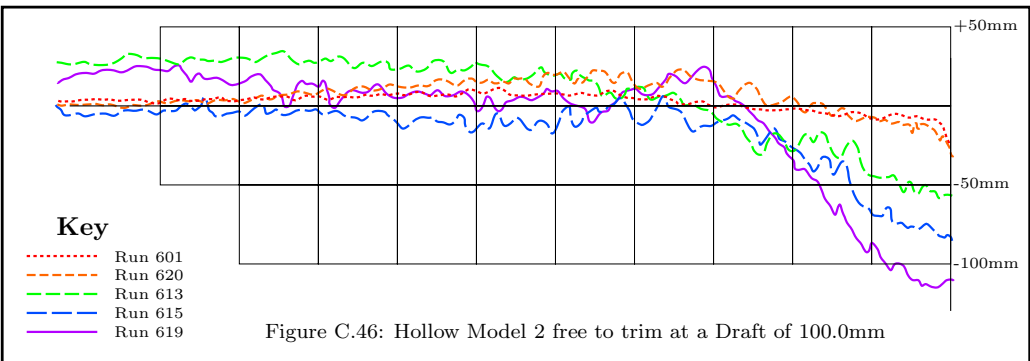
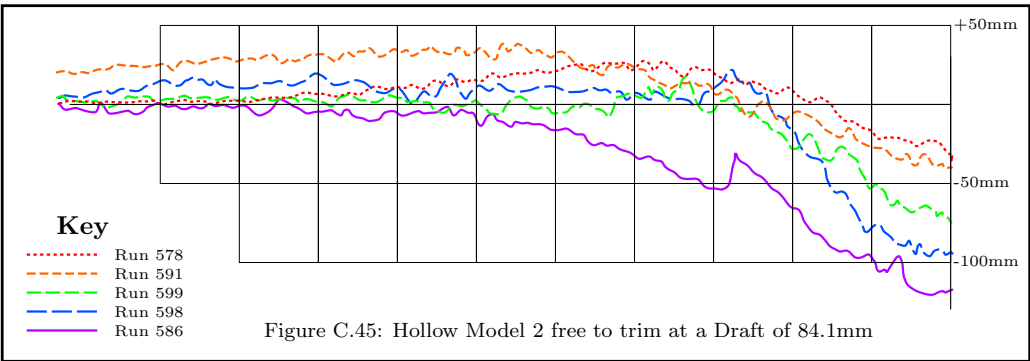
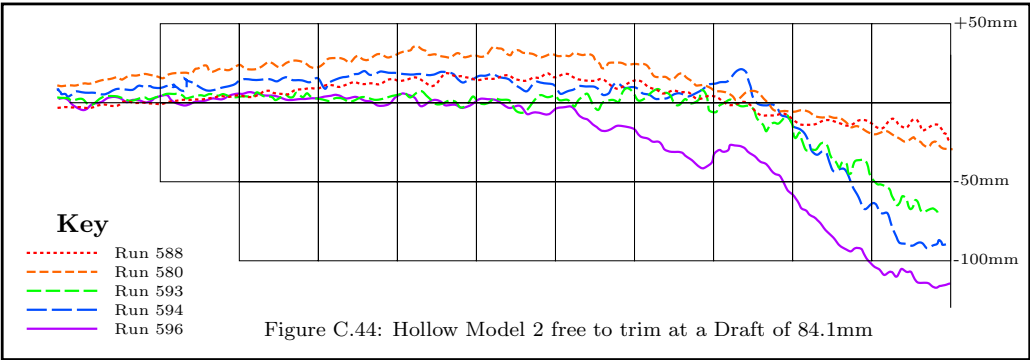
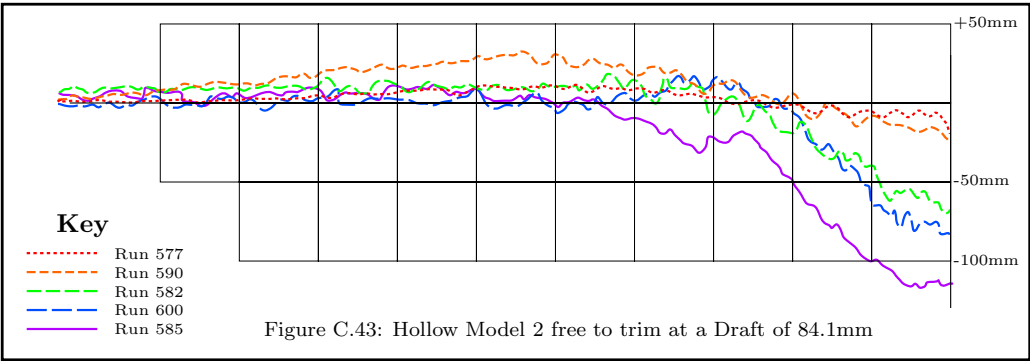


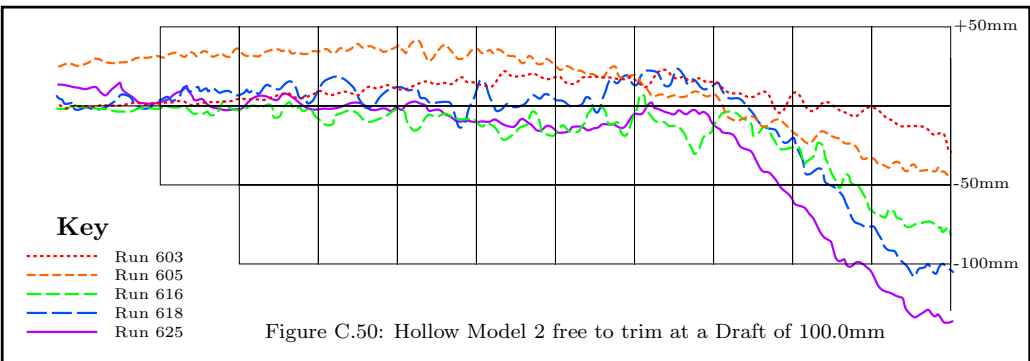
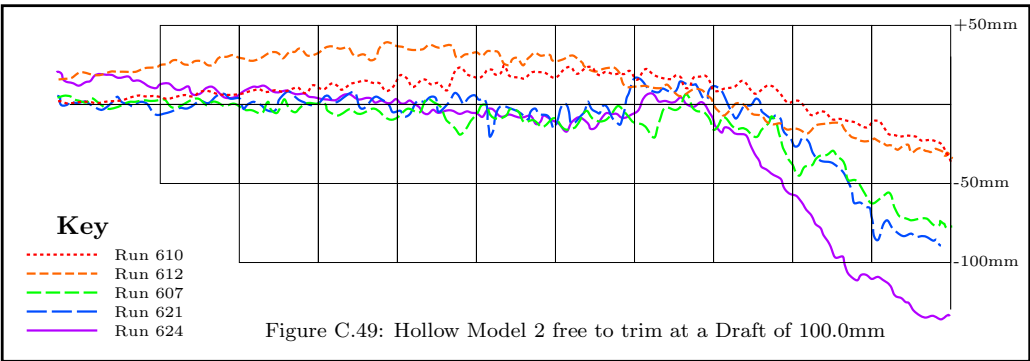
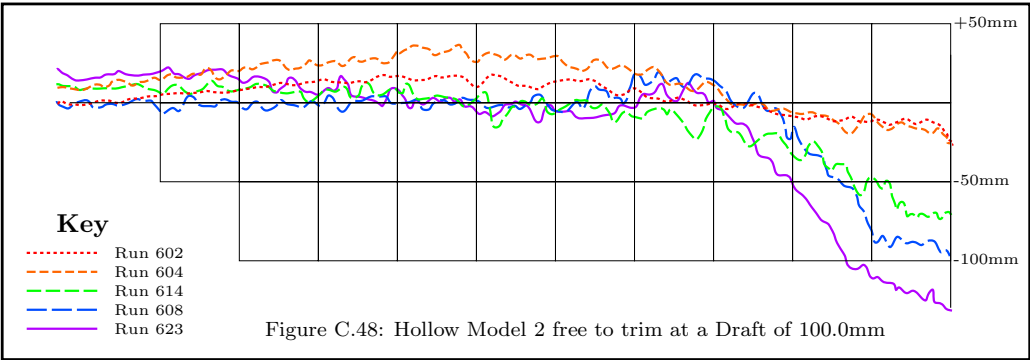
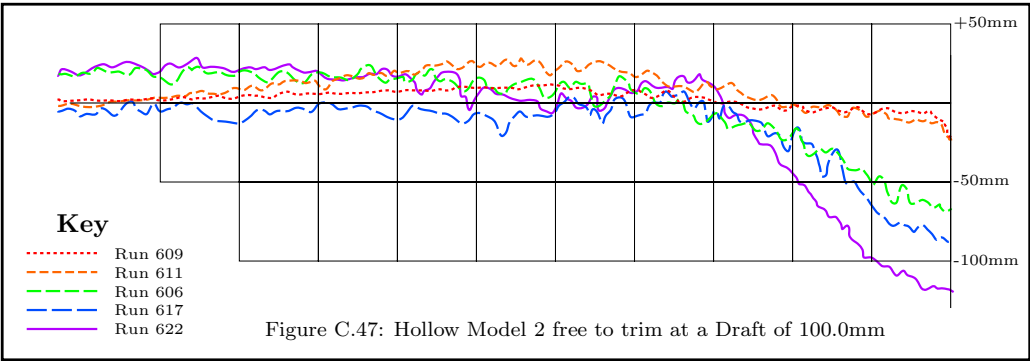


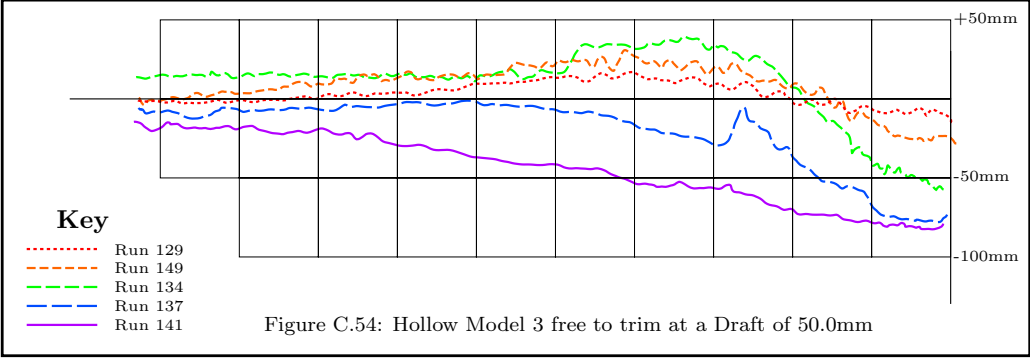
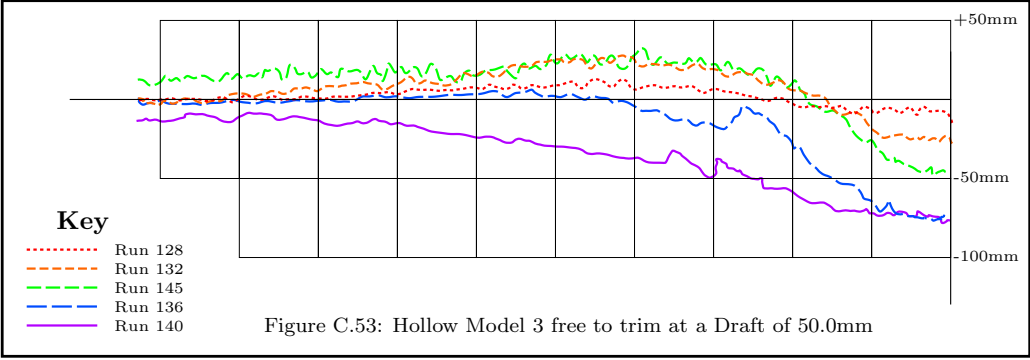
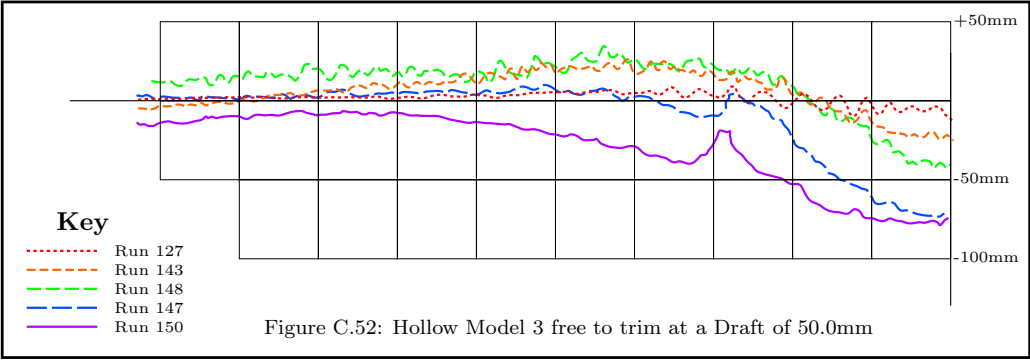
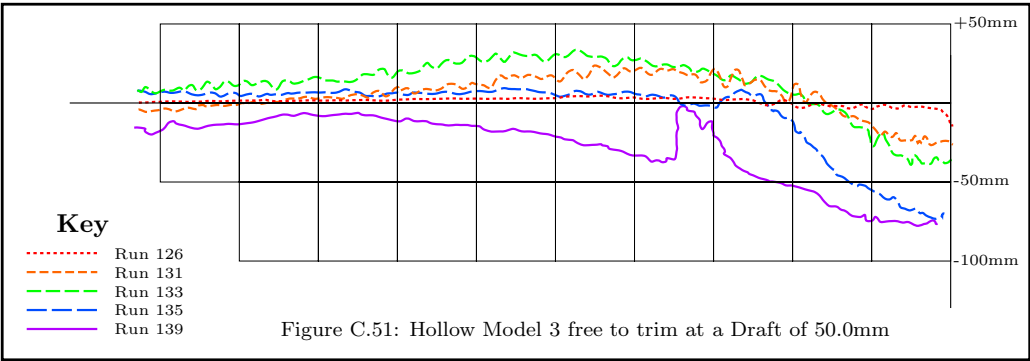


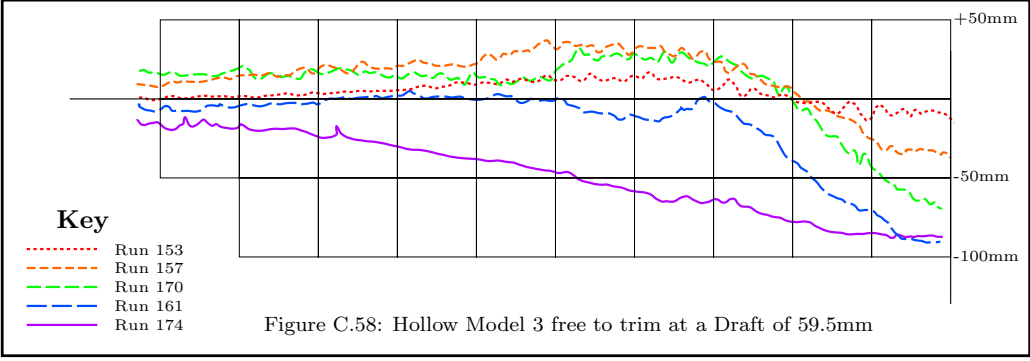
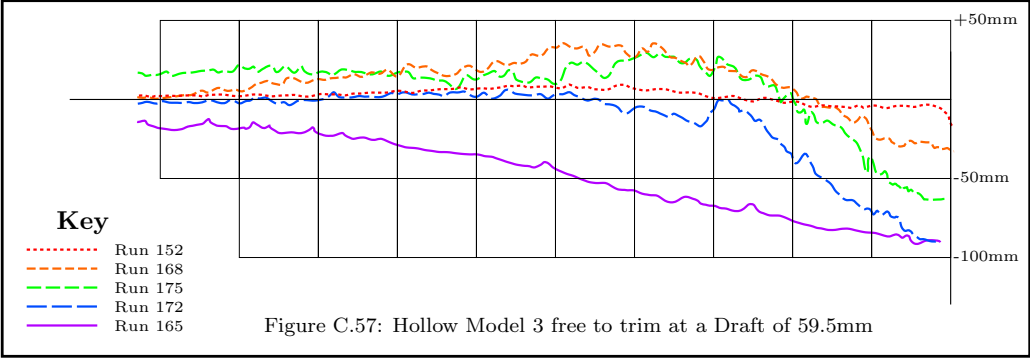
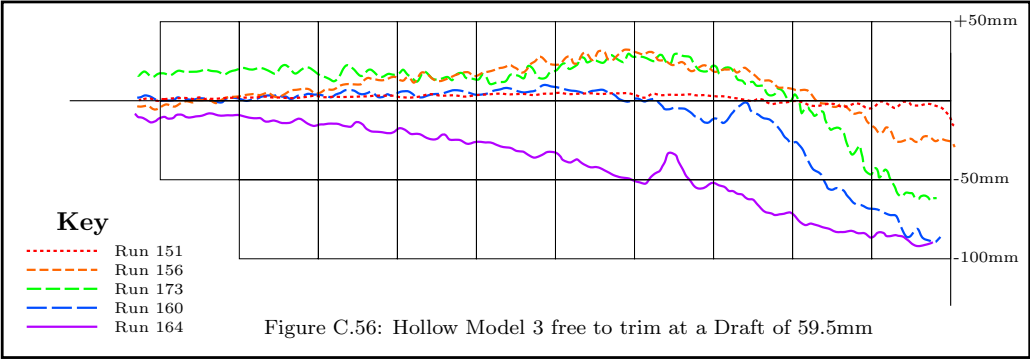
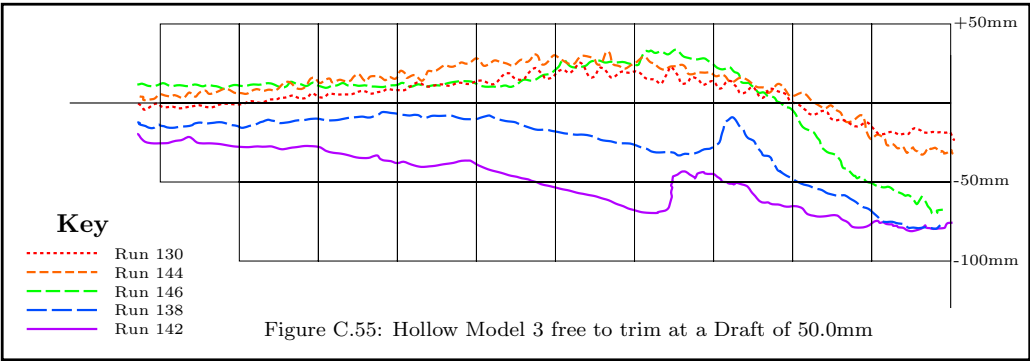


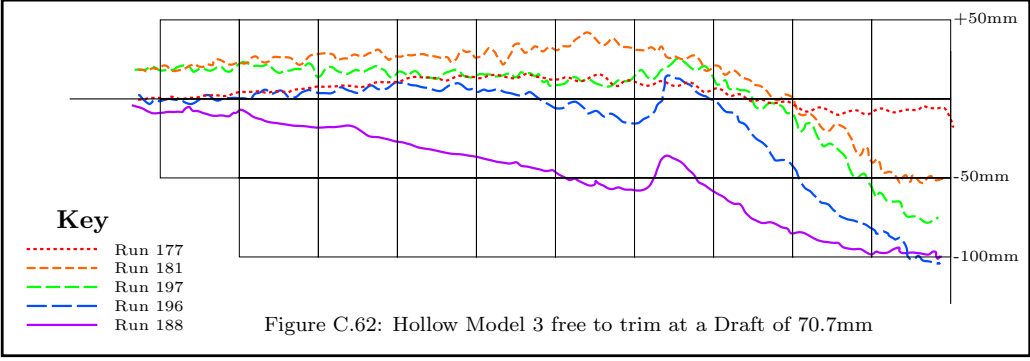
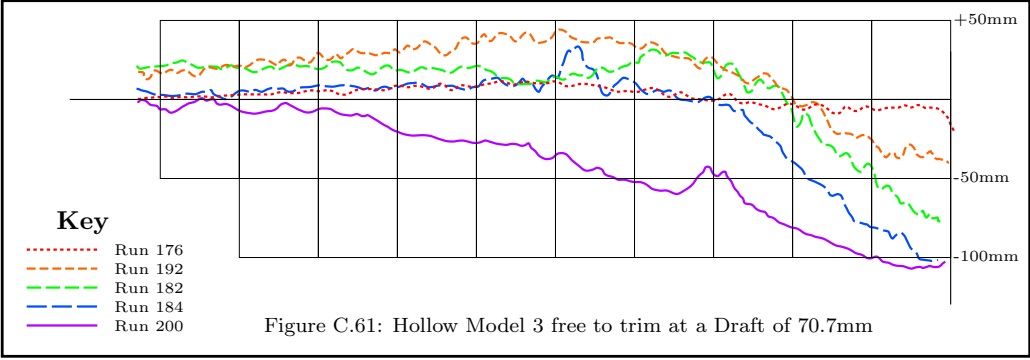
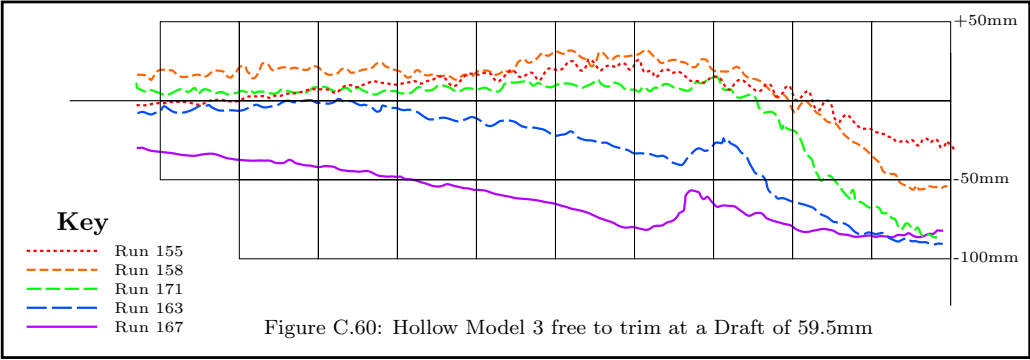
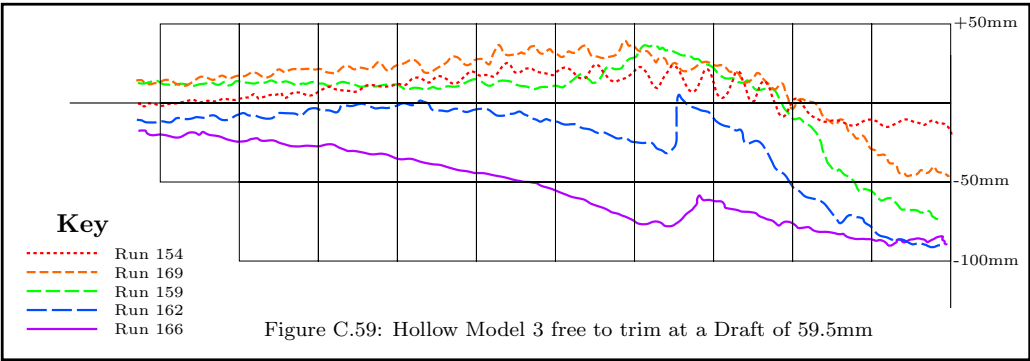


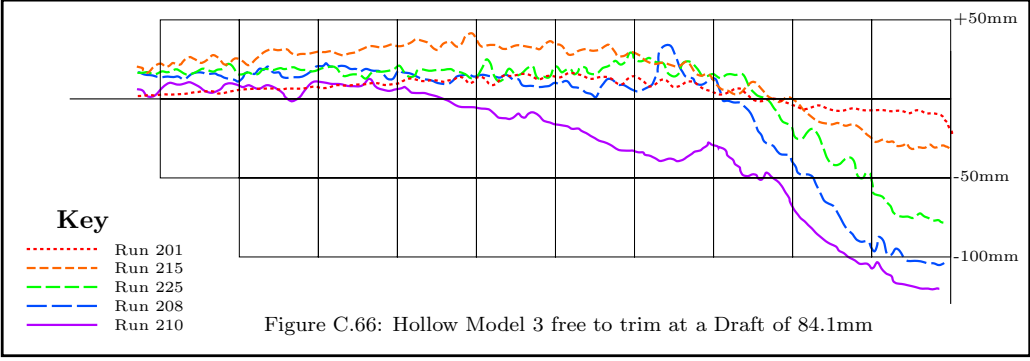
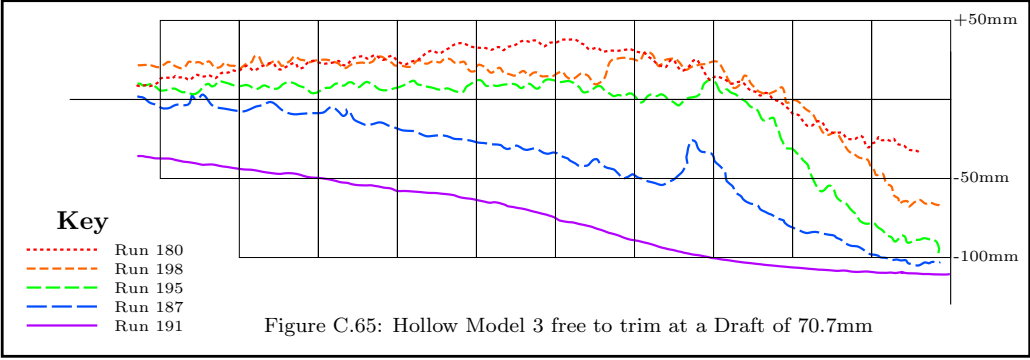
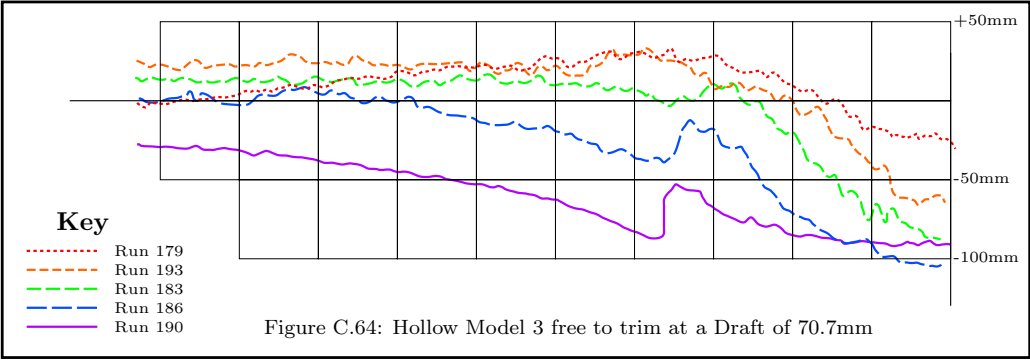
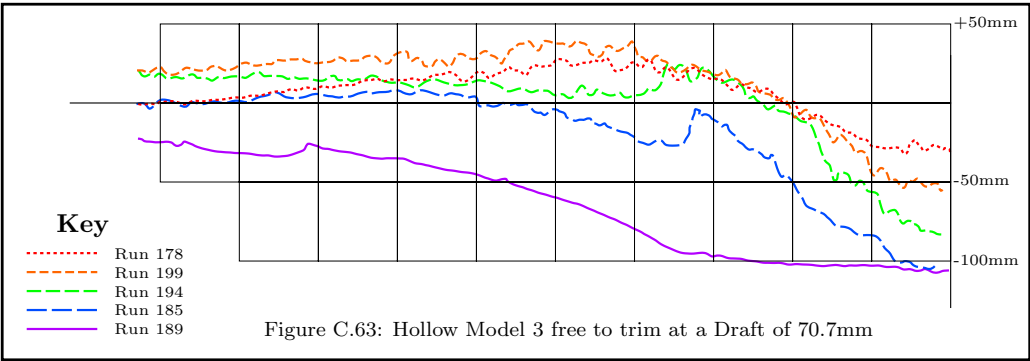


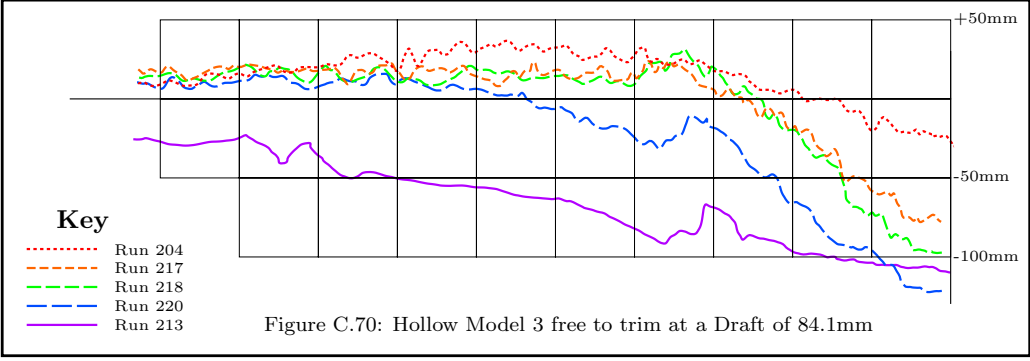
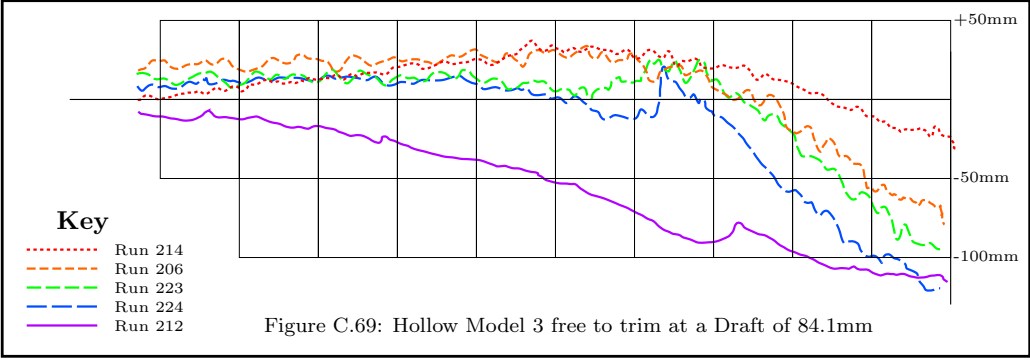
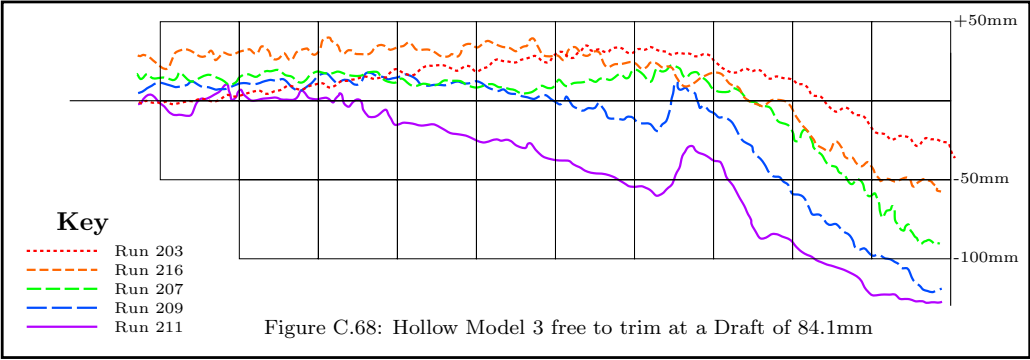
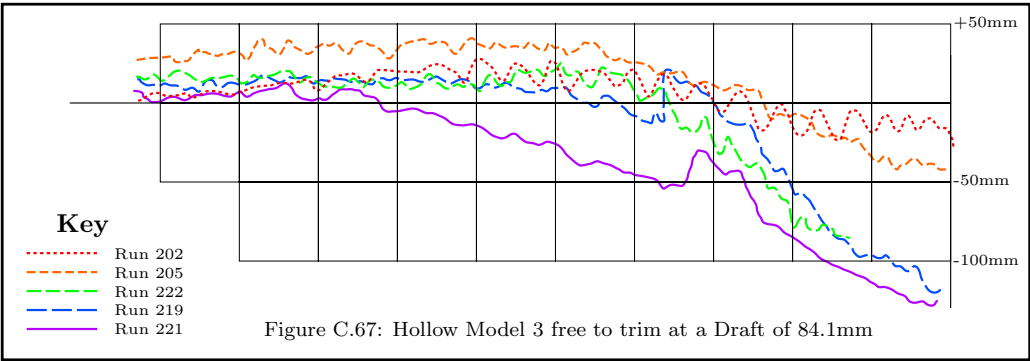


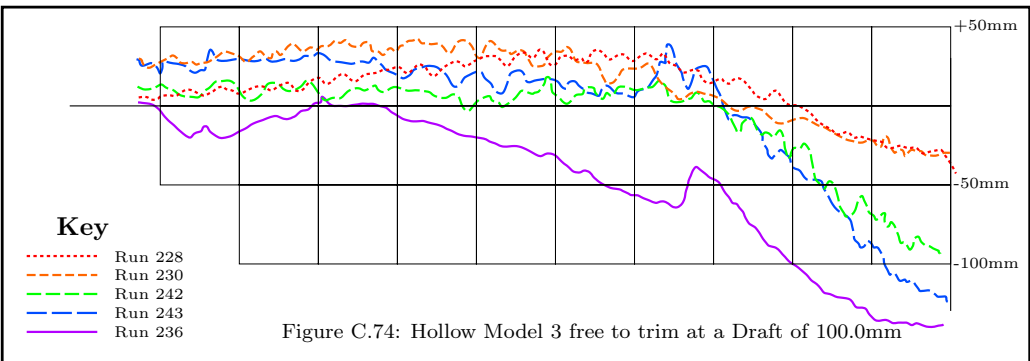
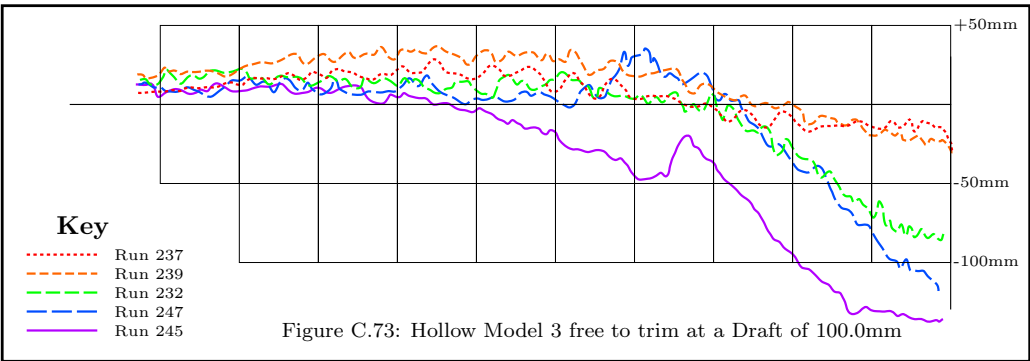
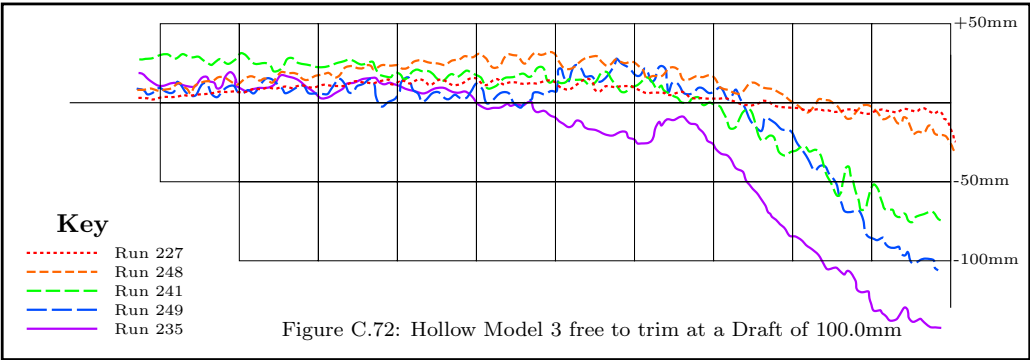
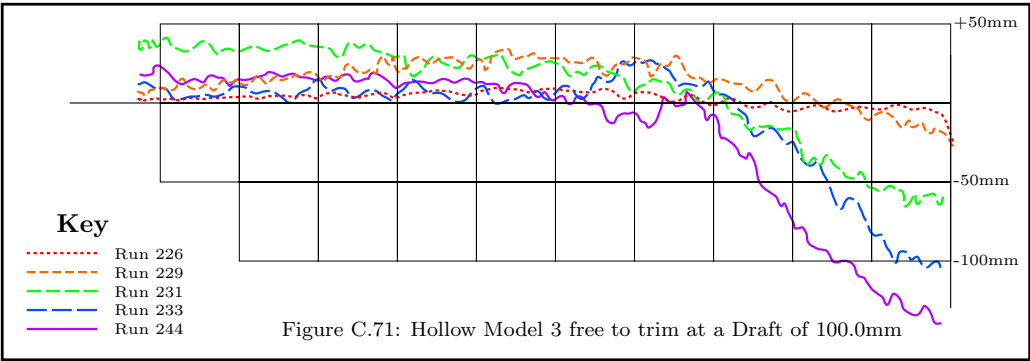


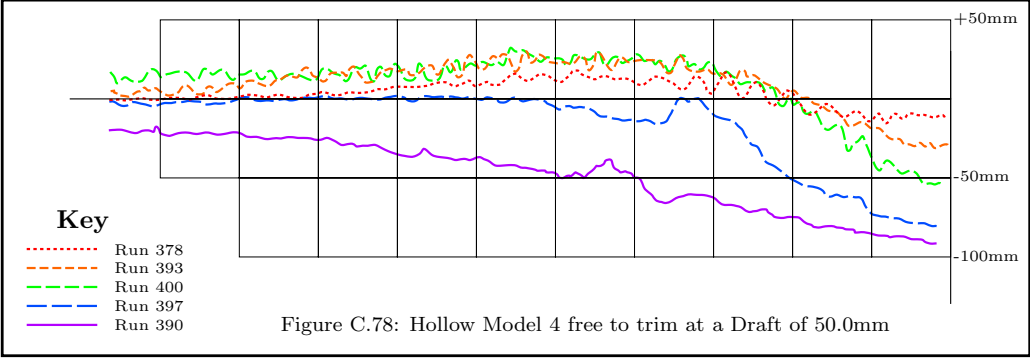
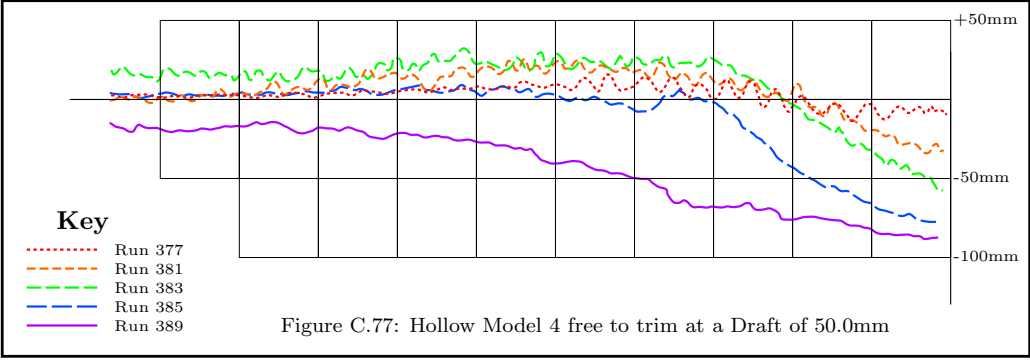
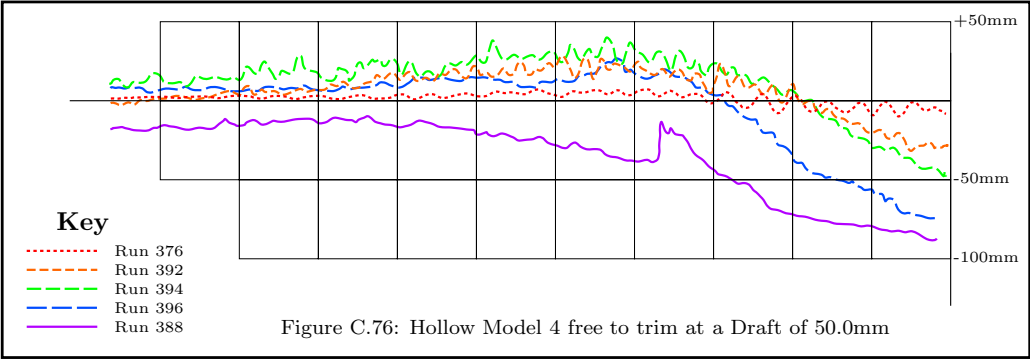
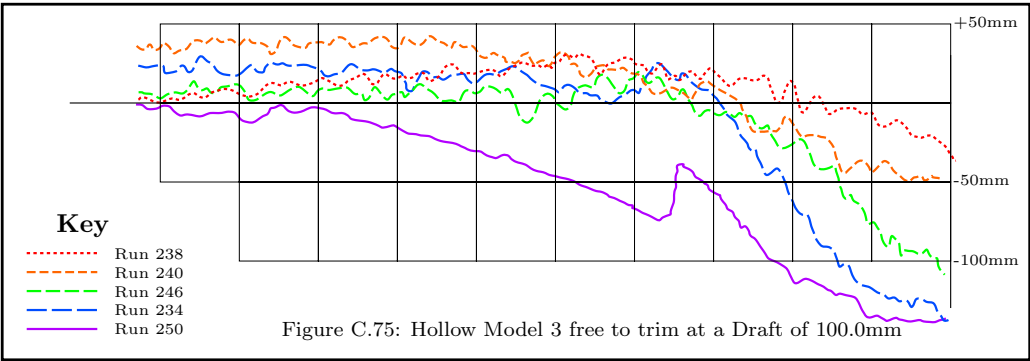


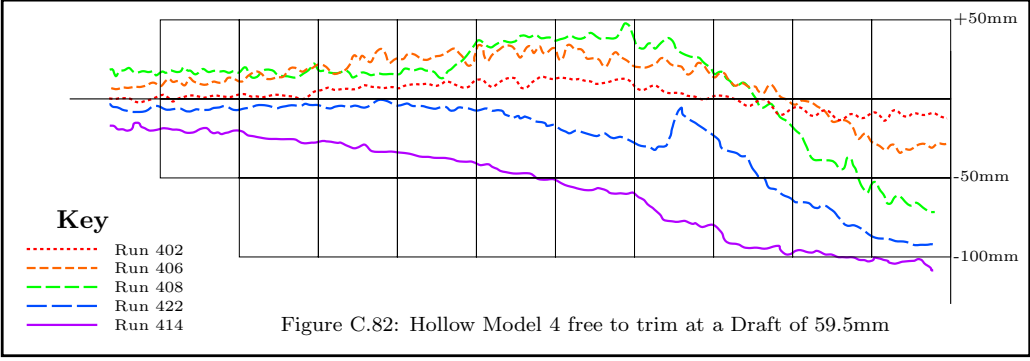
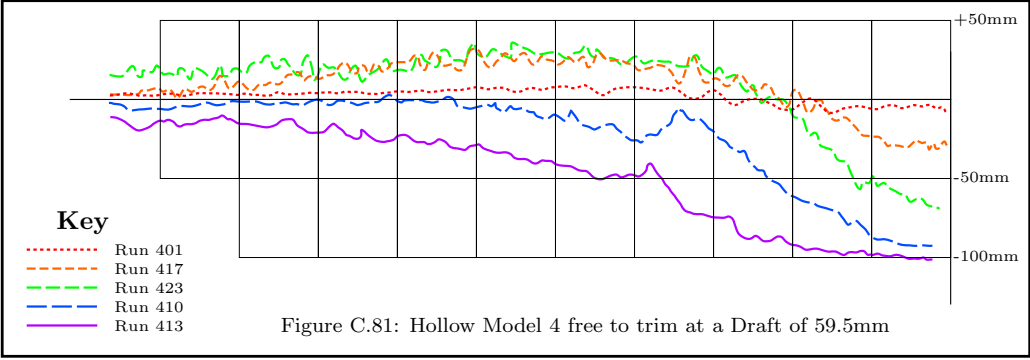
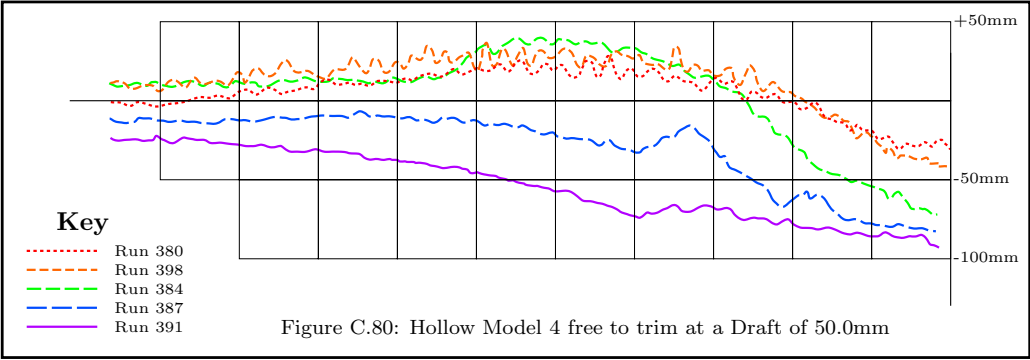
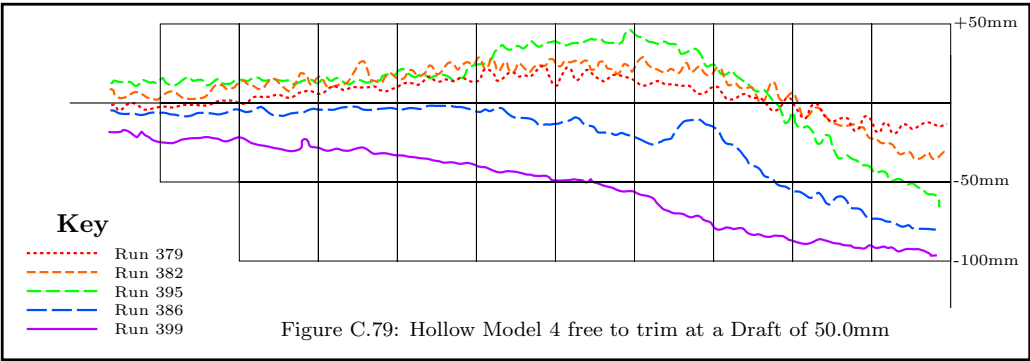


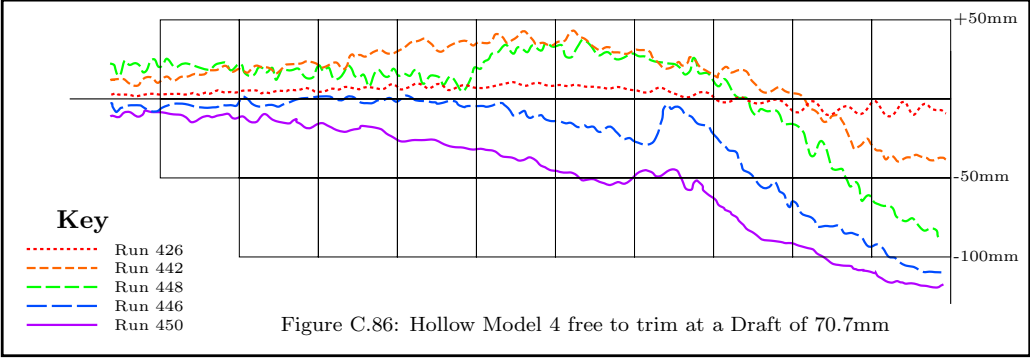
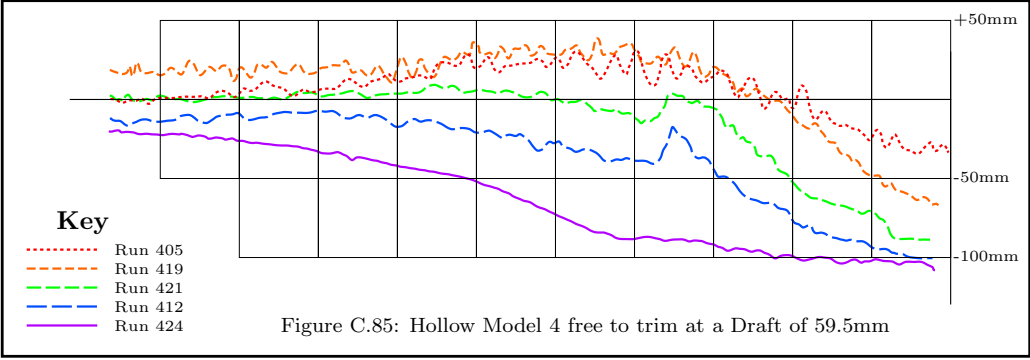
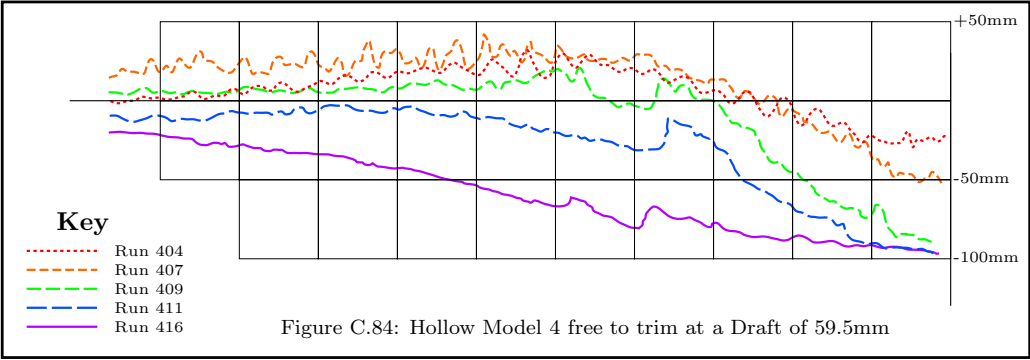
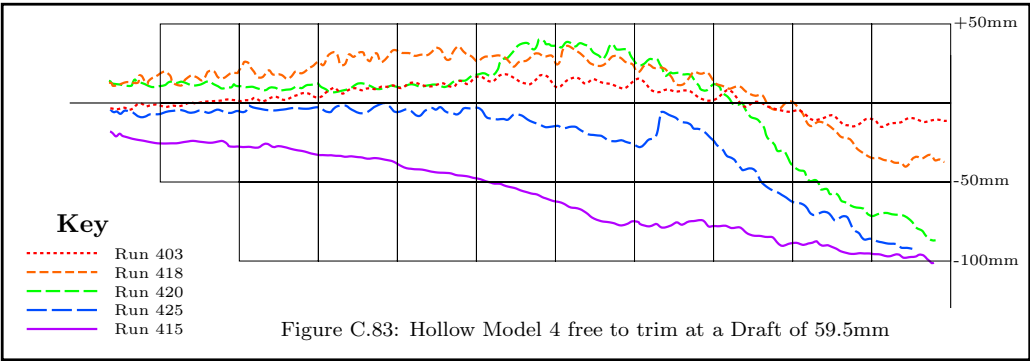


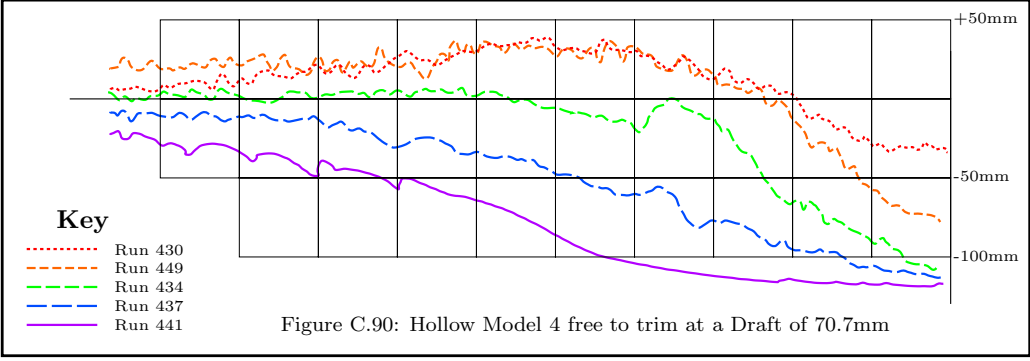
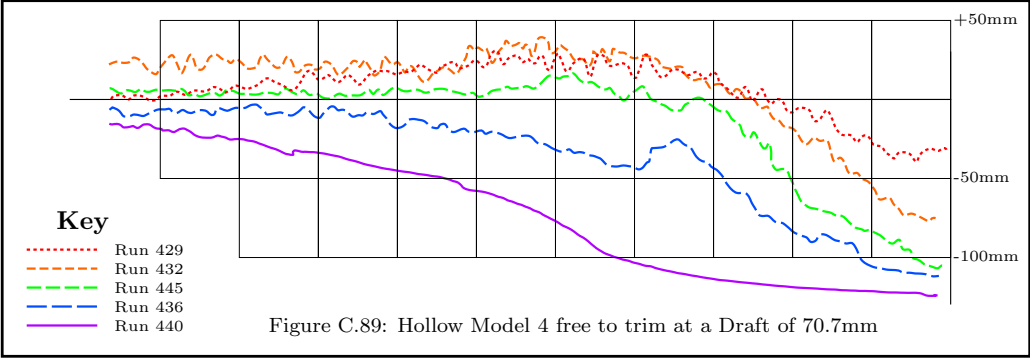
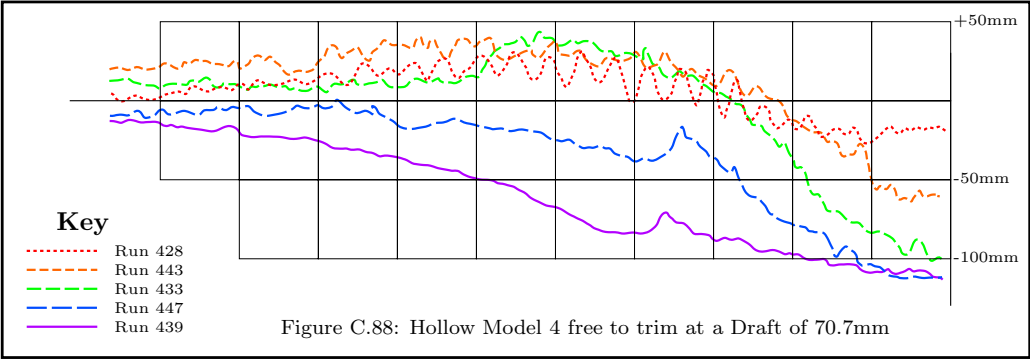
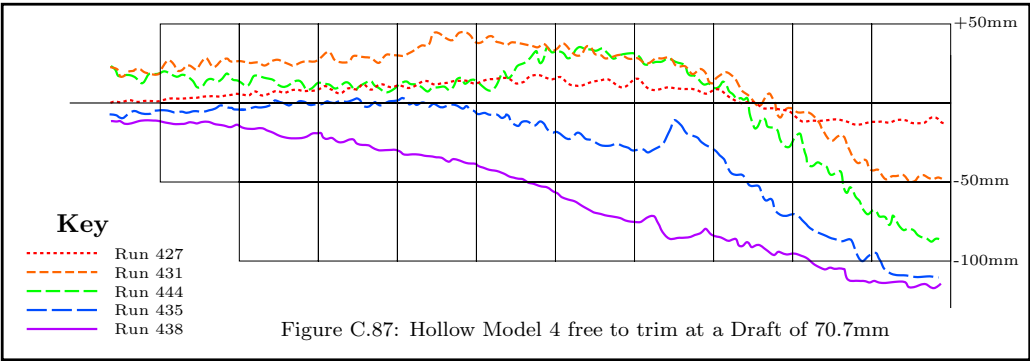


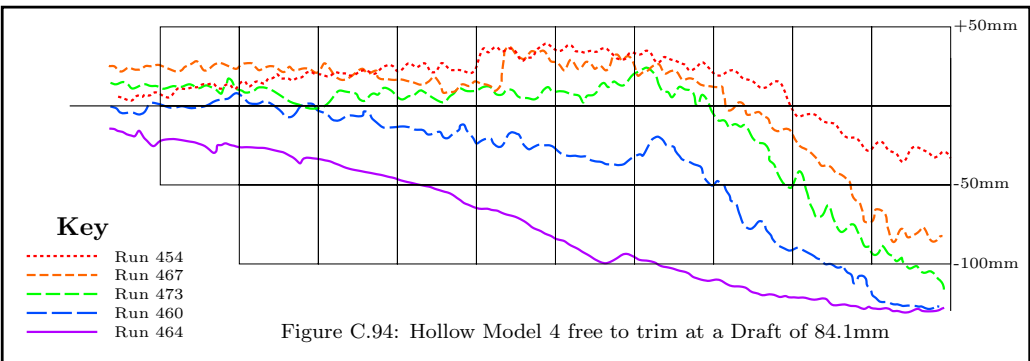
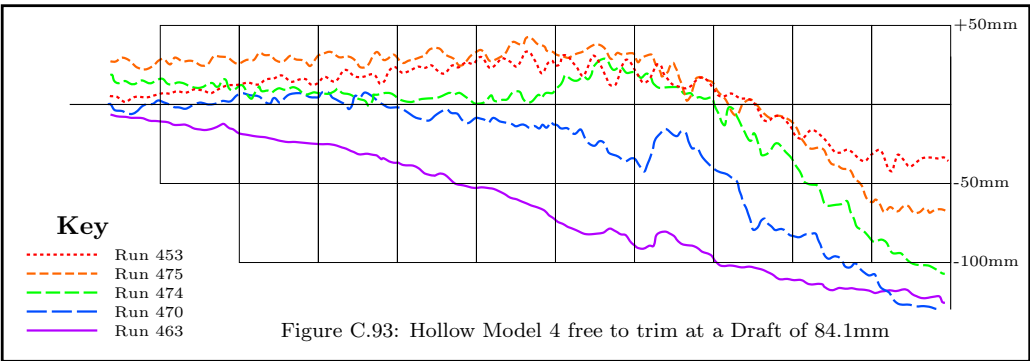
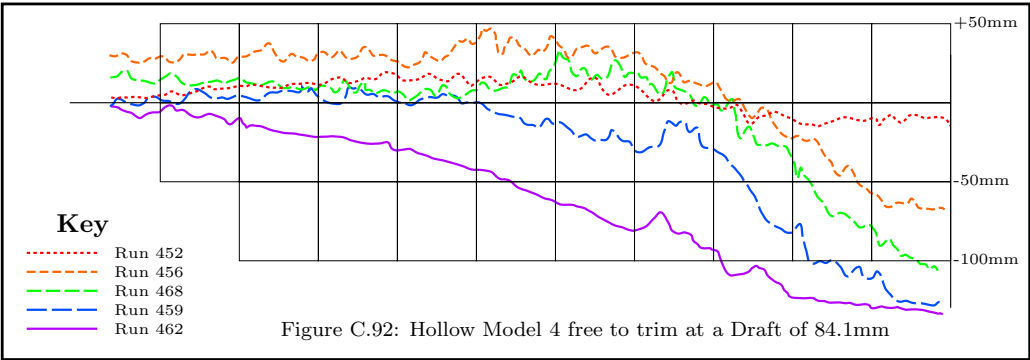
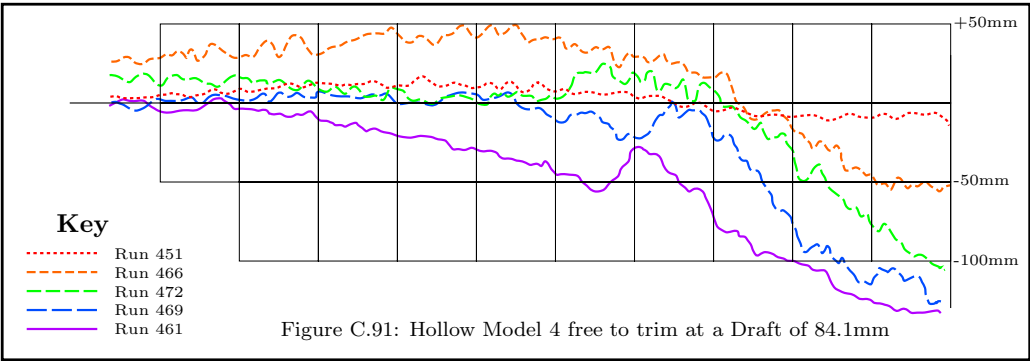


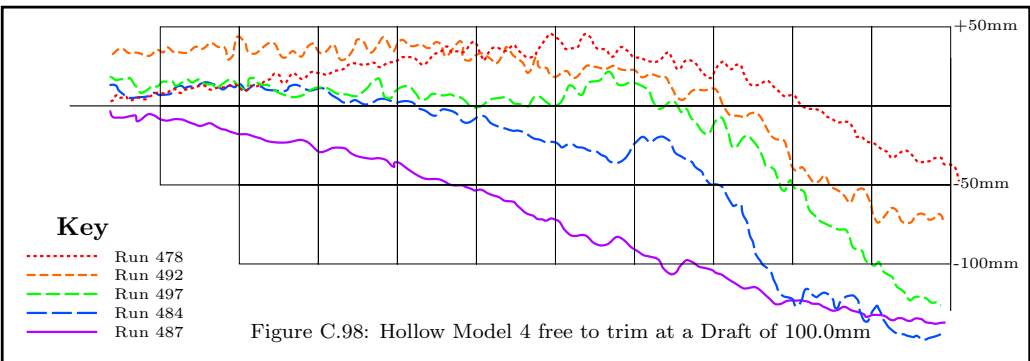
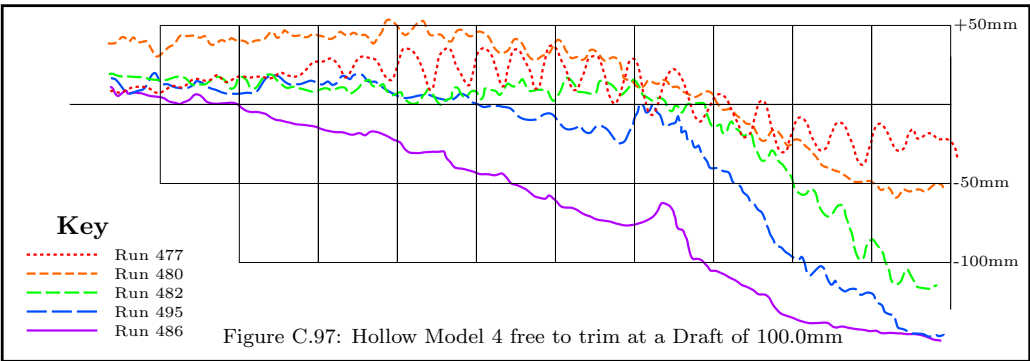
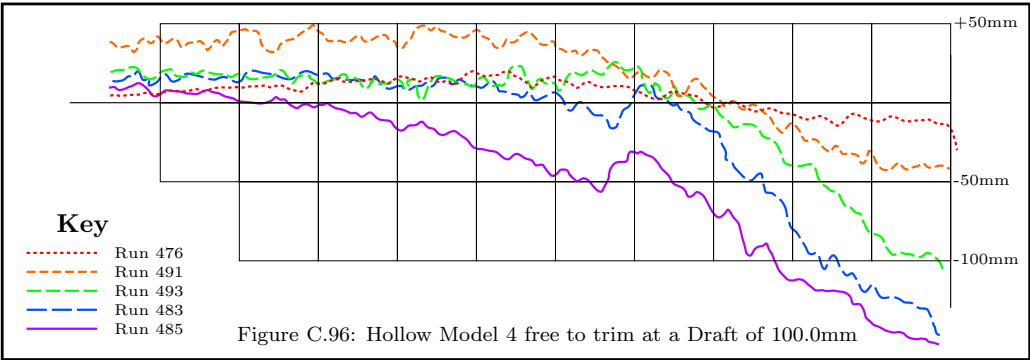
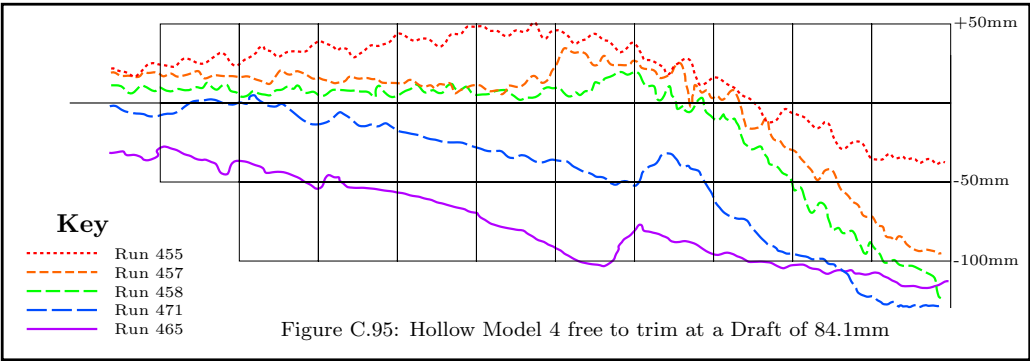


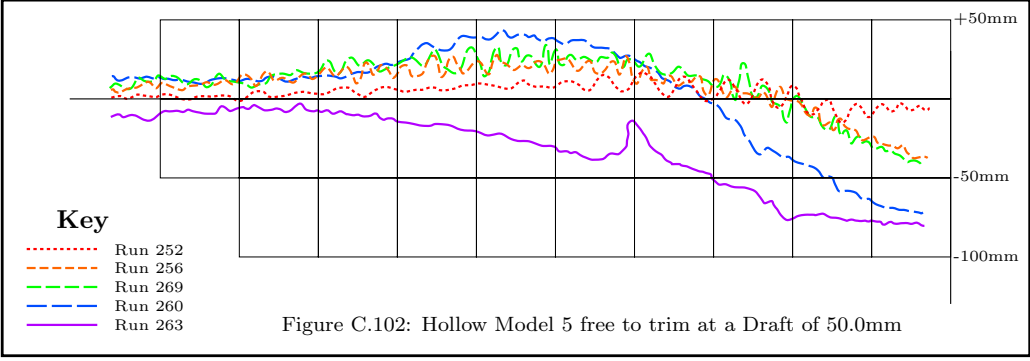
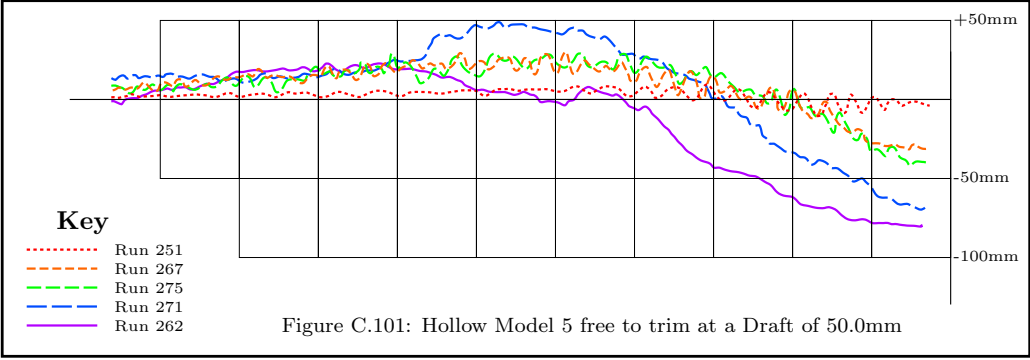
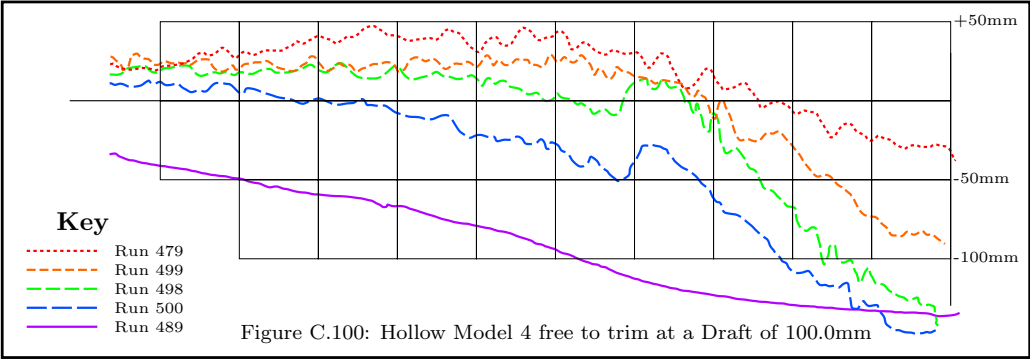
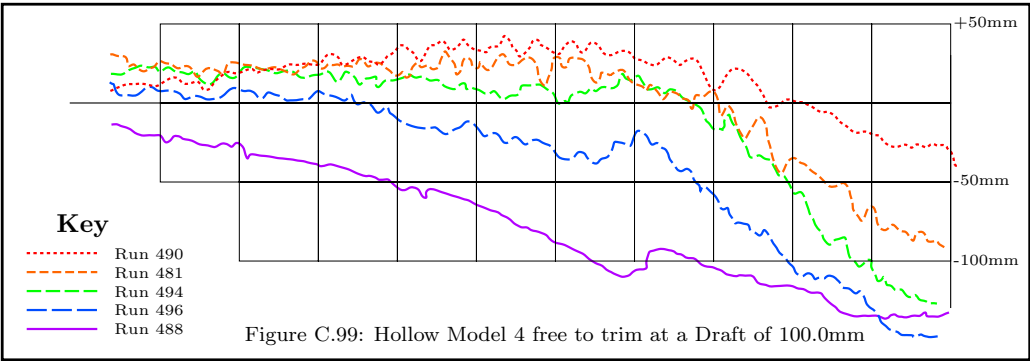


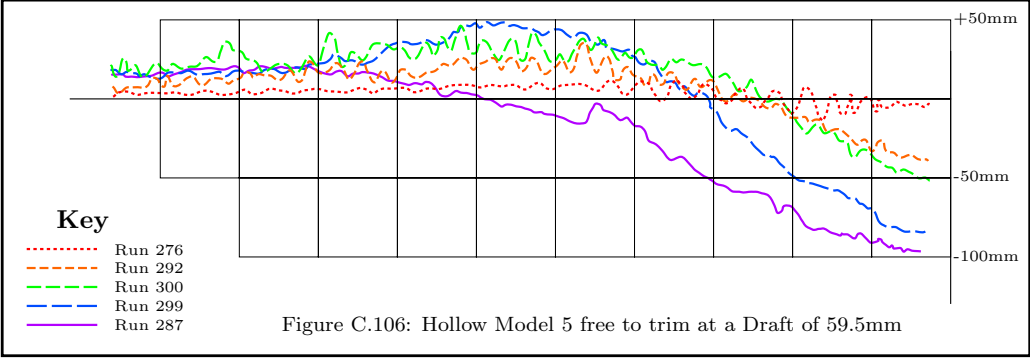
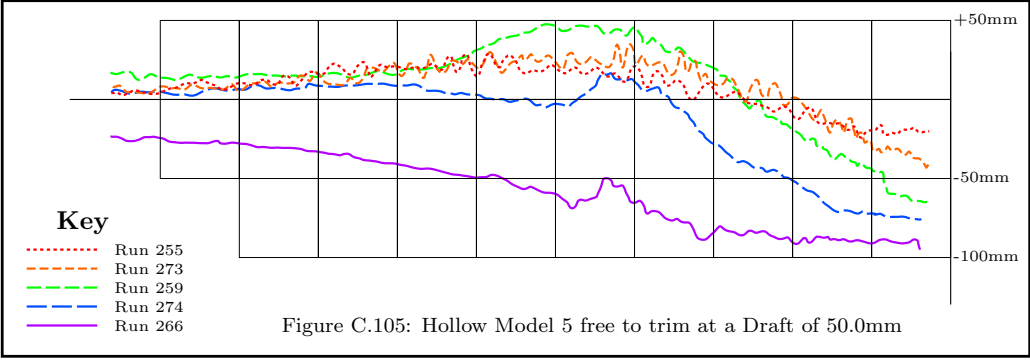
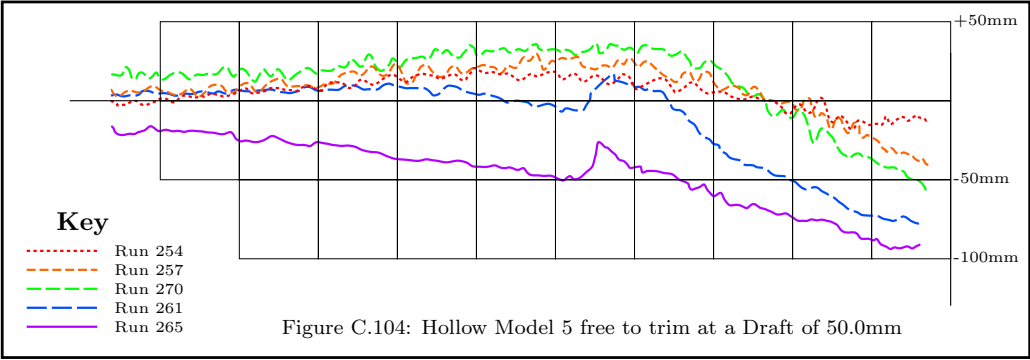
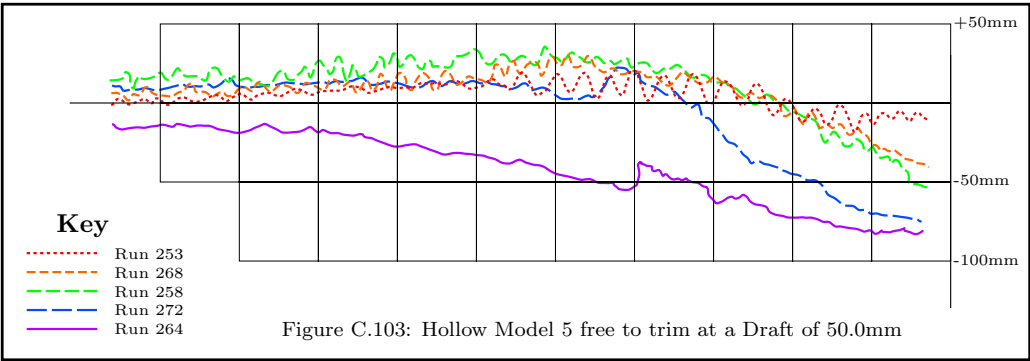


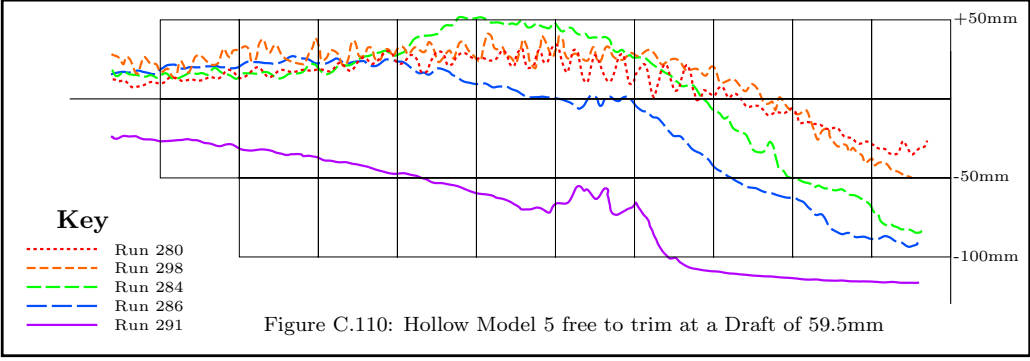
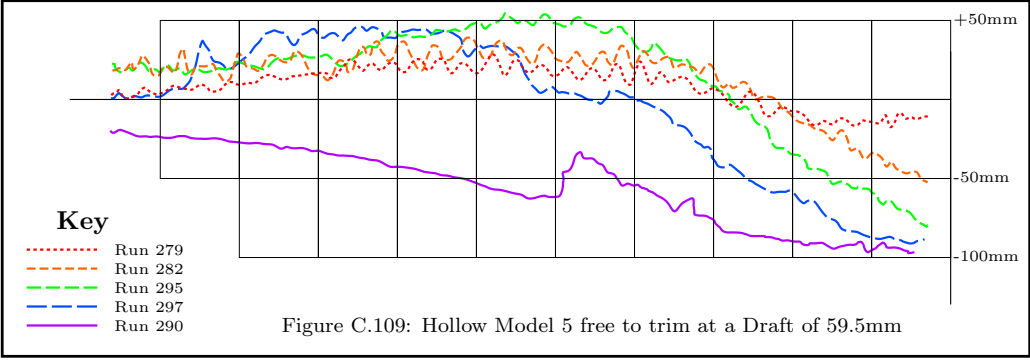
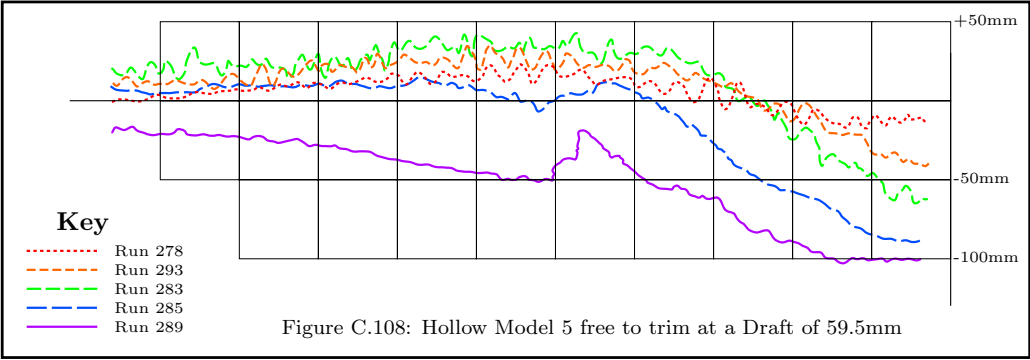
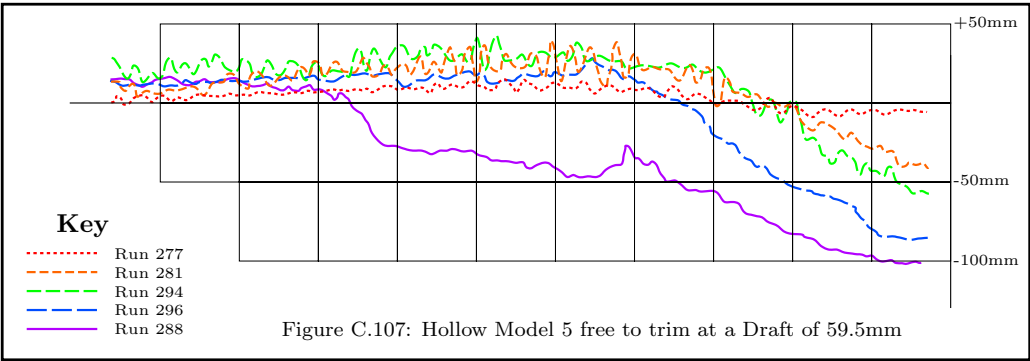


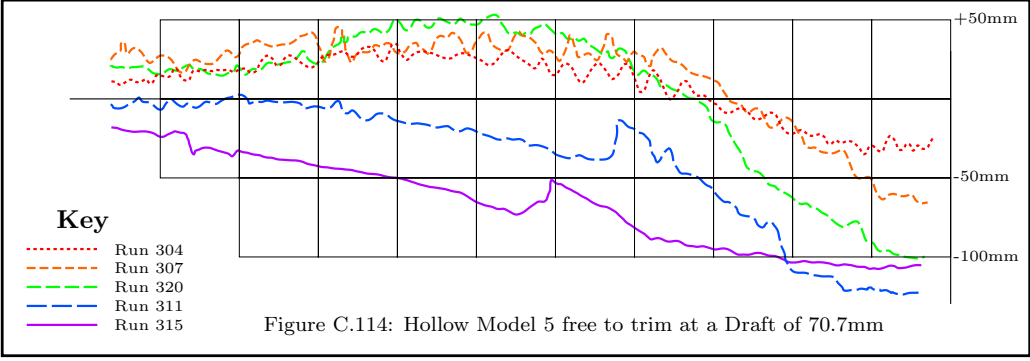
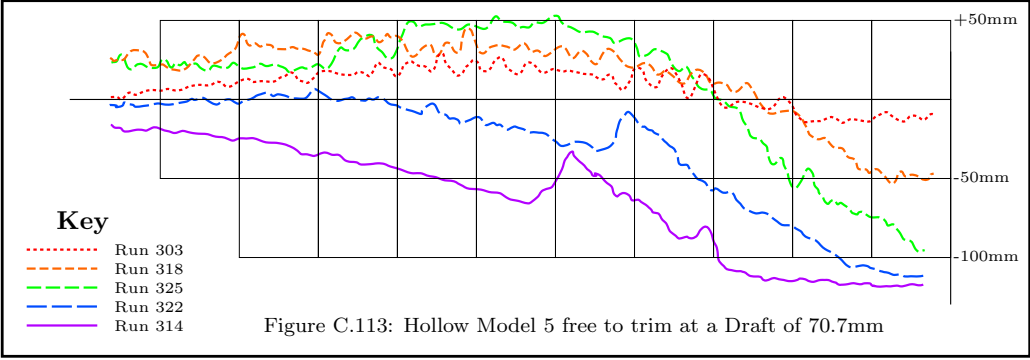
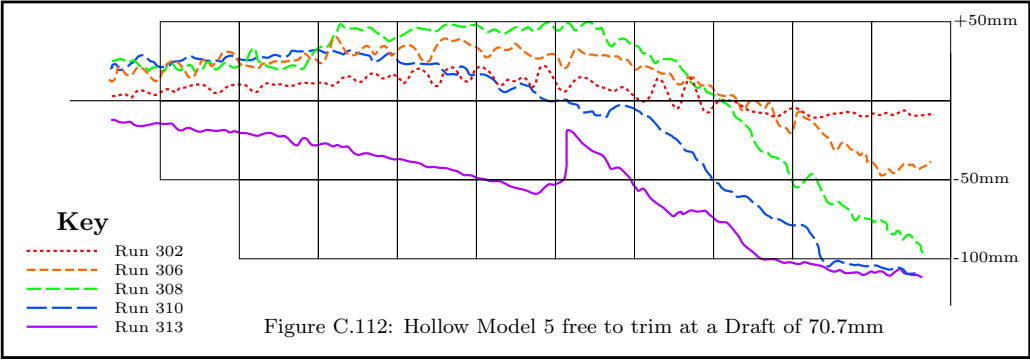
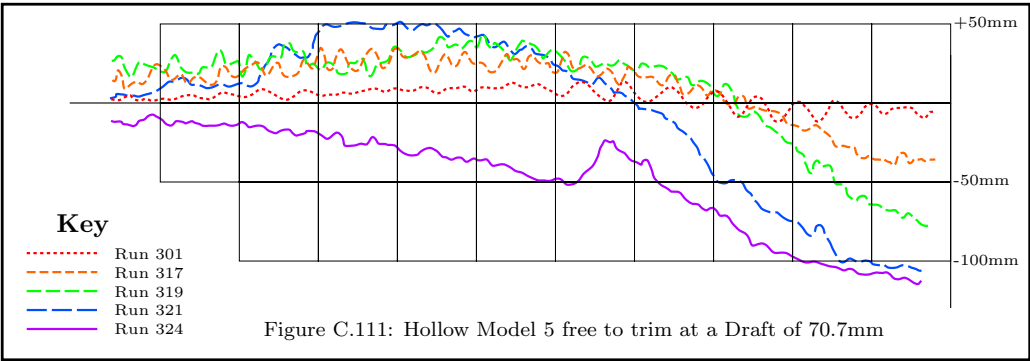


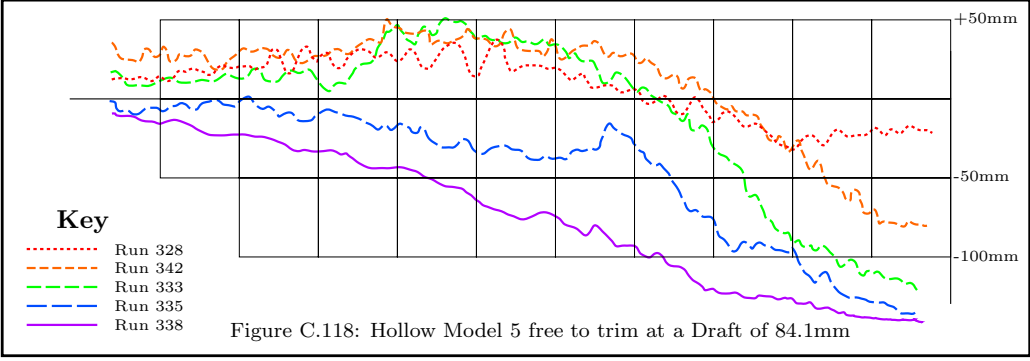
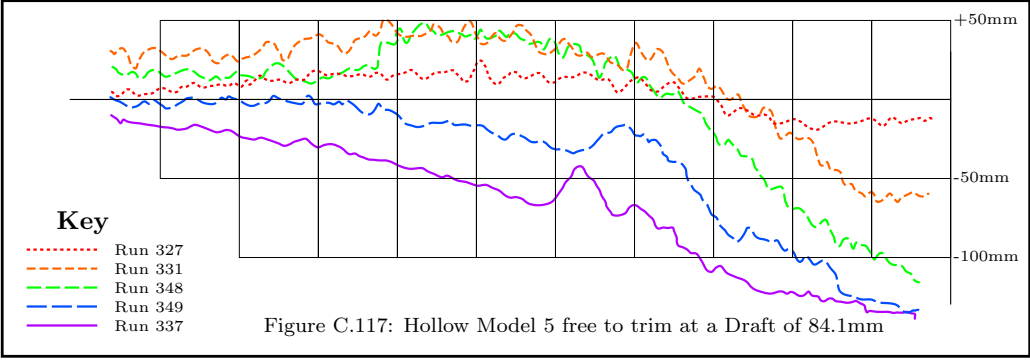
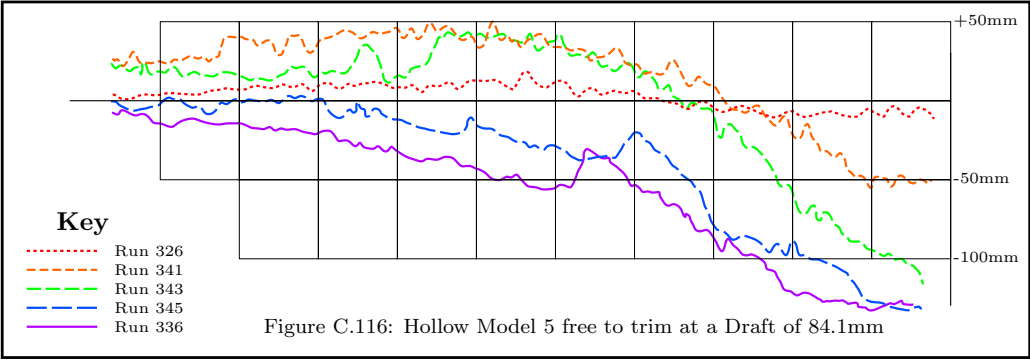
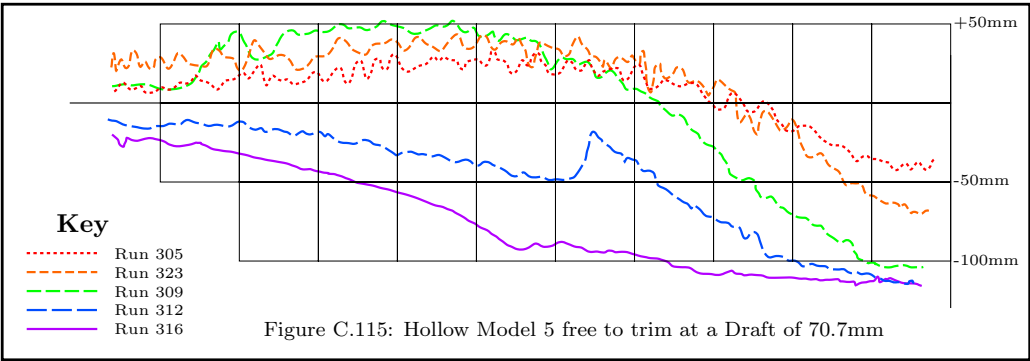


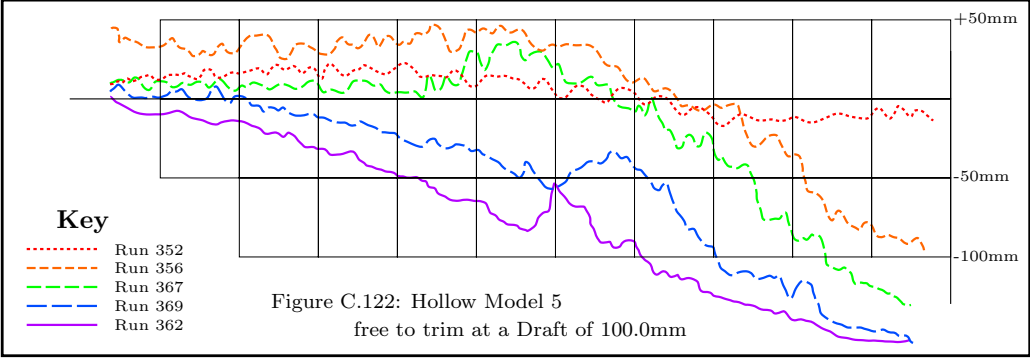
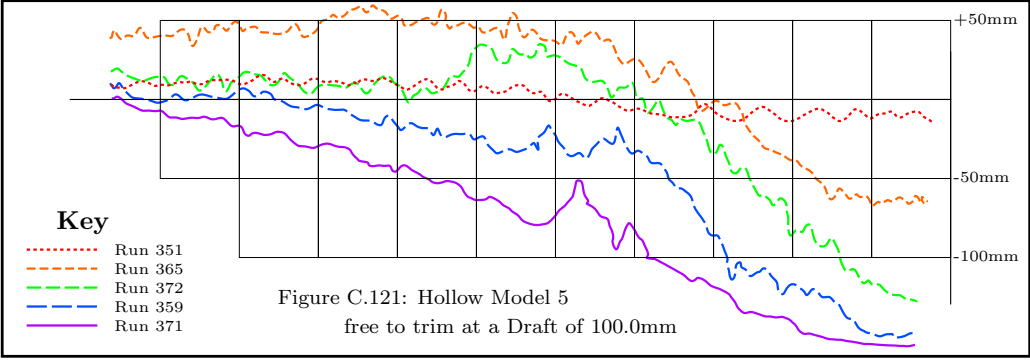
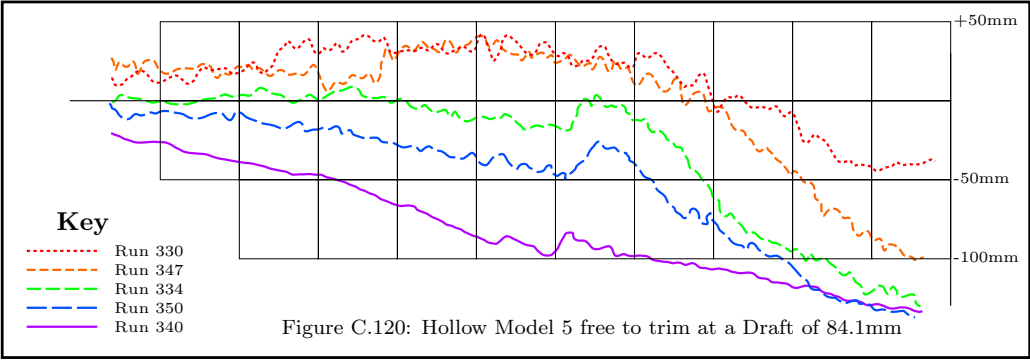
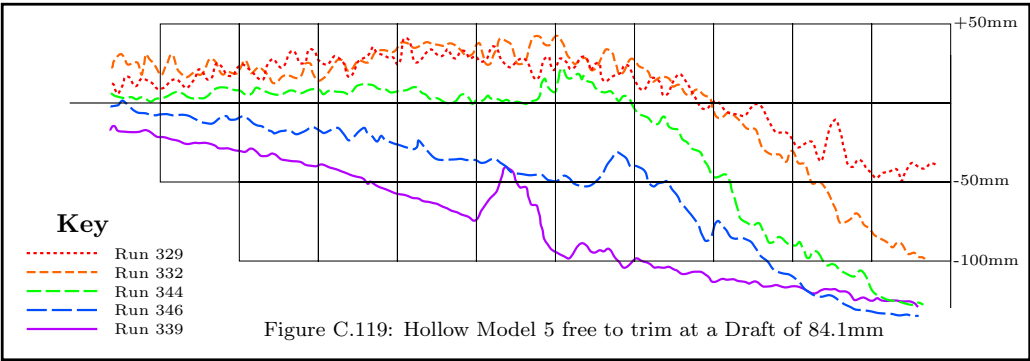


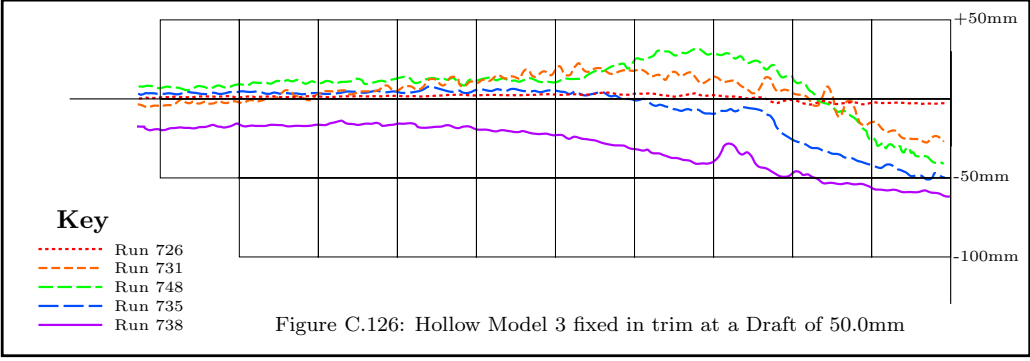
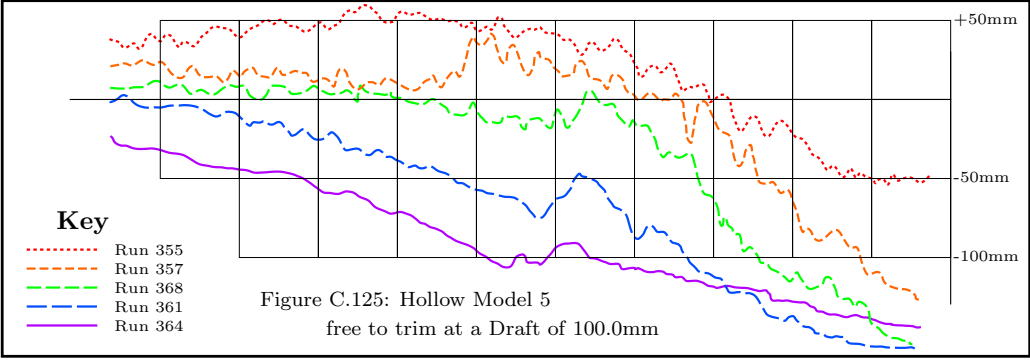
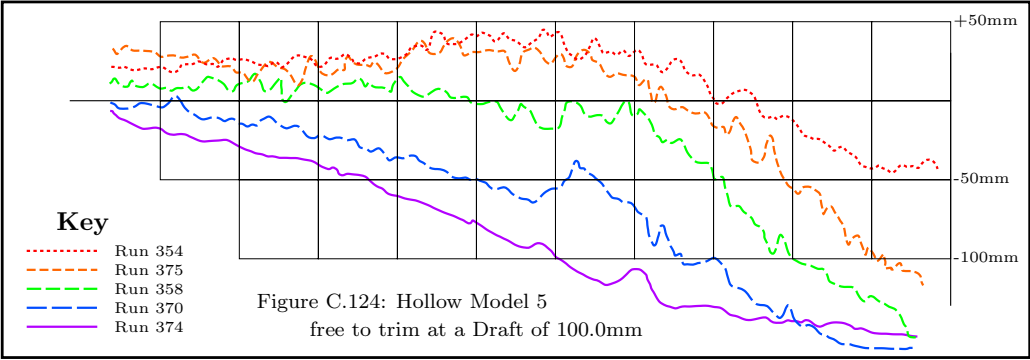
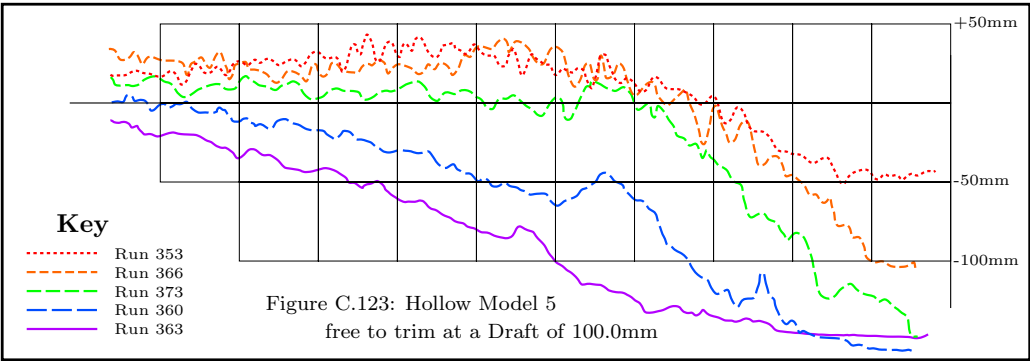


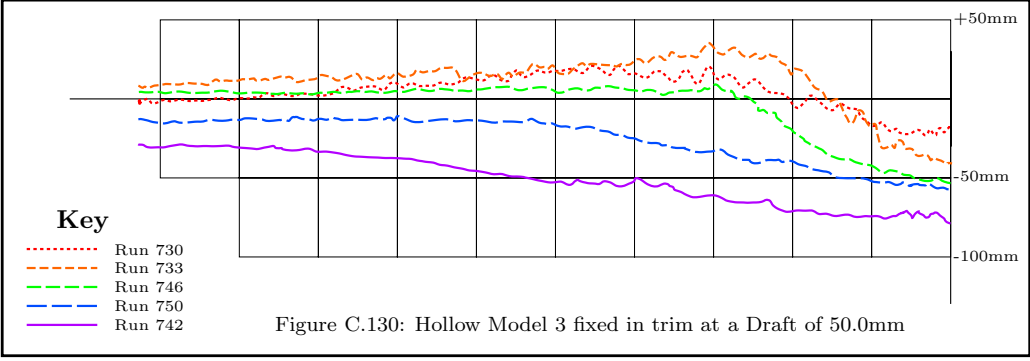
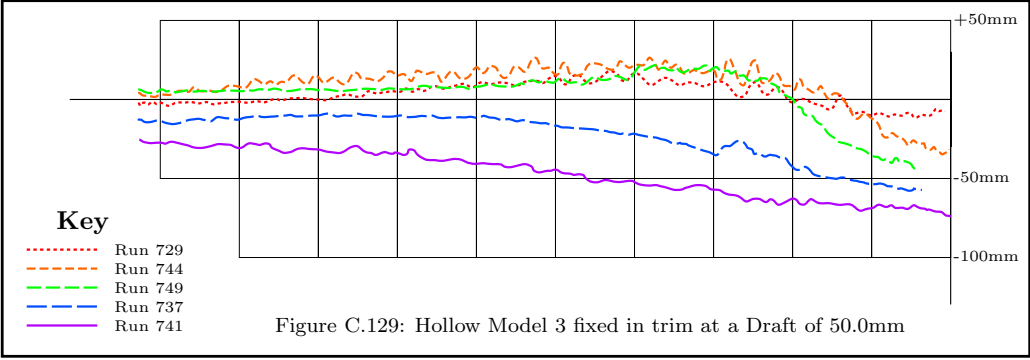
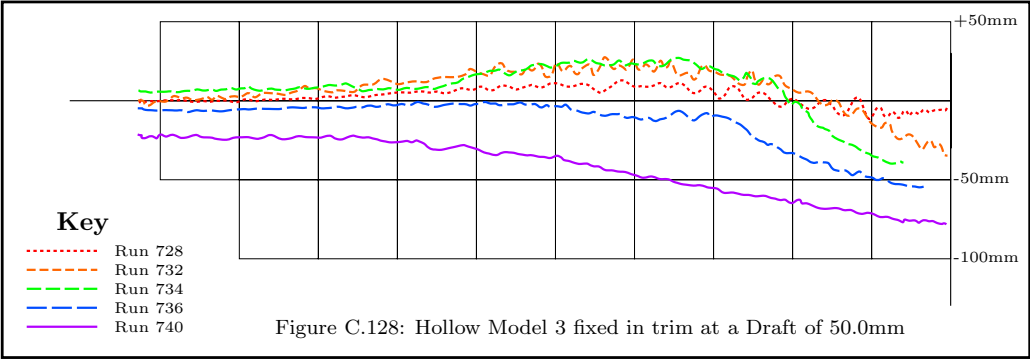
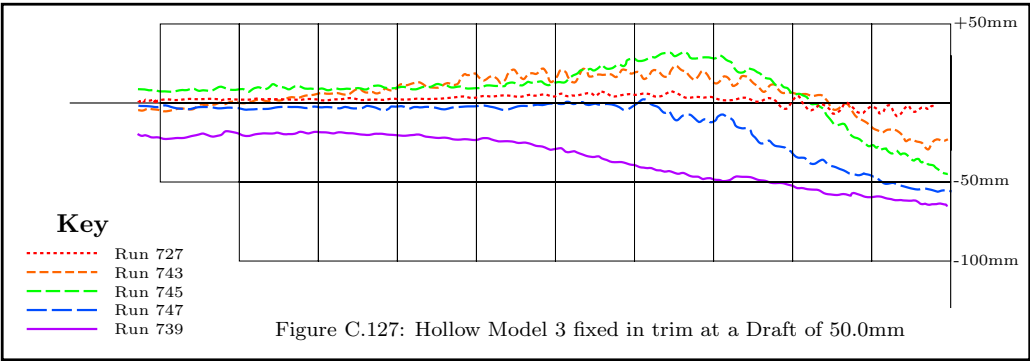


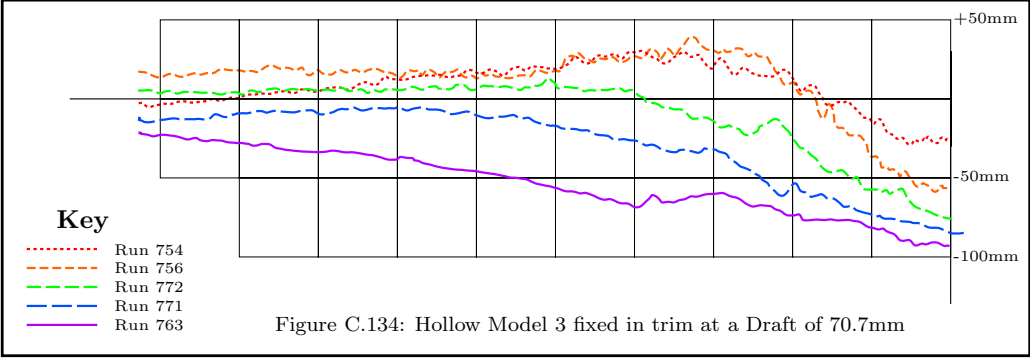
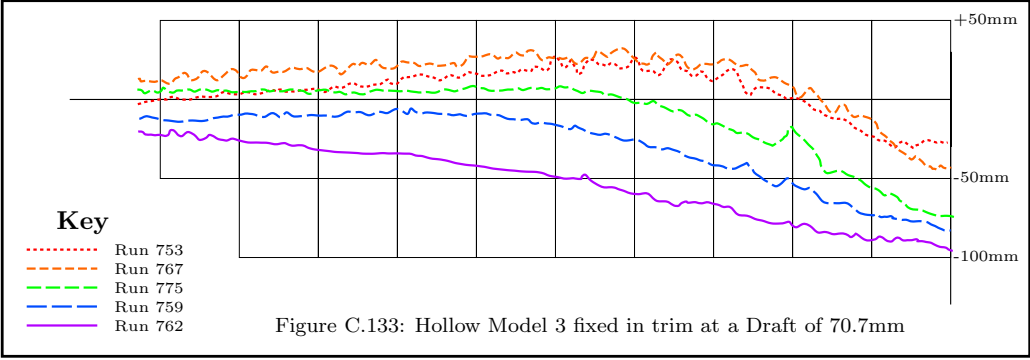
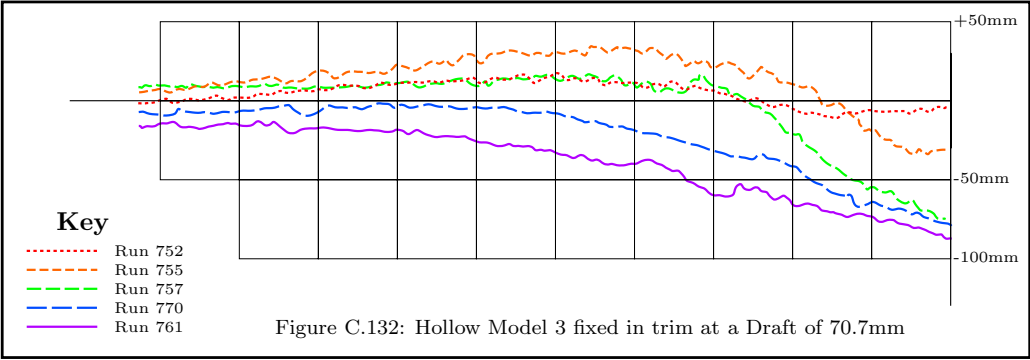
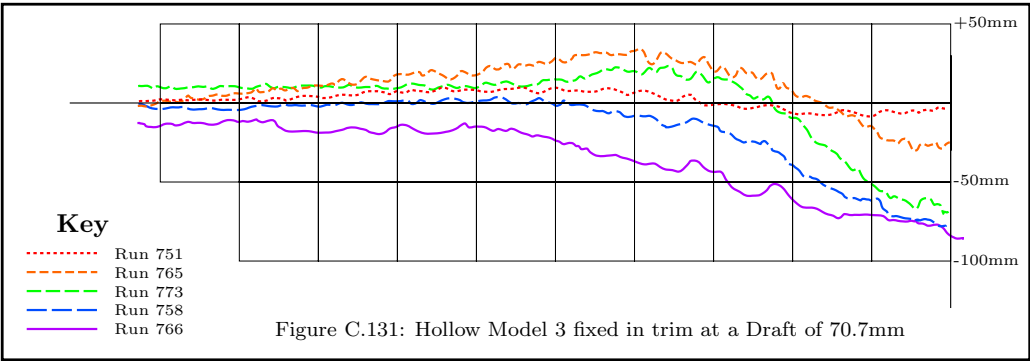


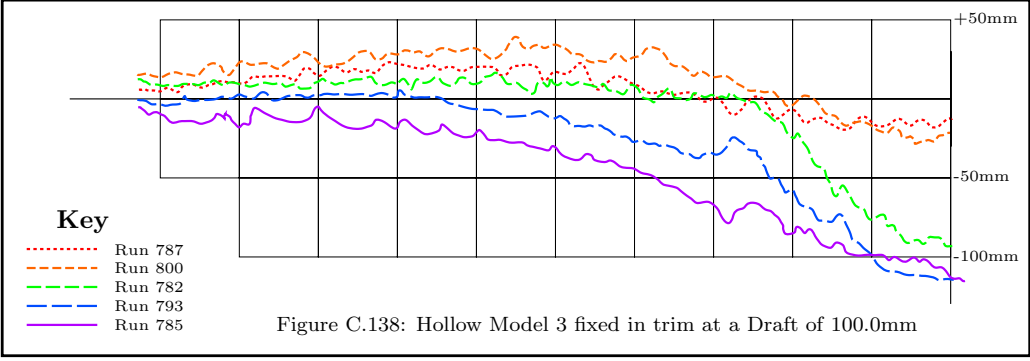
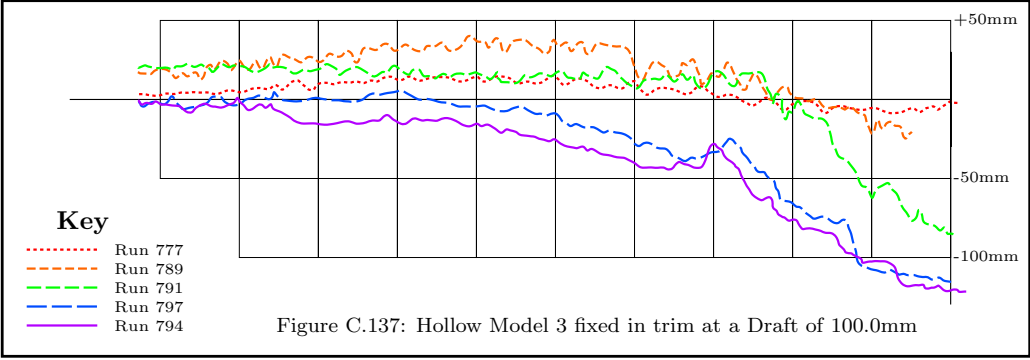
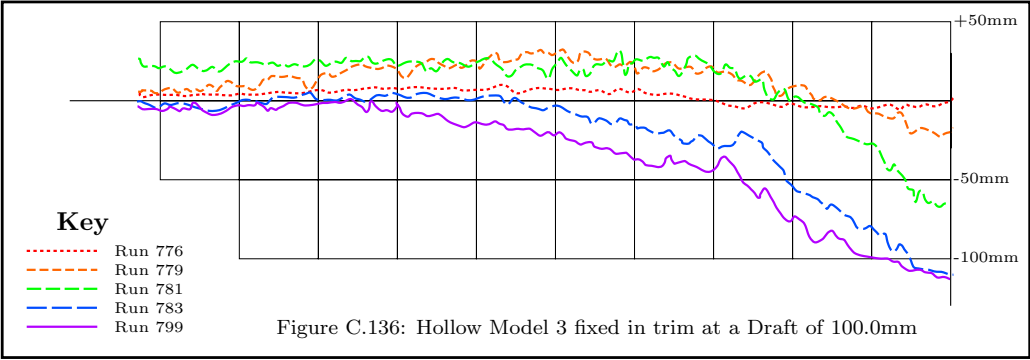
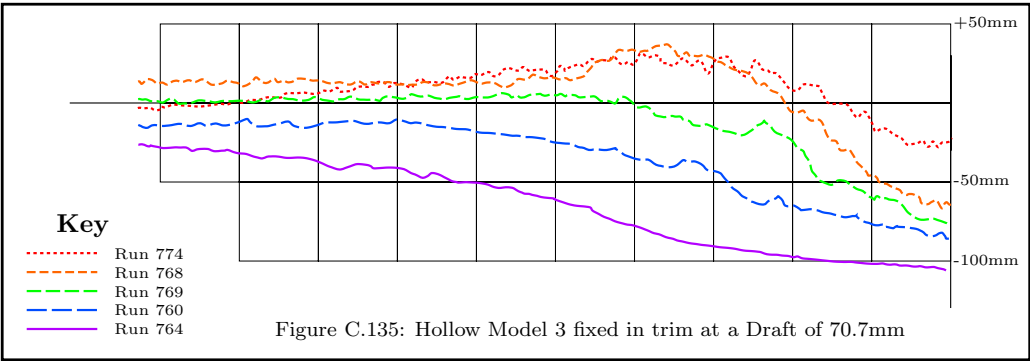


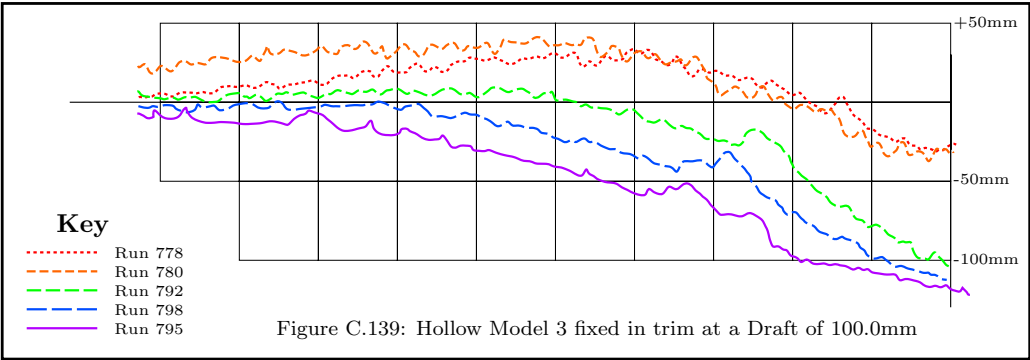












Appendix D

Resistance Curves

This appendix contains the resistance curves for all the models used in the form-factor regression analysis presented in Chapter 7. The resistance data for each model is presented in the form of the total resistance (R_T) non-dimensionalised by the weight (W) and plotted against the length Froude number (F_{n_L}). The experimental data (Expt), as represented by circles in each figure, are as collated from the original references. The blue solid line (Orig) represents the total resistance as predicted using the methodology presented in Section 3.5 with no form factors applied. The red dashed line (Form) in each figure represents the total resistance as predicted using the methodology presented in Section 3.5 but with the form factors calculated in Table 7.21 applied.

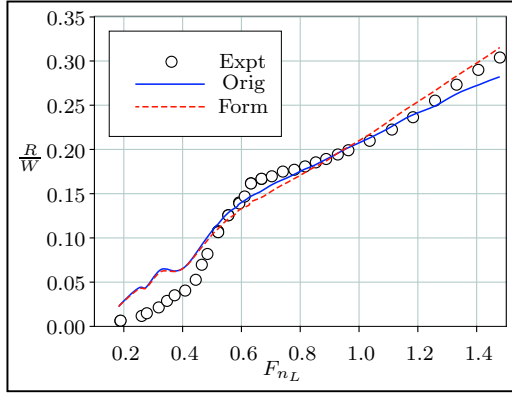


Figure D.1: Lego Model 1

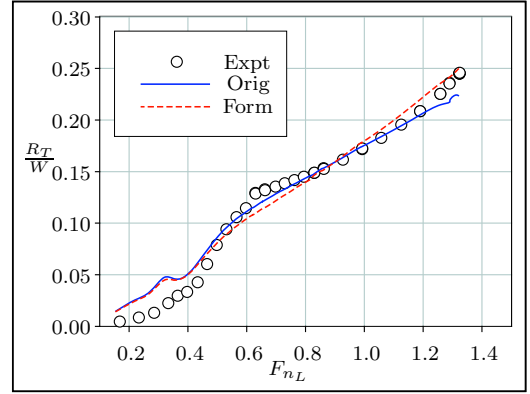


Figure D.2: Lego Model 2

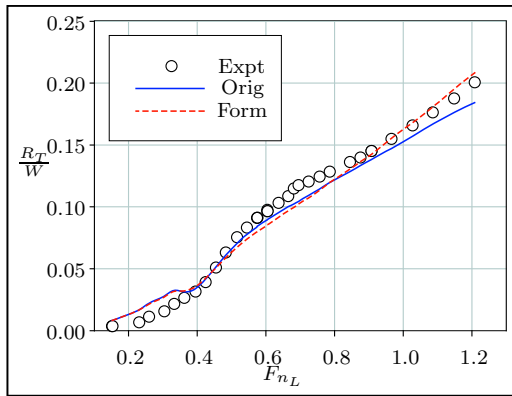


Figure D.3: Lego Model 3

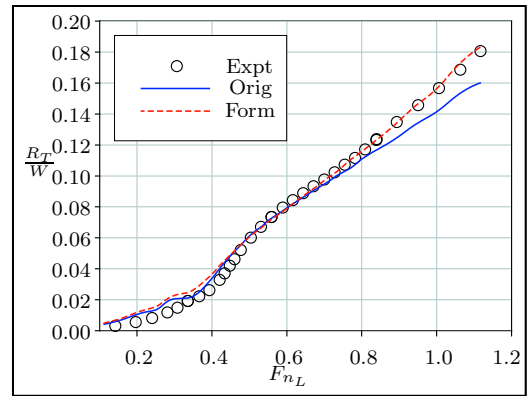


Figure D.4: Lego Model 4

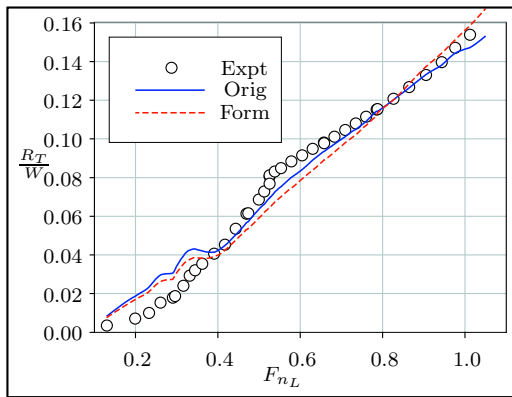


Figure D.5: Lego Model 5

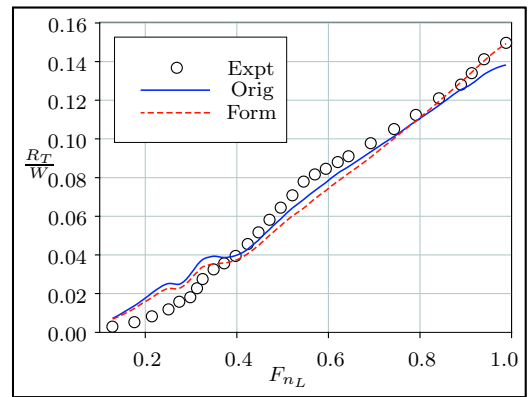


Figure D.6: Lego Model 6

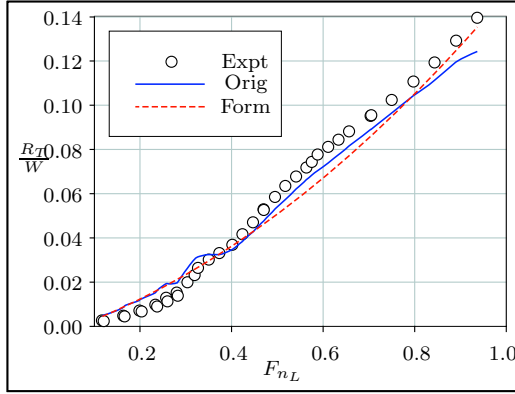


Figure D.7: Lego Model 7

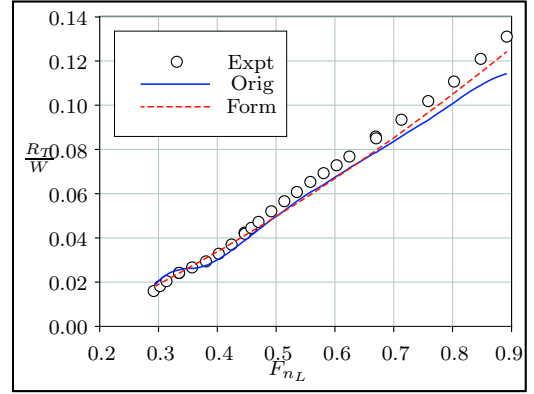


Figure D.8: Lego Model 8

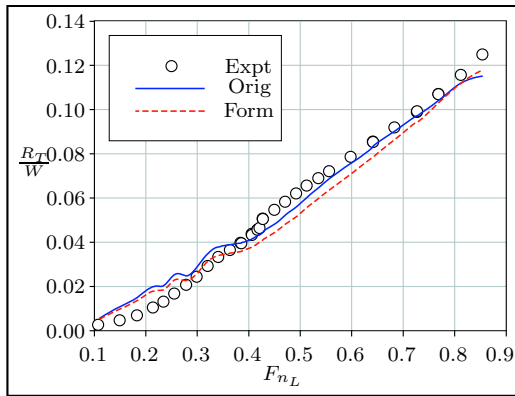


Figure D.9: Lego Model 9

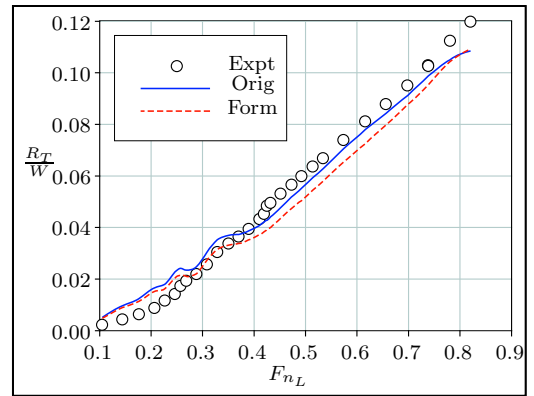


Figure D.10: Lego Model 10

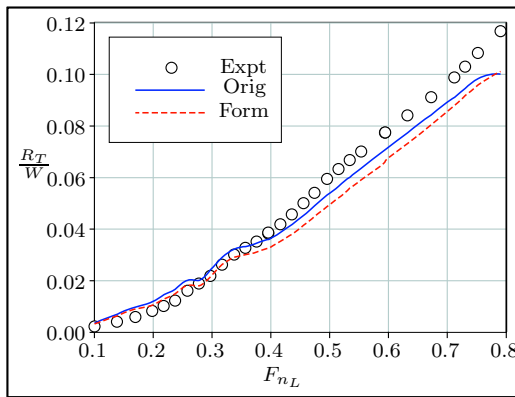


Figure D.11: Lego Model 11

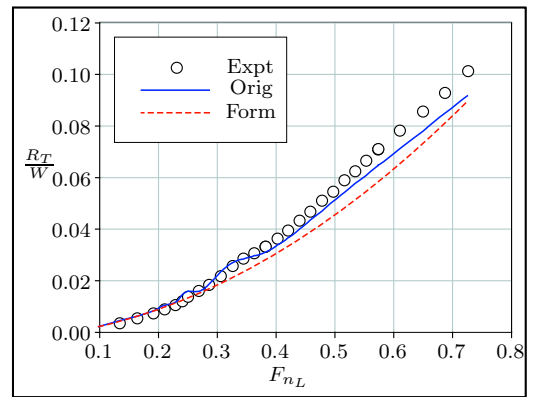


Figure D.12: Lego Model 12

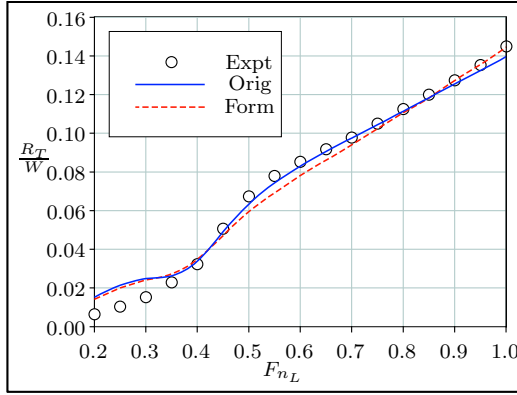


Figure D.13: Uni. of Southampton
Model 3b ($s/L=0.0$)

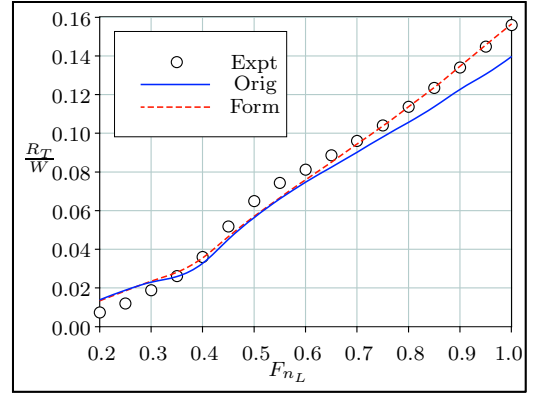


Figure D.14: Uni. of Southampton
Model 4a ($s/L=0.0$)

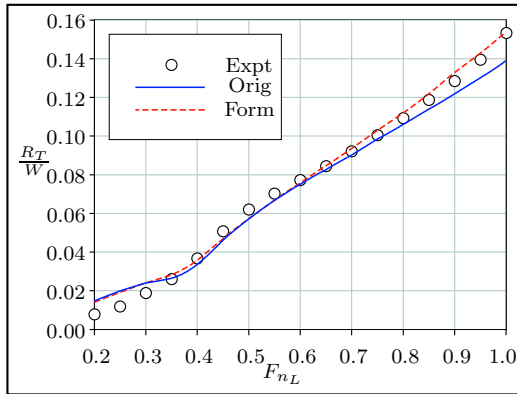


Figure D.15: Uni. of Southampton
Model 4b ($s/L=0.0$)

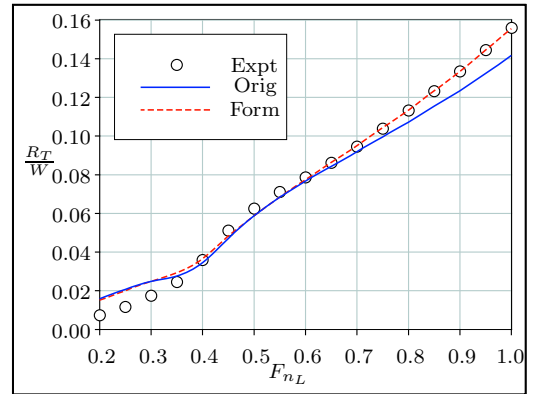


Figure D.16: Uni. of Southampton
Model 4c ($s/L=0.0$)

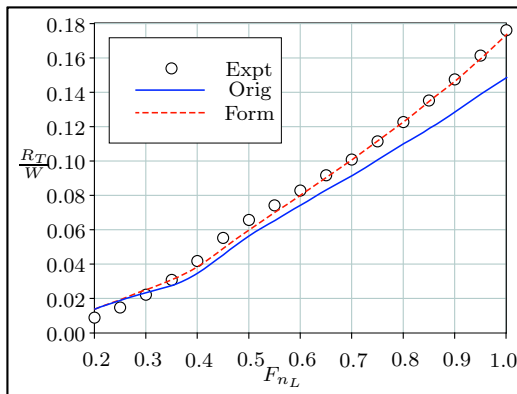


Figure D.17: Uni. of Southampton
Model 5a ($s/L=0.0$)

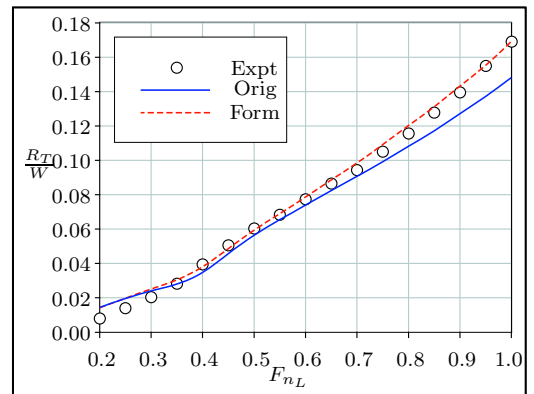


Figure D.18: Uni. of Southampton
Model 5b ($s/L=0.0$)

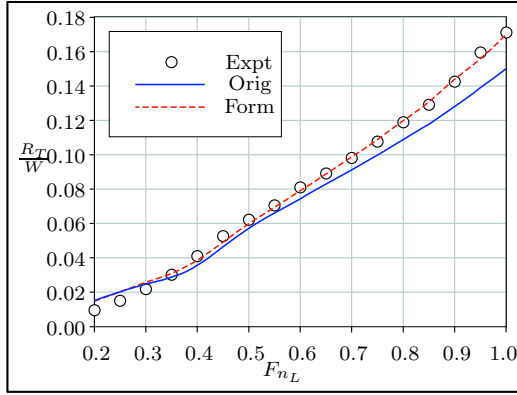


Figure D.19: Uni. of Southampton
Model 5c ($s/L=0.0$)

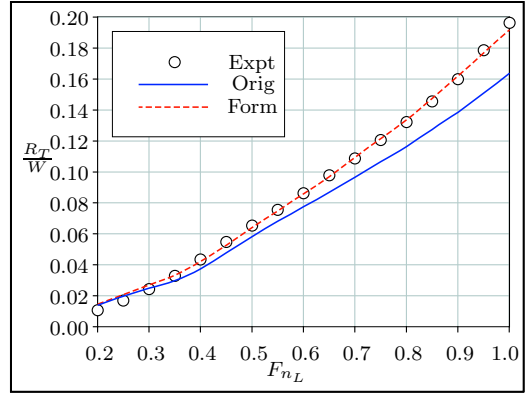


Figure D.20: Uni. of Southampton
Model 6a ($s/L=0.0$)

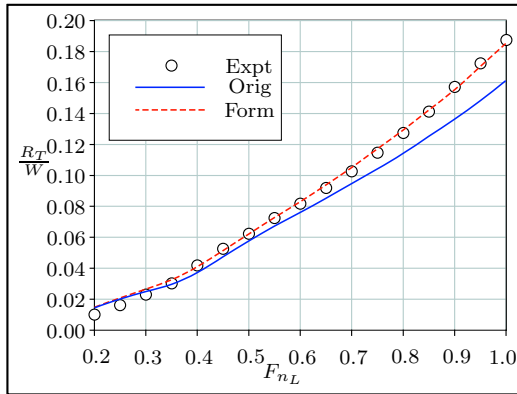


Figure D.21: Uni. of Southampton
Model 6b ($s/L=0.0$)

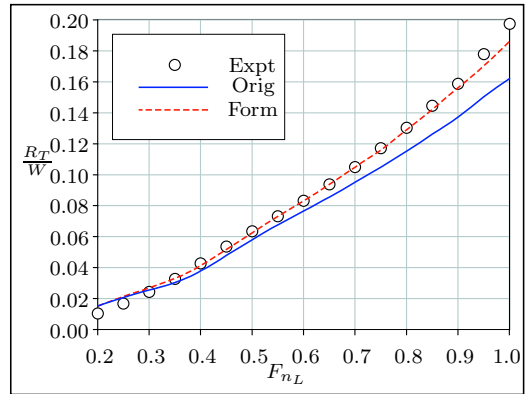


Figure D.22: Uni. of Southampton
Model 6c ($s/L=0.0$)

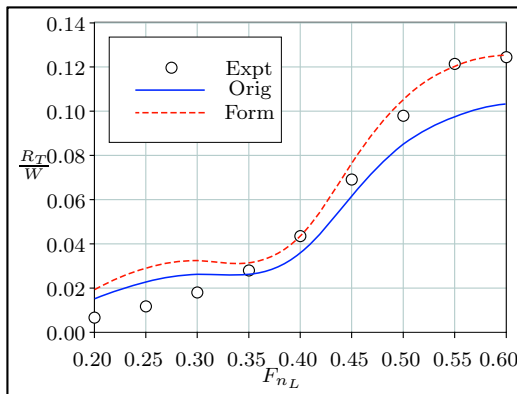


Figure D.23: Uni. of Southampton
Model 3b ($s/L=0.2$)

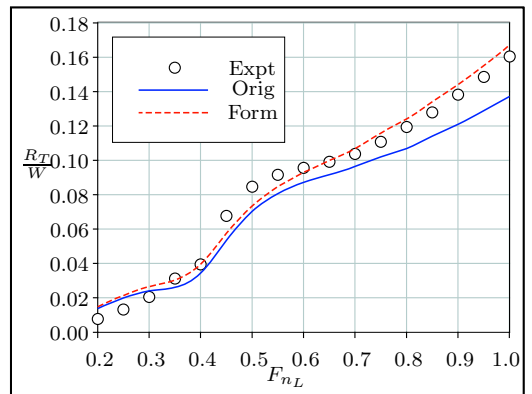


Figure D.24: Uni. of Southampton
Model 4a ($s/L=0.2$)

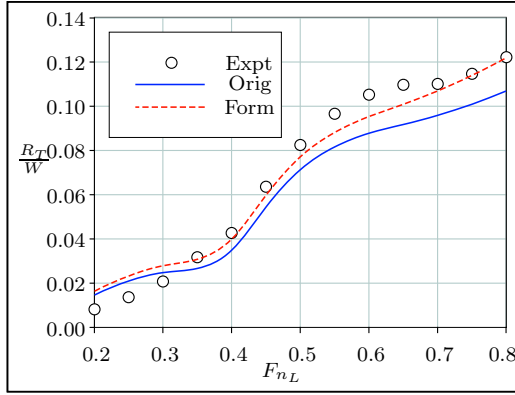


Figure D.25: Uni. of Southampton
Model 4b ($s/L=0.2$)

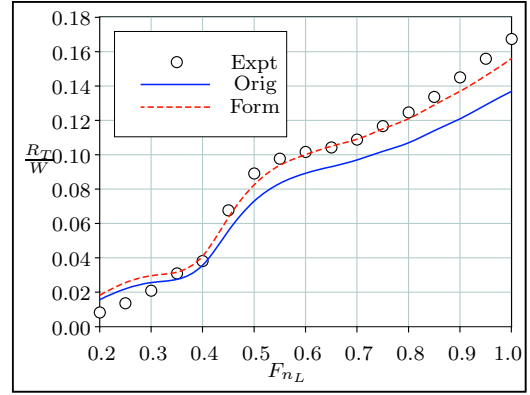


Figure D.26: Uni. of Southampton
Model 4c ($s/L=0.2$)

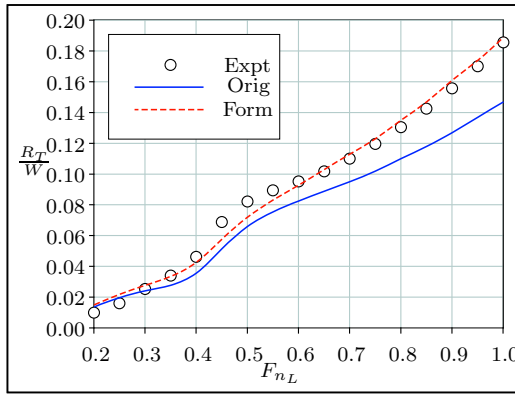


Figure D.27: Uni. of Southampton
Model 5a ($s/L=0.2$)

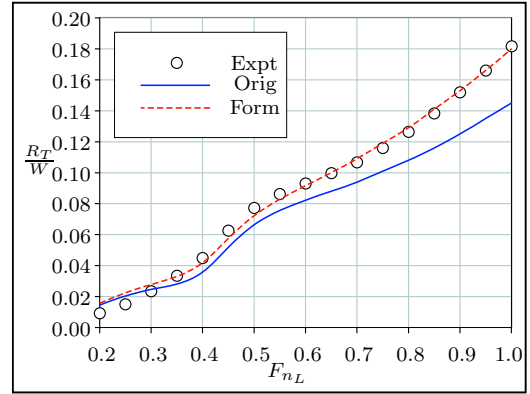


Figure D.28: Uni. of Southampton
Model 5b ($s/L=0.2$)

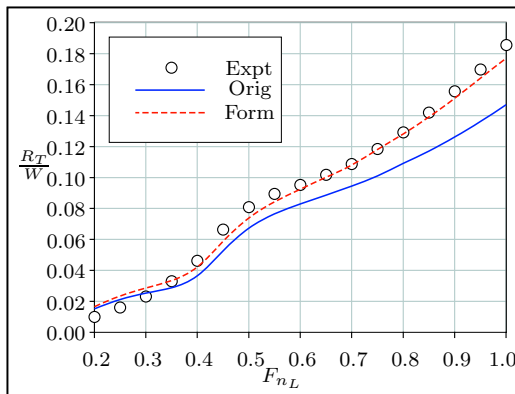


Figure D.29: Uni. of Southampton
Model 5c ($s/L=0.2$)

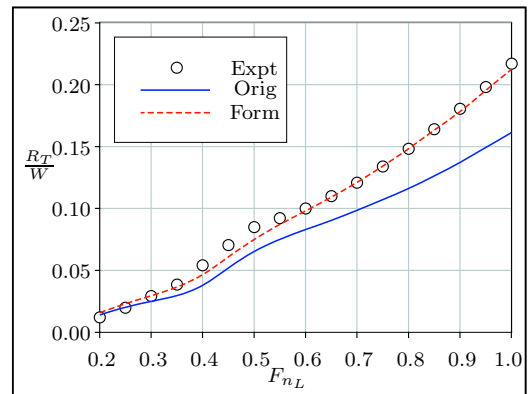


Figure D.30: Uni. of Southampton
Model 6a ($s/L=0.2$)

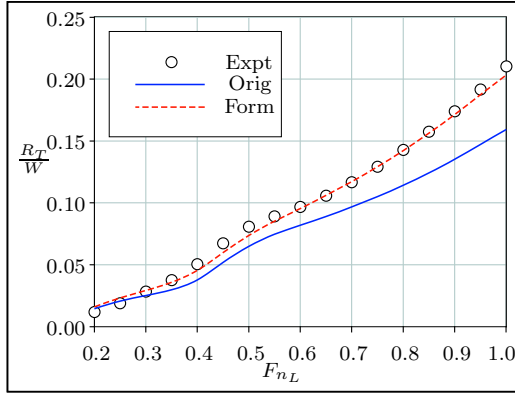


Figure D.31: Uni. of Southampton
Model 6b ($s/L=0.2$)

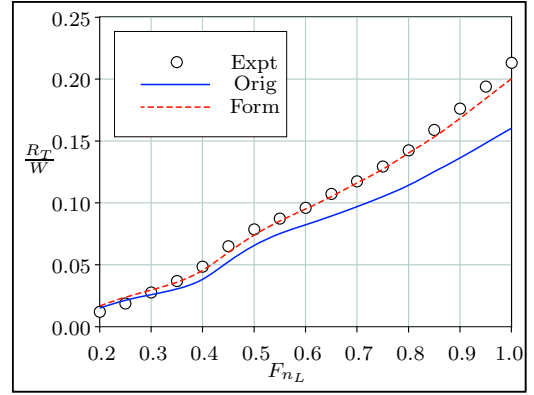


Figure D.32: Uni. of Southampton
Model 6c ($s/L=0.2$)

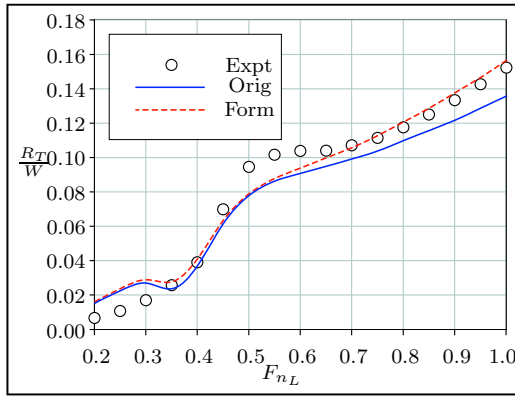


Figure D.33: Uni. of Southampton
Model 3b ($s/L=0.3$)

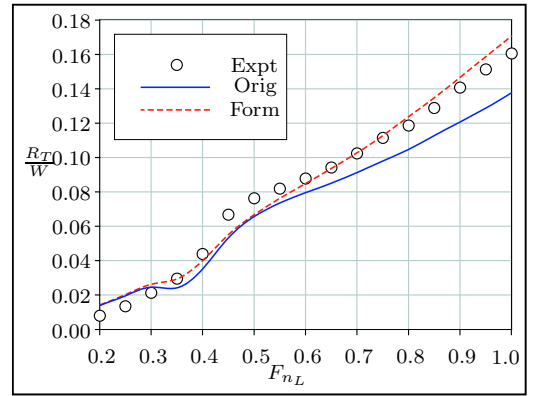


Figure D.34: Uni. of Southampton
Model 4a ($s/L=0.3$)

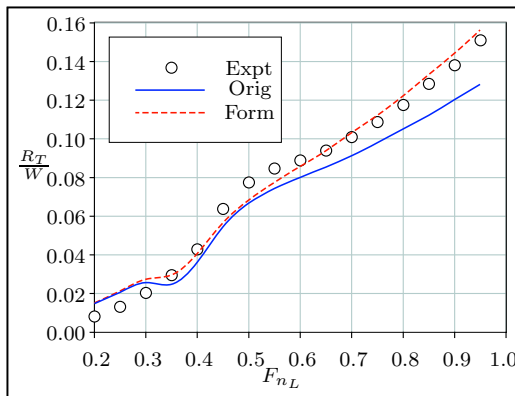


Figure D.35: Uni. of Southampton
Model 4b ($s/L=0.3$)

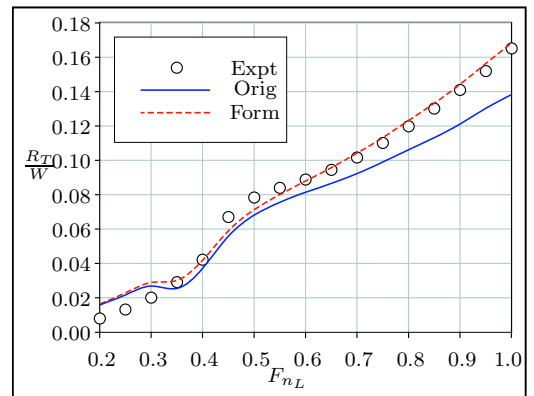


Figure D.36: Uni. of Southampton
Model 4c ($s/L=0.3$)

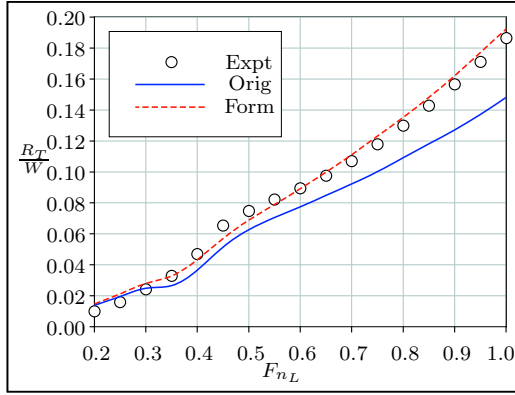


Figure D.37: Uni. of Southampton
Model 5a ($s/L=0.3$)

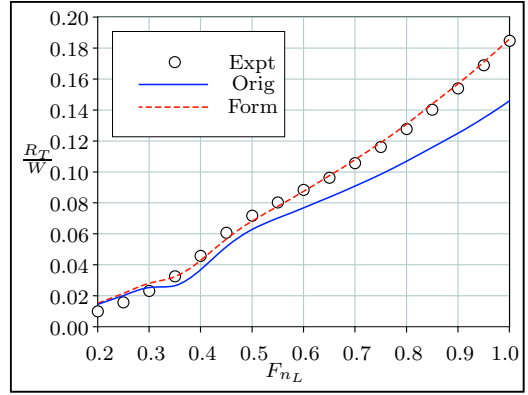


Figure D.38: Uni. of Southampton
Model 5b ($s/L=0.3$)

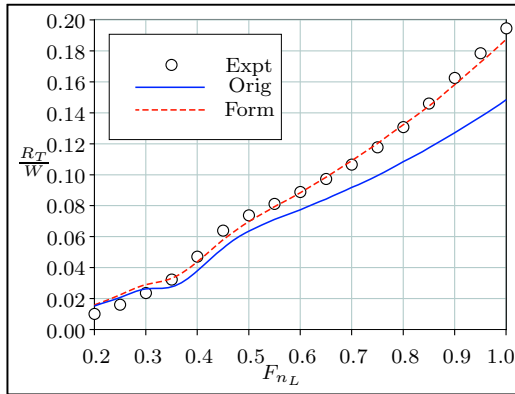


Figure D.39: Uni. of Southampton
Model 5c ($s/L=0.3$)

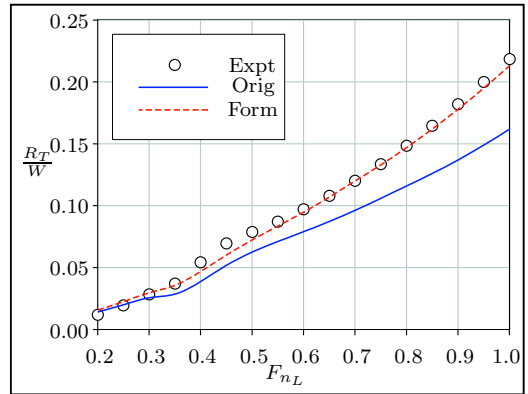


Figure D.40: Uni. of Southampton
Model 6a ($s/L=0.3$)

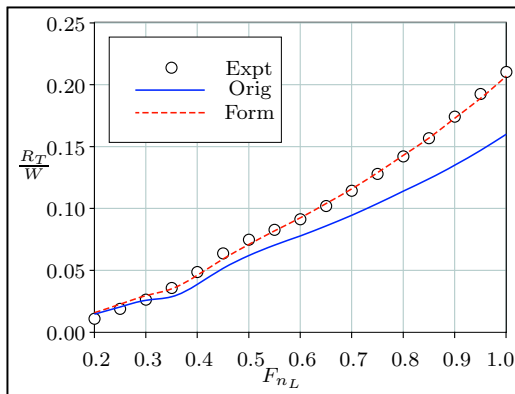


Figure D.41: Uni. of Southampton
Model 6b ($s/L=0.3$)

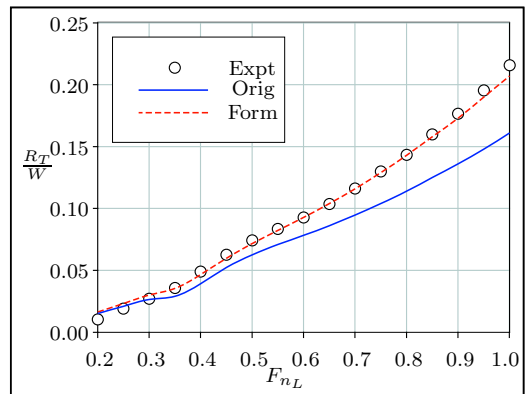


Figure D.42: Uni. of Southampton
Model 6c ($s/L=0.3$)

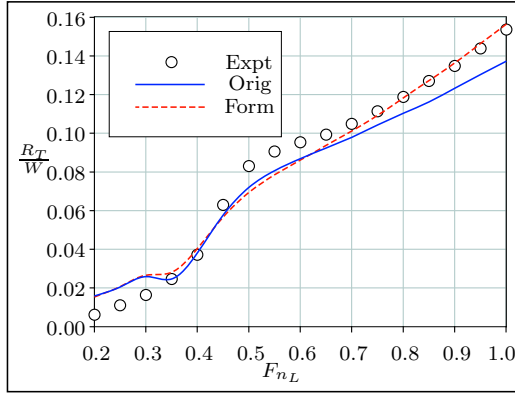


Figure D.43: Uni. of Southampton
Model 3b ($s/L=0.4$)

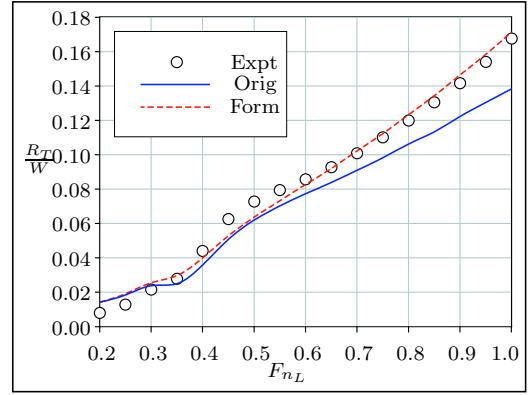


Figure D.44: Uni. of Southampton
Model 4a ($s/L=0.4$)

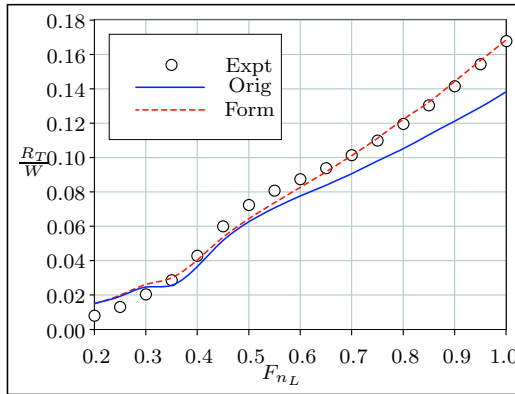


Figure D.45: Uni. of Southampton
Model 4b ($s/L=0.4$)

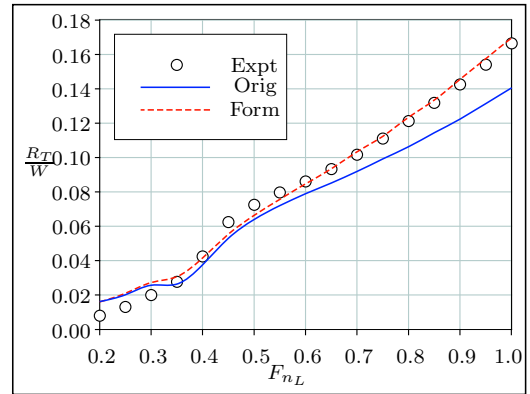


Figure D.46: Uni. of Southampton
Model 4c ($s/L=0.4$)

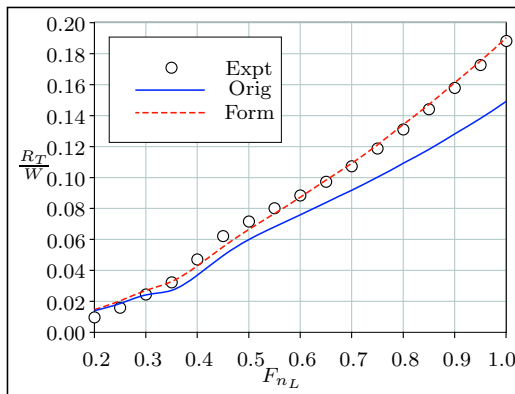


Figure D.47: Uni. of Southampton
Model 5a ($s/L=0.4$)

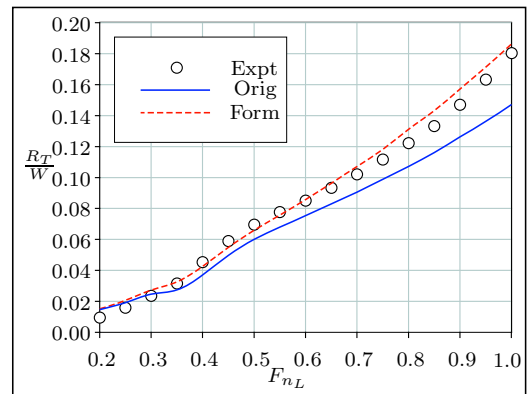


Figure D.48: Uni. of Southampton
Model 5b ($s/L=0.4$)

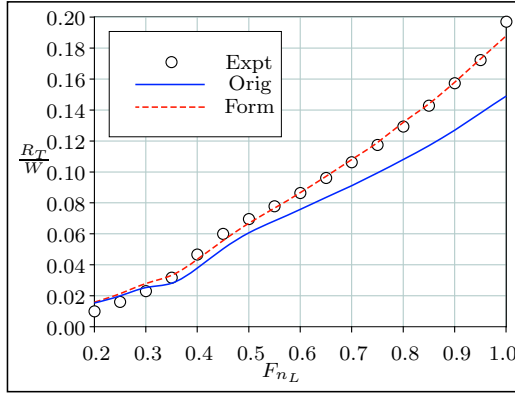


Figure D.49: Uni. of Southampton
Model 5c ($s/L=0.4$)

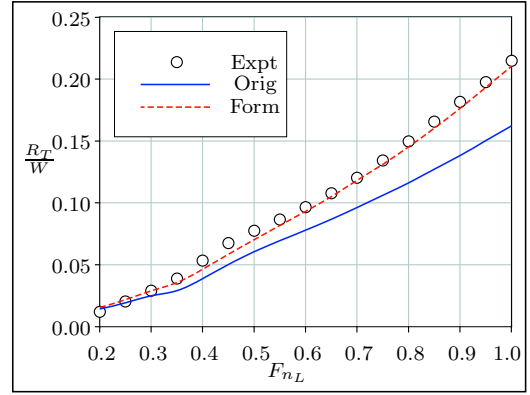


Figure D.50: Uni. of Southampton
Model 6a ($s/L=0.4$)

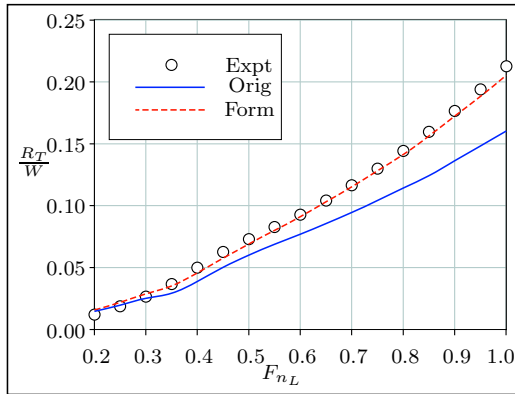


Figure D.51: Uni. of Southampton
Model 6b ($s/L=0.4$)

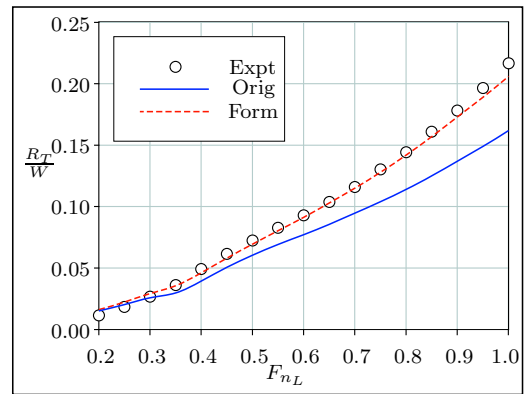


Figure D.52: Uni. of Southampton
Model 6c ($s/L=0.4$)

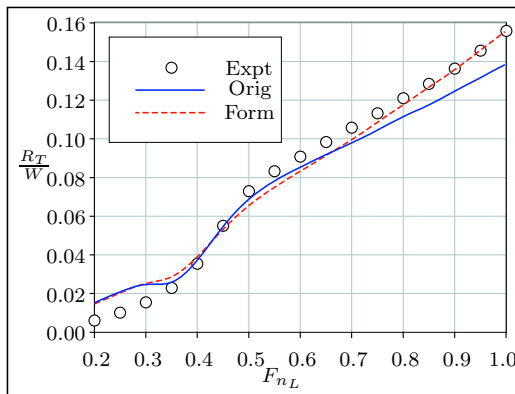


Figure D.53: Uni. of Southampton
Model 3b ($s/L=0.5$)

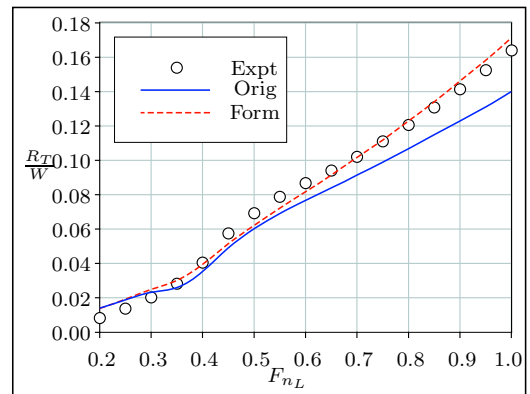


Figure D.54: Uni. of Southampton
Model 4a ($s/L=0.5$)

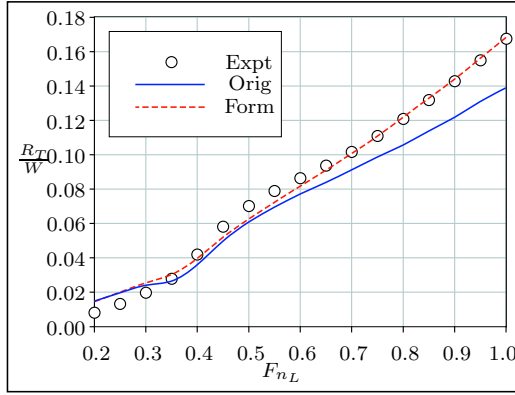


Figure D.55: Uni. of Southampton
Model 4b ($s/L=0.5$)

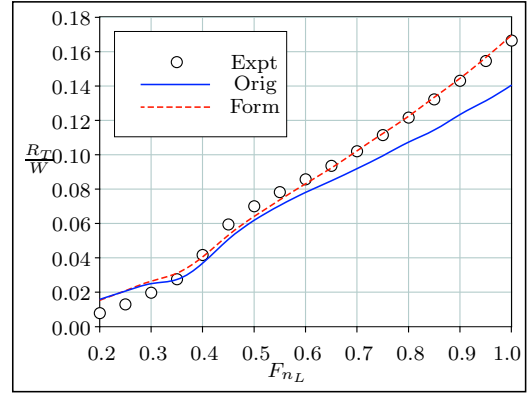


Figure D.56: Uni. of Southampton
Model 4c ($s/L=0.5$)

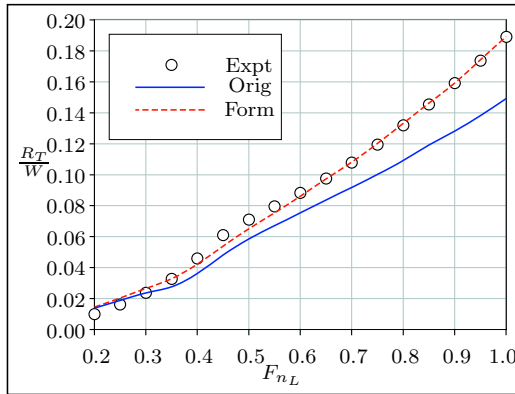


Figure D.57: Uni. of Southampton
Model 5a ($s/L=0.5$)

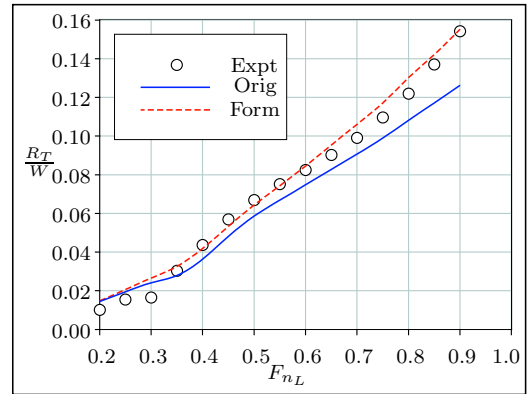


Figure D.58: Uni. of Southampton
Model 5b ($s/L=0.5$)

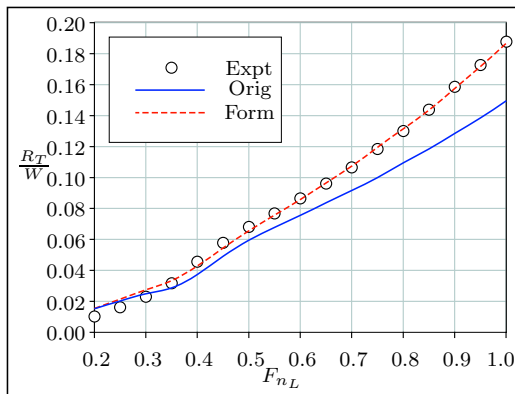


Figure D.59: Uni. of Southampton
Model 5c ($s/L=0.5$)

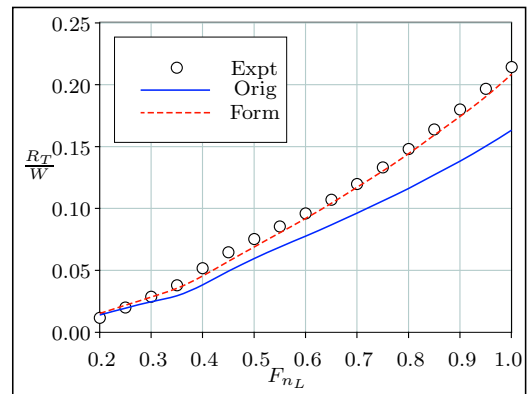


Figure D.60: Uni. of Southampton
Model 6a ($s/L=0.5$)

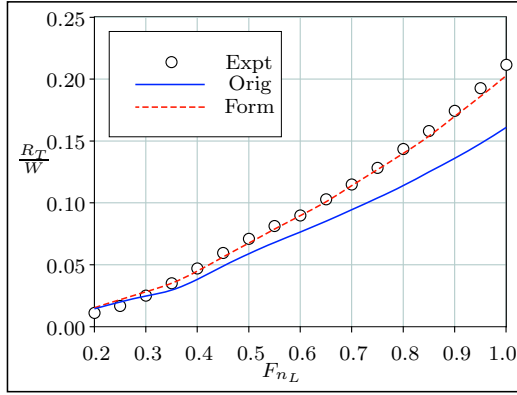


Figure D.61: Uni. of Southampton Model 6b ($s/L=0.5$)

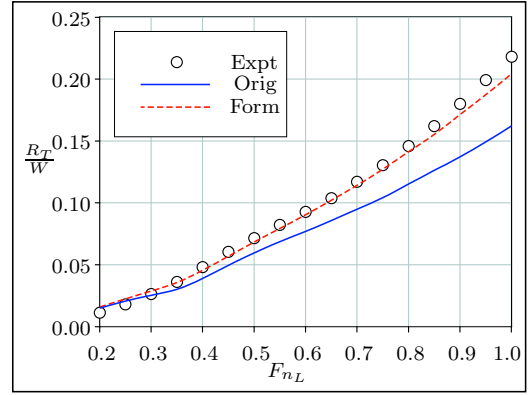


Figure D.62: Uni. of Southampton Model 6c ($s/L=0.5$)

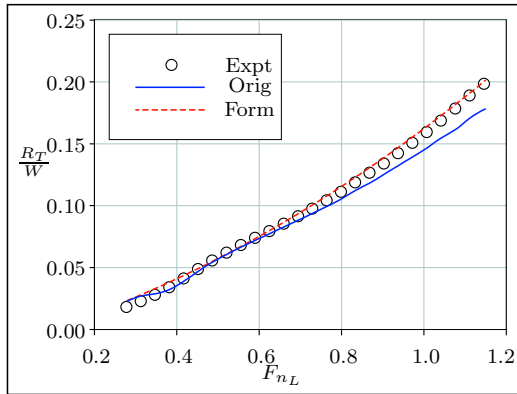


Figure D.63: NPL Model 50Z

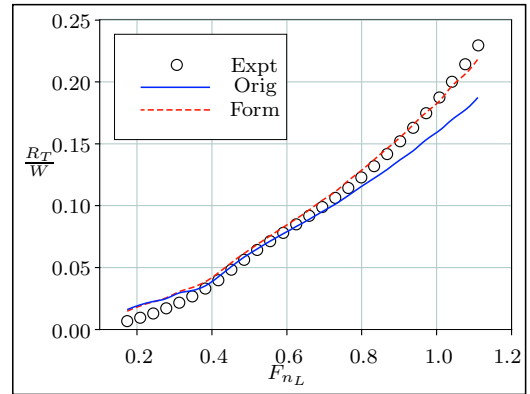


Figure D.64: NPL Model 50A

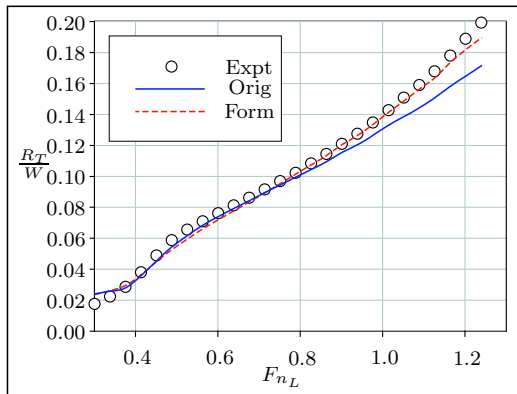


Figure D.65: NPL Model 80Z

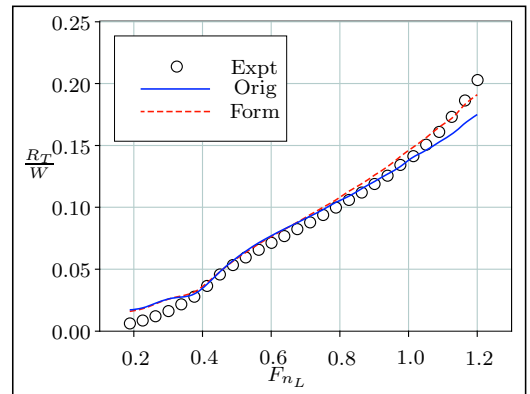


Figure D.66: NPL Model 80A

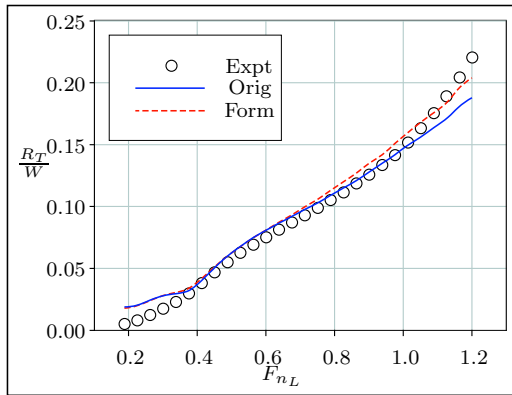


Figure D.67: NPL Model 80B

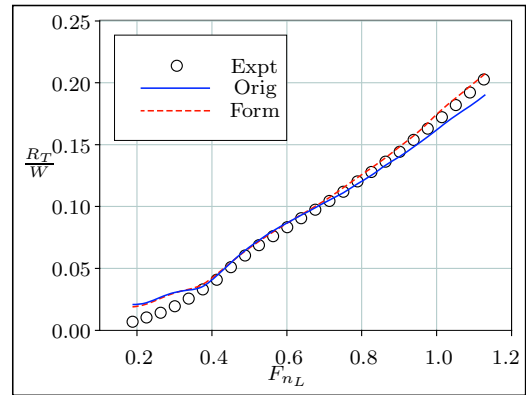


Figure D.68: NPL Model 80C

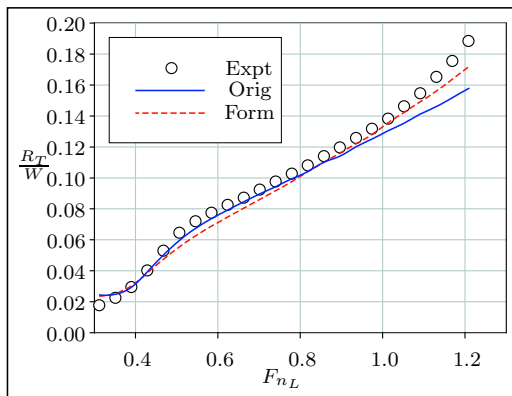


Figure D.69: NPL Model 100Z

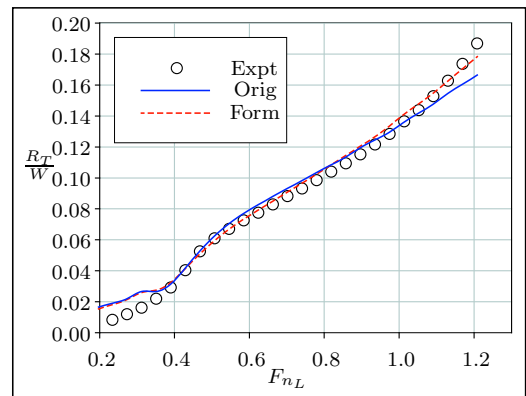


Figure D.70: NPL Model 100A

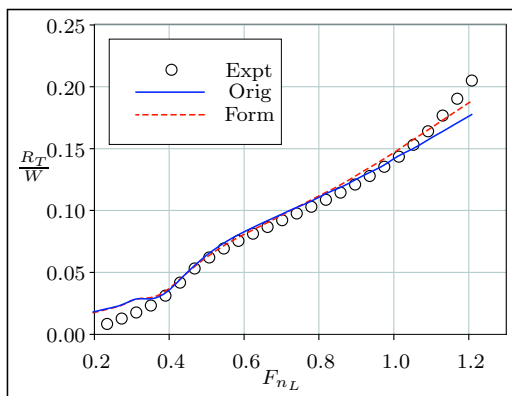


Figure D.71: NPL Model 100B

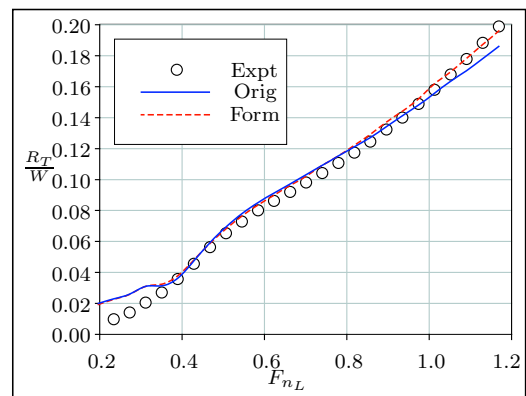


Figure D.72: NPL Model 100C

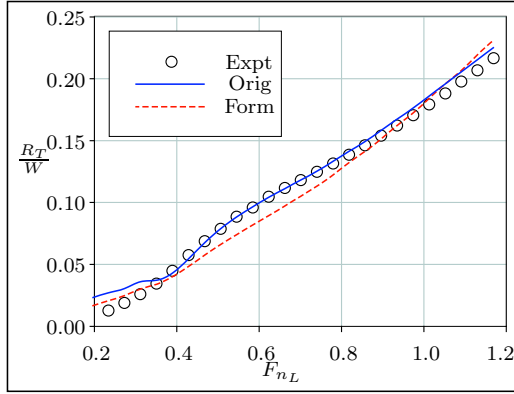


Figure D.73: NPL Model 100D

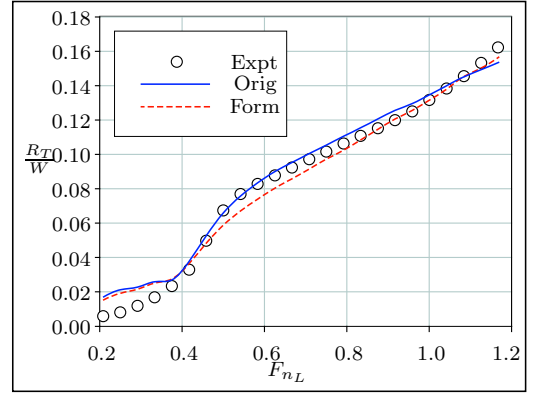


Figure D.74: NPL Model 150A

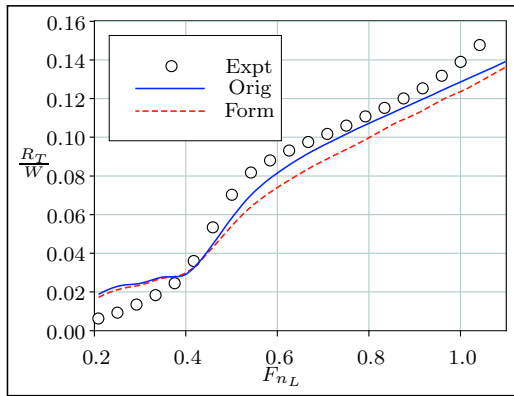


Figure D.75: NPL Model 150B

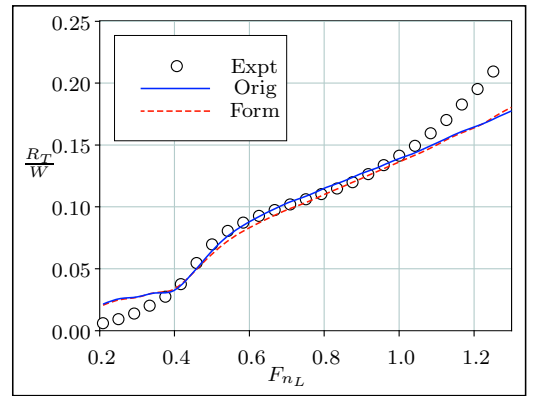


Figure D.76: NPL Model 150C

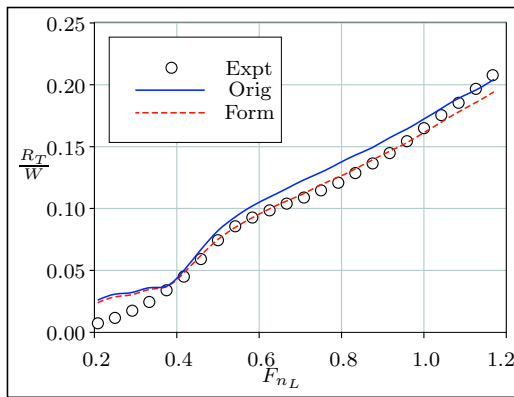


Figure D.77: NPL Model 150D

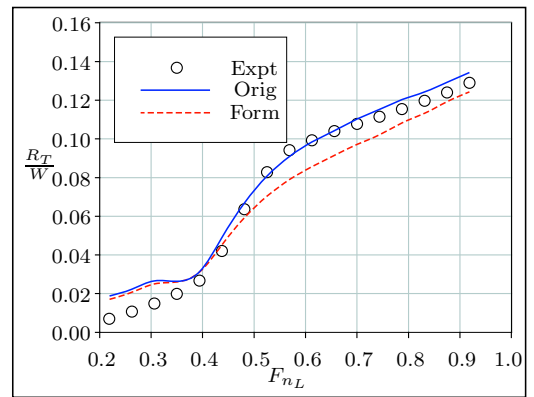


Figure D.78: NPL Model 200B

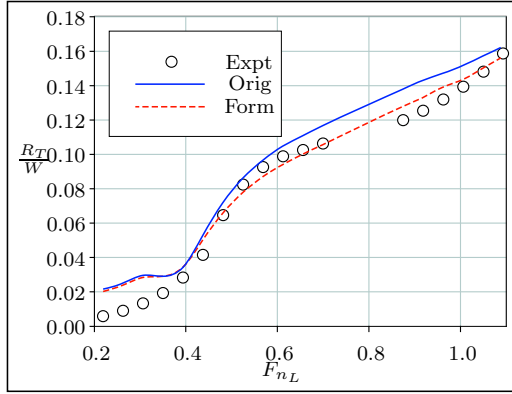


Figure D.79: NPL Model 200C

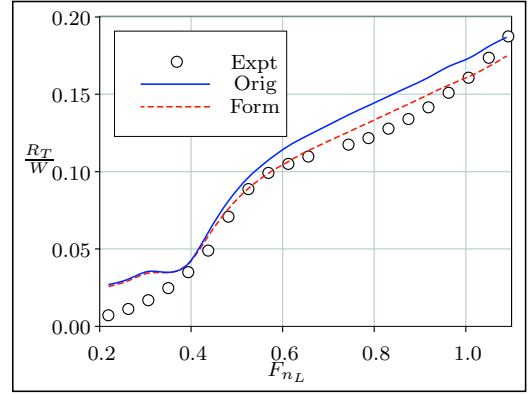


Figure D.80: NPL Model 200D

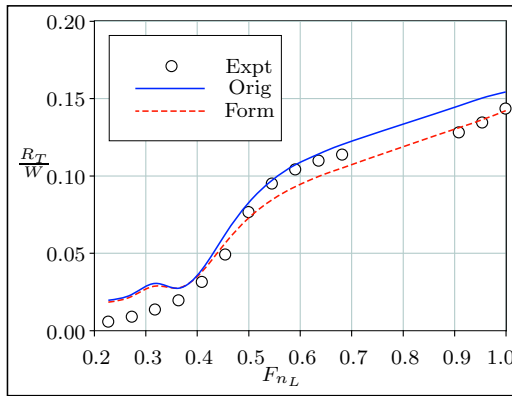


Figure D.81: NPL Model 250C

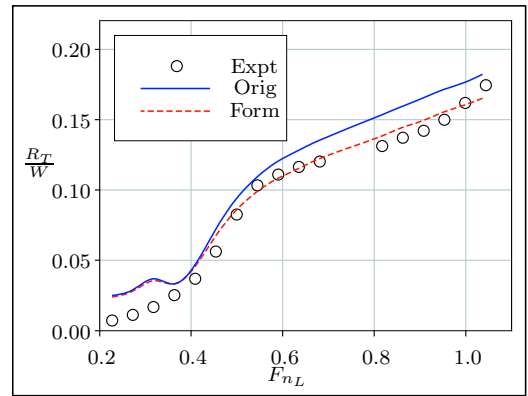


Figure D.82: NPL Model 250D

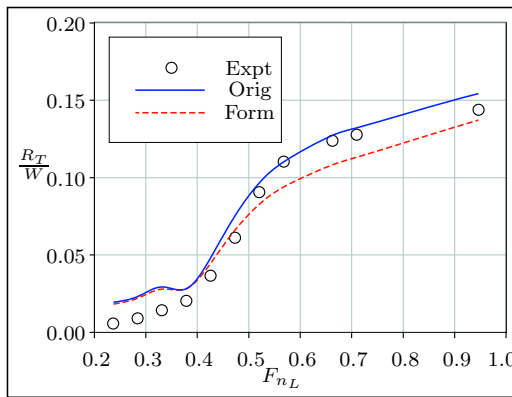


Figure D.83: NPL Model 320C

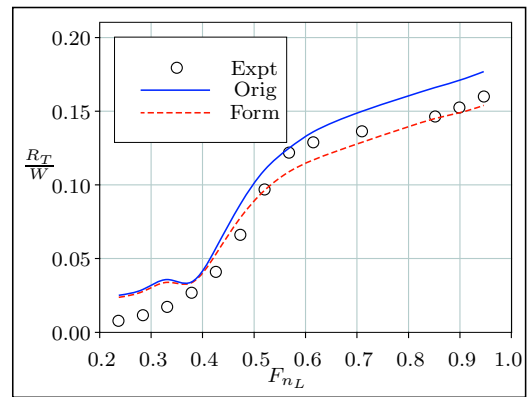


Figure D.84: NPL Model 320D

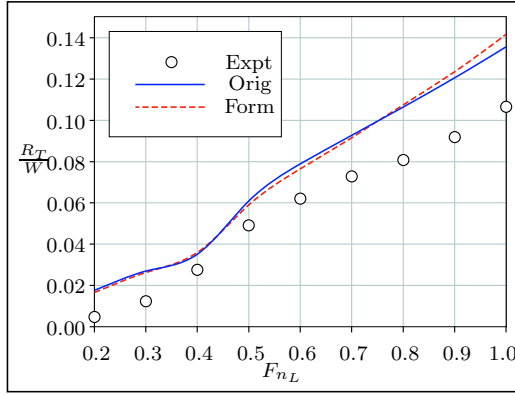


Figure D.85: NPL Model 80A
(110% of Δ_{DWL})

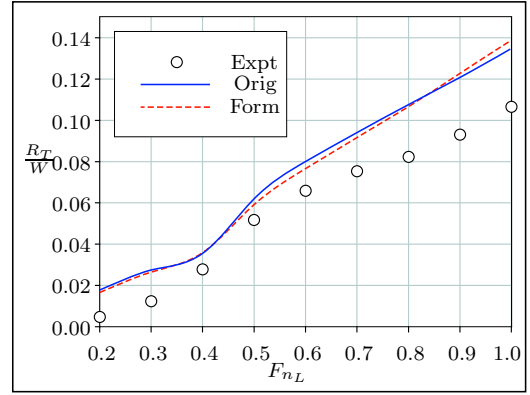


Figure D.86: NPL Model 80A
(120% of Δ_{DWL})

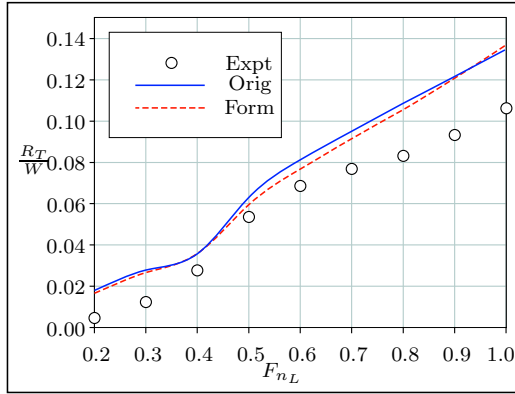


Figure D.87: NPL Model 80A
(130% of Δ_{DWL})

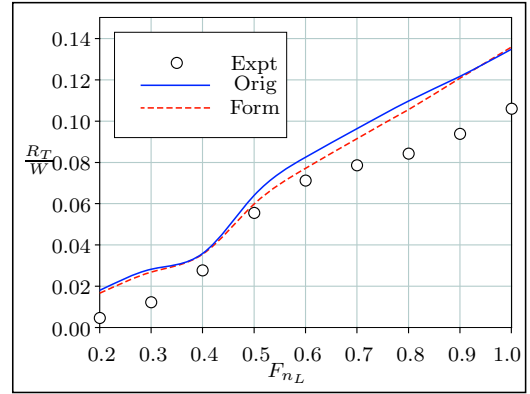


Figure D.88: NPL Model 80A
(140% of Δ_{DWL})

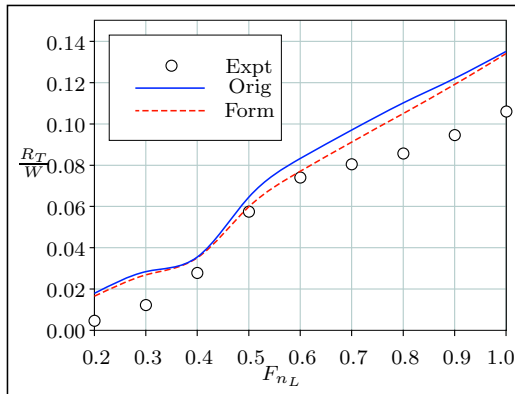


Figure D.89: NPL Model 80A
(150% of Δ_{DWL})

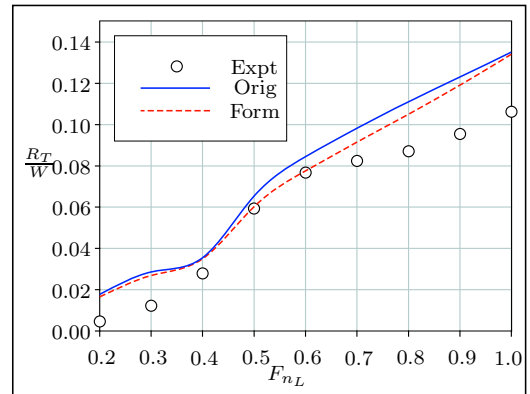


Figure D.90: NPL Model 80A
(160% of Δ_{DWL})

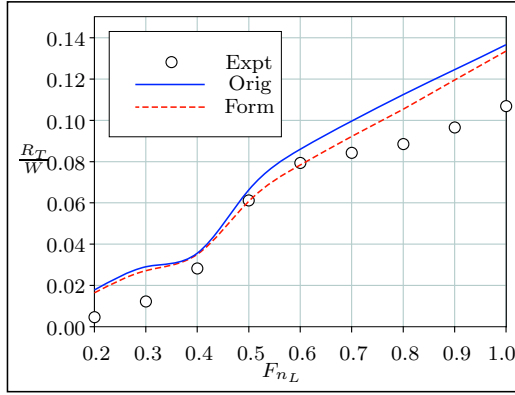


Figure D.91: NPL Model 80A
(170% of Δ_{DWL})

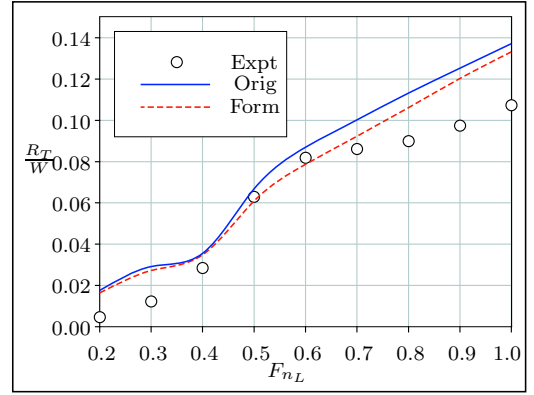


Figure D.92: NPL Model 80A
(180% of Δ_{DWL})

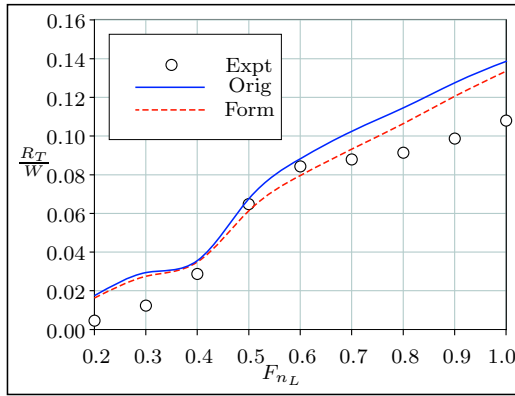


Figure D.93: NPL Model 80A
(190% of Δ_{DWL})

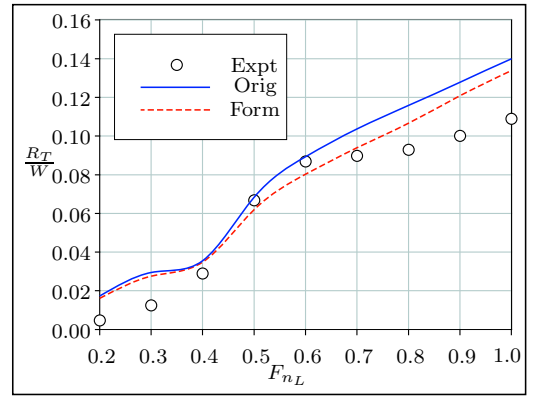


Figure D.94: NPL Model 80A
(200% of Δ_{DWL})

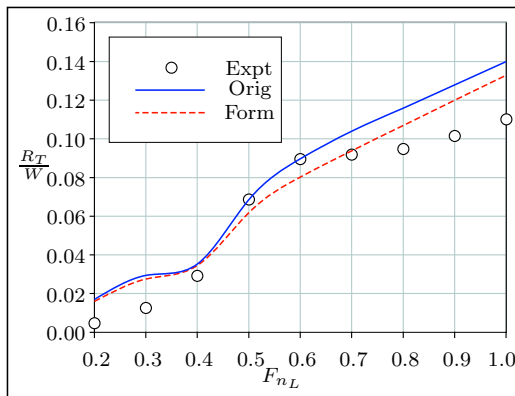


Figure D.95: NPL Model 80A
(210% of Δ_{DWL})

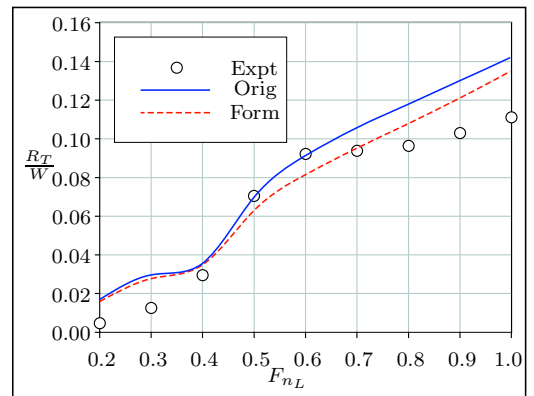


Figure D.96: NPL Model 80A
(220% of Δ_{DWL})

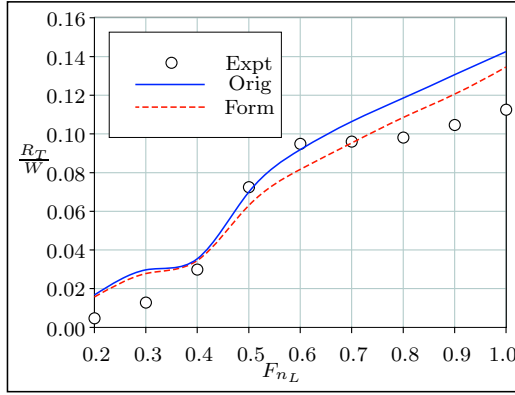


Figure D.97: NPL Model 80A
(230% of Δ_{DWL})

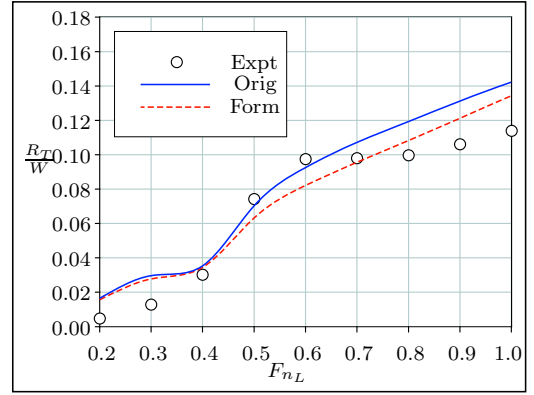


Figure D.98: NPL Model 80A
(240% of Δ_{DWL})

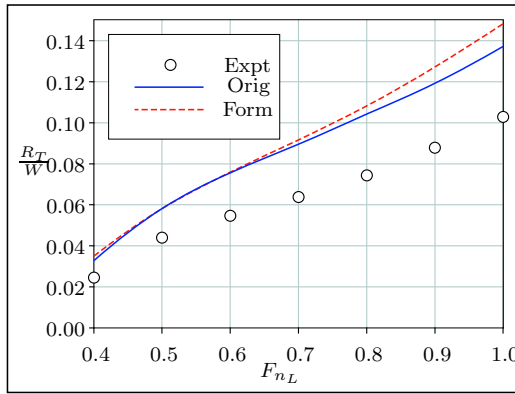


Figure D.99: NPL Model 100A
(80% of Δ_{DWL})

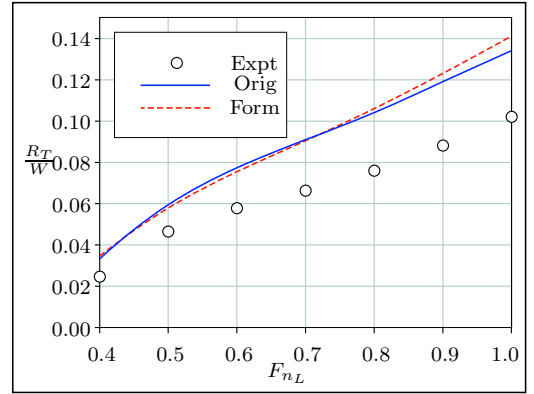


Figure D.100: NPL Model 100A
(90% of Δ_{DWL})

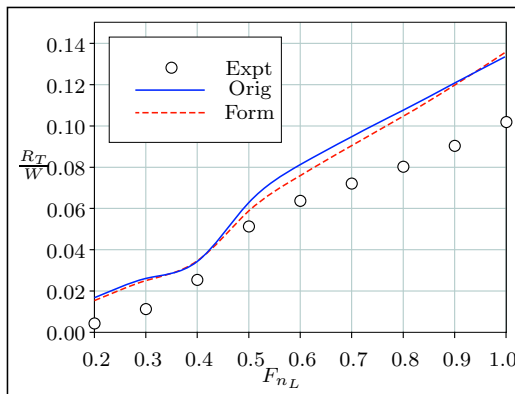


Figure D.101: NPL Model 100A
(110% of Δ_{DWL})

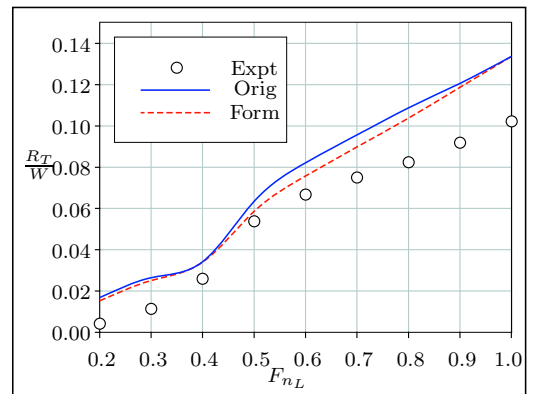


Figure D.102: NPL Model 100A
(120% of Δ_{DWL})

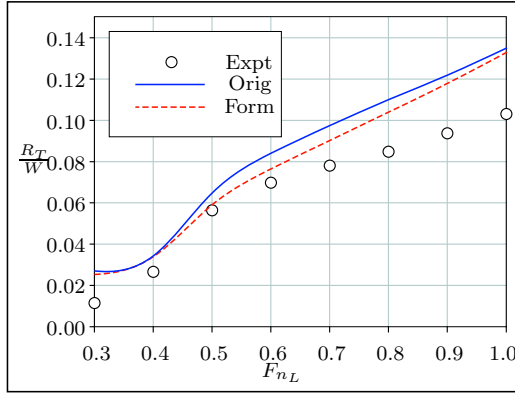


Figure D.103: NPL Model 100A
(130% of Δ_{DWL})

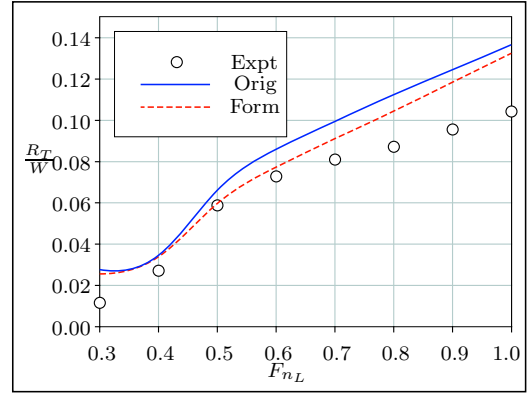


Figure D.104: NPL Model 100A
(140% of Δ_{DWL})

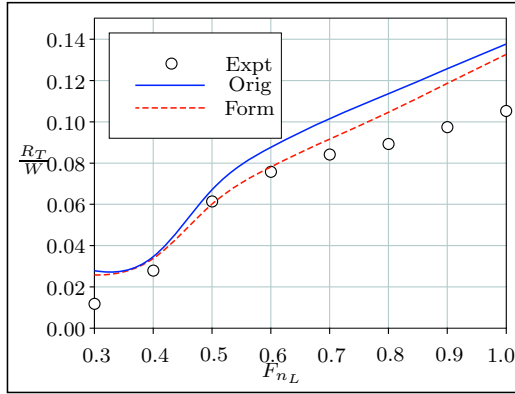


Figure D.105: NPL Model 100A
(150% of Δ_{DWL})

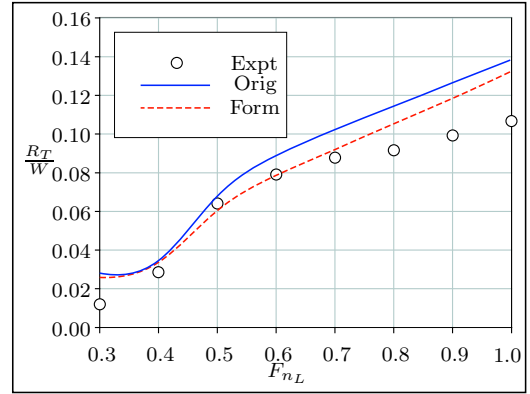


Figure D.106: NPL Model 100A
(160% of Δ_{DWL})

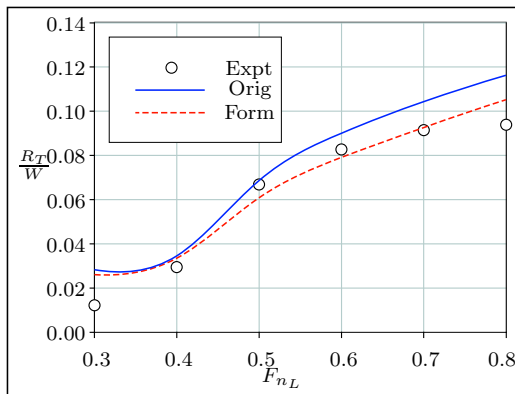


Figure D.107: NPL Model 100A
(170% of Δ_{DWL})

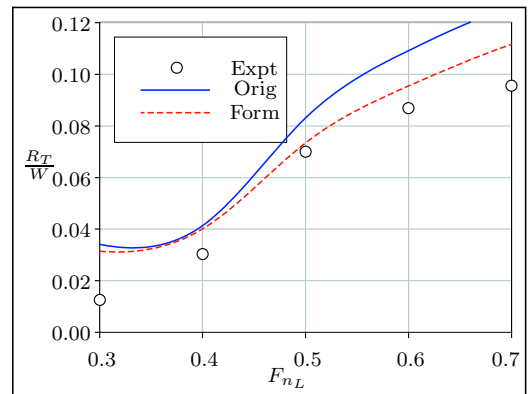


Figure D.108: NPL Model 100A
(180% of Δ_{DWL})

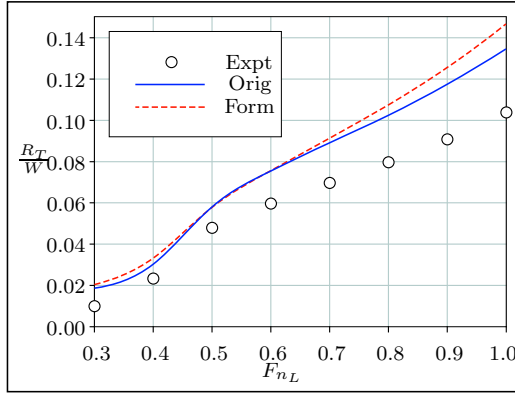


Figure D.109: NPL Model 150A
(60% of Δ_{DWL})

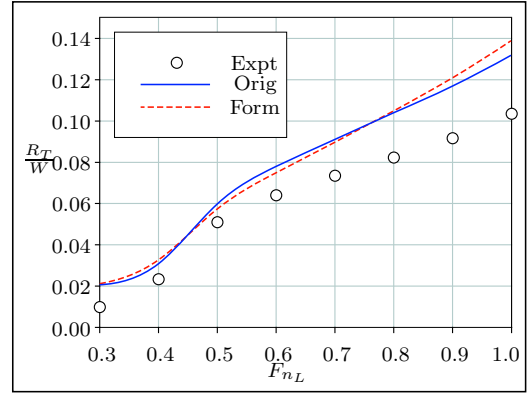


Figure D.110: NPL Model 150A
(70% of Δ_{DWL})

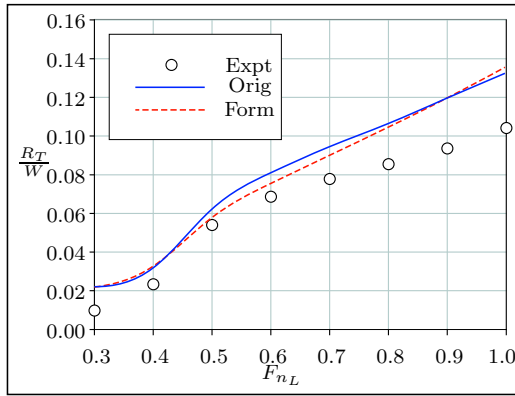


Figure D.111: NPL Model 150A
(80% of Δ_{DWL})

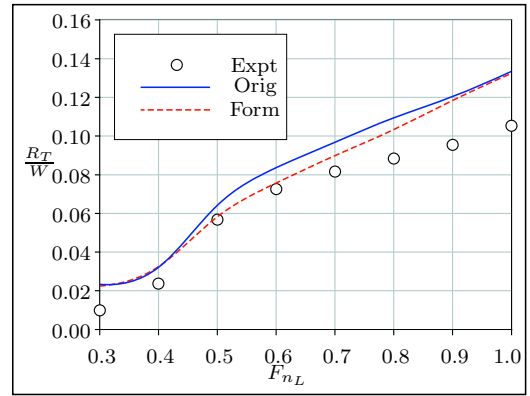


Figure D.112: NPL Model 150A
(90% of Δ_{DWL})

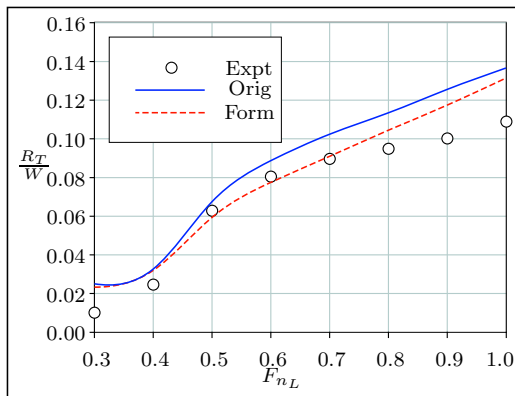


Figure D.113: NPL Model 150A
(110% of Δ_{DWL})

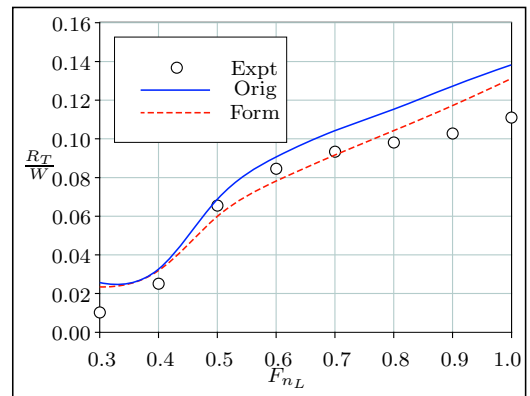


Figure D.114: NPL Model 150A
(120% of Δ_{DWL})

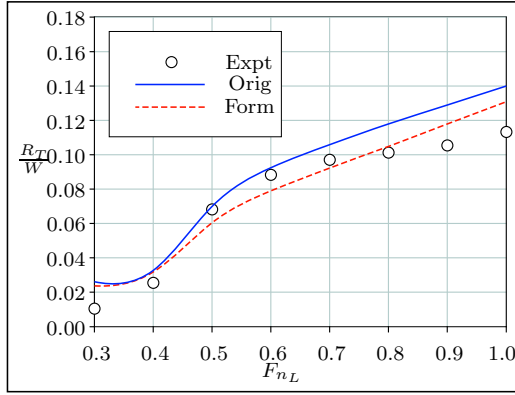


Figure D.115: NPL Model 150A
(130% of Δ_{DWL})

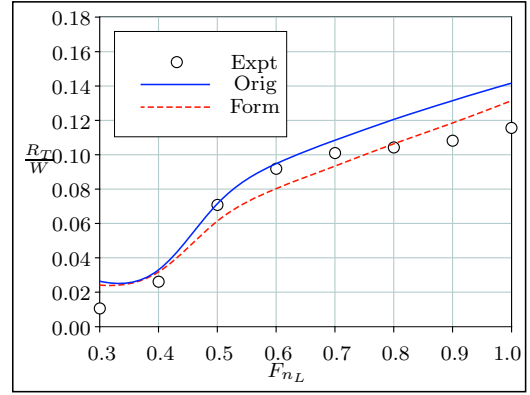


Figure D.116: NPL Model 150A
(140% of Δ_{DWL})

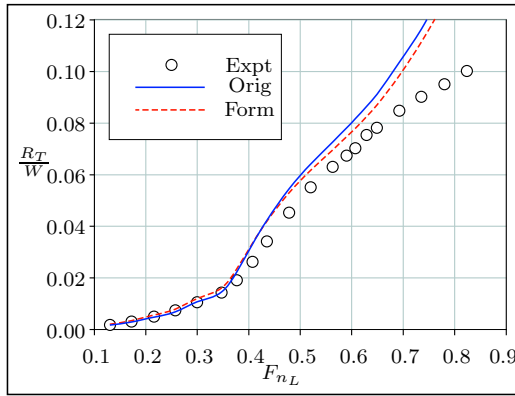


Figure D.117: D-Series Model D1 at
Draft 1

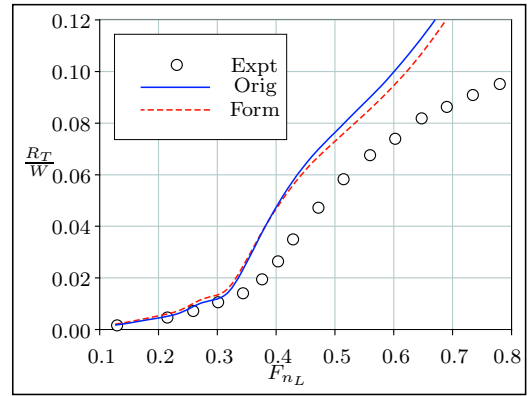


Figure D.118: D-Series Model D2 at
Draft 1

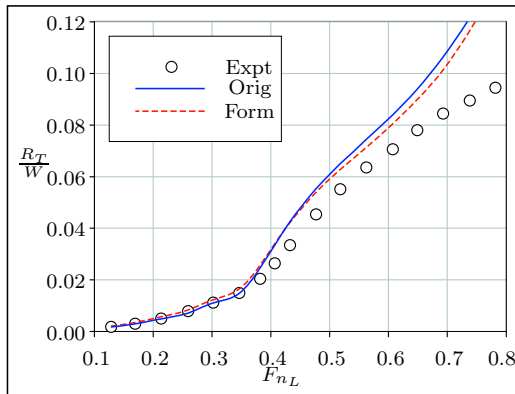


Figure D.119: D-Series Model D3 at
Draft 1

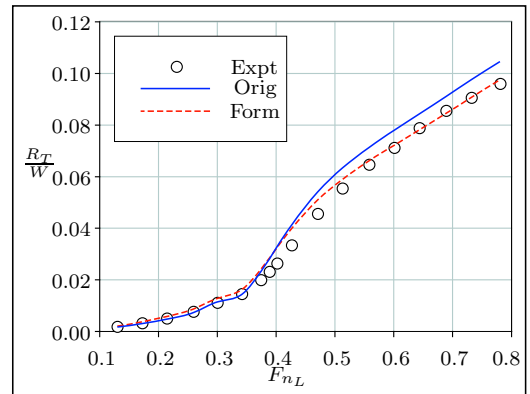


Figure D.120: D-Series Model D4 at
Draft 1

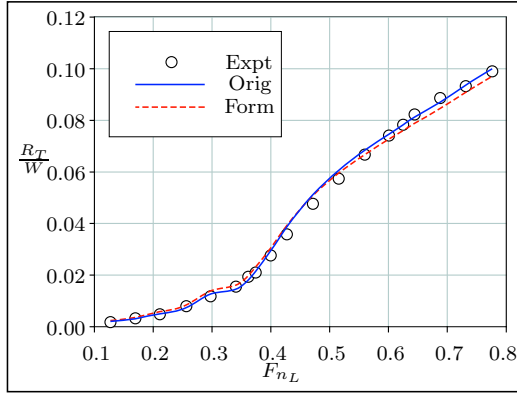


Figure D.121: D-Series Model D5 at Draft 1

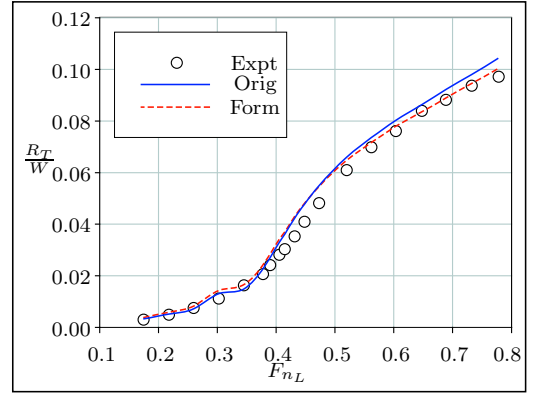


Figure D.122: D-Series Model D6 at Draft 1

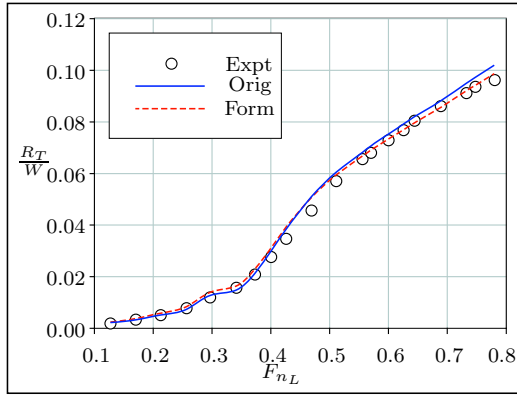


Figure D.123: D-Series Model D7 at Draft 1

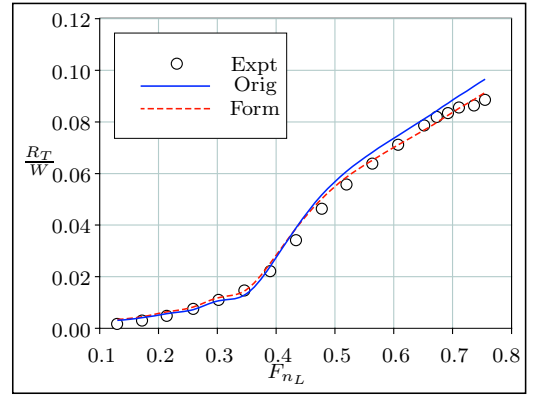


Figure D.124: D-Series Model D1 at Draft 2

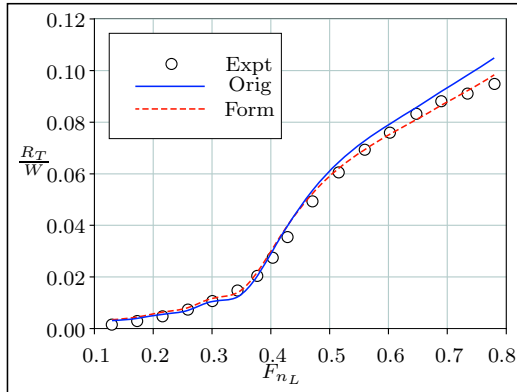


Figure D.125: D-Series Model D2 at Draft 2

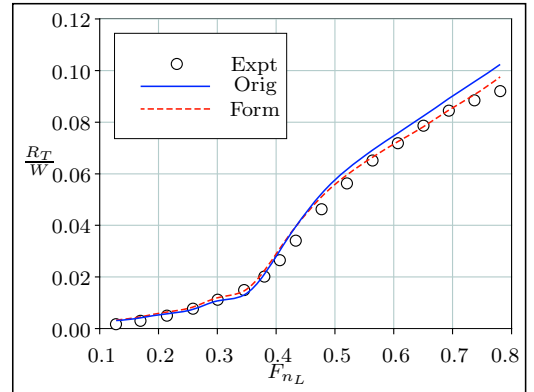


Figure D.126: D-Series Model D3 at Draft 2

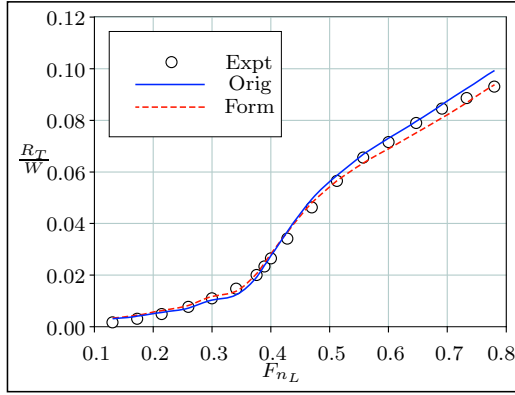


Figure D.127: D-Series Model D4 at Draft 2

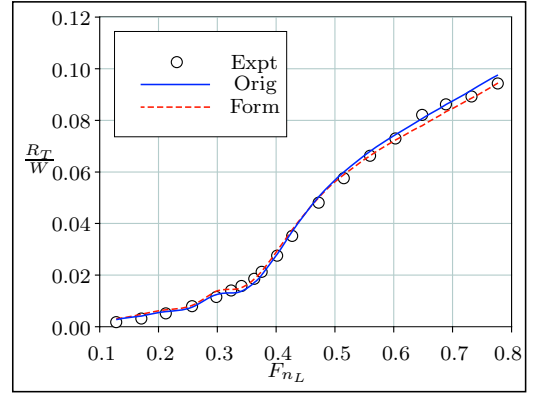


Figure D.128: D-Series Model D5 at Draft 2

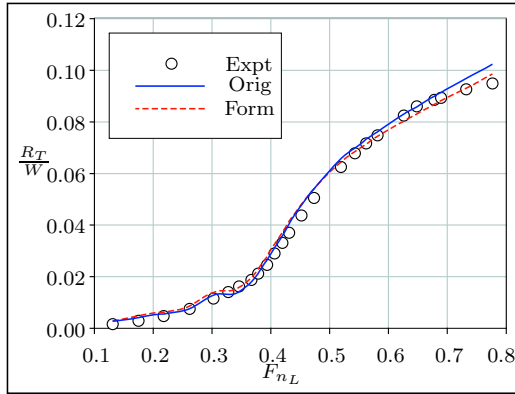


Figure D.129: D-Series Model D6 at Draft 2

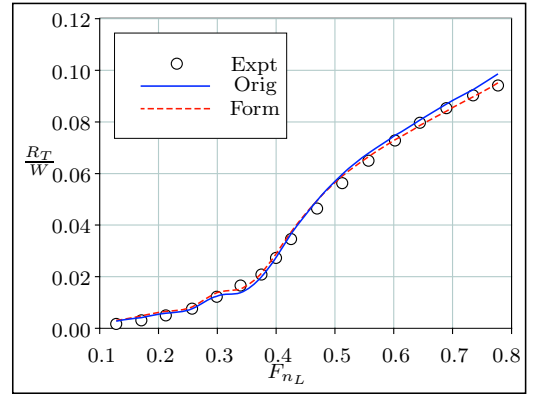


Figure D.130: D-Series Model D7 at Draft 2

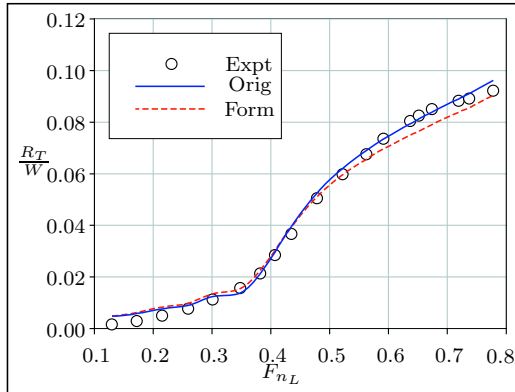


Figure D.131: D-Series Model D1 at Draft 3

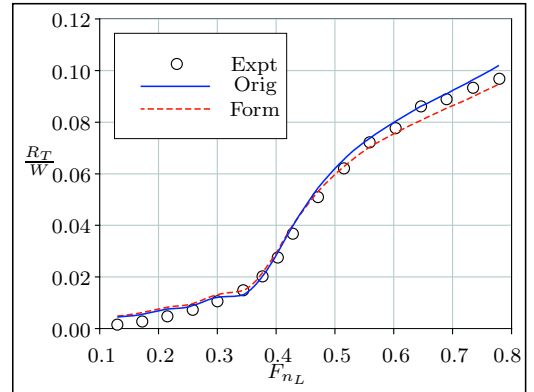


Figure D.132: D-Series Model D2 at Draft 3

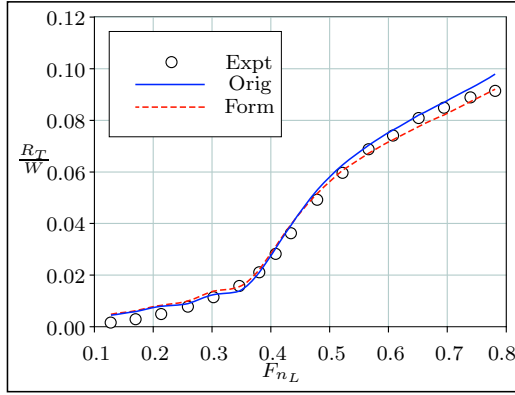


Figure D.133: D-Series Model D3 at Draft 3

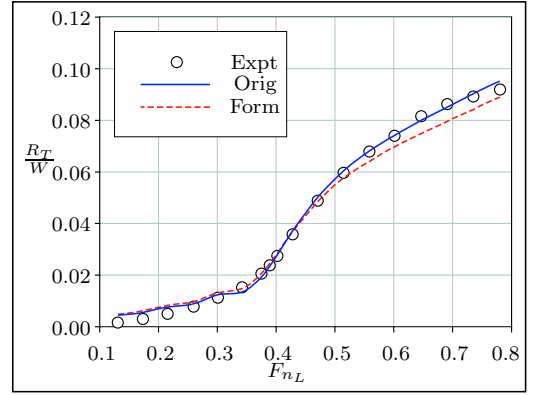


Figure D.134: D-Series Model D4 at Draft 3

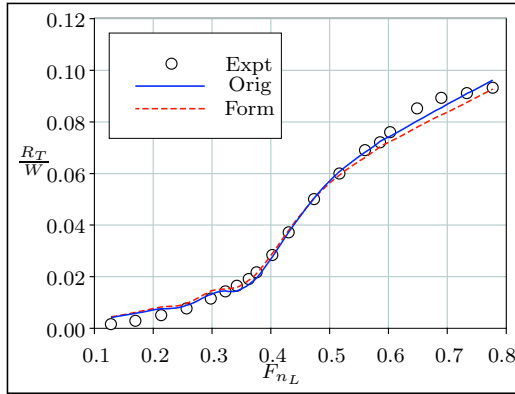


Figure D.135: D-Series Model D5 at Draft 3

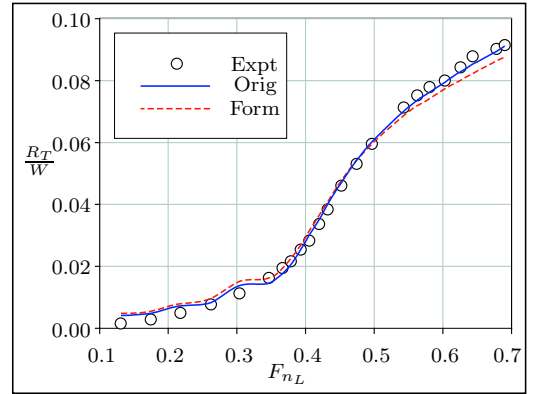


Figure D.136: D-Series Model D6 at Draft 3

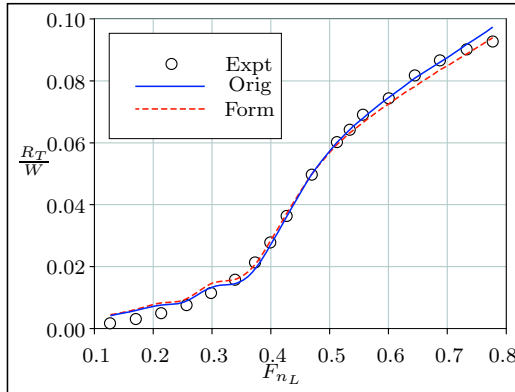


Figure D.137: D-Series Model D7 at Draft 3

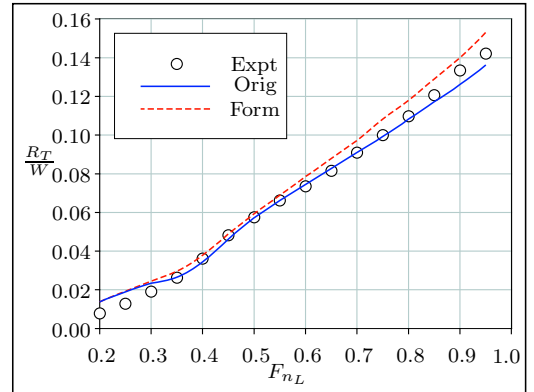


Figure D.138: Uni. of Southampton Model 5d ($s/L=0.0$)

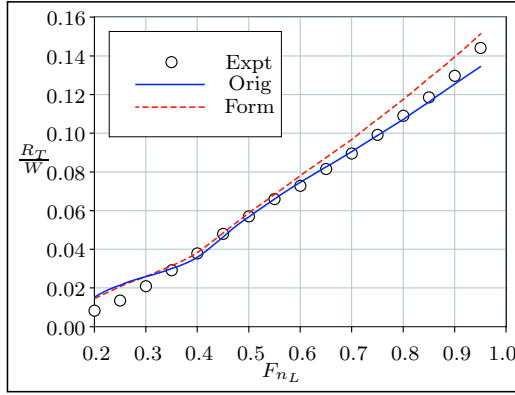


Figure D.139: Uni. of Southampton
Model 5e ($s/L=0.0$)

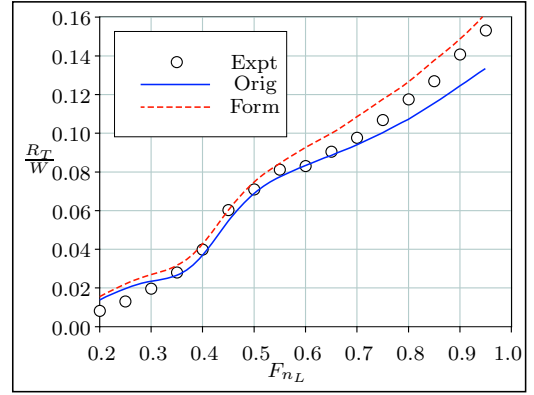


Figure D.140: Uni. of Southampton
Model 5d ($s/L=0.2$)

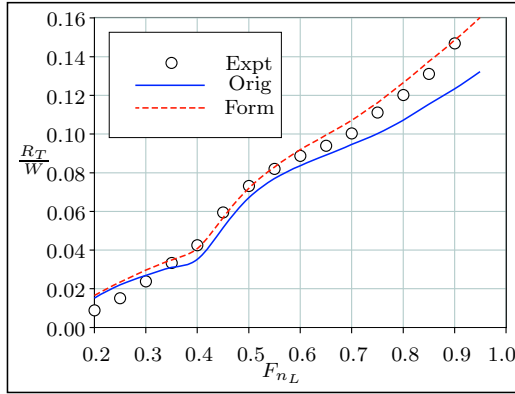


Figure D.141: Uni. of Southampton
Model 5e ($s/L=0.2$)

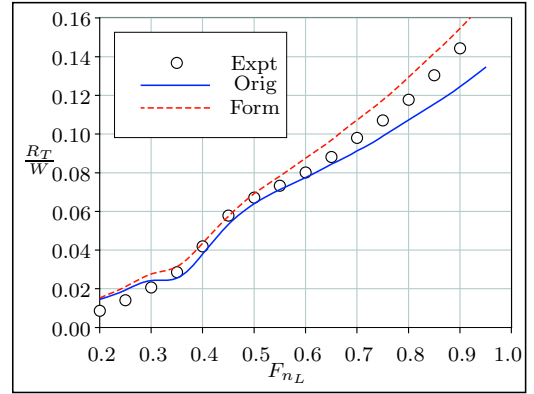


Figure D.142: Uni. of Southampton
Model 5d ($s/L=0.3$)

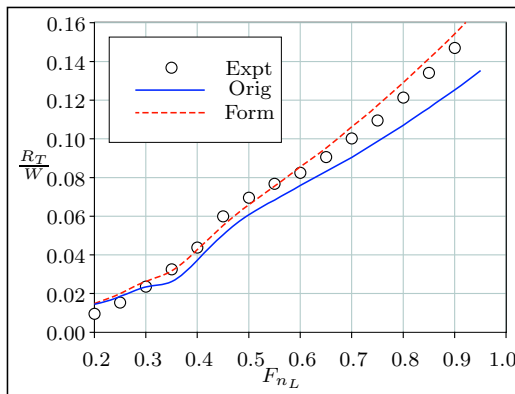


Figure D.143: Uni. of Southampton
Model 5e ($s/L=0.3$)

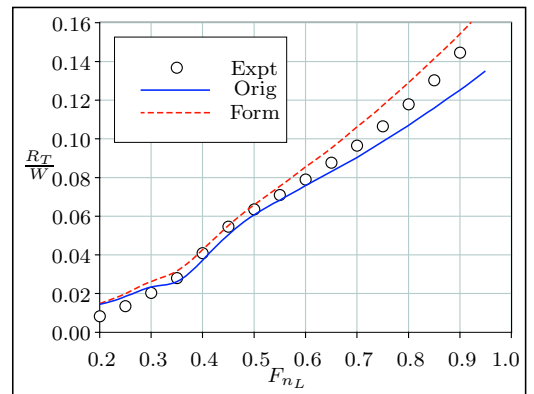


Figure D.144: Uni. of Southampton
Model 5d ($s/L=0.4$)

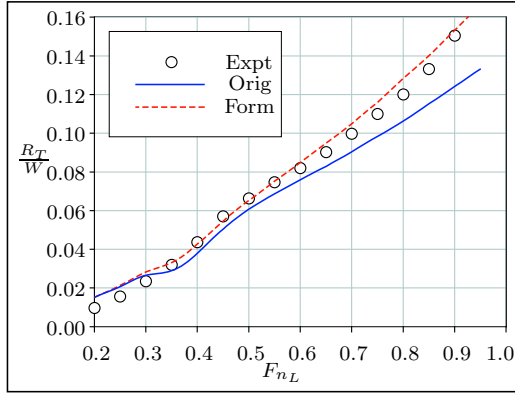


Figure D.145: Uni. of Southampton
Model 5e ($s/L=0.4$)

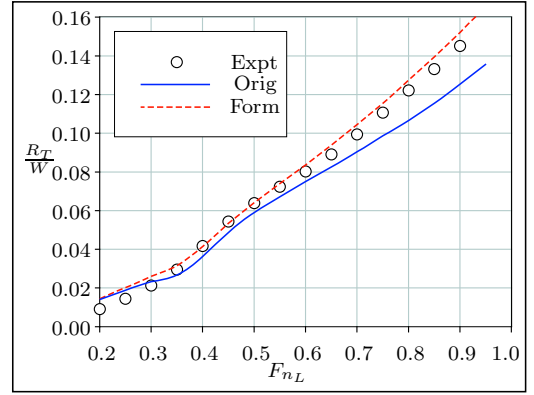


Figure D.146: Uni. of Southampton
Model 5d ($s/L=0.5$)

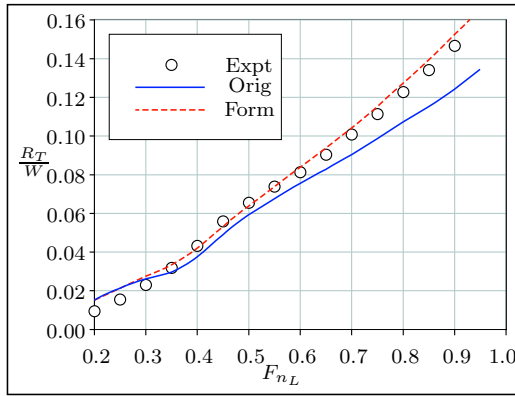


Figure D.147: Uni. of Southampton
Model 5e ($s/L=0.5$)

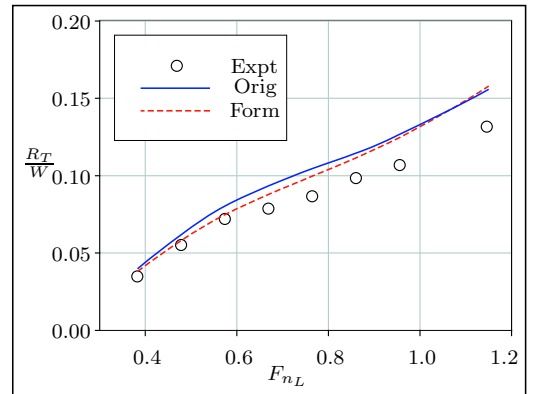


Figure D.148: SKLAD Model M741

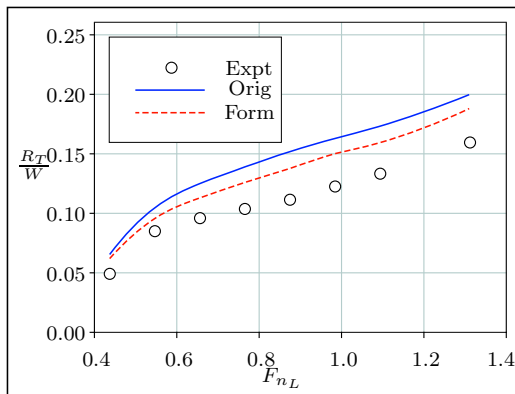


Figure D.149: SKLAD Model M742

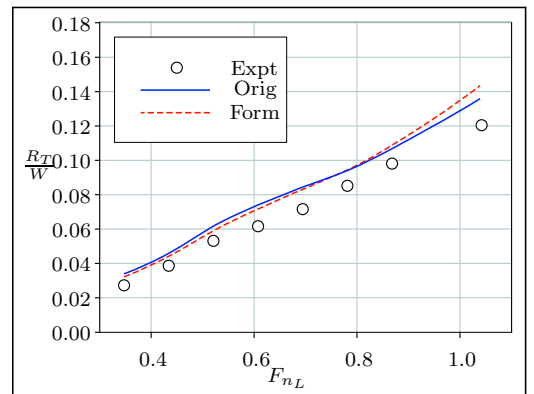


Figure D.150: SKLAD Model M743

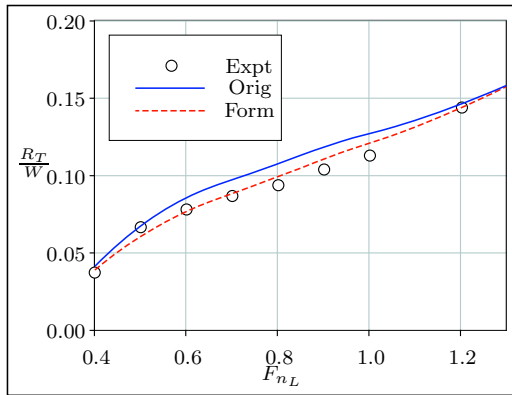


Figure D.151: SKLAD Model M744

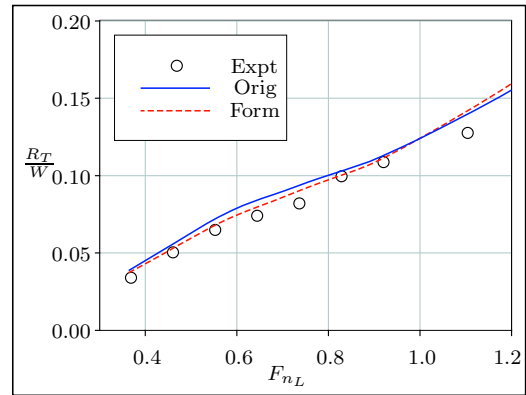


Figure D.152: SKLAD Model M745

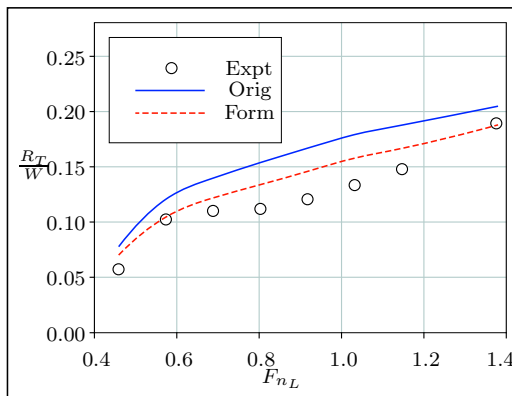


Figure D.153: SKLAD Model M746

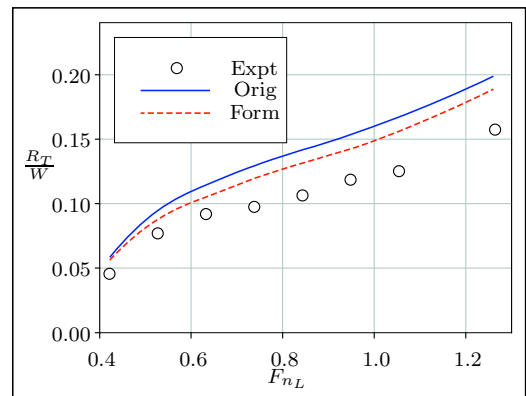


Figure D.154: SKLAD Model M747

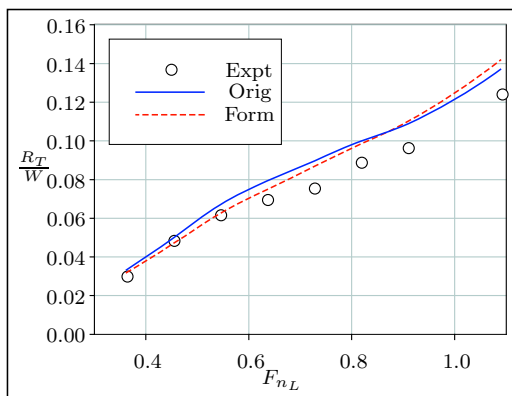


Figure D.155: SKLAD Model M748

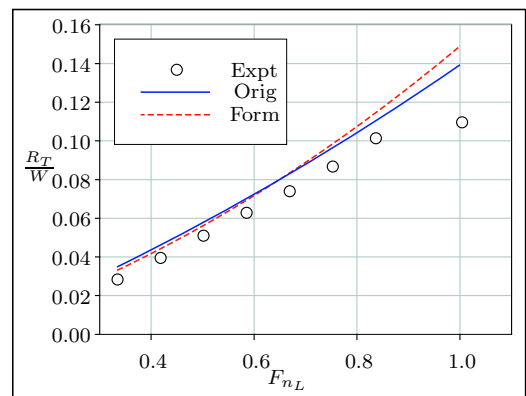


Figure D.156: SKLAD Model M749

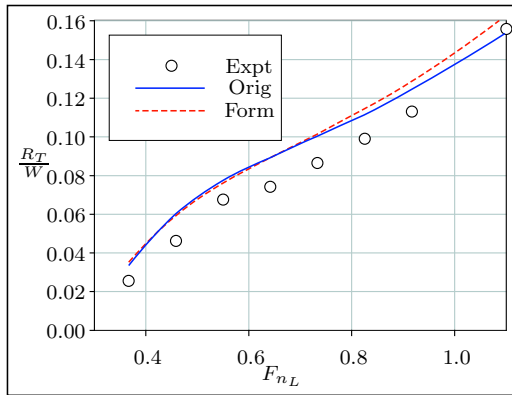


Figure D.157: SKLAD Model M751

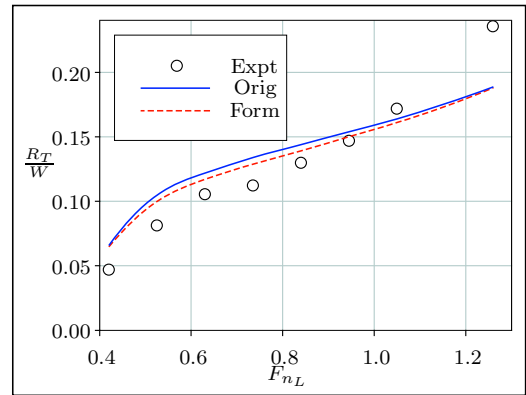


Figure D.158: SKLAD Model M752

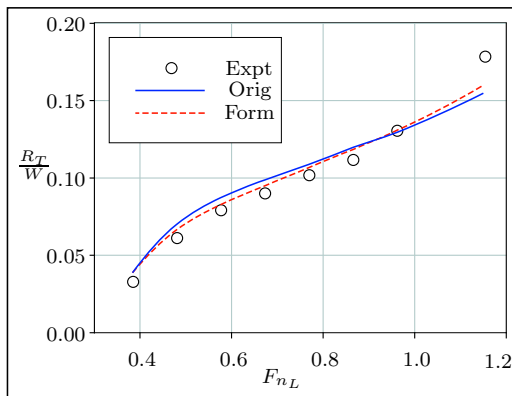


Figure D.159: SKLAD Model M754

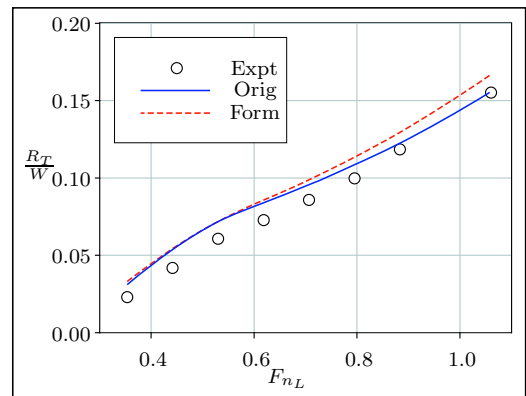


Figure D.160: SKLAD Model M755

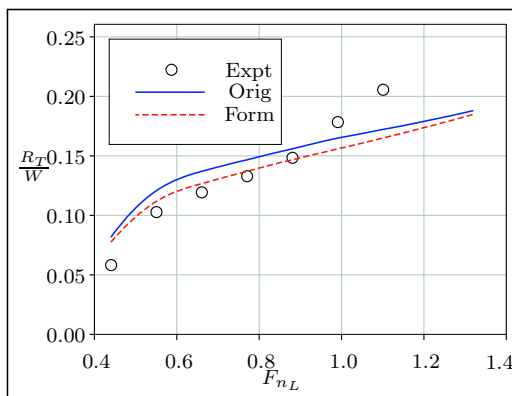


Figure D.161: SKLAD Model M756

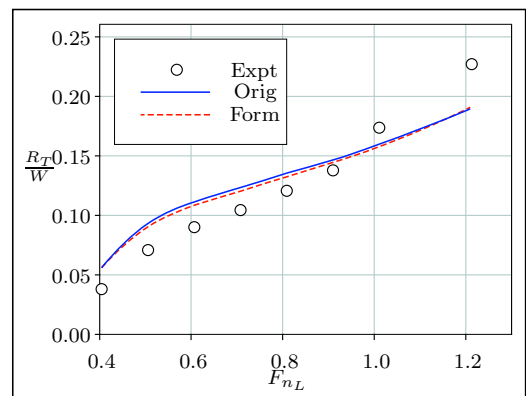


Figure D.162: SKLAD Model M757

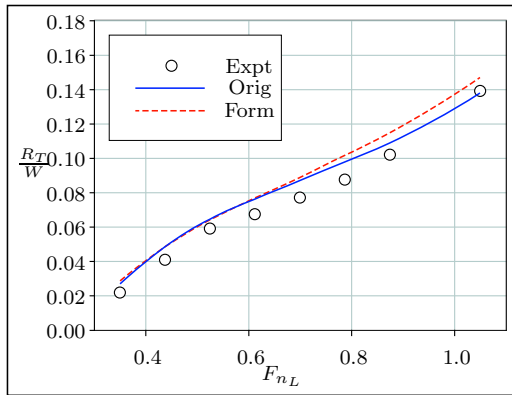


Figure D.163: SKLAD Model M758

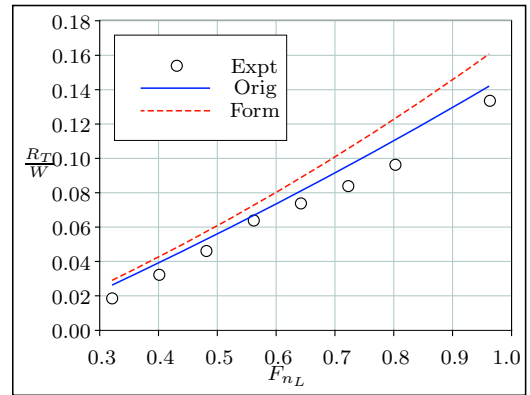


Figure D.164: SKLAD Model M759

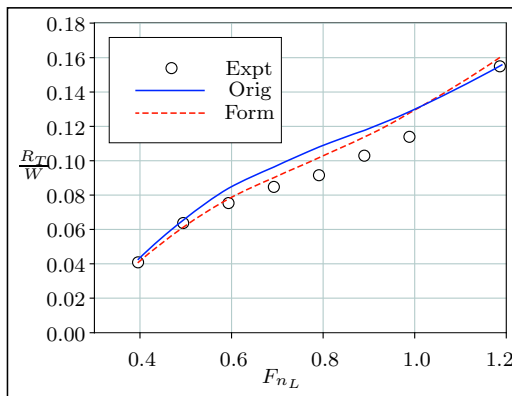


Figure D.165: SKLAD Model M761

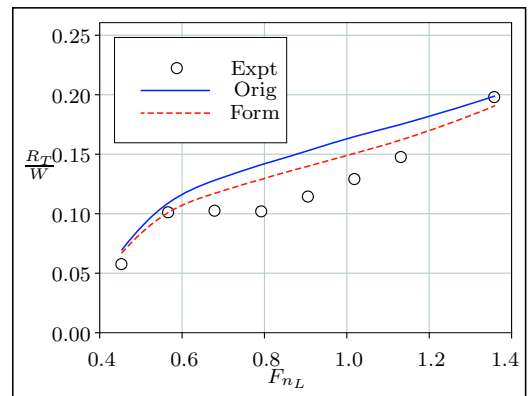


Figure D.166: SKLAD Model M762

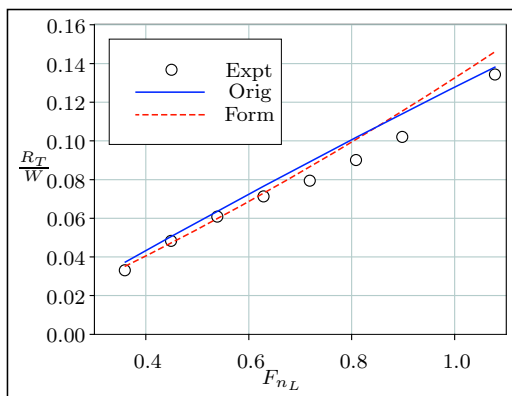


Figure D.167: SKLAD Model M763

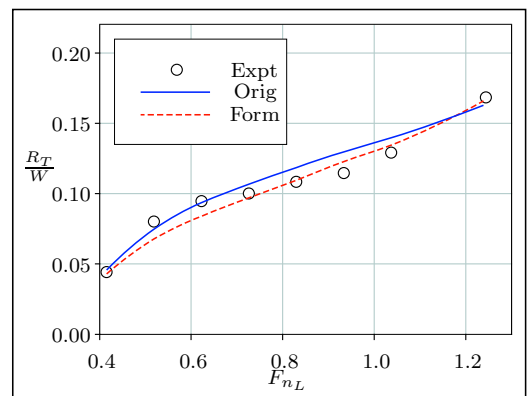


Figure D.168: SKLAD Model M764

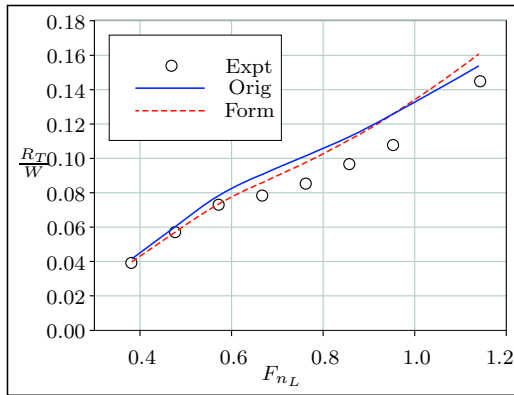


Figure D.169: SKLAD Model M765

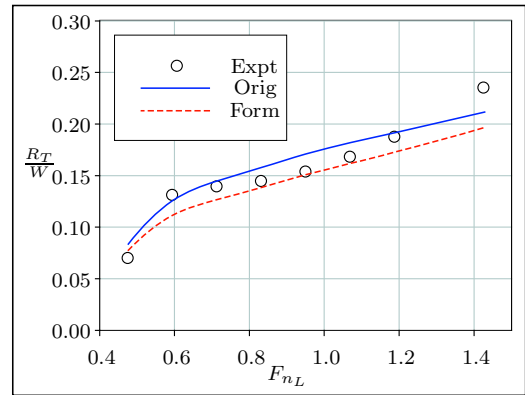


Figure D.170: SKLAD Model M766

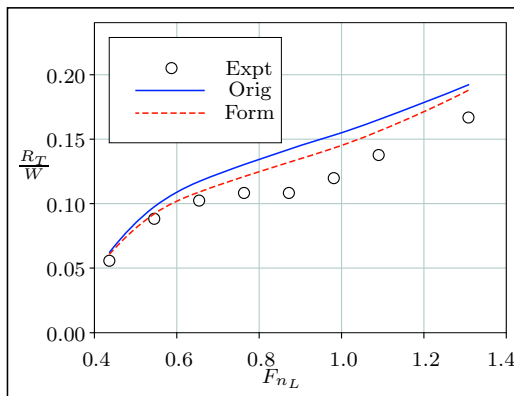


Figure D.171: SKLAD Model M767

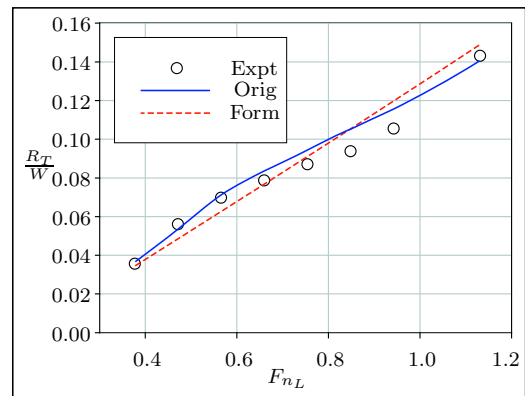


Figure D.172: SKLAD Model M768

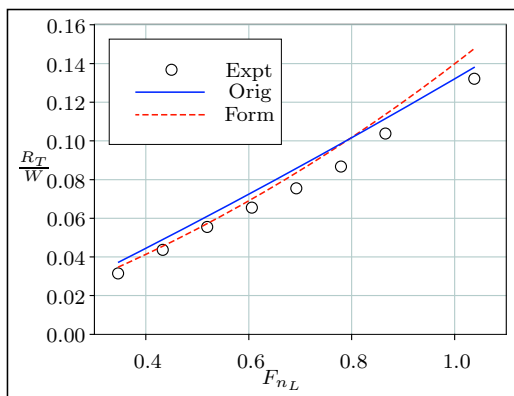


Figure D.173: SKLAD Model M769

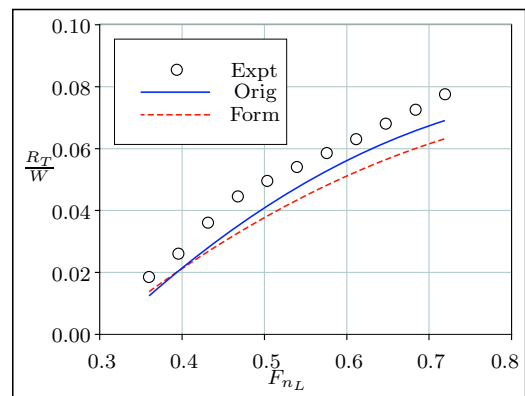


Figure D.174: DeGroot Model 4-I

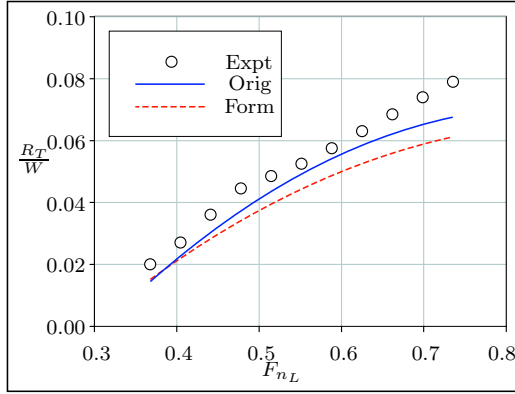


Figure D.175: DeGroot Model 4-II

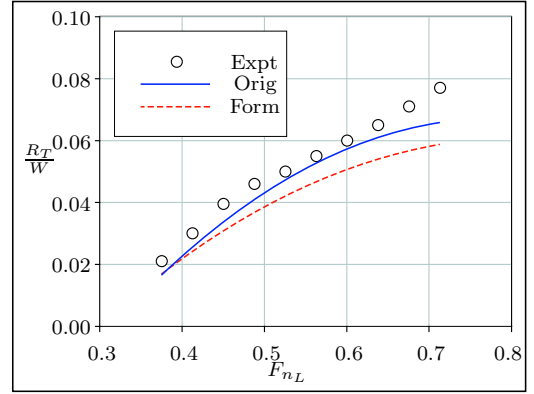


Figure D.176: DeGroot Model 4-III

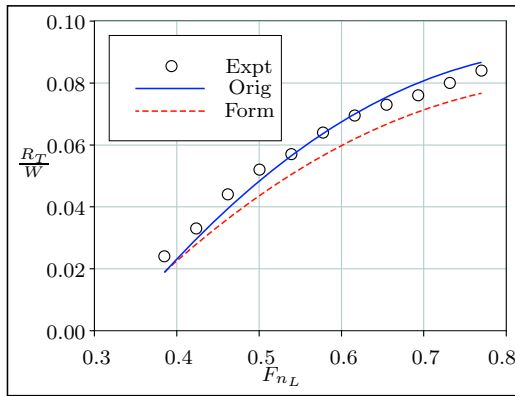


Figure D.177: DeGroot Model 5-I

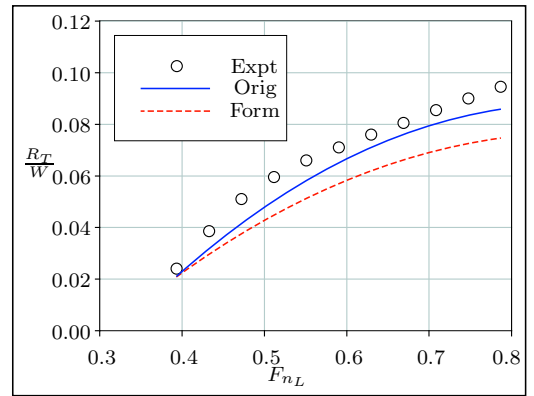


Figure D.178: DeGroot Model 5-II

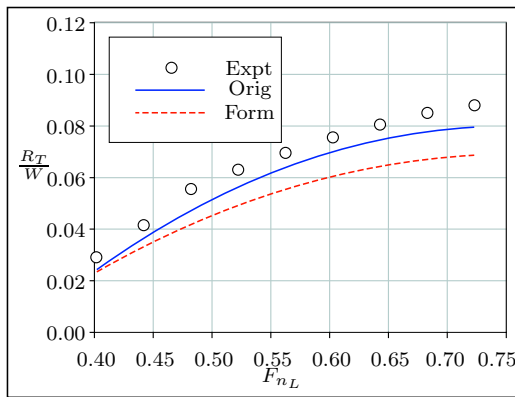


Figure D.179: DeGroot Model 5-III

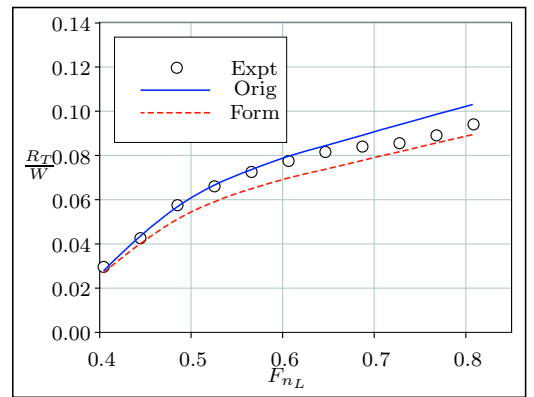


Figure D.180: DeGroot Model 6-I

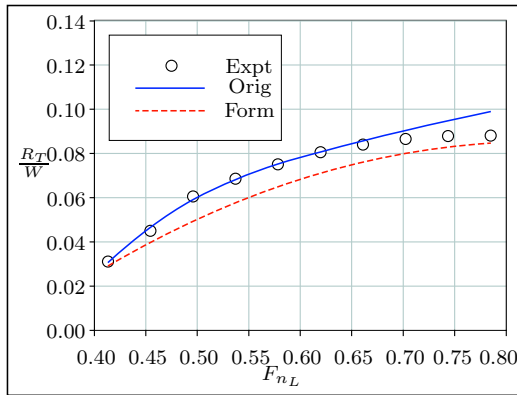


Figure D.181: DeGroot Model 6-II

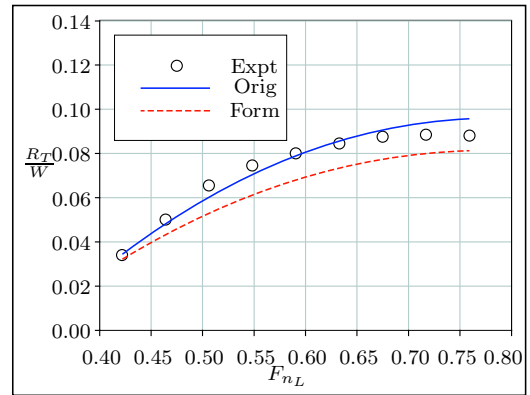


Figure D.182: DeGroot Model 6-III

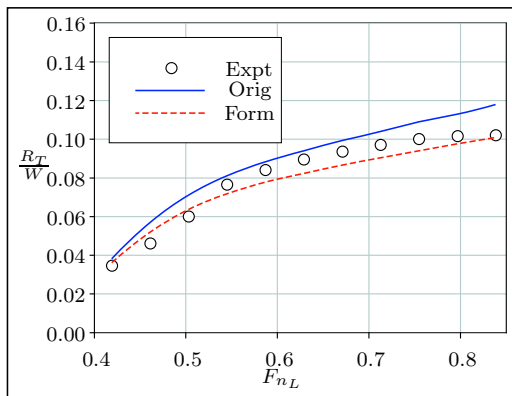


Figure D.183: DeGroot Model 7-I

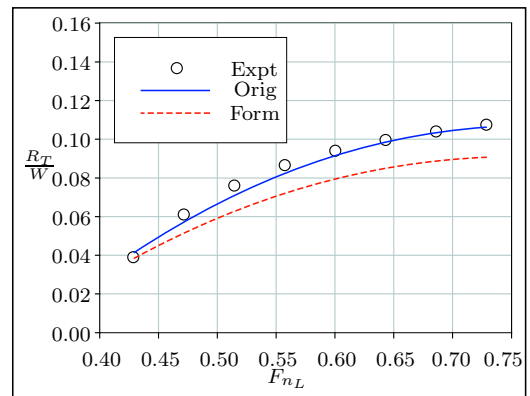


Figure D.184: DeGroot Model 7-II

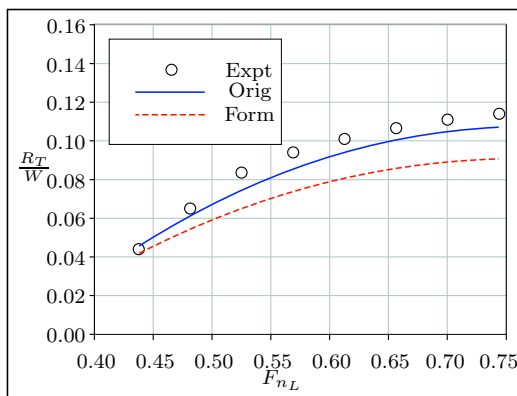


Figure D.185: DeGroot Model 7-III

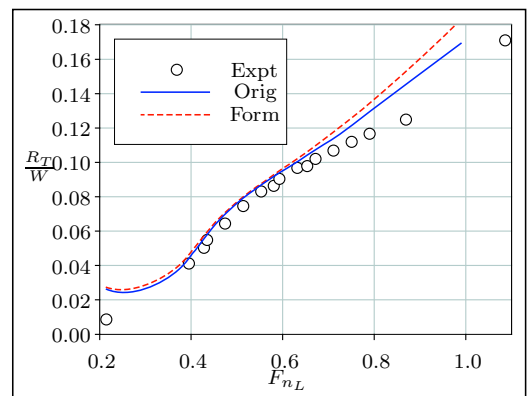
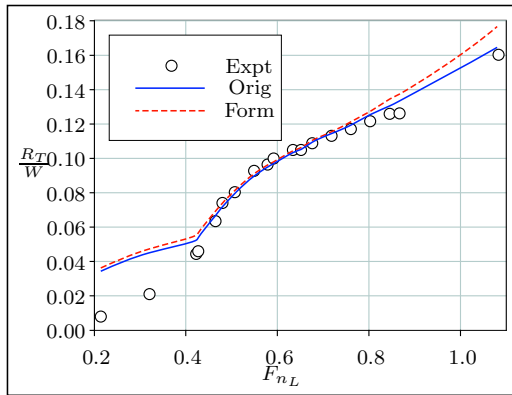
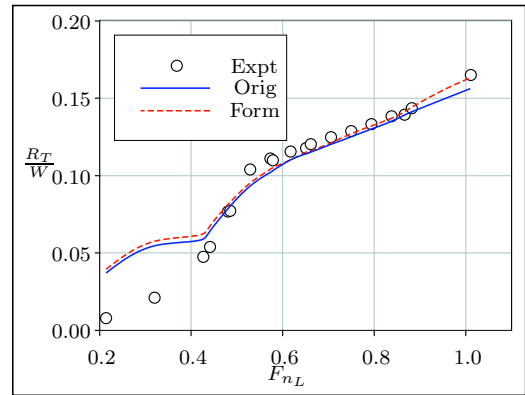
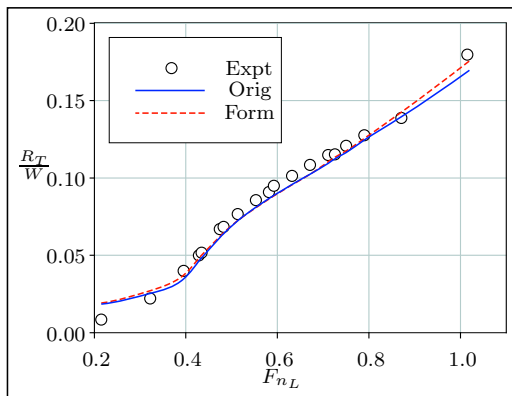
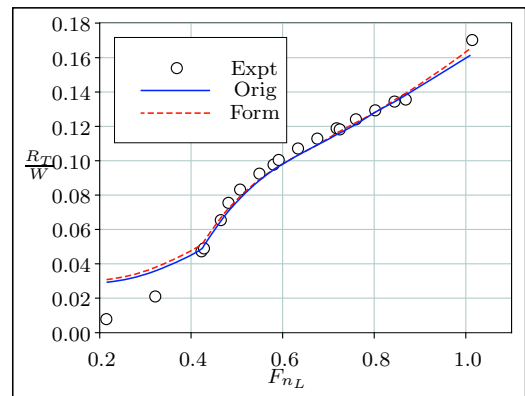
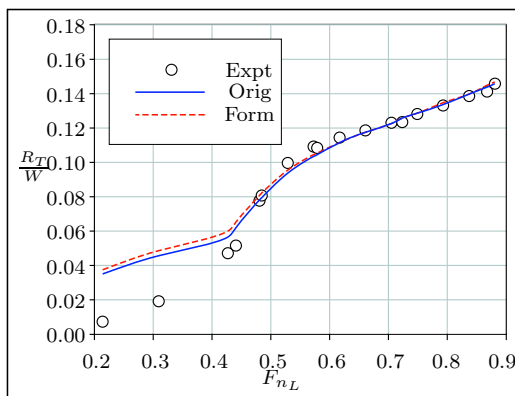
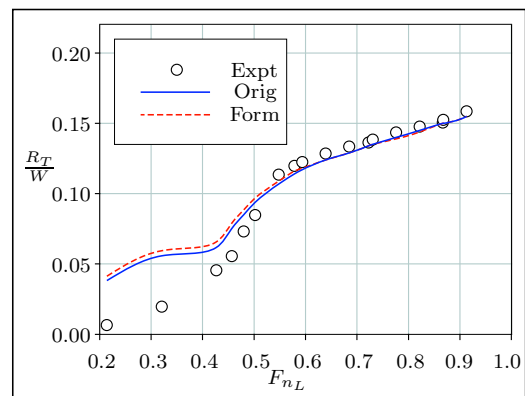
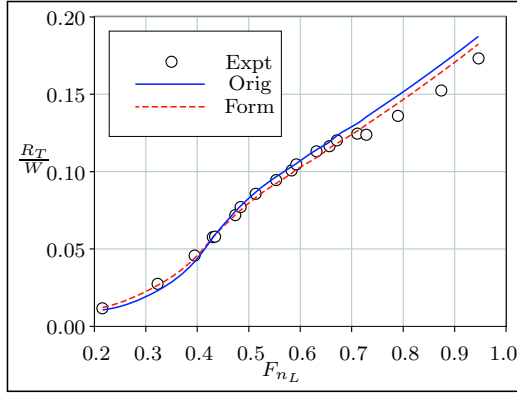
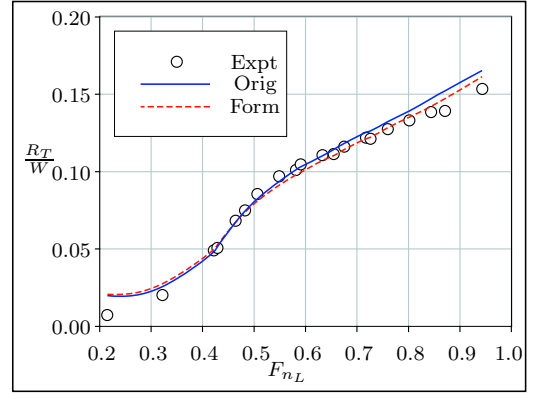
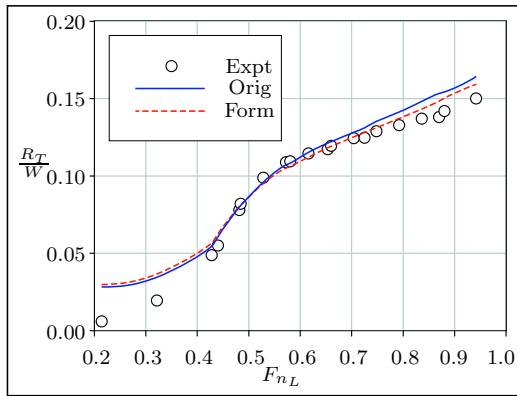
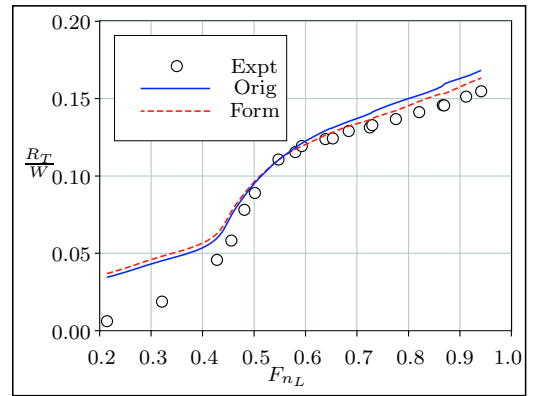
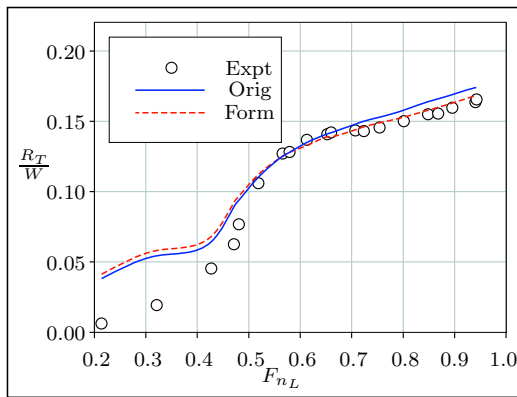
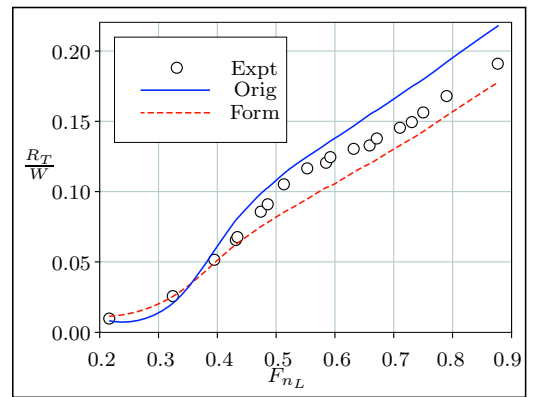
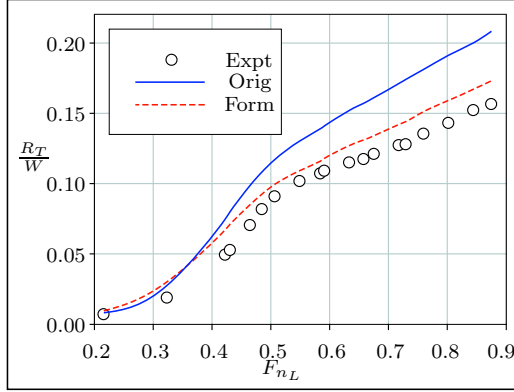
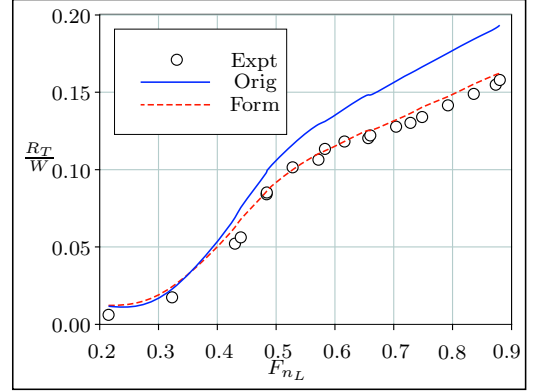
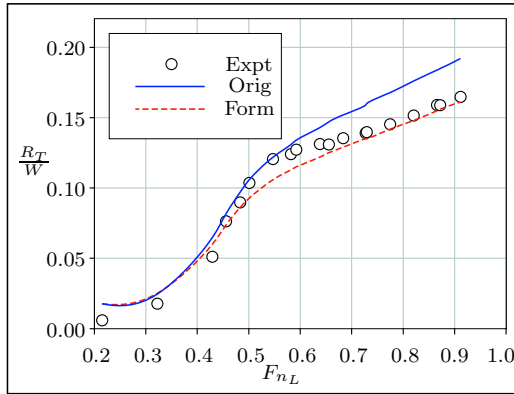
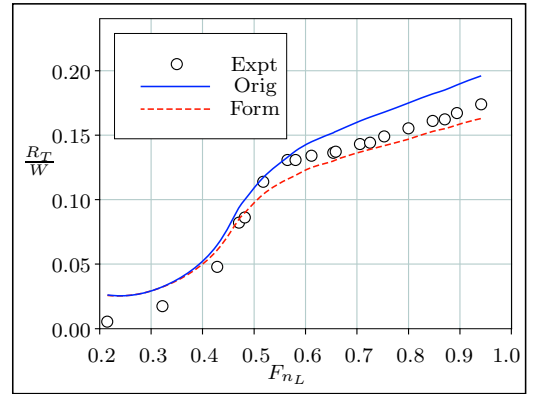
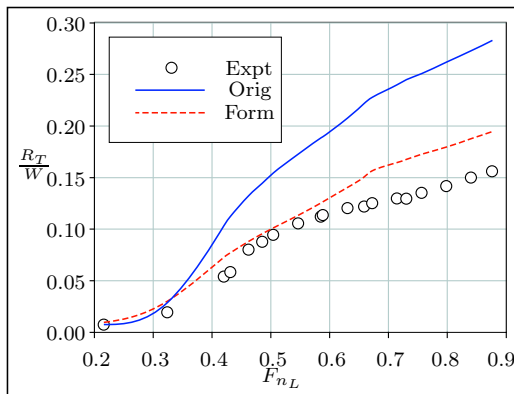
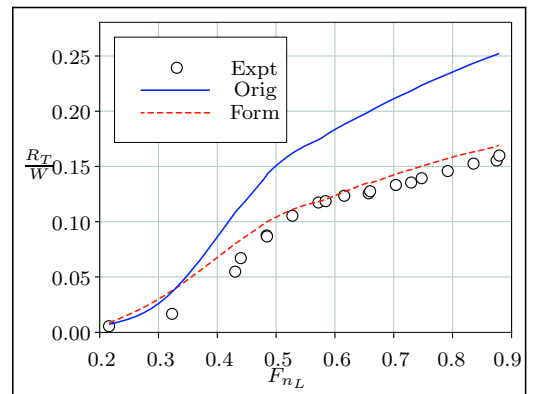


Figure D.186: Series 63 Model 4781-I

**Figure D.187:** Series 63 Model 4781-II**Figure D.188:** Series 63 Model 4781-III**Figure D.189:** Series 63 Model 4780-I**Figure D.190:** Series 63 Model 4780-II**Figure D.191:** Series 63 Model 4780-III**Figure D.192:** Series 63 Model 4780-IV

**Figure D.193:** Series 63 Model 4777-I**Figure D.194:** Series 63 Model 4777-II**Figure D.195:** Series 63 Model 4777-III**Figure D.196:** Series 63 Model 4777-IV**Figure D.197:** Series 63 Model 4777-V**Figure D.198:** Series 63 Model 4779-I

**Figure D.199:** Series 63 Model 4779-II**Figure D.200:** Series 63 Model 4779-III**Figure D.201:** Series 63 Model 4779-IV**Figure D.202:** Series 63 Model 4779-V**Figure D.203:** Series 63 Model 4778-II**Figure D.204:** Series 63 Model 4778-III

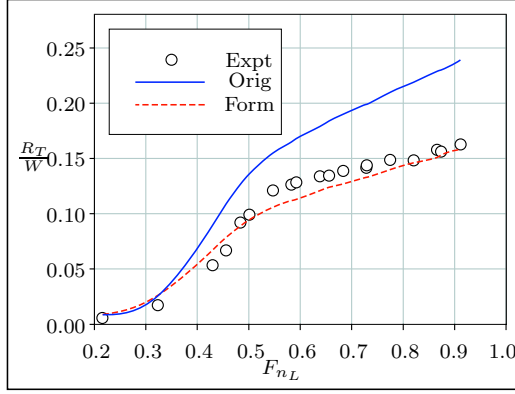


Figure D.205: Series 63 Model 4778-IV

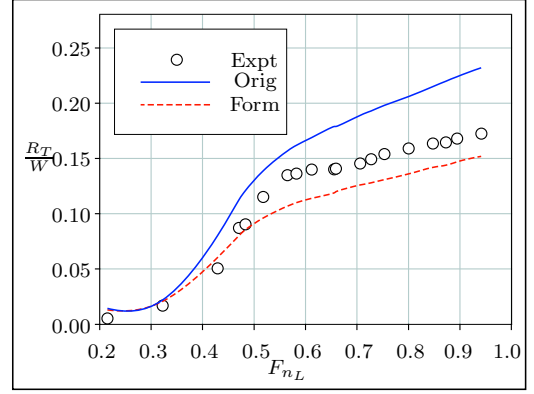


Figure D.206: Series 63 Model 4778-V

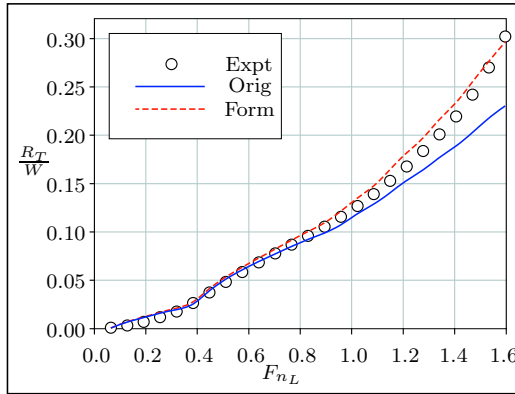


Figure D.207: Series 64 Model 4787

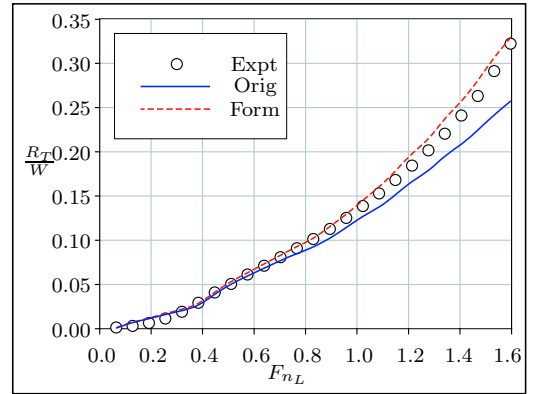


Figure D.208: Series 64 Model 4788

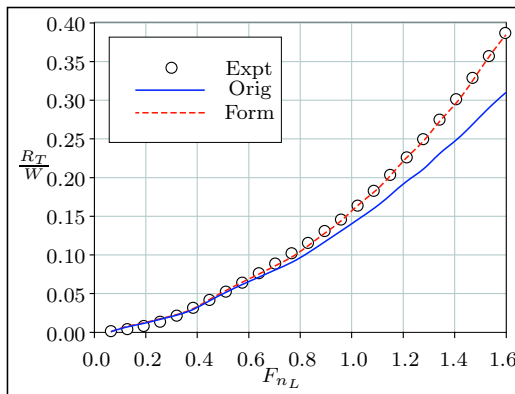


Figure D.209: Series 64 Model 4789

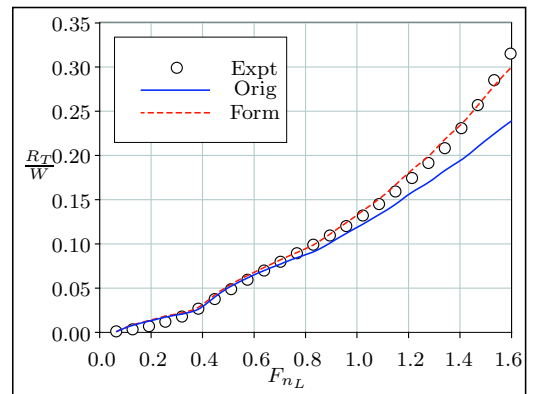


Figure D.210: Series 64 Model 4790

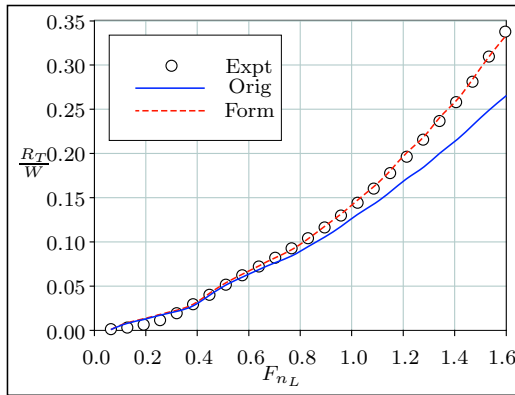


Figure D.211: Series 64 Model 4791

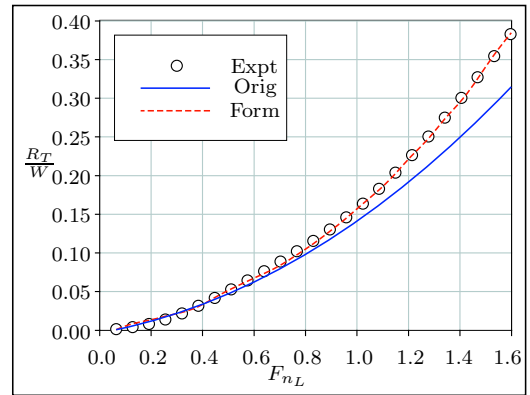


Figure D.212: Series 64 Model 4792

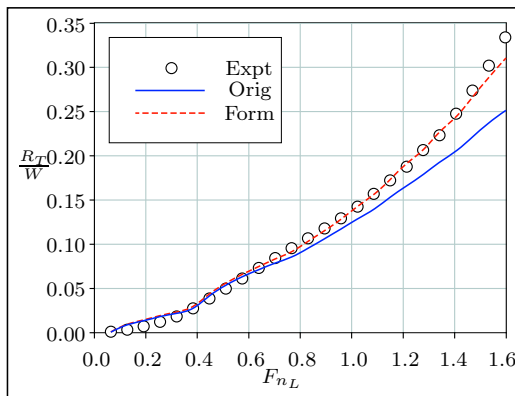


Figure D.213: Series 64 Model 4793

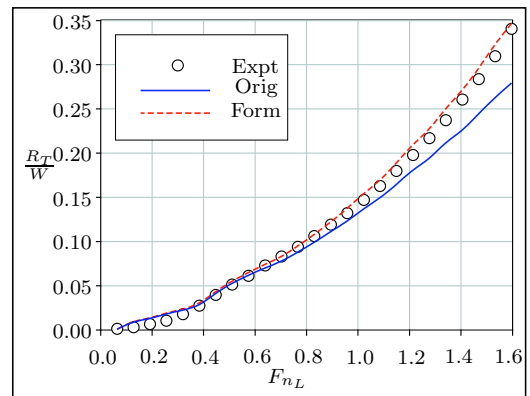


Figure D.214: Series 64 Model 4794

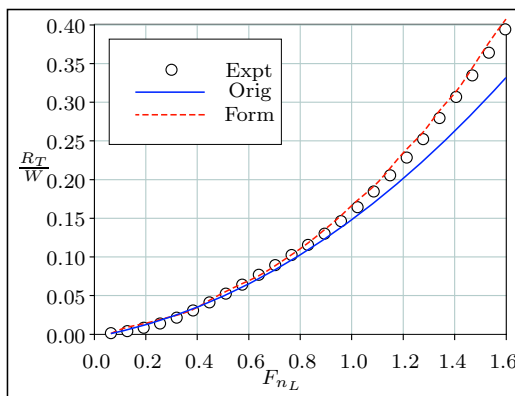


Figure D.215: Series 64 Model 4795

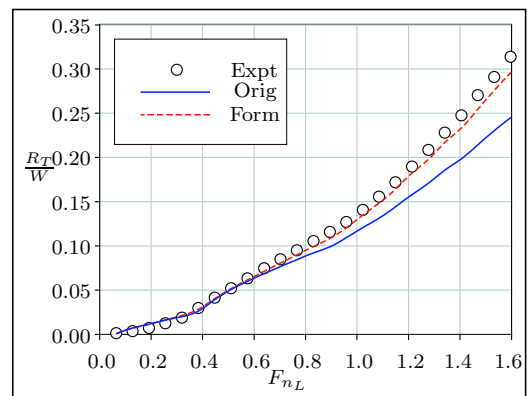


Figure D.216: Series 64 Model 4796

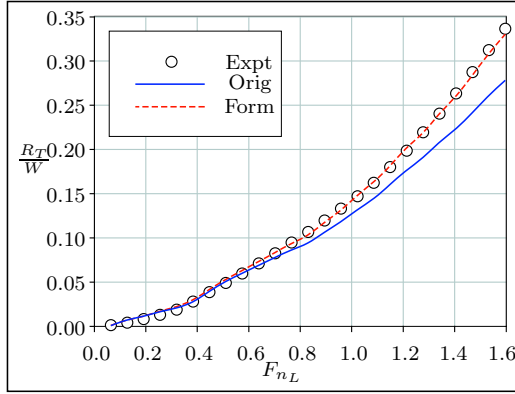


Figure D.217: Series 64 Model 4797

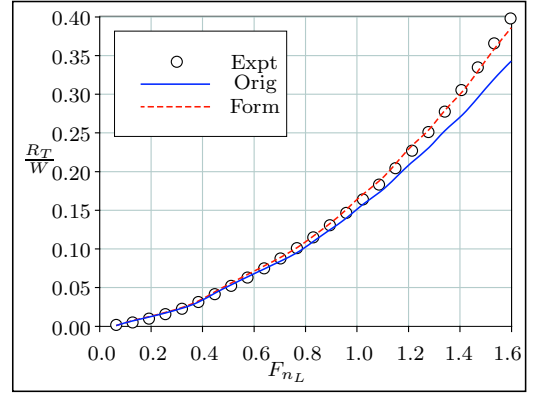


Figure D.218: Series 64 Model 4798

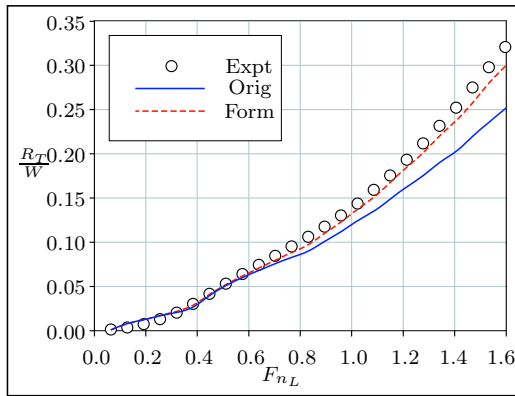


Figure D.219: Series 64 Model 4799

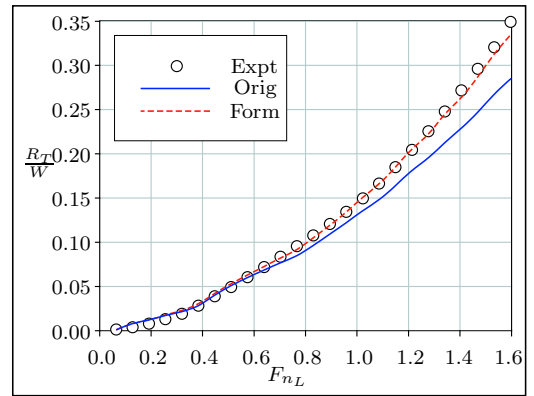


Figure D.220: Series 64 Model 4800

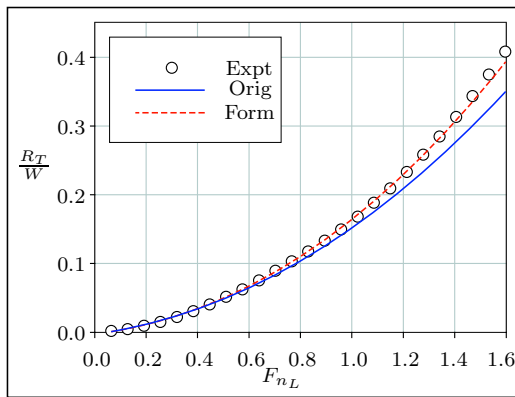


Figure D.221: Series 64 Model 4801

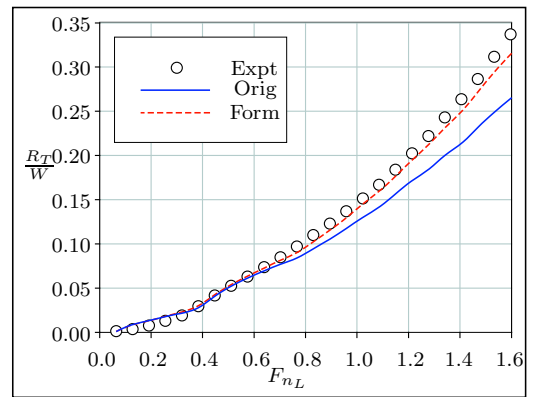


Figure D.222: Series 64 Model 4802

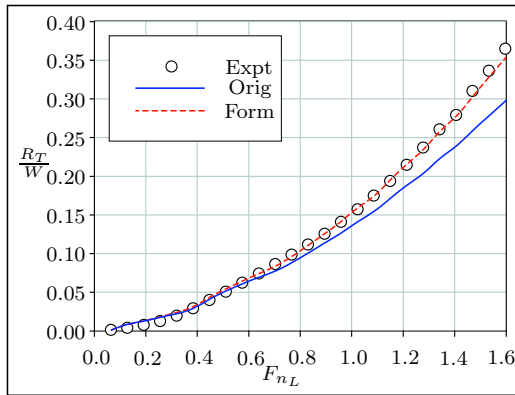


Figure D.223: Series 64 Model 4803

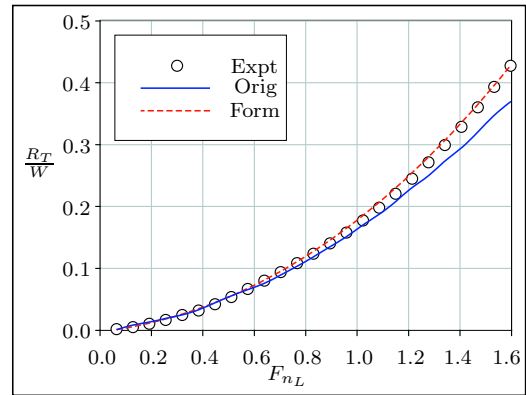


Figure D.224: Series 64 Model 4804

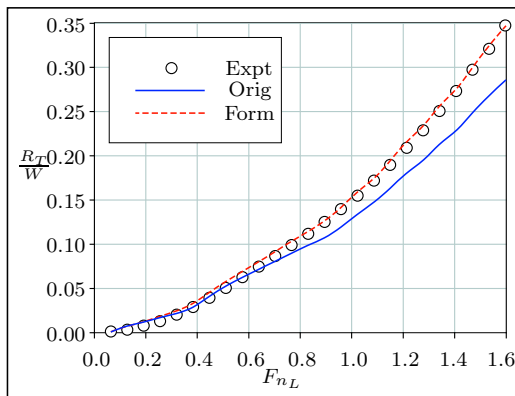


Figure D.225: Series 64 Model 4805

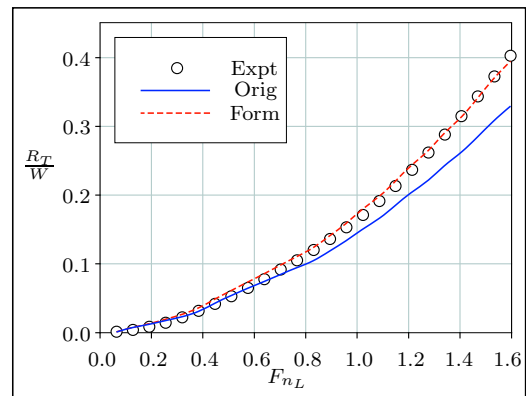


Figure D.226: Series 64 Model 4806

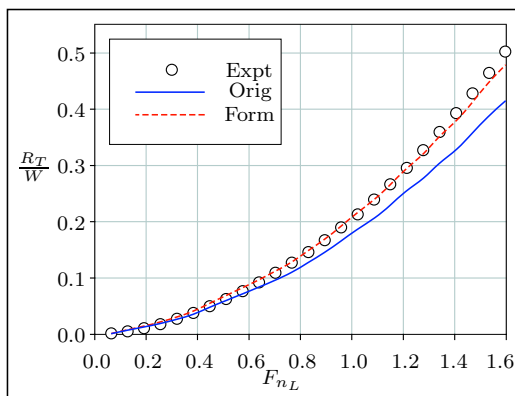


Figure D.227: Series 64 Model 4807

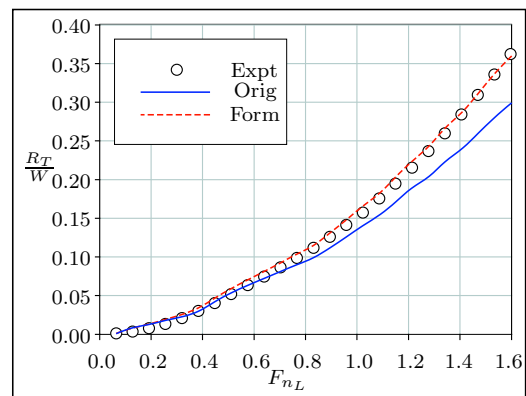


Figure D.228: Series 64 Model 4808

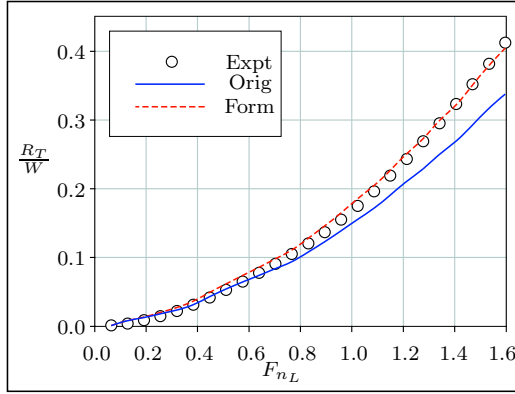


Figure D.229: Series 64 Model 4809

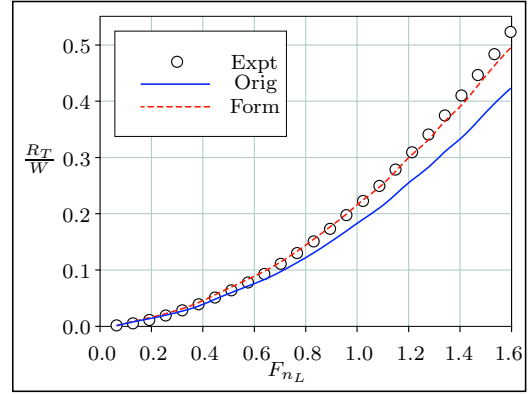


Figure D.230: Series 64 Model 4810

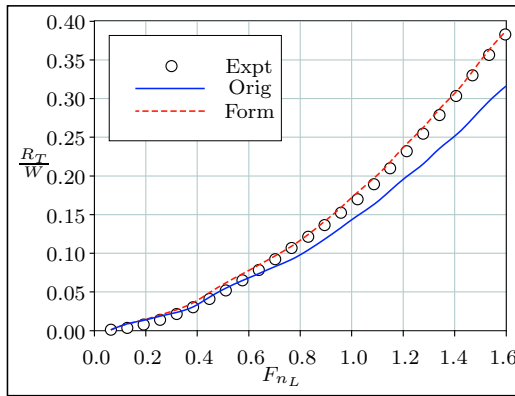


Figure D.231: Series 64 Model 4811

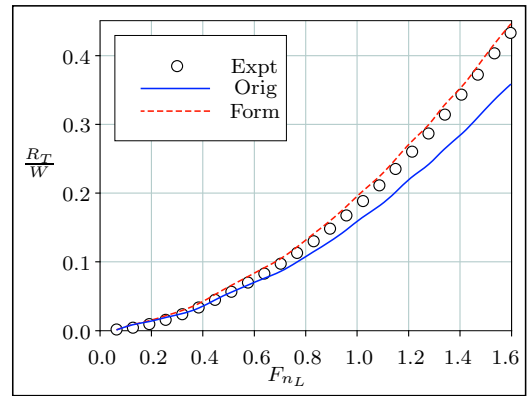


Figure D.232: Series 64 Model 4812

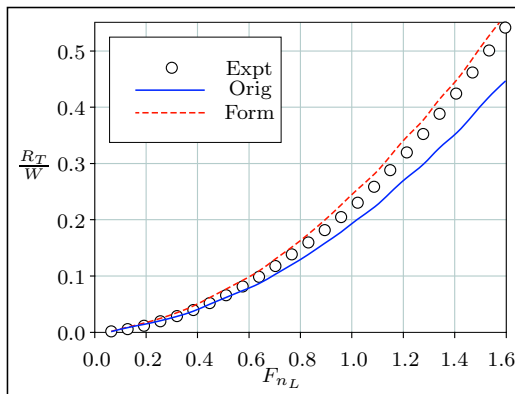


Figure D.233: Series 64 Model 4813

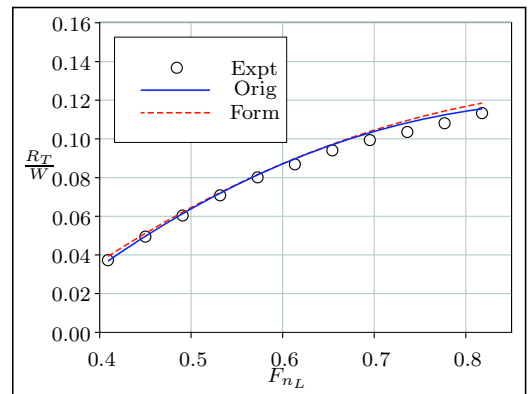


Figure D.234: SSPA Model 1209-A

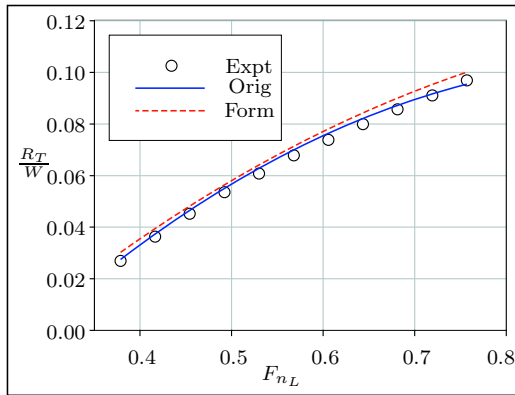


Figure D.235: SSPA Model 1210-A

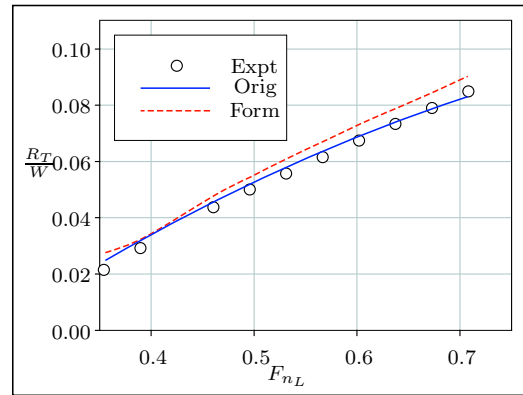


Figure D.236: SSPA Model 1211-A

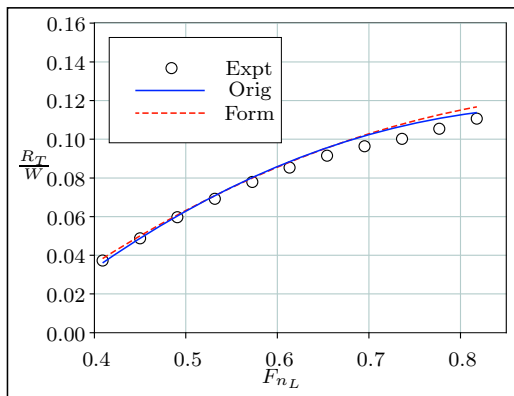


Figure D.237: SSPA Model 1212-A

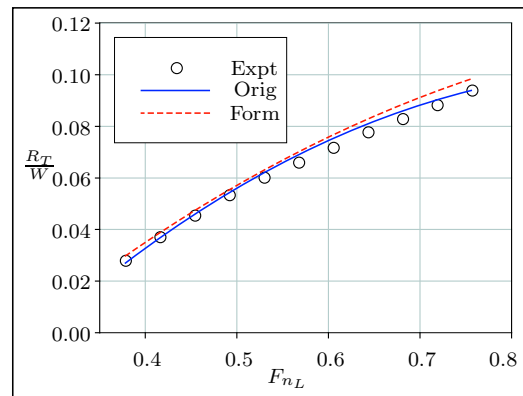


Figure D.238: SSPA Model 1213-A

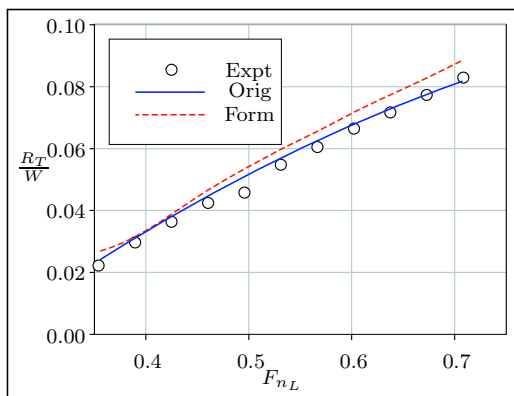


Figure D.239: SSPA Model 1214-A

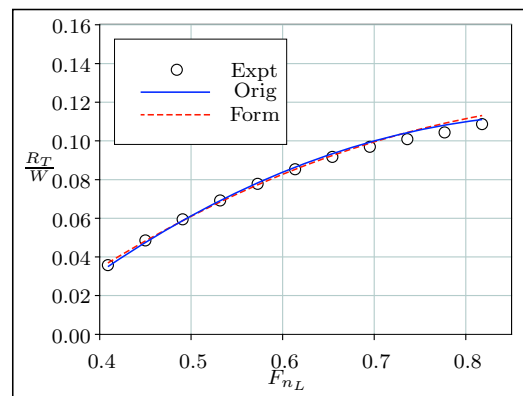


Figure D.240: SSPA Model 1215-A

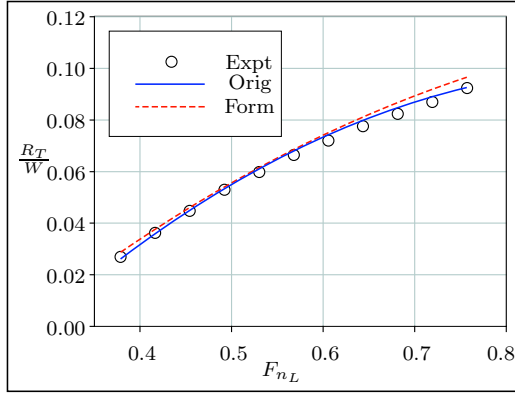


Figure D.241: SSPA Model 1216-A

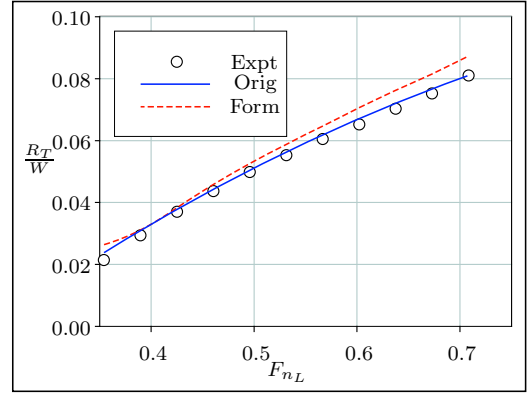


Figure D.242: SSPA Model 1217-A

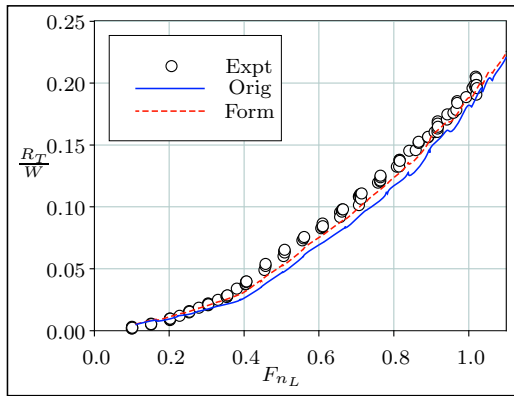


Figure D.243: AMECRC Model 1

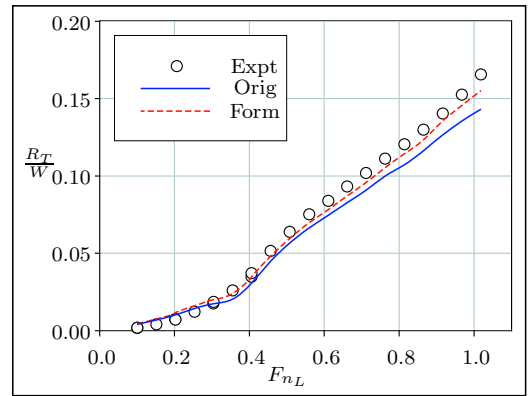


Figure D.244: AMECRC Model 2

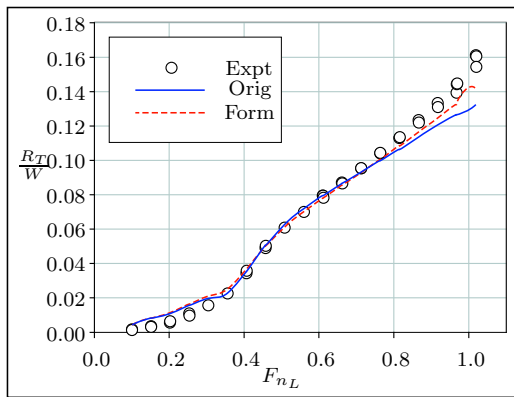


Figure D.245: AMECRC Model 3

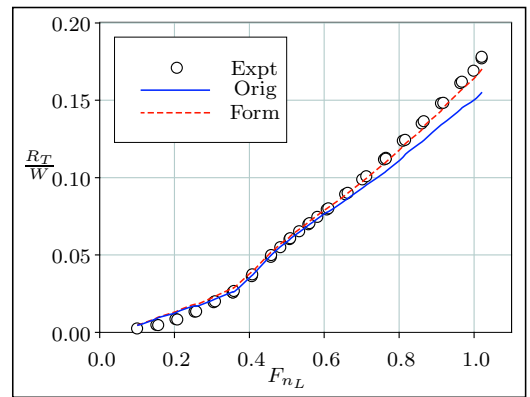


Figure D.246: AMECRC Model 4

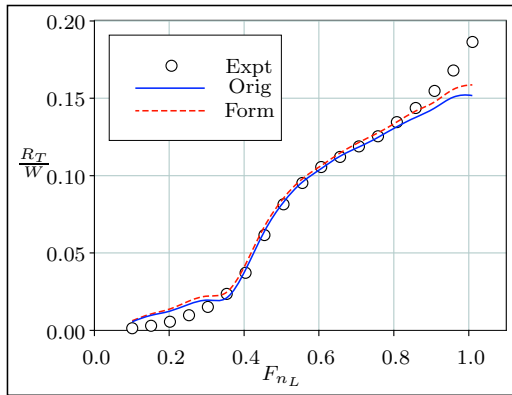


Figure D.247: AMECRC Model 5

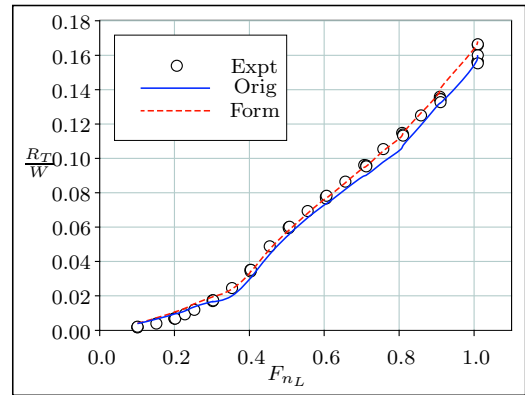


Figure D.248: AMECRC Model 6

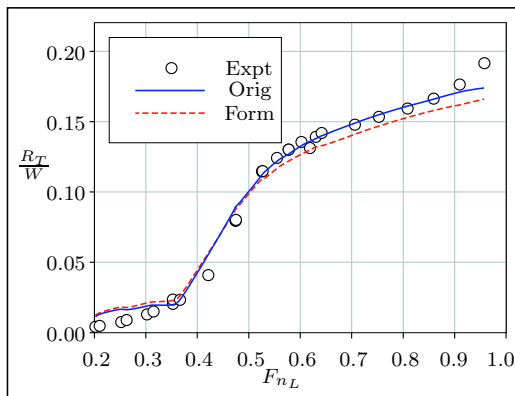


Figure D.249: AMECRC Model 7

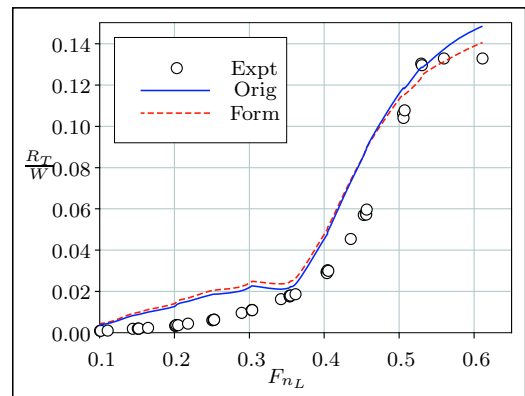


Figure D.250: AMECRC Model 8

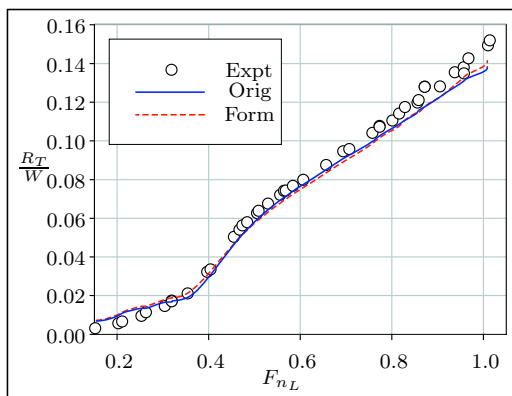


Figure D.251: AMECRC Model 9

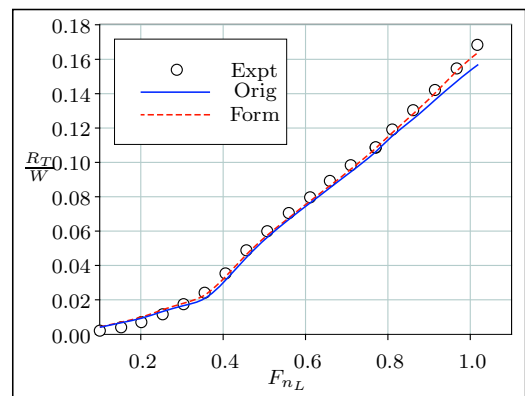


Figure D.252: AMECRC Model 10

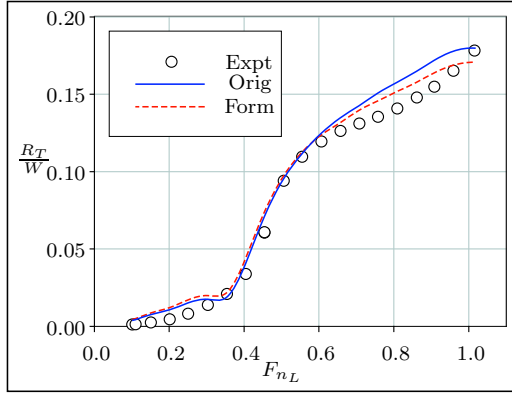


Figure D.253: AMECRC Model 11

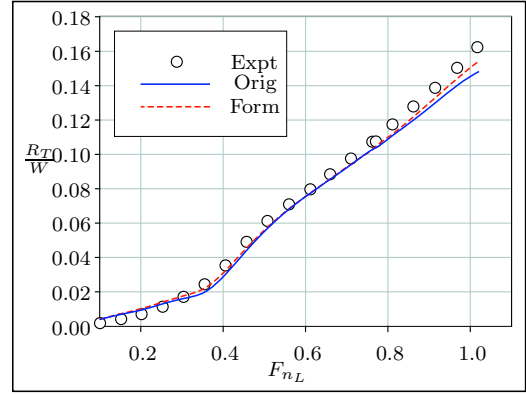


Figure D.254: AMECRC Model 12

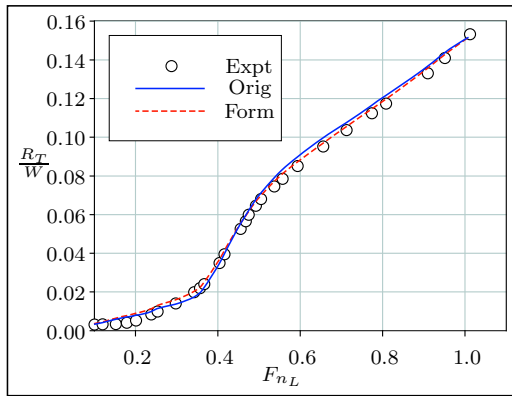


Figure D.255: AMECRC Model 13

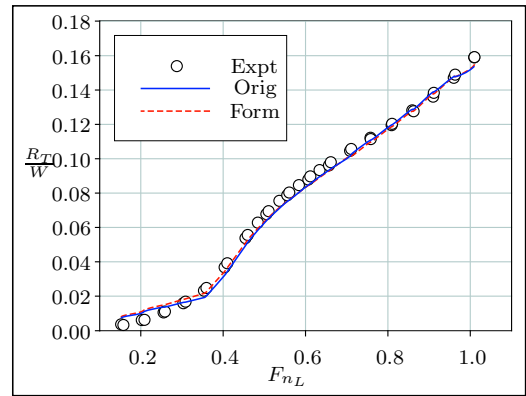
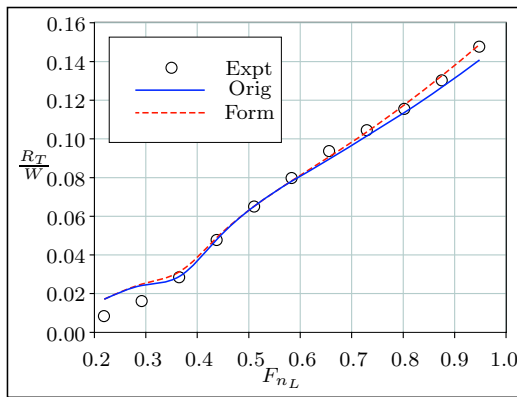
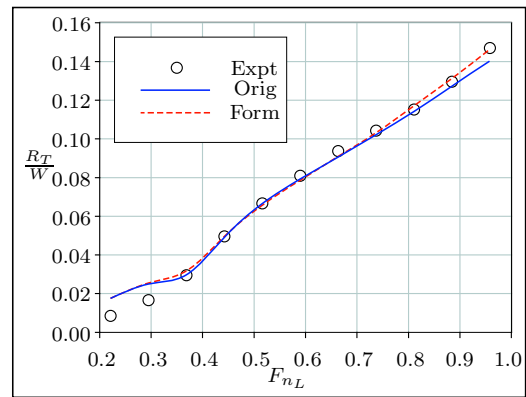
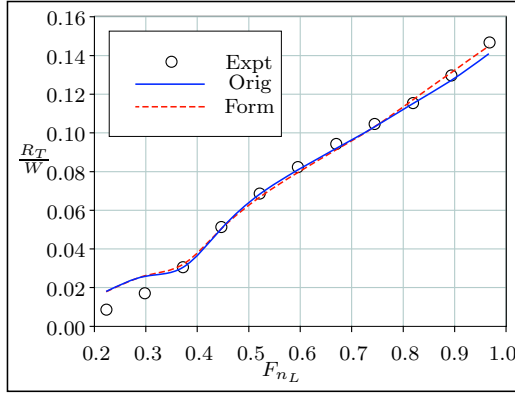
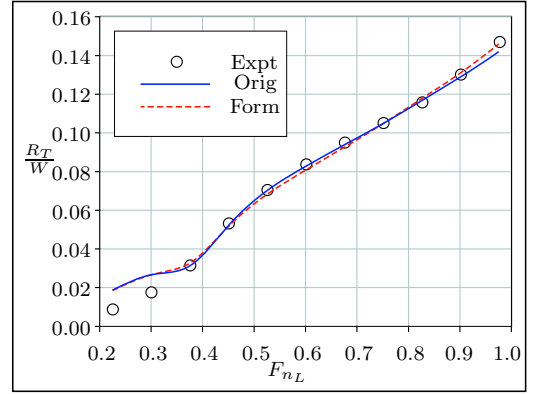
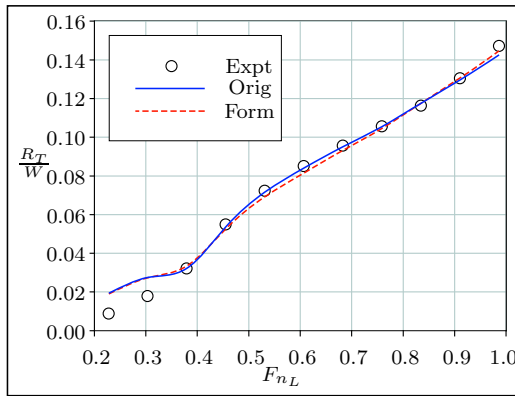
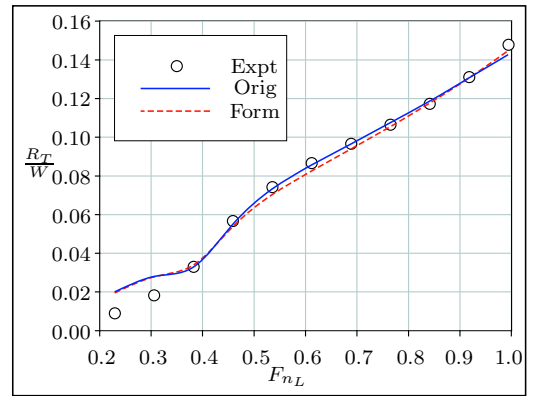
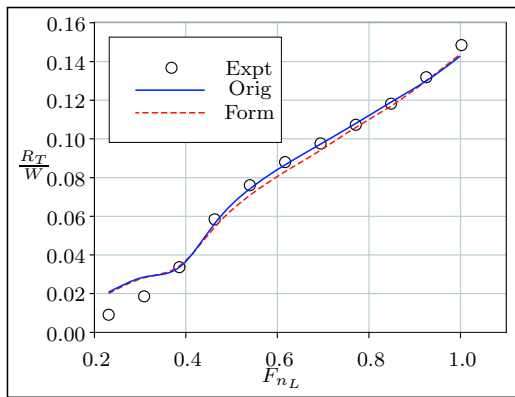
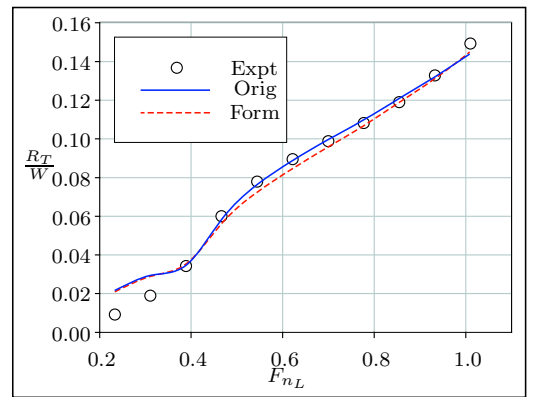
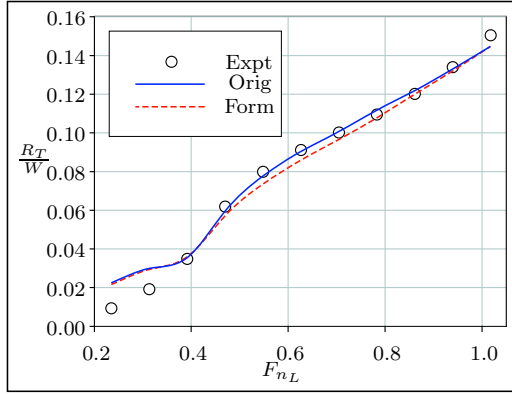
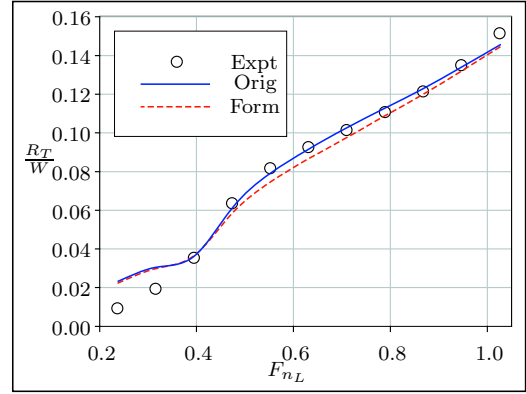
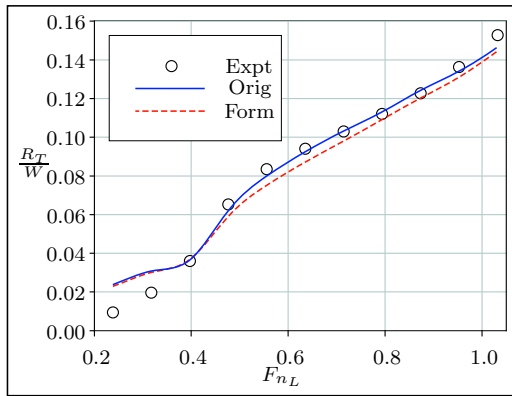
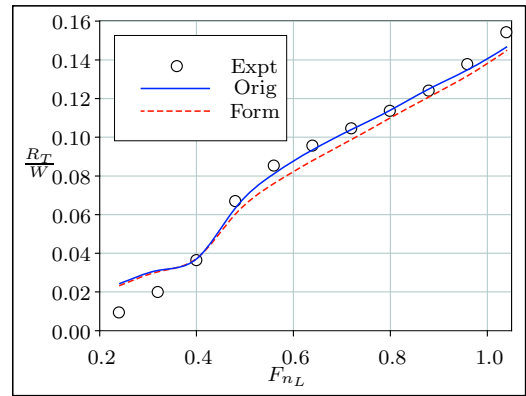
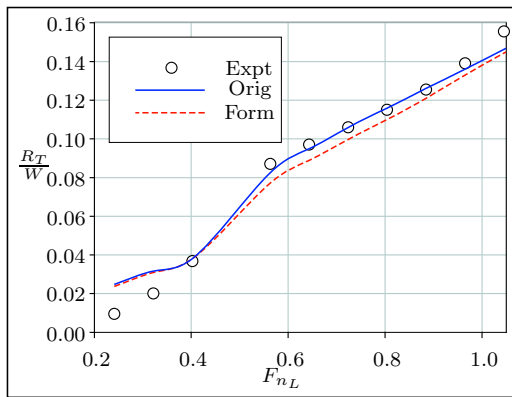
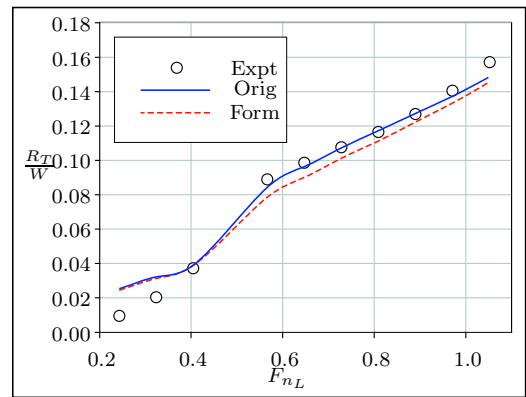
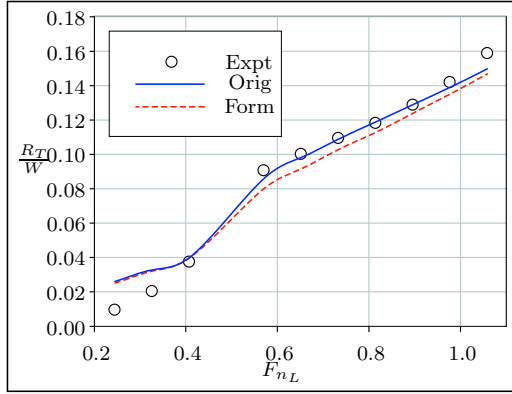
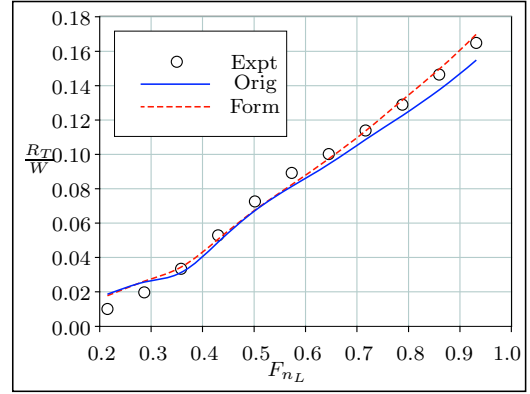
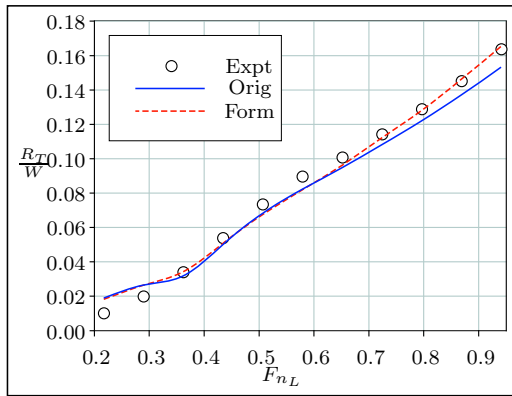
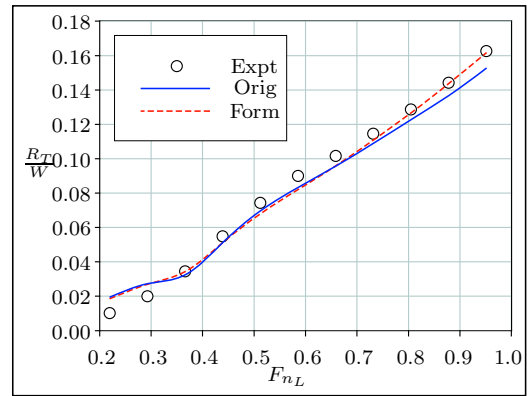
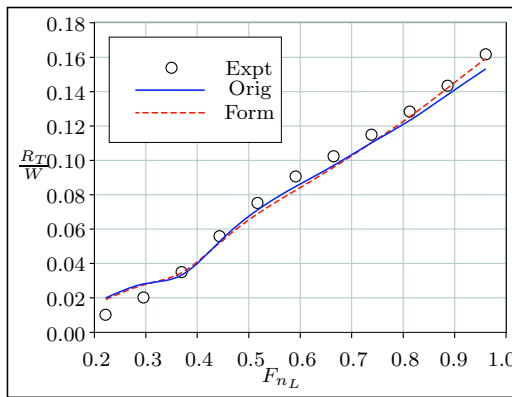
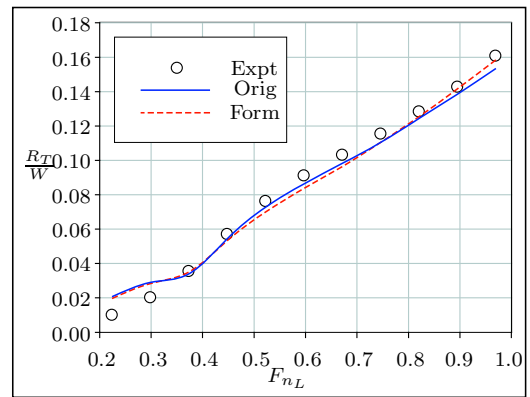


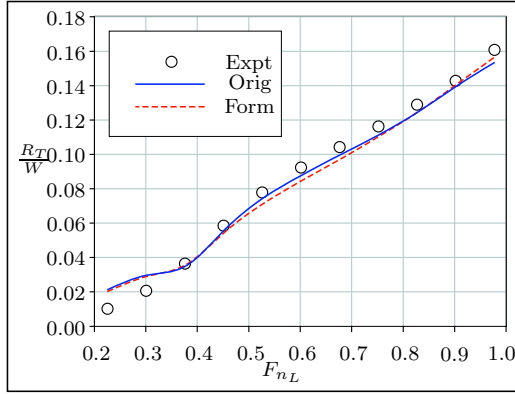
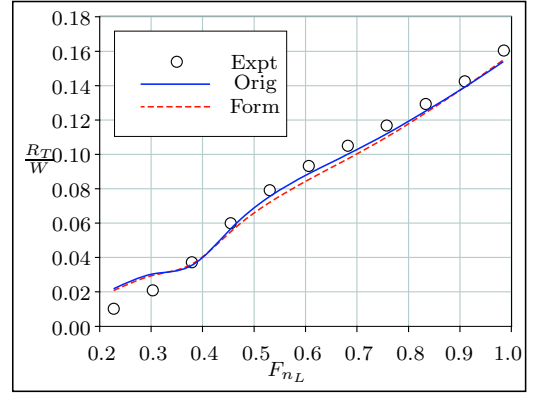
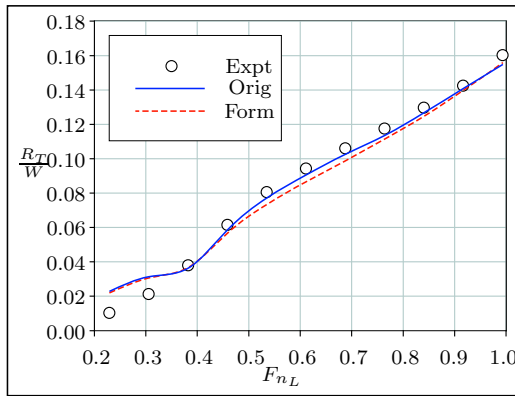
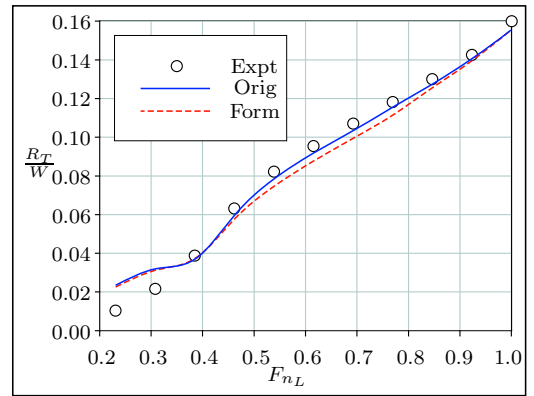
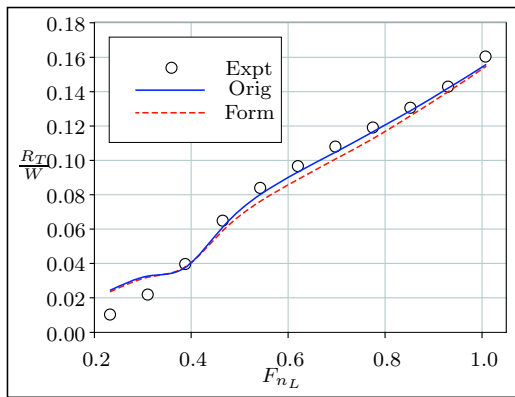
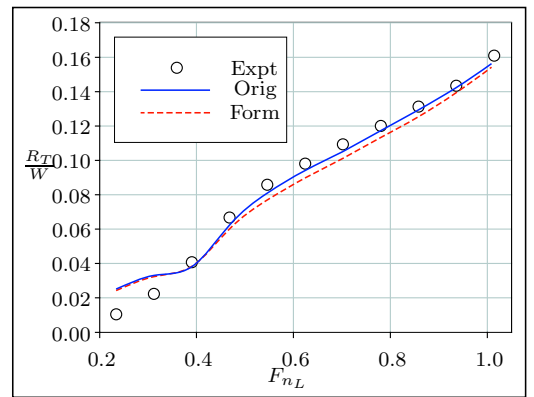
Figure D.256: AMECRC Model 14

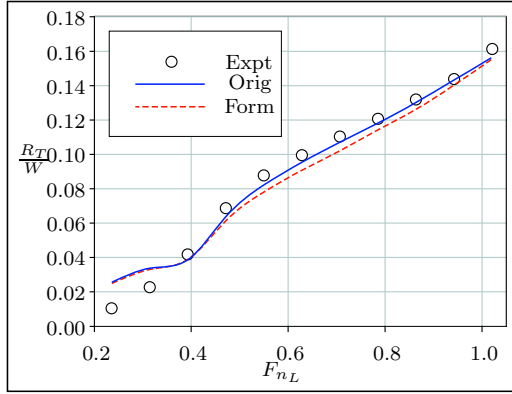
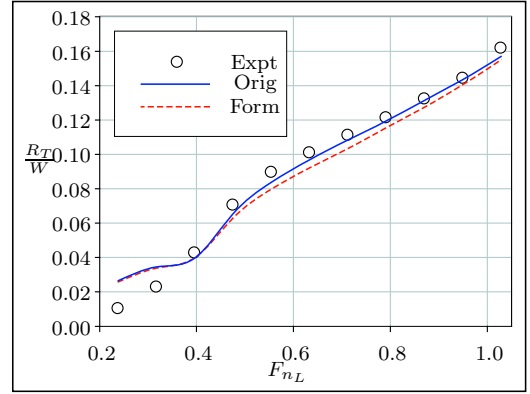
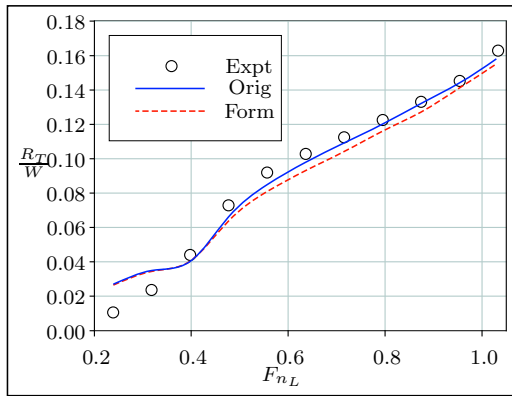
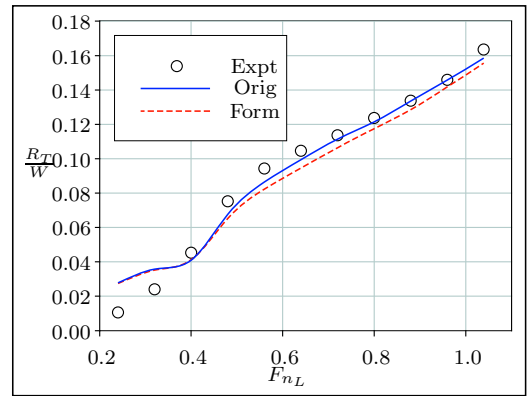
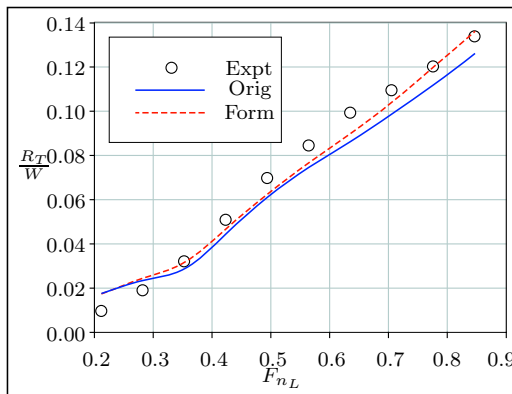
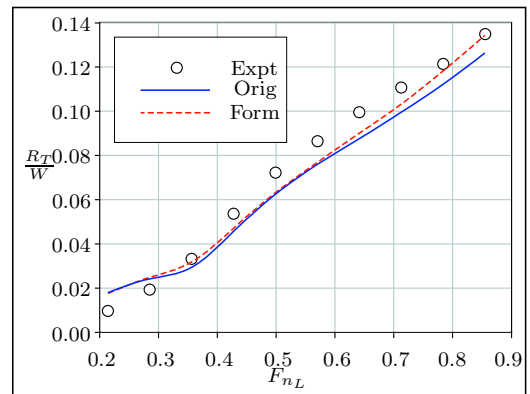
Figure D.257: NOVA-I at 75% Δ_{DWL} Figure D.258: NOVA-I at 80% Δ_{DWL}

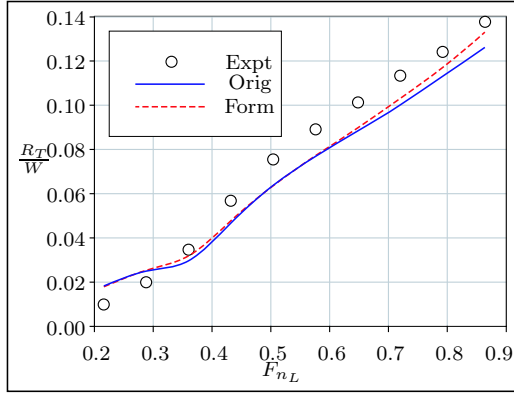
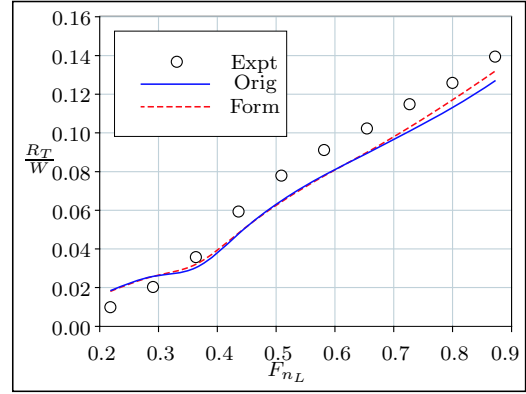
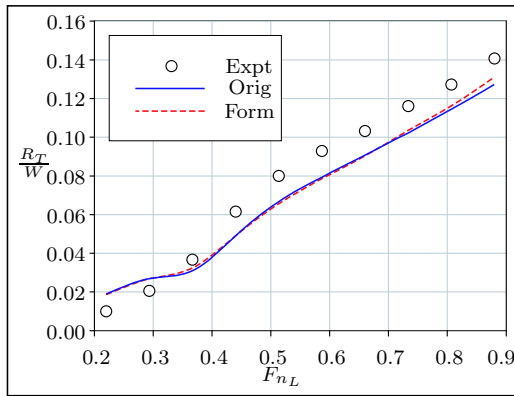
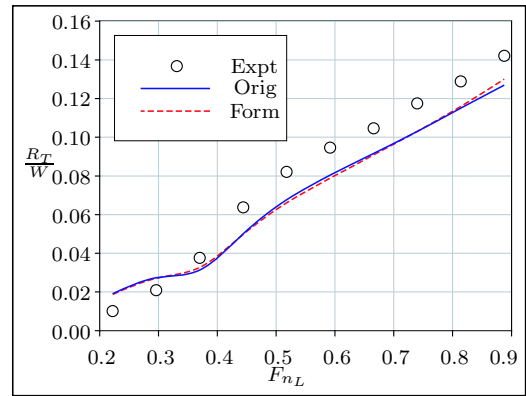
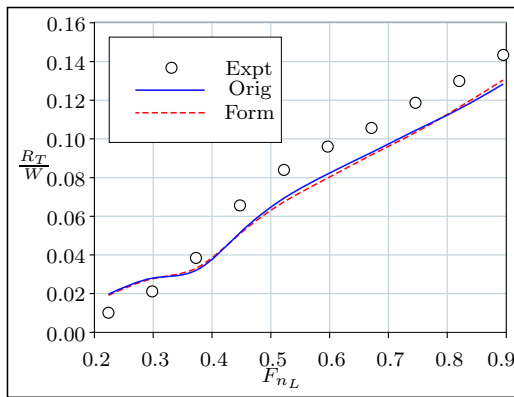
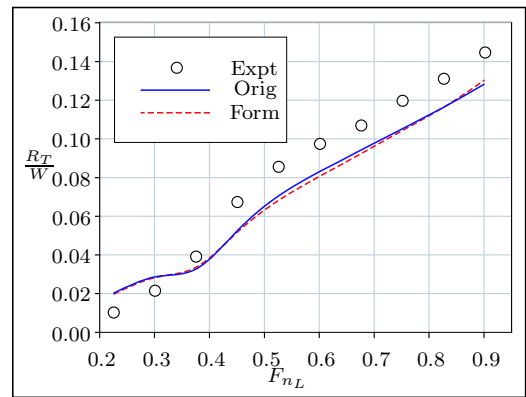
Figure D.259: NOVA-I at 85% Δ_{DWL} Figure D.260: NOVA-I at 90% Δ_{DWL} Figure D.261: NOVA-I at 95% Δ_{DWL} Figure D.262: NOVA-I at 100% Δ_{DWL} Figure D.263: NOVA-I at 105% Δ_{DWL} Figure D.264: NOVA-I at 110% Δ_{DWL}

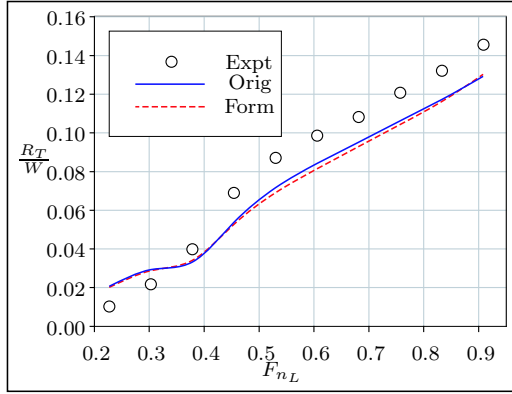
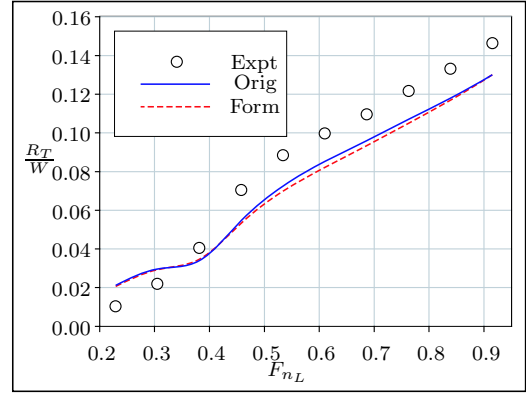
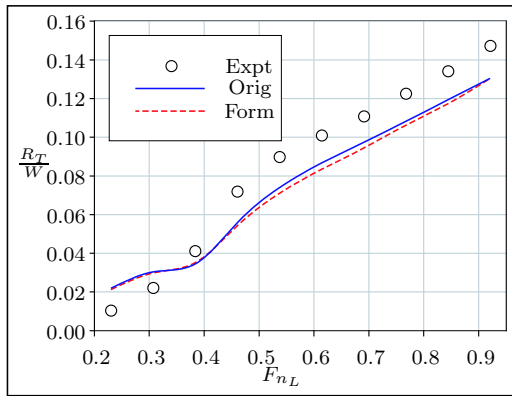
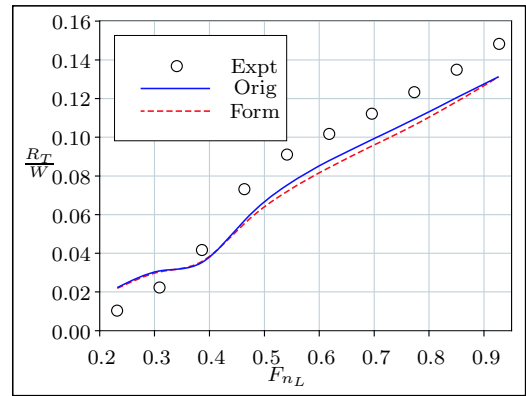
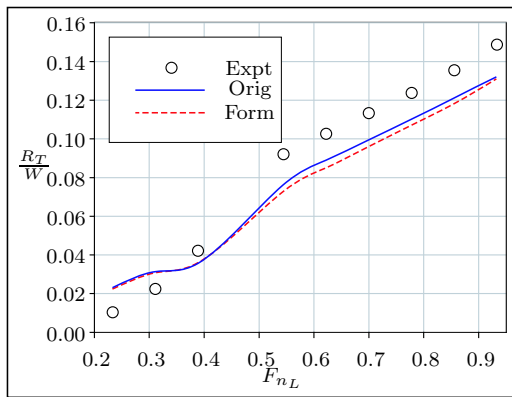
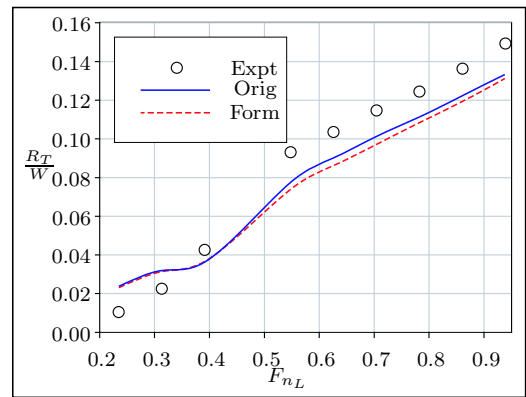
Figure D.265: NOVA-I at 115% Δ_{DWL} Figure D.266: NOVA-I at 120% Δ_{DWL} Figure D.267: NOVA-I at 125% Δ_{DWL} Figure D.268: NOVA-I at 130% Δ_{DWL} Figure D.269: NOVA-I at 135% Δ_{DWL} Figure D.270: NOVA-I at 140% Δ_{DWL}

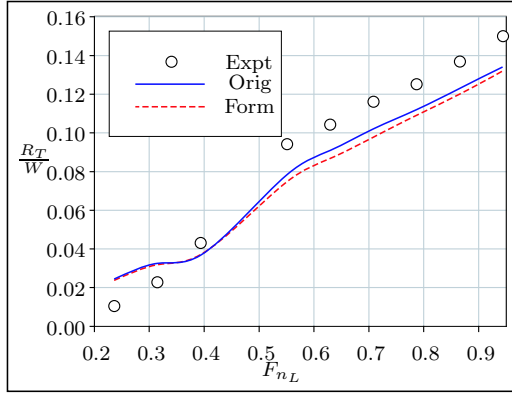
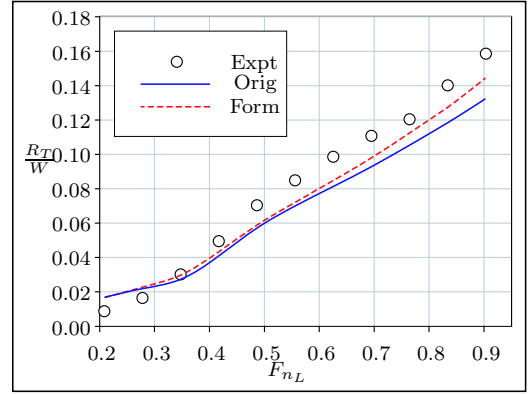
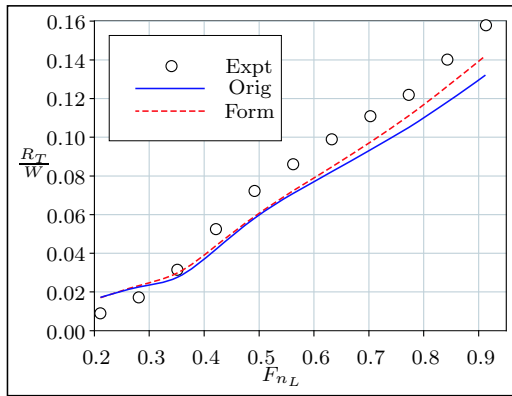
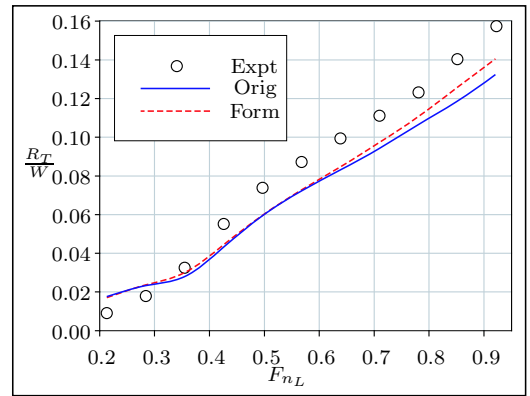
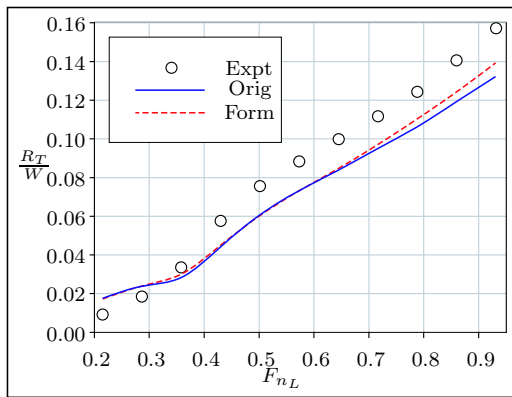
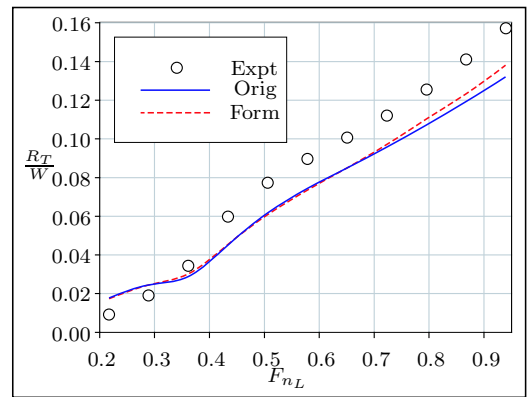
**Figure D.271:** NOVA-I at 145% Δ_{DWL} **Figure D.272:** NOVA-II at 75% Δ_{DWL} **Figure D.273:** NOVA-II at 80% Δ_{DWL} **Figure D.274:** NOVA-II at 85% Δ_{DWL} **Figure D.275:** NOVA-II at 90% Δ_{DWL} **Figure D.276:** NOVA-II at 95% Δ_{DWL}

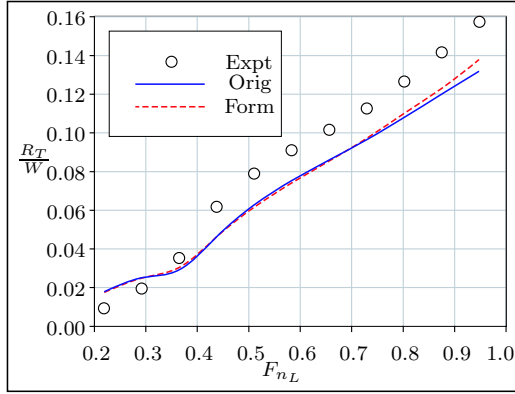
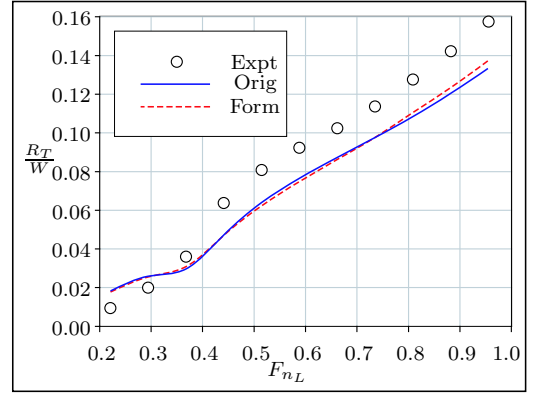
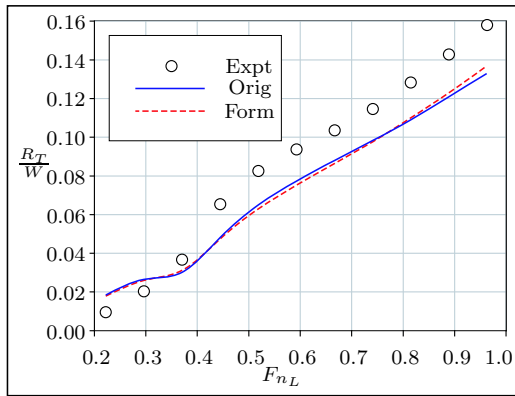
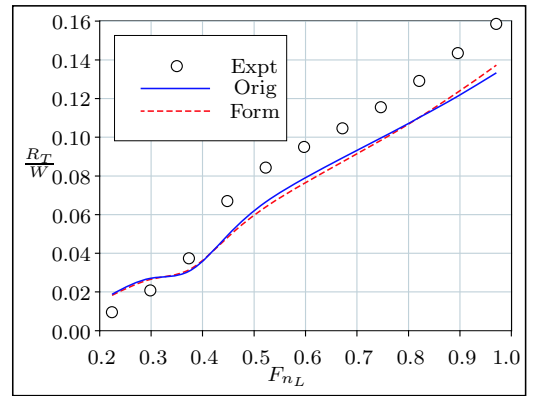
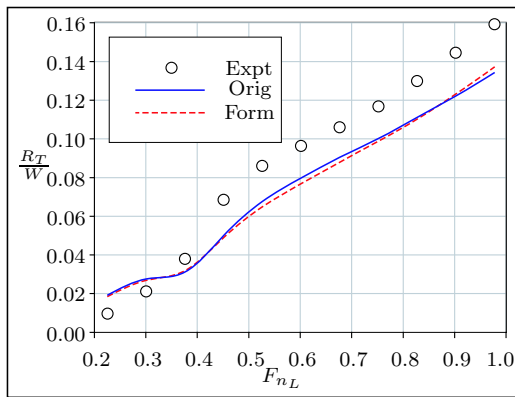
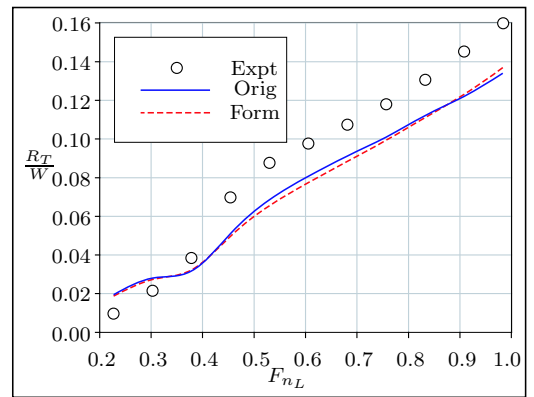
Figure D.277: NOVA-II at 100% Δ_{DWL} Figure D.278: NOVA-II at 105% Δ_{DWL} Figure D.279: NOVA-II at 110% Δ_{DWL} Figure D.280: NOVA-II at 115% Δ_{DWL} Figure D.281: NOVA-II at 120% Δ_{DWL} Figure D.282: NOVA-II at 125% Δ_{DWL}

Figure D.283: NOVA-II at 130% Δ_{DWL} Figure D.284: NOVA-II at 135% Δ_{DWL} Figure D.285: NOVA-II at 140% Δ_{DWL} Figure D.286: NOVA-II at 145% Δ_{DWL} Figure D.287: NOVA-III at 75% Δ_{DWL} Figure D.288: NOVA-III at 80% Δ_{DWL}

Figure D.289: NOVA-III at 85% Δ_{DWL} Figure D.290: NOVA-III at 90% Δ_{DWL} Figure D.391: NOVA-III at 95% Δ_{DWL} Figure D.292: NOVA-III at 100% Δ_{DWL} Figure D.293: NOVA-III at 105% Δ_{DWL} Figure D.294: NOVA-III at 110% Δ_{DWL}

Figure D.295: NOVA-III at 115% Δ_{DWL} Figure D.296: NOVA-III at 120% Δ_{DWL} Figure D.297: NOVA-III at 125% Δ_{DWL} Figure D.298: NOVA-III at 130% Δ_{DWL} Figure D.299: NOVA-III at 135% Δ_{DWL} Figure D.300: NOVA-III at 140% Δ_{DWL}

Figure D.301: NOVA-III at 145% Δ_{DWL} Figure D.302: NOVA-IV at 75% Δ_{DWL} Figure D.303: NOVA-IV at 80% Δ_{DWL} Figure D.304: NOVA-IV at 85% Δ_{DWL} Figure D.305: NOVA-IV at 90% Δ_{DWL} Figure D.306: NOVA-IV at 95% Δ_{DWL}

Figure D.307: NOVA-IV at 100% Δ_{DWL} Figure D.308: NOVA-IV at 105% Δ_{DWL} Figure D.309: NOVA-IV at 110% Δ_{DWL} Figure D.310: NOVA-IV at 115% Δ_{DWL} Figure D.311: NOVA-IV at 120% Δ_{DWL} Figure D.312: NOVA-IV at 125% Δ_{DWL}

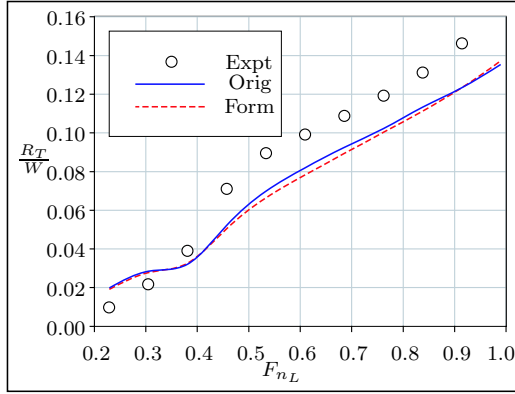
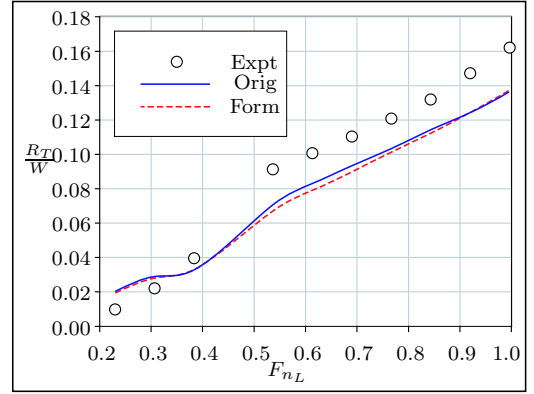
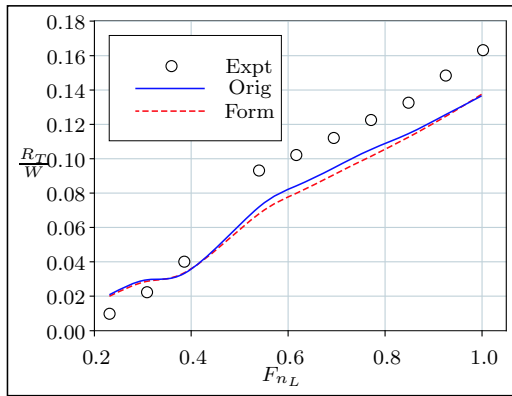
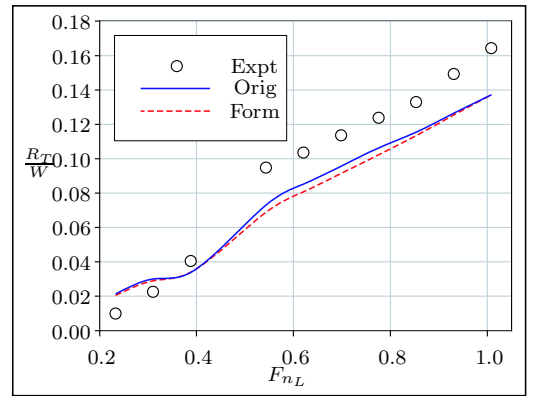
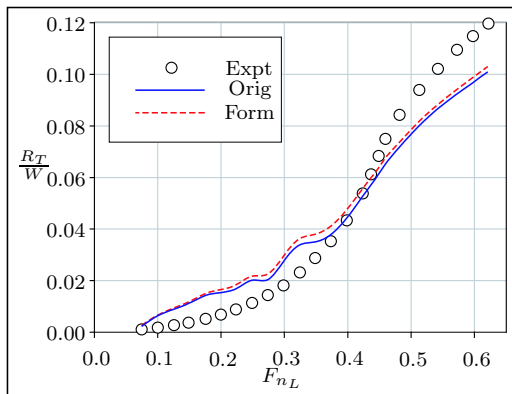
Figure D.313: NOVA-IV at 130% Δ_{DWL} Figure D.314: NOVA-IV at 135% Δ_{DWL} Figure D.315: NOVA-IV at 140% Δ_{DWL} Figure D.316: NOVA-IV at 145% Δ_{DWL} 

Figure D.317: COMPTON 1 at Draft 1

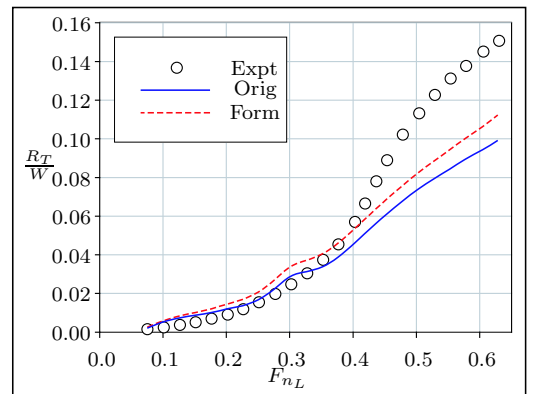


Figure D.318: COMPTON 1 at Draft 2

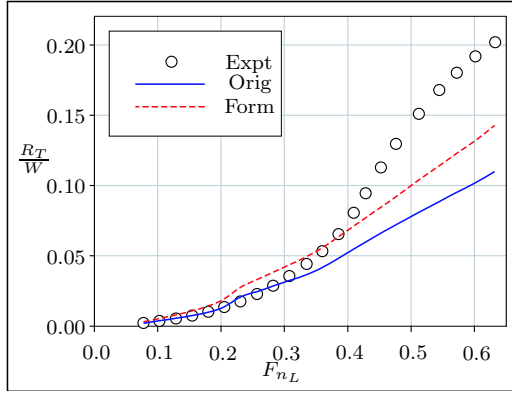


Figure D.319: COMPTON 1 at Draft 3

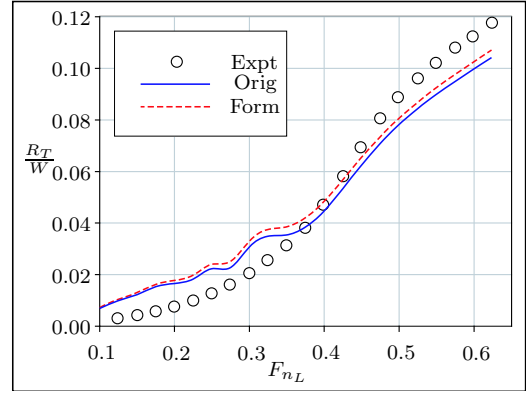


Figure D.320: COMPTON 2 at Draft 1

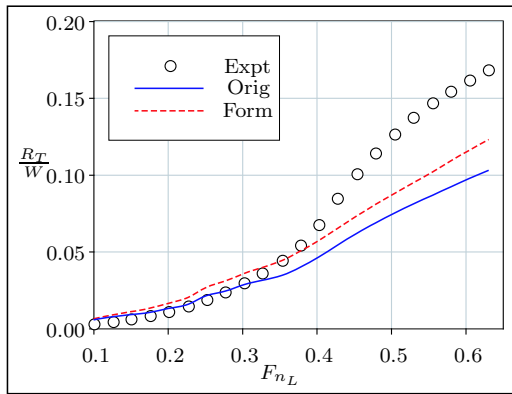


Figure D.321: COMPTON 2 at Draft 2

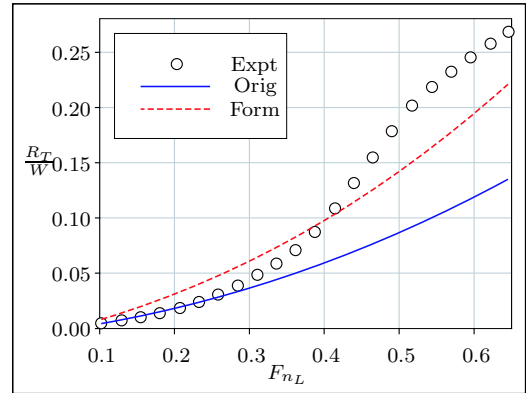


Figure D.322: COMPTON 2 at Draft 3

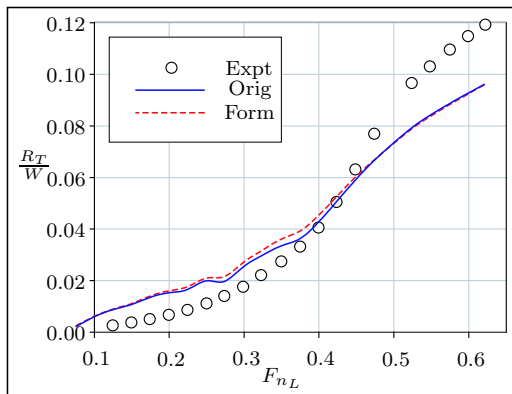


Figure D.323: COMPTON 3 at Draft 1

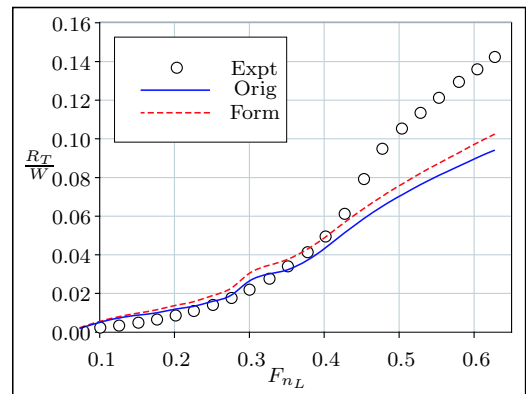


Figure D.324: COMPTON 3 at Draft 2

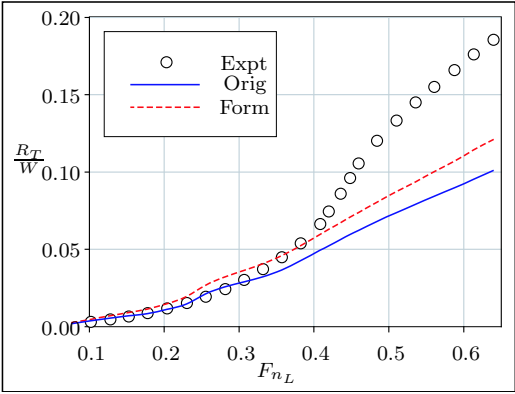


Figure D.325: COMPTON 3 at Draft 3